Univerza v Ljubljani

Fakulteta za elektrotehniko

Davorka Šel

DOLOČITEV ČASOVNO DISKRETNEGA MODELA ELEKTROPERMEABILIZACIJE TKIVA

DOKTORSKA DISERTACIJA

Ljubljana, 2003

Univerza v Ljubljani

Fakulteta za elektrotehniko

Davorka Šel

DOLOČITEV ČASOVNO DISKRETNEGA MODELA ELEKTROPERMEABILIZACIJE TKIVA

DOKTORSKA DISERTACIJA

Mentor: prof. dr. Damijan Miklavčič

Ljubljana, 2003

ACKNOWLEDGMENTS

I am gratefully indebted to prof. dr. Damijan Miklavčič, my mentor, for introducing me to this exciting field and leading me through the research labyrinth with the valuable discussions. I am also grateful for his patience, understanding and support in finishing the present thesis.

Special thanks also to prof. dr. Tomaž Slivnik for his suggestions in developing the model of tissue permeabilisation with analytical description of electric field distribution.

I greatly appreciate the interesting discussions in the field of system control I have had with dr. Igor Škrjanc, especially about the feasibility of real time control of tissue permeabilisation.

The experiments on tissue phantom were conducted at The Institute of Pharmacology and Structural Biology (Toulouse, France) by dr. Serge Mazeres, supervised by dr. Justin Teissie and I am greatly appreciative of their results. Particular thanks are also extended to dr. Justin Teissie for his detailed discussions about experiments and measurement techniques.

The *in vivo* experiments were conducted at The Institute Gustave-Roussy (Villejuif, France) by dr. David Cukjati and dr. Danute Batiuskaite under the supervision of dr. Lluis M. Mir. For their efforts and cooperation in providing me with the critically important results I am very thankful. I am also indebted to dr. Lluis M. Mir for his suggestions and extensive discussions about permeabilisation which has enhanced my understanding of the field.

Thanks are also due to the employees at The Institute of Oncology (Ljubljana, Slovenia), who scanned the CT images.

The extensive discussions with dr. Alenka Maček Lebar and her help with image recognition are greatly appreciated.

Thanks to all the people in The Laboratory of Biocybernetics for their pleasant collaboration and precious moments in the Laboratory.

Thanks to all people at Government Centre for IT, Republic of Slovenia, who supported me in finishing the thesis and tolerated my desire for research work.

I am deeply indebted to my parents who were extremely supportive during the whole period of my education and for encouraging me in my research work. I am also indebted to both my grandfathers who initially developed the enthusiasm for research in me.

Thanks to all my closest friends, who have put up with me through this process and filled my every day life with warmth and laughter which I needed through both bright and darker moments.

Thanks are due to Vince Pool for reading the thesis and correcting my grammatical inventions.

Some parts of the thesis were supported by the European Commission, within the 5th framework programme under the grant Cliniporator QLK3-1999-00484.

TABLE OF CONTENT

POVZETEK

Elektropermeabilizacija celic in posledično tudi tkiva je pojav, ki označuje spremembo prepustnosti celične membrane zaradi vzbujanja s kratkimi, visokonapetostnimi pulzi. Pri električnem vzbujanju je celica izpostavljena zunanjemu električnemu polju, zaradi katerega se na celični membrani pojavi električni potencial. Le-ta je odvisen od oblike in velikosti celice ter jakosti zunanjega električnega polja. V primeru, ko je vsiljena potencialna razlika na celični membrani zaradi zunanjega električnega polja dovolj velika, se poveča prepustnost celične membrane. Sprememba prepustnosti celične membrane pa je lahko reverzibilna ali ireverzibilna, na kar vpliva velikost jakosti zunanjega električnega polja. Poleg jakosti električnega polja pa vplivajo na permeabilizacijo celične membrane tudi trajanje in število električnih pulzov ter njihova frekvenca. Sprememba prepustnosti celične membrane pod vplivom zunanjega električnega polja je posledica sprememb v strukturi membrane. Natančni mehanizmi tega pojava doslej še niso v celoti pojasnjeni zaradi pomanjkanja eksperimentalnih rezultatov.

S povečanjem prepustnosti celične membrane omogočimo vnos snovi v celico, za katere celična membrana sicer predstavlja neprehodno oviro. Take snovi so nekatere zdravilne učinkovine (npr. kemoterapevtiki), barvila, beljakovine, DNK in druge snovi. Zaradi možnosti vnosa omenjenih snovi v celico je elektropermeabilizacija celične membrane z visokonapetostnimi pulzi postala zanimiva za uporabo v medicini.

Trenutno v kliniki za terapijo tumorjev že uporabljajo terapevtski pristop, ki združuje kemoterapijo in elektropermeabilizacijo. Pri tem kombiniranem pristopu z električnim vzbujanjem tkiva s kratkimi visokonapetostnimi pulzi omogočimo vnos kemoterapevtika v tumorske celice. Ustrezna terapevtska metoda zdravljenja je poimenovana elektrokemoterapija. Za uspešno elektrokemoterapijo je potrebno celotni volumen tumorja izpostaviti poljskim jakostim, višjim od reverzibilnega praga.

Podobno se za vnos genskega materiala v celice uporablja kombinacija visokonapetostnih pulzov, ki permeabilizirajo celično membrano in pulzov nižjih amplitud, ki omogočajo prehod genskega materiala prek permeabilizirane celične membrane z elektroforezo. Opisana metoda, poimenovana elektro-genska terapija, je trenutno predmet predkliničnih raziskav. Zaradi številnih prednosti, ki jih ima pred drugimi metodami genskega vnosa, pa lahko pričakujemo, da jo bodo v kratkem pričeli uporabljati tudi v kliniki. Pogoj za uspešno elektro-gensko terapijo je porazdelitev poljskih jakosti med reverzibilnim in ireverzibilnim pragom v obravnavanem delu tkiva.

Uspešnost elektrokemoterapije in elektro-genske terapije je torej odvisna od porazdelitve poljske jakosti v obravnavanem območju tkiva. Tako je potrebno za vsako od naštetih metod glede na tip in razsežnosti obravnavanega tkiva posebej, določiti električne parametre signala vzbujanja in izbrati ustrezno postavitev elektrod. Za določitev pragovih vrednosti poljske jakosti je bila doslej uporabljena kombinacija modelov in tako imenovanih hitrih testov. Pri teh se v tkivo vbrizga snov, ki lahko prehaja v celico zgolj skozi permeabilizirano celično membrano. Temu sledi vzbujanje tkiva z visokonapetostnimi pulzi različnih amplitud. Amplitude električnih pulzov, pri katerih dosežemo vnos snovi v celico se uporabi za modelski izračun porazdelitve električnega polja.

Pragovne vrednosti električnega polja nato določimo s primerjavo področja permeabiliziranega tkiva in na tem mestu z modelom izračunanih vrednosti električnega polja. Ena od pomanjkljivosti tega pristopa je, da ne upošteva električnih sprememb v tkivu zaradi izpostavljenosti zunanjemu električnemu polju.

S povečanjem prepustni celične membrane se namreč pri elektropermeabilizaciji poveča tudi prepustnost membrane za ione, kar se posledično odraža v povečani električni prevodnosti celice. To ima za posledico tudi povečanje prevodnosti celotnega tkiva, kar seveda vpliva na drugačno porazdelitev električnega polja kot v nepermeabiliziranem tkivu.

V okviru tega dela smo tako razvili časovno diskretni model permeabilizacije tkiva. Model upošteva spreminjanje električne prevodnosti v tkivu pod vplivom zunanjega električnega polja zadostnih jakosti. Obnašanje modela smo potrdili v okviru študije parametrov in posebej v ta namen razvitega simulacijskega okolja. Vrednotenje modela na eksperimentalnih podatkih pa je pokazalo zelo dobro ujemanje izmerjenih in izračunanih vrednosti. Na podlagi predstavljenega modela permeabilizacije smo raziskali možnosti njegove uporabe za optimizacijo parametrov električnih pulzov in razdalje med elektrodama za uporabo v elektrokemoterapiji na geometriji človeških možganov s tumorjem.

Osnovni namen uporabe predstavljenega časovno diskretnega modela je torej določitev optimalnih parametrov za učinkovito permeabilizacijo tkiva na neinvaziven način pred terapijo.

SIMULACIJSKO OKOLJE ZA SPREMLJANJE ELEKTROPERMEABILIZACIJE TKIVA NA OSNOVI ČASOVNO DISKRETNEGA MODELA

Simulacijsko okolje za spremljanje elektropermeabilizacije tkiva smo razvili za geometrijo dveh koncentričnih valjastih elektrod, med kateri je vstavljeno biološko tkivo. To geometrijo smo izbrali, ker omogoča analitičen izračun porazdelitve električnega polja, obenem pa je porazdelitev polja med koncentričnima valjastima elektrodama podobna porazdelitvi polja okrog igelnih elektrod.

Elektropermeabilizacijo tkiva med koncentričnima valjastima elektrodama smo opisali s časovno diskretnim modelom (Slika i). Le-ta je zasnovan na dejstvu, da se pri vzbujanju tkiva z električnim pulzom zaradi elektropermeabilizacije tkiva poveča električna prevodnost v delu tkiva, ki je bilo izpostavljeno električni poljski jakosti, višji od reverzibilnega praga. Način spreminjanja električne prevodnosti tkiva zaradi električne poljske jakosti je podan s funkcijsko odvisnostjo $\sigma(E)$, ki jo je potrebno vnaprej določiti za vsak tip tkiva. Električno polje v posameznem časovnem trenutku obravnavamo kot kvazistacionarno in ga opišemo z enačbami za tokovno polje v prevodniku.

Začetno stanje ob vzbujanju z visokonapetostnim električnim pulzom v času k=1 predpostavlja v celotnem tkivu tako prevodnost, kot jo ima nepermeabilzirano tkivo. V primeru, da ima v času k=1 izračunano električno polje v delu tkiva višjo jakost od reverzibilnega praga, temu delu tkiva ustrezno spremenimo prevodnost na podlagi odvisnosti $\sigma(E)$. Tako dobimo prevodnost tkiva v časovnem trenutku k=2. Zaradi povečane električne prevodnosti v permeabiliziranem delu tkiva, se v časovnem trenutku k=2, posledično spremeni tudi porazdelitev električnega polja. Pri izračunu porazdelitve električnega polja smo zaradi spremenjene prevodnosti upoštevali prestopni pogoj za električno poljsko jakost na meji dveh snovi z različnima prevodnostma. Nova porazdelitev električne poljske jakosti vpliva na nadaljnjo permeabilizacijo tkiva in spremembo prevodnosti. Razširjanje permeabilizacije se tako nadaljuje, dokler električna poljska jakost ne doseže ustaljenega stanja. Pri spreminjanju prevodnosti v časovno diskretnem modelu smo upoštevali, da se med trajanjem električnega pulza prevodnost nikoli ne zmanjša, saj je proces zacelitve bistveno počasnejši in tako daljši od časa trajanja pulza. Tako tudi v primeru, ko bi zaradi odvisnosti $\sigma(E)$

morala biti v izbrani točki prevodnost nižja, kot je bila v predhodnem časovno diskretnem trenutku, se le-ta ne zmanjša, ker traja učinek permeabilizacije dlje, kot je dolžina pulza.

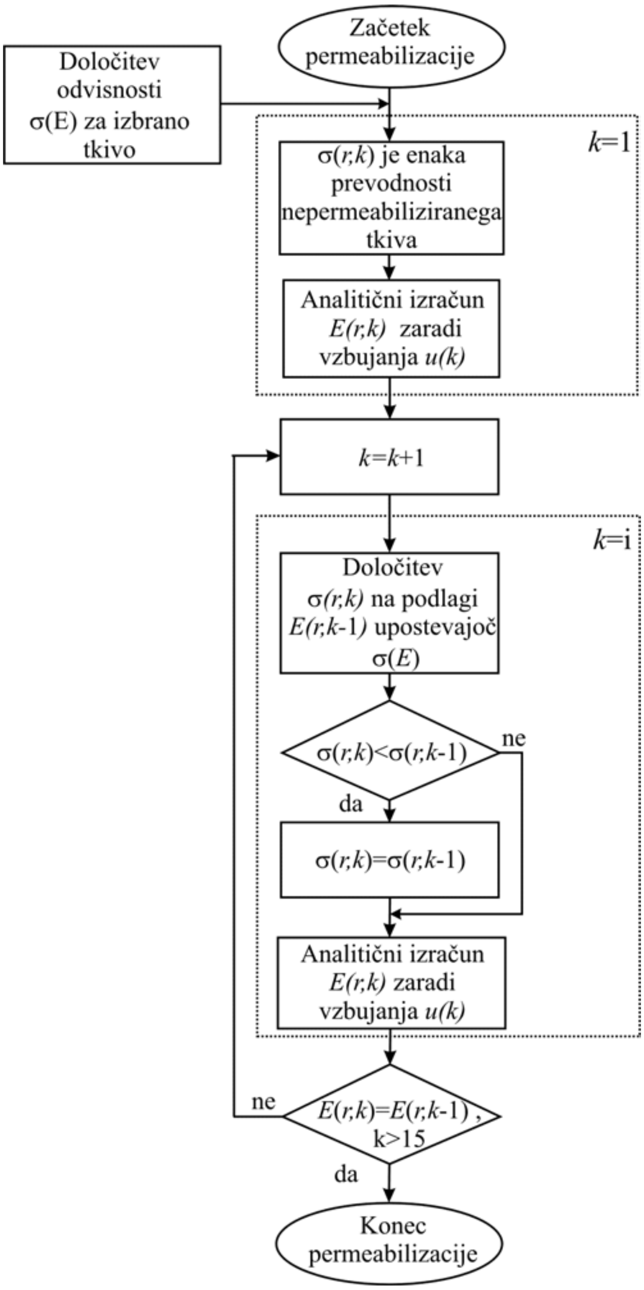

Slika i: Časovno diskretni model permeabilizacije tkiva – shematski prikaz.

Opisani časovno diskretni model permeabilizacije tkiva smo nato vključili v simulacijsko okolje. Namen izdelave simulacijskega okolja je bil omogočiti spremljanje poteka permeabilizacije pri različnih amplitudah pulzov, različnih prevodnostih tkiva in različnih razdaljah med valjastima elektrodama. V simulacijskem okolju smo upoštevali možnost, da ima lahko funkcijska odvisnost σ(E) stopničast, linearen, eksponenten ali sigmoiden potek. Grafični vmesnik simulacijskega okolja prikazuje Slika ii. Nastavitev parametrov permeabilizacije in izbiro funkcijske odvisnosti σ(E) izvedemo v spodnjem levem oknu grafičnega vmesnika. Potek permeabilizacije pa je v okviru simulacijskega okolja predstavljen s porazdelitvijo električnega polja (zgoraj desno) in specifične prevodnosti tkiva (zgoraj levo) med elektrodama za vsak časovno diskretni korak ter radijem, do katerega je bilo tkivo permeabilizirano, v posameznem časovne koraku (spodaj desno).

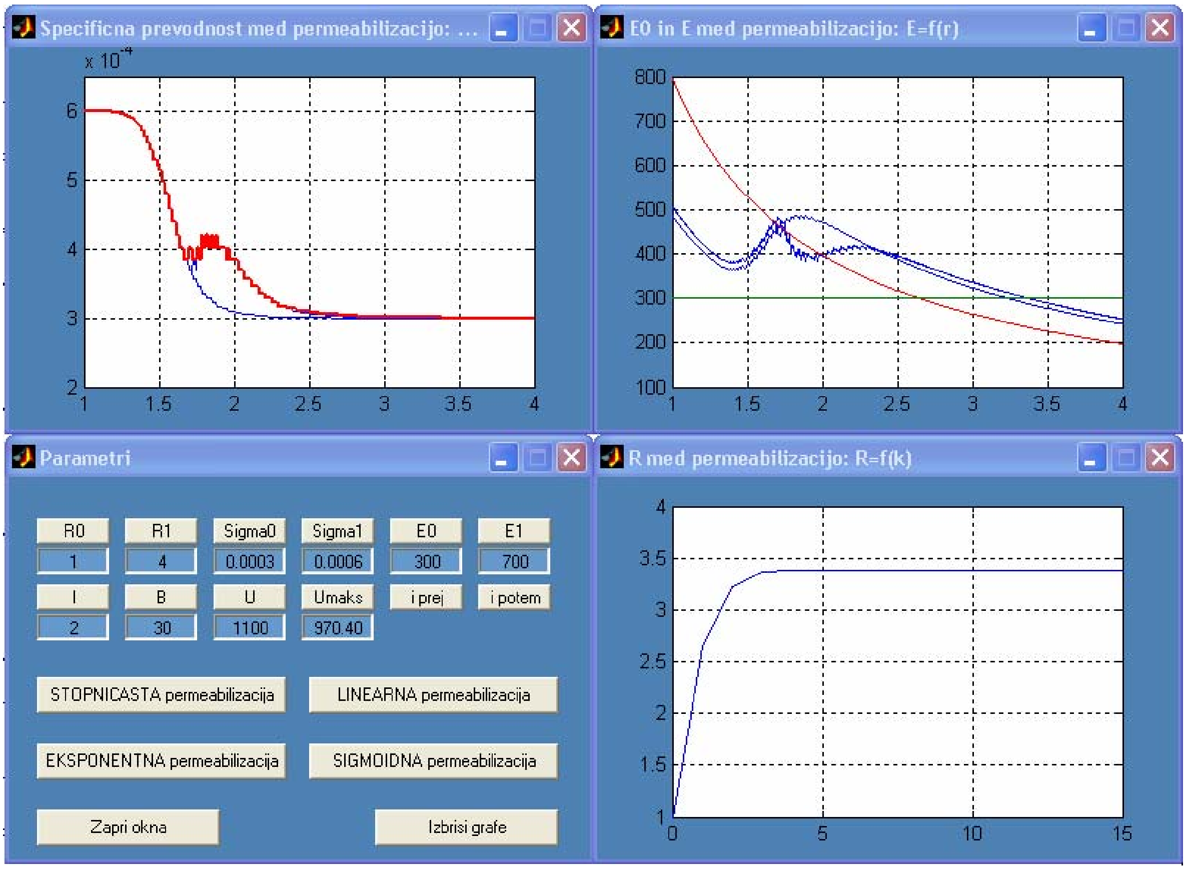

R0	R1	Sigma0	Sigma1	E0	E1
1	4	0.0003	0.0006	300	700
I	B	U	Umaks	i prej	i potem
2	30	1100	970.40		

Slika ii: Grafični vmesnik simulacijskega okolja, s prikazom poteka permeabilizacije ob izbiri sigmoidne odvisnosti σ(E).

Prikazano simulacijsko okolje bi lahko zaradi podobne porazdelitve električnega polja, kot je okrog igelnih elektrod, uporabljali v klinične namene za grobo, a hitro oceno permeabilizacije tkiva. Poleg tega bi lahko služilo v pomoč pri izbiri parametrov – razdalje med elektrodami in napetosti električnih pulzov, potrebnih za permeabilizacijo želenega dela tkiva.

Znotraj simulacijskega okolja smo predvideli štiri različne oblike funkcijskih odvisnosti σ(E). Njihov vpliv, kot tudi vpliv amplitude pulzov in razdalje med elektrodama na potek permeabilizacije smo sistematično raziskali v okviru študije parametrov. Namen študije parametrov je bila tudi potrditev časovno diskretnega modela, saj s spreminjanjem posameznih parametrov lahko preverimo, ali so modelski izračuni skladni z eksperimentalno ugotovljenimi pojavi pri elektropermeabilizaciji tkiva.

Študija parametrov je potrdila, da električne lastnosti tkiva (prevodnost permeabiliziranega in nepermeabiliziranega tkiva ter reverzibilni in ireverzibilni prag električne poljske jakosti) vplivajo na radij permeabilizacije. Ravno tako je potrdila, da je porazdelitev električnega polja, ki jo določata razdalja med elektrodama in amplituda pulzov odločilna za potek permeabilizacije. Iz tega sledi, da je potrebno za učinkovito permeabilizacijo tkiva poznati električne lastnosti tkiva ter le-tem ustrezno izbrati amplitudo pulzov in razdaljo med elektrodama.

Pri primerjavi vpliva funkcijskih odvisnosti σ(E) smo izbrali take parametre le-teh, da so imele vse funkcijske odvisnosti iste vrednosti prevodnosti permeabiliziranega in nepermeabiliziranega tkiva. Simulacijsko okolje in študija parametrov sta pokazala, da v primeru stopničaste funkcijske odvisnosti σ(E) permeabilizacija poteka dlje, kot v primeru ostalih odvisnosti. Stopničasta odvisnost namreč povzroča nezveznosti v porazdelitvi električnega polja na meji med snovmi z različno prevodnostjo, ki je posledica prestopnega pogoja za vektor električne poljske jakosti na tej meji. V primeru linearne, eksponentne in sigmoidne funkcijske odvisnosti σ(E) vpliv prestopnega pogoja ni tako izrazit, ker so le-te zvezne oziroma vsaj odsekoma zvezne. Primerjava med slednjimi funkcijskimi odvisnostmi pa je pokazala, da je bil največji del tkiva permeabiliziran pri upoštevanju linearne funkcijske odvisnosti σ(E). Vzrok temu je porazdelitev polja med elektrodama, ki pada obratno sorazmerno z razdaljo od središča valjastih elektrod. Tako je bil v področju med elektrodama večji del tkiva izpostavljen poljskim jakostim, ki so nižje od povprečne vrednosti poljskih jakosti na veznici med elektrodama. Pri nižjih vrednostih električne poljske jakosti pa linearna funkcijska odvisnost predvideva večje povečanje specifične prevodnosti, kot eksponentna ali sigmoidna odvisnost.

Vpliv posameznih funkcijskih odvisnosti σ(E) je seveda odvisen tudi od porazdelitve električnega polja v tkivu. Večji kot je del tkiva, ki je izpostavljeno poljskim jakostim med pragovnima vrednostma, večji je vpliv različnih funkcijskih odvisnosti. V odvisnosti od porazdelitve električnega polja tako lahko oblika funkcijske odvisnosti σ(E) pomembno vpliva na izračun radija permeabilizacije. Na podlagi zgornjih ugotovitev in primerjave z rezultati poskusov *in vivo* smo izbrali sigmoidno obliko funkcijske odvisnosti σ(E) za uporabo v nadaljnjih modelih. Sigmoidna oblika je namreč zvezna v celotnem področju električnih poljskih jakosti, obenem pa se ujema z rezultati, dobljenimi pri poskusih *in vivo*. Poskusi so namreč pokazali, da je v tkivu, ki je bilo izpostavljeno poljskim jakostim tik nad reverzibilnim pragom, le del celic permeabiliziran. Z večanjem poljske jakosti je bil tudi večji del celic permeabiliziran. Pri poljskih jakostih velikosti ireverzibilnega praga, je nato odmrlo sprva le nekaj celic, pri še višjih poljskih jakostih pa je prišlo do nekroze tkiva. Tak potek permeabilizacije v odvisnosti od električne poljske jakosti je mogoče opisati s sigmoidno funkcijsko odvisnostjo. Upoštevajoč dejstvo, da se pri permeabilizaciji tkiva poveča električna prevodnost tkiva, ima tudi slednja sigmoidni potek v odvisnosti od poljske jakosti.

Določitev parametrov sigmoidne funkcijske odvisnosti σ(E) je mogoče opraviti zgolj s pomočjo eksperimentalnih podatkov za vsak tip tkiva posebej. Tako smo v nadaljevanju predlagali metodo določitve parametrov funkcijske odvisnosti. Metoda temelji na minimizaciji razlike med izmerjenim in modelsko izračunanim tokom, s spreminjanjem parametrov sigmoidne funkcijske odvisnosti σ(E), ki je vključena v model. Območje, v katerem se z optimizacijo išče optimalne vrednosti parametrov, smo določili na podlagi meritev vnosa Cr^{51}-EDTA, ki je indikator volumna reverzibilno permeabiliziranega tkiva. Primerjavo izmerjenega in izračunanega toka z modelom, v katerega je vključena sigmoidna funkcijska odvisnost z optimiziranimi vrednostmi parametrov prikazuje Slika iii.

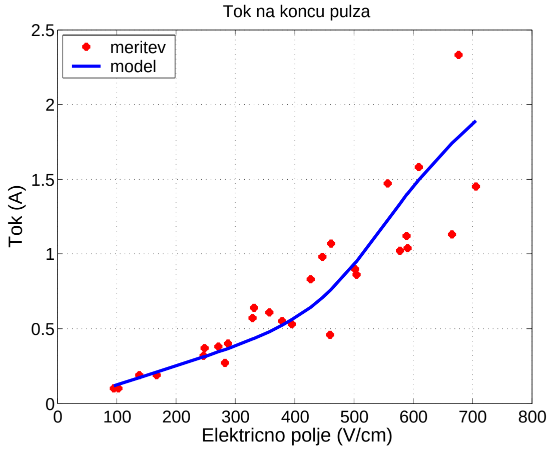

Slika iii: Izmerjeni tok (*) in izračunani tok (polna črta) pri optimiziranih parametrih sigmoidne odvisnosti σ(E).

V simulacijskem okolju in študiji parametrov smo pri izračunu modela upoštevali vzbujanje s pravokotnimi električnimi pulzi. V nadaljevanju pa nas je zanimalo, kako oblika pulza vpliva na potek permeabilizacije tkiva. Zato smo izvedli dodatne izračune modela pri dveh različnih oblikah vhodne napetosti in sicer v obliki rampe, a z nasprotnima naklonoma. Simulacije so pokazale, da je radij permeabiliziranega področja v obeh primerih približno enak (Tabela i), z razliko, da je v primeru linearno padajoče napetosti maksimalni radij dosežen že na samem začetku vzbujanja, medtem ko je v primeru linearno naraščajoče napetosti maksimalni radij dosežen tik pred koncem vzbujanja (Slika iv). Primerjava radijev permeabilizacije z radijem, ki ga dobimo pri vzbujanju s konstantnim pulzom amplitude povprečne vrednosti signalov rampe je pokazala, da je v primeru vzbujanja s konstantno napetostjo radij permeabilizacije bistveno nižji (Tabela i). Iz tega sledi, da na radij permeabilizacije odločilno vpliva maksimalna vrednost pritisnjene napetosti.

Tabela i: Primerjava radijev permeabilizacije pri različnih oblikah vhodne napetosti za različne funkcijske odvisnosti σ(E).

	Linearno naraščajoča *u*	Linearno padajoča *u*	Konstantna *u*
σ(E)	Radij permeabilizacije (enota)		
Stopničasta	1.75	1.61	1.12
Linerana	2.77	2.81	1.97
Eksponentna	2.52	2.53	1.83
Sigmoidna	2.63	2.72	1.89

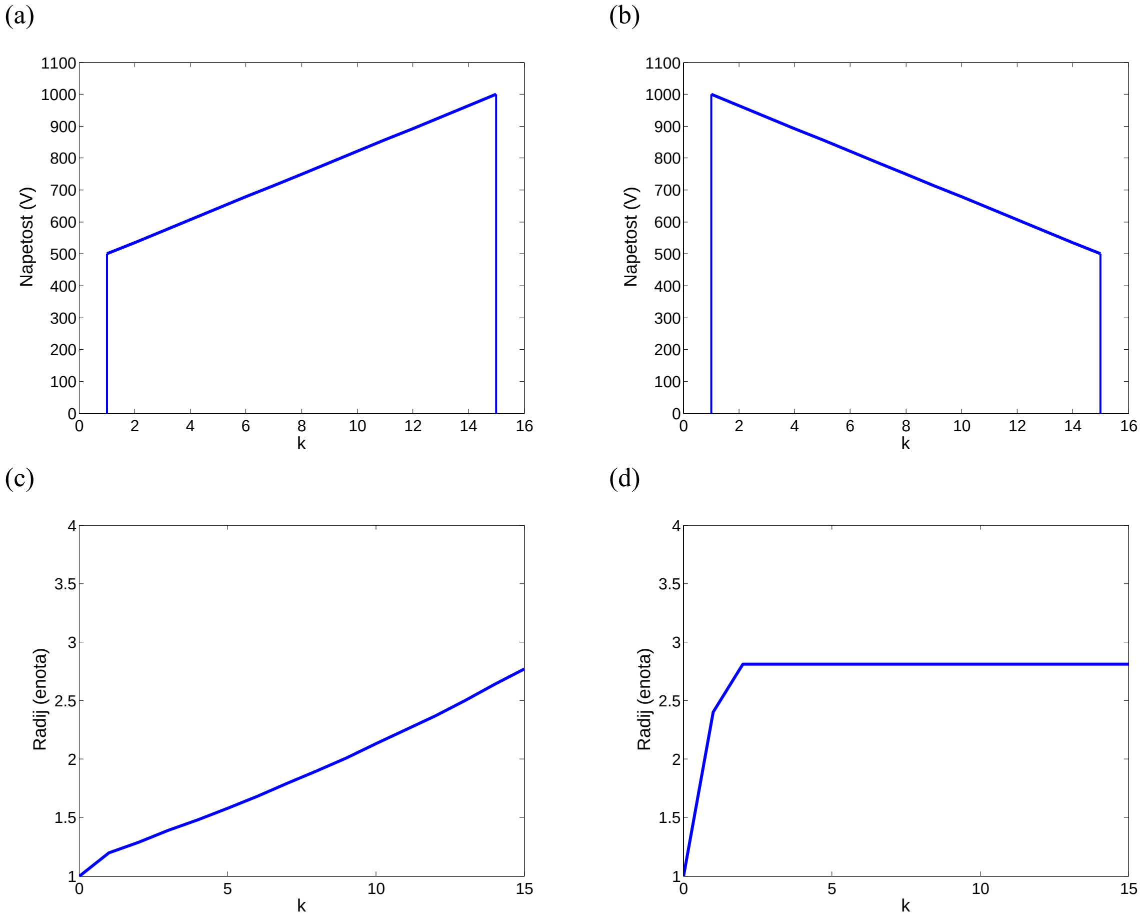

Slika iv: (c) radij permeabilizacije pri vzbujanju z linearno naraščajočo napetostjo (a); (d) radij permeabilizacije pri vzbujanju z linearno padajočo napetostjo (b). Upoštevana je sigmoidna oblike funkcijske odvisnosti σ(E).

Ker lahko z obliko pritisnjene napetosti vplivamo na radij permeabilizacije tkiva, smo v nadaljevanju raziskali možnosti zaprtozančnega vodenja permeabilizacije s proporcionalno integrirnim (PI) regulatorjem. Naloga regulatorja je bila določiti ustrezno napetost vzbujanja na podlagi razlike med trenutnim in želenim obsegom permeabilizacije tkiva. Rezultati, ki smo jih pridobili s pomočjo časovno diskretnega modela (Slika v) so pokazali, da je uporaba tega pristopa možna. Vendar pa bi bila uporaba sprotnega vodenje permeabilizacije za klinične namene težavna, saj je določitev obsega permeabilizacije v realnem času praktično nemogoča. Ta podatek pa je nujno potreben tako za določitev parametrov PI regulatorja, kot tudi za sprotno vodenje permeabilizacije. Podatka o obsegu permeabilizacije prav tako ni mogoče dobiti posredno iz drugih meritev, saj npr. podatek o spremembi celotne prevodnosti tkiva, ki bi ga lahko pridobili iz sprotnih meritev toka in napetosti, ne daje informacije o tem ali je bilo neko področje tkiva permeabilizirano. Edini način za pridobitev podatka o obsegu permeabilizacije bi lahko bil dinamični model permeabilizacije in posledično pristop vodenja permeabilizacije na osnovi modela. To obenem predstavlja tudi dodatno področje uporabe predstavljenega časovno diskretnega modela.

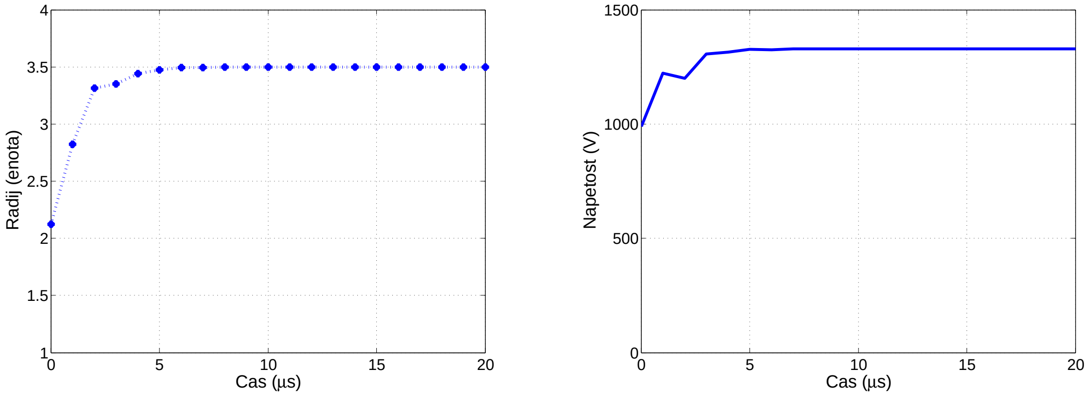

Slika v: (a) regulirani signal – radij in (b) regulirni signal – napetost pri vodenju s proporcionalno integrirnim regulatorjem.

Porazdelitev električnega polja lahko v časovno diskretnem modelu izračunamo tudi s pomočjo numeričnih metod. Ta pristop je praktično nujen, ko geometrije in snovnih lastnosti prevodnika ni mogoče opisati v istem koordinatnem sistemu. Takrat namreč analitični opis porazdelitve električnega polja ni mogoč. Glede na dejstvo, da je potrebno v časovno diskretnem modelu večkrat izračunati porazdelitev električnega polja, in upoštevajoč računsko zahtevnost numeričnih izračunov, je čas izračuna časovno diskretnega modela z numeričnim izračunom porazdelitve polja bistveno daljši, kot v primeru analitičnega modela. To je pokazala tudi primerjava časovno diskretnih modelov permeabilizacije tkiva z analitičnim in numeričnim izračunom polja med dvema koncentričnima valjastima elektrodama.

DOLOČITEV OPTIMALNE GEOMETRIJE IGELNIH ELEKTROD ZA MODELIRANJE Z METODO KONČNIH ELEMENTOV

Igelne elektrode se v kliniki uporabljajo za elektropermeabilizacijo globlje ležečega tkiva. Pri modelskem izračunu porazdelitve električnega polja okrog igelnih elektrod, pa je pogosto potrebno uporabiti numerične metode, še posebej v primerih, ko želimo opazovati porazdelitev polja okrog vrha elektrod. Za reševanje tovrstnih problemov se je metoda končnih elementov izkazala kot zelo primerna. Modeliranje igelnih elektrod z metodo končnih elementov pa je dostikrat zahtevno, saj so dimenzije elektrod ponavadi bistveno manjše od dimenzij okoliškega tkiva. V takih primerih je potrebno v okolici elektrod zgraditi zelo gosto mrežo končnih elementov, kar ima za posledico daljši čas, potreben za izračun modela.

V okviru tega dela naloge smo tako raziskali načine modeliranja geometrije igelnih elektrod z metodo končnih elementov, z namenom, da bi določiti tako geometrijo, ki bi omogočila hitrejši izračun modela, obenem pa ne bi bistveno vplivala na porazdelitev električnega polja v tkivu. Določitev optimalne geometrije elektrod in vrednotenje le-te smo izvedli s pomočjo eksperimentalnih podatkov, pri katerih je bil merjen celotni tok pri vzbujanju z določeno napetostjo. Eksperimenti z igelnimi elektrodami so bili izvedeni v gelu, ki ima podobne električne lastnosti, kot biološko tkivo. Za izbiro ustrezne geometrije elektrod smo vpeljali kriterijsko funkcijo, ki so jo sestavljale utežena relativna razlika med izmerjenim in modelsko izračunanim tokom, utežena relativna razlika med časom, potrebnim za izračun modela in najkrajšim časom izračuna ter utežena relativna razlika med presekom elektrod in presekom okroglih igelnih elektrod.

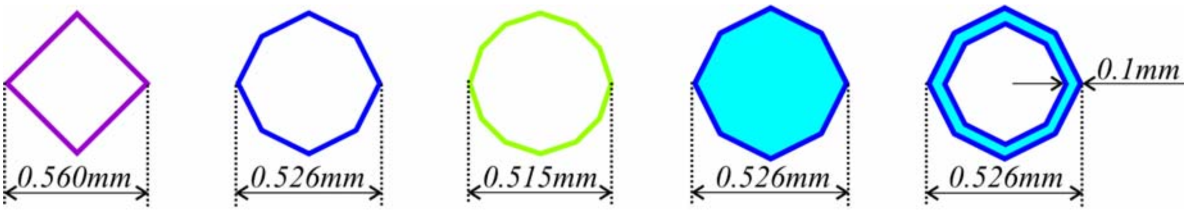

Slika vi: Različni preseki, uporabljeni za modeliranje igelnih elektrod.

Osem kotni presek igelnih elektrod je bil na podlagi kriterijske funkcije in eksperimentalnih podatkov, dobljenih pri električnem vzbujanju z enim parom igelnih elektrod, izbran kot najustreznejši. Model z osem kotnimi igelnimi elektrodami smo nato ovrednotili na eksperimentalnih podatkih, dobljenih pri vzbujanju s poljem igelnih elektrod. Maksimalno odstopanje med modelsko izračunanim in izmerjenim tokom je bilo 9%, razen v primeru zelo tankega gela. Razlog za odstopanje je bila polarizacija elektrod, ki je pri nižjih napetostih bistveno vplivala na odstopanje med modelom in meritvami. Učinek polarizacije elektrod smo nato vključili v model, kar je zmanjšalo odstopanje med modelom in meritvami na 3%. Primerjava izračunane porazdelitve električnega polja pri vzbujanju s poljem igelnih elektrod (Slika vii) in porazdelitve podane v literaturi za isto geometrijo elektrod je pokazala, da model z osem kotnimi igelnimi elektrodami zadosti dobro opisuje porazdelitev polja.

Vrednotenje modela na podlagi celotnega toka pa je pokazalo, da je ta pristop mogoče uporabiti za hitro vrednotenje modela pod pogojem, da so geometrija in električne lastnosti tkiva zadosti dobro opisane z modelom.

VREDNOTENJE ČASOVNO DISKRETNEGA MODELA PERMEABILIZACIJE JETRNEGA TKIVA S PAROM IGELNIH ELEKTROD

Med pomembnejše korake pri procesu modeliranja sodita vsekakor potrditev in vrednotenje modela. Potrditev časovno diskretnega modela smo opravili v okviru študije parametrov. Vrednotenje modela, pri katerem ugotavljamo, ali daje model take rezultat kot realni sistem, pa smo opravili v okviru tega poglavja.

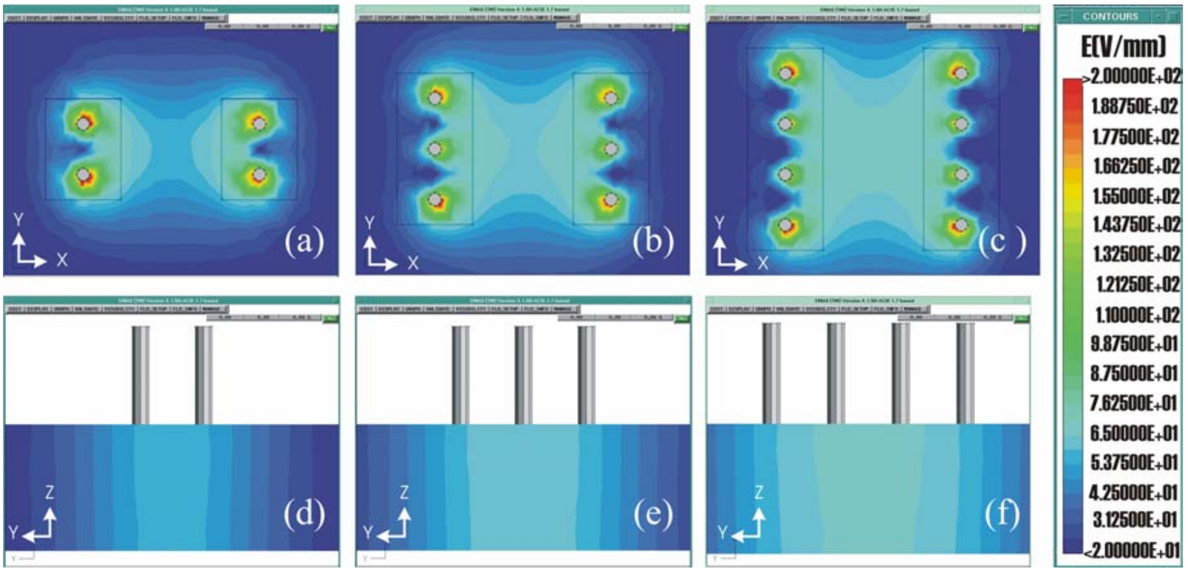

Slika vii: Porazdelitev električnega polja pri vzbujanju z dvema paroma igelnih elektrod v *xy* ravnini (a) in *yz* ravnini (d); s tremi pari igelnih elektrod v *xy* ravnini (b) in *yz* ravnini (e) in s štirimi pari igelnih elektrod v *xy* ravnini (c) in *yz* ravnini (f).

Eksperimenti, potrebni za vrednotenje modela, so bili opravljeni na institutu Gustave-Roussy v Franciji. Za permeabilizacijo jetrnega tkiva zajcev so uporabili igelne elektrode. Električno vzbujanje so izvedli z vlakom osmih pulzov, trajanja 100 µs in frekvence 1 Hz. Posamezni eksperimenti so se med seboj razlikovali v amplitudi pulzov, ki je bila v območju med 200 V in 1200 V. V eksperimentih so izmerili celoten tok in napetost med trajanjem pulza. V predhodno opravljenih eksperimenti na jetrnem tkivu zajcev z enakim električnim vzbujanjem pa so določili tudi območje permeabiliziranega in nepermeabiliziranega tkiva. Meritve obeh skupin eksperimentov smo uporabili za ocenjevanje parametrov funkcijske odvisnosti σ(E) in vrednotenje modela.

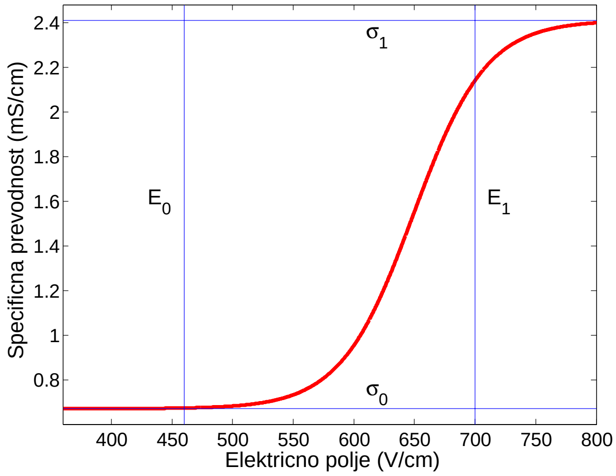

Slika viii: Funkcijska odvisnost σ(E). Ocenjevanje parametrov je izvedeno z optimizacijo na eksperimentalnih podatkih o toku.

Za izdelavo ustreznega časovno diskretnega modela permeabilizacije smo morali najprej določiti parametre funkcijske odvisnosti σ(E) za jetrno tkivo zajcev. Iz razlogov, podanih pri analizi časovno diskretnega modela z analitičnim opisom porazdelitve električnega polja med valjastima elektrodama, smo izbrali sigmoidno obliko funkcijske odvisnosti. Ocenjevanje parametrov funkcijske odvisnosti σ(E) pa smo izvedli s prav tako predhodno predlagano metodo, torej z optimizacijo na eksperimentalnih meritvah toka. Za ocenjevanje parametrov smo izbrali le del eksperimentalnih meritev toka, preostale meritve pa smo kasneje uporabili za vrednotenje modela. Funkcijsko odvisnost σ(E), s tako ocenjenimi parametri prikazuje Slika viii. Z ocenjevanjem parametrov smo med drugim določili tudi reverzibilni (460 V/cm) in ireverzibilni (700 V/cm) prag električne poljske jakosti za jetrno tkivo zajcev. Dobljena pragova se razlikujeta od podanih vrednosti v literaturi. Vzrok temu je dejstvo, da so bili v literaturi podani pragovi določeni brez upoštevanja spreminjanja prevodnosti tkiva zaradi permeabilizacije. Razlago razlike v dobljenih vrednostih pragov prikazuje Slika ix. Razlaga je podana za geometrijo dveh koncentričnih valjastih elektrod, ker ima le-ta podobno porazdelitev polja kot je v okolici igelnih elektrod in omogoča analitični opis polja. Črta, označena z E_{00}, podaja vrednost reverzibilnega praga, ki jo dobimo v nepermeabiliziranem tkivu, ob upoštevanju podatka, da je bil eksperimentalno ugotovljen radij permeabilizacije pri vrednosti 2.6 enote (navpična črta). Ker se pri permeabilizaciji tkiva poveča njegova električna prevodnost, to vpliva na spremembo porazdelitev električnega polja v tkivu. Če torej upoštevamo porazdelitev polja v delno permeabiliziranem tkivu, dobimo reverzibilni prag permeabilizacije pri vrednosti E_0-dejanski, ki je višji od predhodno določenega.

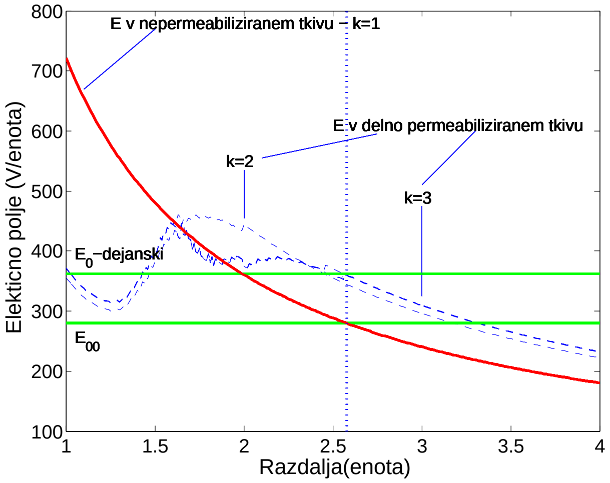

Slika ix: Razlaga razlike v pragovnih vrednostih, dobljenih z ocenjevanjem parametrov funkcijske odvisnosti σ(E) in podanimi vrednostmi v literaturi.

Časovno diskretni model permeabilizacije jetrnega tkiva smo nato ovrednotili na eksperimentalnih podatkih. Najprej smo primerjali območje reverzibilno permeabiliziranega tkiva, izmerjenega z eksperimenti in območje permeabilizacije, izračunano z modelom, ob upoštevanju enake amplitude pulza, kot v ustreznem eksperimentu. Slika x prikazuje porazdelitev električnega polja, izračunane z modelom v petih časovno diskretnih korakih. Porazdelitev polja v petem koraku ustreza stanju, ki ga dobimo po zaključku razširjanja permeabilizacije v tkivu. Vidimo, da na sredini med elektrodama poljska jakost ravno doseže reverzibilni prag (460 V/cm), kar se ujema z eksperimentalnimi ugotovitvami, ki so pri enaki amplitudi pulza pokazale reverzibilno permeabilizacijo jetrnih celic na celotni veznici med elektrodama.

V nadaljevanju smo vrednotili območje ireverzibilne permeabilizacije, ki ga predvideva model z eksperimentalno določenim območjem. Slika xi prikazuje porazdelitev električnega polja pri električnem vzbujanju s pulzom amplitude 960 V. S temno rdeče je prikazano območje, ki je izpostavljeno poljskim jakostim nad 700 V/cm in torej ireverzibilno permeabilizirano. S črno konturo je označeno eksperimentalno določeno območje ireverzibilne permeabilizacije, ki se zelo dobro ujema z modelsko izračunanim območjem.

Nazadnje smo opravili vrednotenje modela še z eksperimentalnimi podatki o celotnem toku, izmerjenem pri različnih amplitudah pulzov. Slika xii prikazuje primerjavo izračunanega toka po zaključeni permeabilizaciji in izmerjenega toka na kocu pulza. Ujemanje med izračunanim in izmerjenim tokom smo ovrednotili z merami, kot sta srednji kvadratični pogrešek (RMSE) in neenakostni kriterij po Theil-u (TIC). Slednji pravi, da je ujemanje med dvema vrstama dobro za vrednosti TIC manjše od 0.3. Na podlagi obeh mer, katerih vrednosti prikazuje Slika xii vidimo, da je ujemanje med modelskim in izmerjenim tokom zelo dobro.

Tok, izračunan v posameznih časovno diskretnih korakih smo primerjali tudi s tokom, izmerjenim med trajanjem pulza (Slika xiii). Trajanje intervalov med posameznima časovnima korakoma pa smo določili s prilagajanjem izračunanega in izmerjenega toka. Primerjava je pokazala, da se modelsko izračunani tok ustali pred koncem trajanja pulza pri vseh napetostih vzbujanja, medtem ko merjeni tok pri višjih napetostih narašča ves čas trajanja pulza. Vzrok temu bi lahko bilo povišanje prevodnosti tkiva zaradi segrevanja ter tudi ionska disociacija. To sta pojava, ki bi lahko bila prisotna pri vzbujanju z višjimi napetostmi, vendar nista vsebovana v modelu.

Vrednotenje časovno diskretnega modela permeabilizacije je pokazalo, da model zelo dobro opisuje permeabilizacijo tkiva. Med vrednotenjem modela smo postavili tudi nekaj hipotez, s katerimi smo poskusili pojasniti dogajanje med permeabilizacijo tkiva. Pri transportu snovi skozi permeabilizirano celično membrano sodelujejo različni transportnih mehanizmi, kot je npr. elektroforetski transport ionov, ki se odraža v povečani prevodnosti tkiva in difuzijski transport manjših molekul, kot npr. bleomicyn, s katero smo določali področje reverzibilne permeabilizacije. Oba transportna mehanizma sta povezana z enako vrednostjo reverzibilnega praga električnega polja, saj le-ta vpliva na permeabilizacijo celične membrane, vendar je transport ionov bistveno hitrejši od transporta molekul. Domnevamo tudi, da povečani transport ionov prek celične membrane omogoča veliko število majhnih prehodno prepustnih struktur (por), ki izginejo po prenehanju trajanja pulza. Transport molekul čez celično membrano, ki poteka z difuzijo, pa omogoča manjše število večjih, stabilnih por, ki nastajajo z združevanjem manjših por in trajajo tudi po več minut. Ker majhne prehodno prepustne pore nastajajo hitro – takoj po začetku vzbujanja z električnim pulzom in ker je transport ionov hiter, se prevodnost tkiva med pulzom zelo hitro spreminja in posledično tudi porazdelitev električnega polja. Proces se nadaljuje, dokler ni doseženo ustaljeno stanje. V ustaljenem stanju pa je v permeabiliziranem delu tkiva poljska jakost nižja, kot na začetku vzbujanja. Domnevamo, da šele ustaljena porazdelitev poljske jakosti povzroča nastanek stabilnih por, ki posledično omogočajo transport molekul čez celično membrano.

Z modelom smo tudi ugotovili, da poljska jakost med permeabilizacijo tkiva v posameznih časovnih korakih presega vrednost ireverzibilnega praga (Slika x(c)), kljub temu pa po zaključeni permeabilizaciji tkivo v teh delih ni ireverzibilno permeabilizirano. Zato domnevamo, da je za ireverzibilno permeabilizacijo tkiva potrebno daljše izpostavljanje tkiva poljski jakosti nad ireverzibilnim pragom. Domnevamo, da šele vrednosti polja v ustaljenem stanju, pod pogojem, da so višje od ireverzibilnega praga, povzročajo nekrozo tkiva.

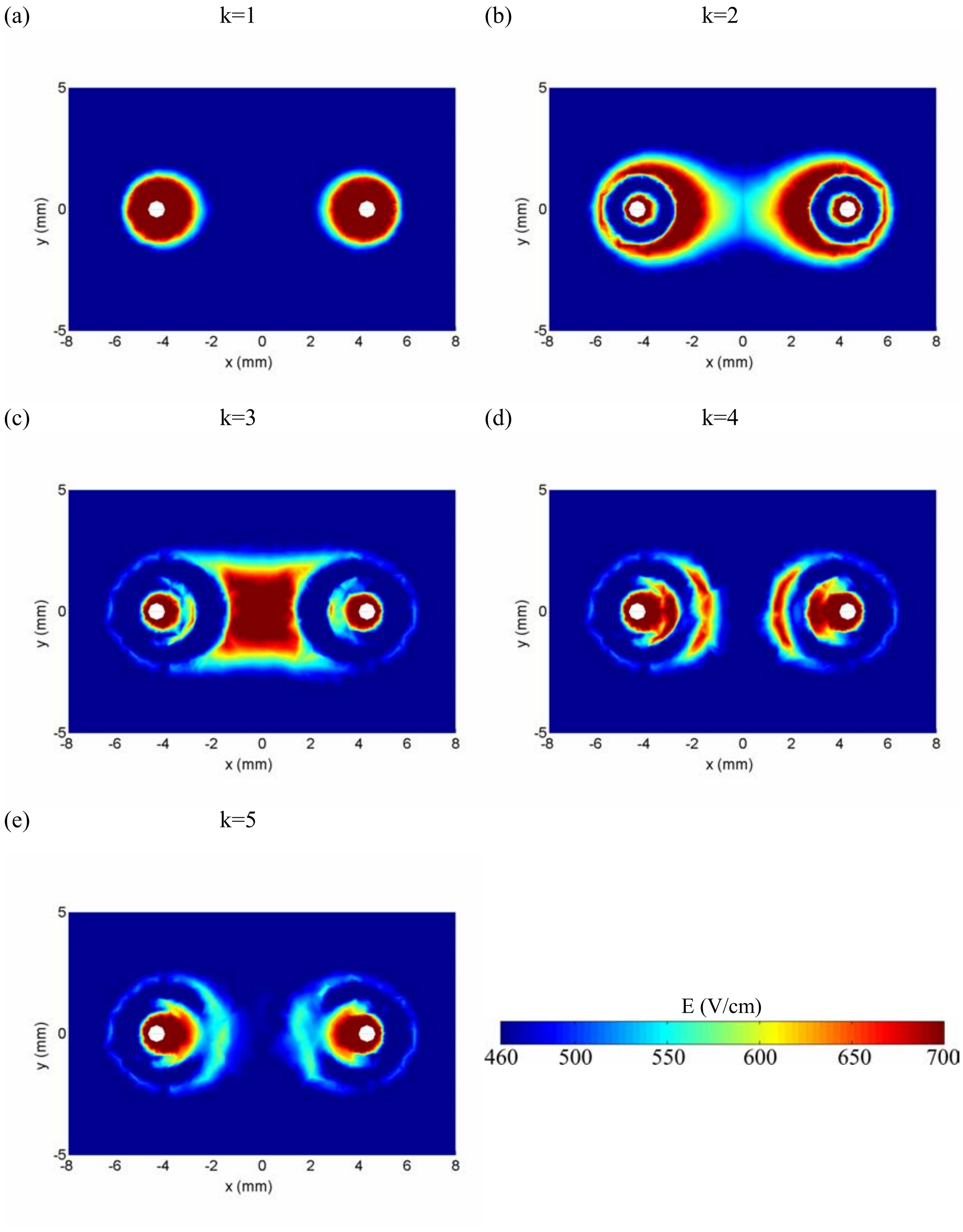

Slika x: Porazdelitev električnega polja v petih časovno diskretnih korakih med permeabilizacijo jetrnega tkiva. Slike (a) do (e) prikazujejo porazdelitev električnega polja za ustrezne časovno diskretne korake k=1 do k=5.

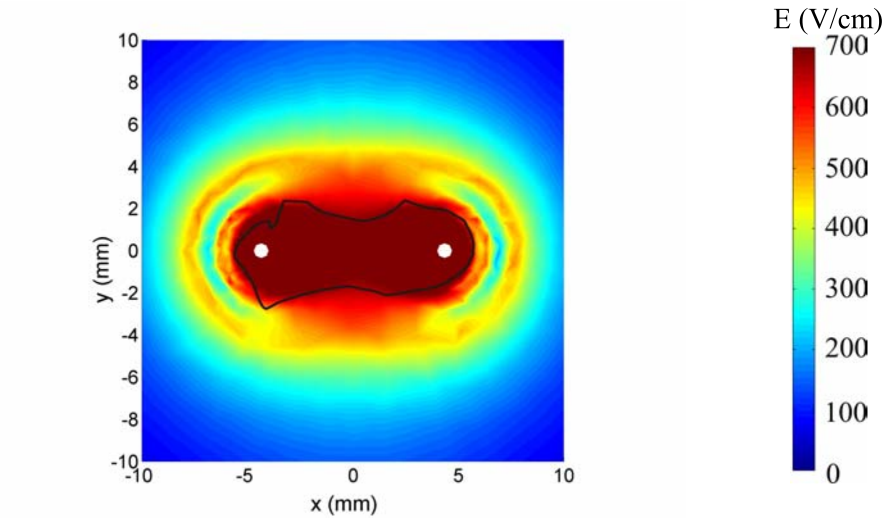

Slika xi: Izmerjeno področje (črna kontura) in izračunano področje (temno rdeče) ireverzibilne permeabilizacije.

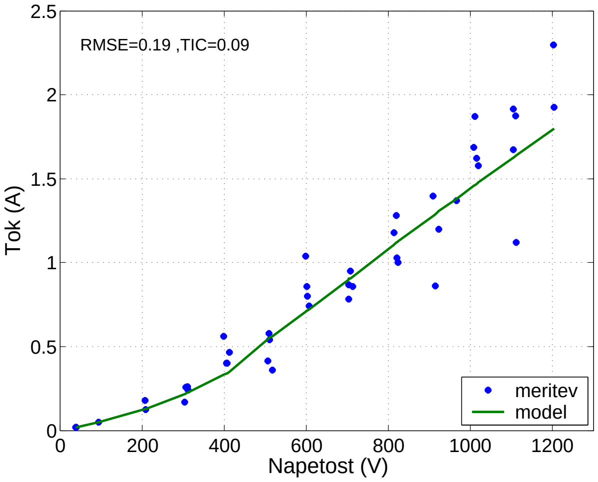

Slika xii: Izmerjeni (polna črta) in izračunani tok (*) na koncu pulza.

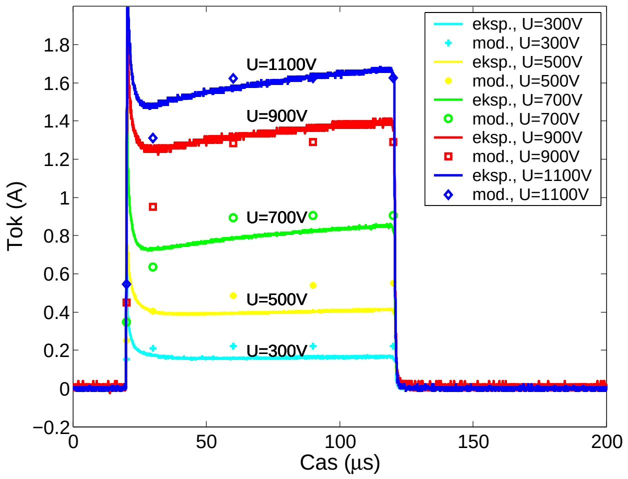

Slika xiii: Izmerjeni tok pri vzbujanju s pulzi različnih amplitud (polne črte) in tok izračunan z modelom v petih časovno diskretnih korakih (simboli) pri enakih amplitudah pulzov.

OPTIMIZACIJA PARAMETROV PERMEABILIZACIJE NA OSNOVI ČASOVNO DISKRETNEGA MODELA

Kot smo že uvodoma omenili, je eden bistvenih razlogov za izdelavo modela, uporaba le-tega za optimizacijo parametrov elektropermeabilizacije – t.j. amplitude električnih pulzov in določitev postavitve elektrod za dosego izbranega cilja terapije. V primeru elektrokemoterapije je tako potrebno določiti amplitudo pulzov in postavitev elektrod, ki bi v tumorju povzročili jakosti električnega polja, višje od reverzibilnega praga. S tem bi dosegli permeabilizacijo celotnega volumna tumorja in torej vnos kemoterapevtika v vse tumorske celice.

V zadnjem poglavju smo tako raziskali možnosti za določanje parametrov permeabilizacije z optimizacijo na osnovi modela za uporabo v elektrokemoterapiji. Optimizacijo parametrov smo najprej izvedli na modelih preprostih geometrij (Slika xiv) nato pa na modelu človeških možganov s tumorjem. Električne parametre možganov in tumorja smo določili na podlagi vrednosti, zbranih iz literature, potek odvisnosti σ(E) pa smo določili hipotetično. Natančen potek odvisnosti σ(E), ki bi ga lahko pridobili samo z dodatnimi eksperimenti, ne bi vplival na zaključke študije možnosti.

V primeru geometrije, ki jo prikazuje Slika xiv(a), smo želeli določiti optimalno amplitudo pulza, ki ga moramo pritisniti na ploščati elektrodi, da celotni volumen tumorja izpostavimo poljskim jakostim nad reverzibilnim pragom. V primeru geometrije, ki jo prikazuje Slika xiv(b), pa smo iskali optimalno napetost pulza in hkrati optimalno razdaljo med elektrodama, da dosežemo permeabilizacijo celotnega tumorja. Izračun porazdelitve polja na osnovi optimalnih parametrov je dal želeni rezultat (Slika xv). V primeru prve geometrije je bilo celotno področje tumorja izpostavljeno poljskim jakostim tik nad reverzibilnim pragom, ker je polje med ploščatima elektrodama precej homogeno. V drugem primeru je bil vrhnji del tumorja (bližje elektrodam) izpostavljen bistveno višjim poljskim jakostim, kot spodnji del, kjer so jakosti električnega polja bile tik nad reverzibilnim pragom. Vzrok temu je nehomogena porazdelitev električnega polja pri taki postavitvi elektrod.

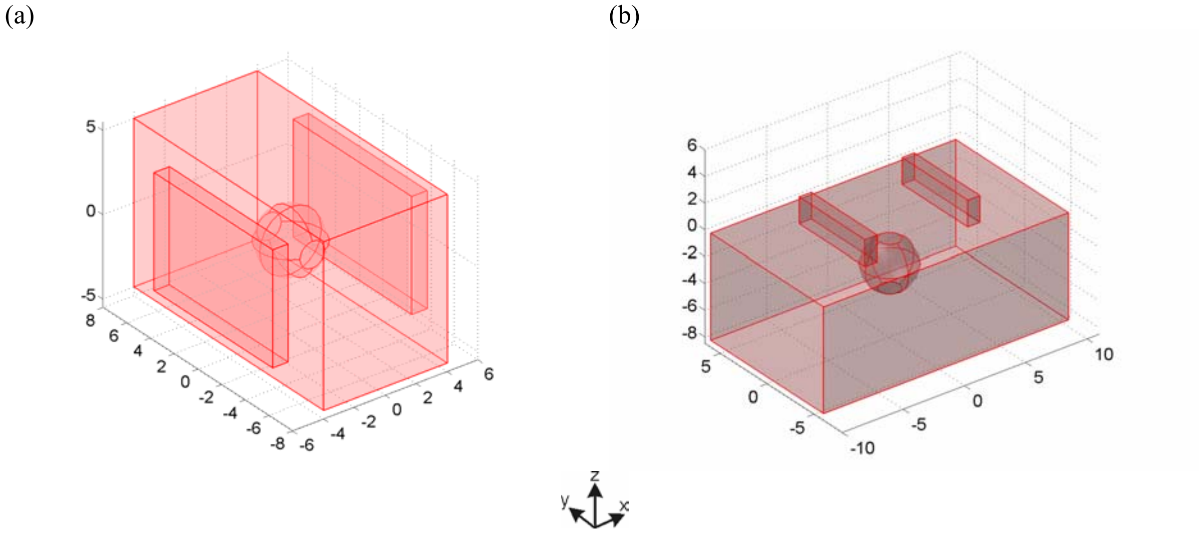

Slika xiv: (a) Tkivo s krogelnim tumorjem in elektrodami položenimi ob straneh ter (b) tkivo s krogelnim tumorjem in elektrodami položenimi na vrhu.

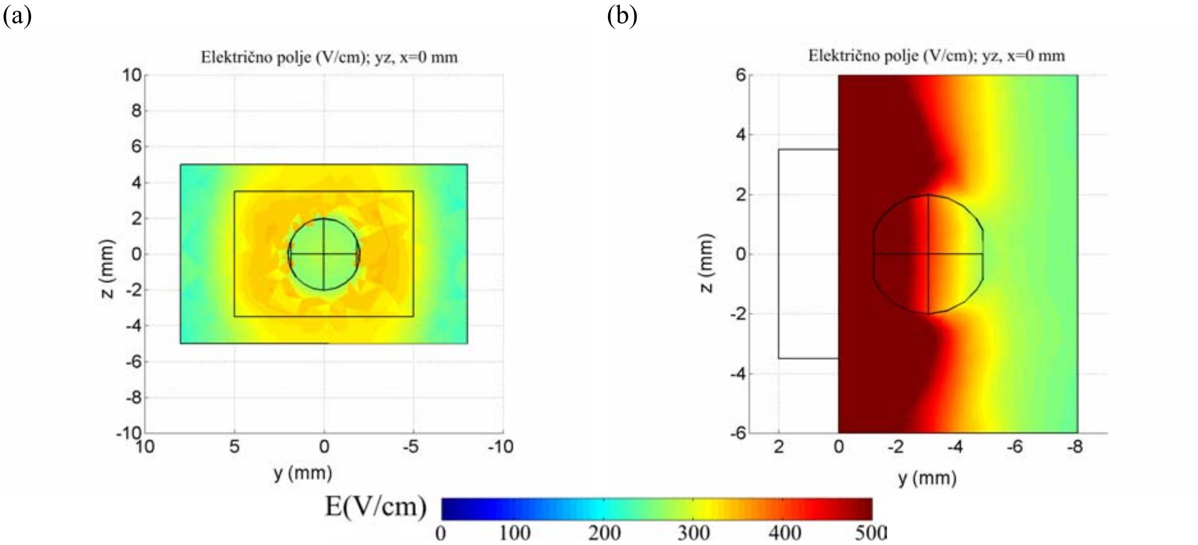

Slika xv: Porazdelitev električnega polja v *yz* ravnini za geometriji, ki ju prikazuje Slika xiv: (a) ustreza geometriji na Sliki xiv (a) in (b) ustreza geometriji na Sliki xiv (b).

Optimizacijo parametrov smo nato izvedli na modelu možganov s tumorjem. Trirazsežnostni model možganov smo izdelali na podlagi prereznih slik glave, pridobljenih z računalniško tomografijo (CT). Za izgradnjo trirazsežnostnega modela možganov smo izdelali poseben program, ki na osnovi podane pragovne vrednosti avtomatično razpozna rob možganov iz slik CT in zgradi trirazsežnostno geometrijo možganov. Izgradnja modela tumorja pa je zahtevala ročno določitev roba tumorja na podlagi podatkov iz slik CT, ker je bil rob tumorja premalo jasen za avtomatsko določanje s programom. Nadaljnja izdelava trirazsežnostne geometrije tumorja je potekala na enak način kot pri možganih.

Slika xvi prikazuje trirazsežnostni model možganov s tumorjem. Model je zasukan za kot 24° glede na vodoravno ravnino, ker so pod takim kotom bile posnete tudi slike CT. Za dovajanje električnega vzbujanja smo upoštevajoč razsežnosti tumorja izbrali polje štirih parov igelnih elektrod, ki jih prav tako prikazuje Slika xvi. Pri definiciji optimizacijskega problema smo upoštevali omejitve generatorja električnih pulzov Cliniporator in sicer 16 A za maksimalni tok in 1000 V za maksimalno napetost. Obenem smo upoštevali zahtevo, da mora biti v izbranih točkah tumorja poljska jakost nad reverzibilnim pragom. Izbrane točke tumorja smo določili tako, da smo upoštevali tiste robne točke tumorja, v katerih so bile izračunane najnižje vrednosti polja.

Z optimizacijo smo želeli določiti amplitudo pulzov in razdaljo med elektrodama za učinkovito permeabilizacijo tumorja. Pri optimizaciji amplitud pulzov se je izkazalo, da pri podanih omejitvah rešitev optimizacijskega problema ne obstaja. Če bi namreč želeli izpolniti pogoj, da poljska jakost preseže reverzibilni prag v izbranih točkah tumorja, bi morali izbrati bistveno višjo amplitudo pulzov, kot 1000 V. Tako smo v nadaljevanju pri optimizaciji parametrov upoštevali samo omejitvi toka in napetosti. Pri tem smo se zavedali možnosti, da na ta način dobljena poljska jakost ne bo nujno presegla reverzibilnega praga v izbranih točkah tumorja in da bo ta pogoj mogoče doseči samo s ponovno terapijo, pri kateri bodo elektrode postavljene na drugem mestu.

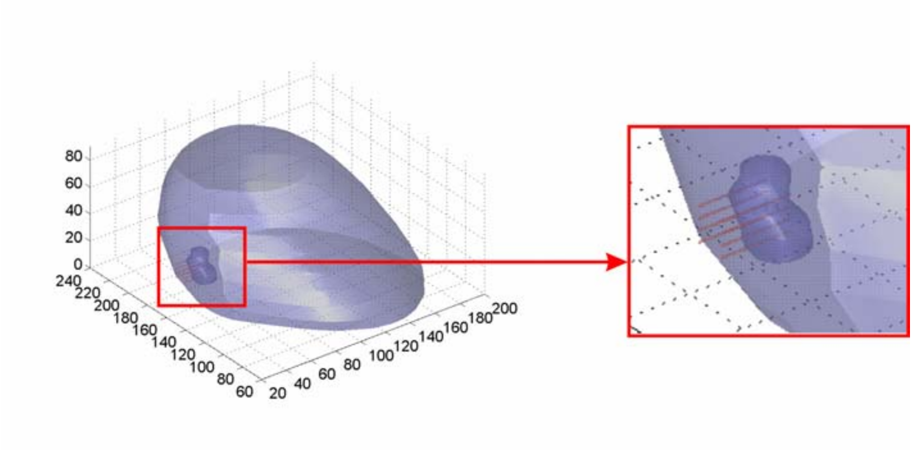

Slika xvi: Trirazsežnostni model možganov s tumorjem in vstavljenim poljem štirih parov igelnih elektrod.

Ker je bila izgradnja mreže končnih elementov za model možganov s tumorjem in poljem igelnih elektrod izredno zahtevna, smo problem hkratne optimizacije amplitude pulza in razdalje med dvema paroma elektrod poenostavili tako, da smo naenkrat optimirali samo napetost pulza ter postopek ponovili za dve različni razdalji med paroma elektrod. Pri obeh razdaljah med paroma elektrod je bila z optimizacijo napetosti dosežena ena od omejitev generatorja - bodisi omejitev toka ali napetosti. Dobljeni optimalni napetosti pulza (za obe razdalji med paroma elektrod) pa nista dali take porazdelitve polja, ki bi povzročila permeabilizacijo celotnega tumorja. Podoben rezultat smo dobili tudi z optimizacijo amplitude pulza na štirih parih igelnih elektrod in sicer za primer, ko smo pritisnili na vse pare enako napetost (Slika xvii) in tudi za primer, ko smo vsakemu paru pritisnili drugačno – optimalno napetost.

Omejitve generatorja pulzov so bile vzrok za le delno permeabilizacijo tumorja. Za permeabilizacijo celotnega volumna tumorja bi potemtakem morali spremeniti lego polja igelnih elektrod in postopek ponoviti ali pa uporabiti zmogljivejši generator. V povezavi s slednjim smo z optimizacijo želeli ugotoviti, kakšno napetost bi morali pritisniti posamičnemu paru igelnih elektrod, da bi dosegli permeabilizacijo celotnega tumorja. Za napetost na posamičnem paru igelnih elektrod smo dobili naslednje vrednosti: u_1=1088.2 V, u_2=485.7 V, u_3=1200.1 V, in u_4=1880.9 V. Pri vzbujanju s takimi pulzi pa bi skozi tkivo stekel tok 28.7 A.

ZAKLJUČEK

Predstavljeni časovno diskretni model permeabilizacije tkiva lahko po uspešnem vrednotenju uporabimo za simulacijo procesa permeabilizacije. Na ta način lahko spoznamo učinek vzbujanja z različnimi amplitudami pulzov in učinek postavitve elektrod na obseg permeabilizacije tkiva. Z modelom lahko izračunamo tudi tok, ki steče skozi tkivo pri izbrani postavitvi elektrod. Na podlagi tega podatka lahko v generatorju pulzov omejimo tok na vrednost, ki ne sme biti presežena, da ne bi prišlo do uničenja tkiva. Podatek o napetosti in ustreznem toku za učinkovito permeabilizacijo tkivo z izbranimi elektrodami lahko uporabimo tudi pri izbiri oziroma določanju tehničnih lastnosti generatorja pulzov.

S pomočjo modela lahko ugotovimo, ali je bil posamezni del tkiva izpostavljen želenim jakostim električnega polja, prav tako pa lahko ugotovimo, ali je bila zdravemu tkivu, ki ni bilo predmet terapije, povzročena škoda.

Za uspešno uporabo modela je potrebno natančno določiti funkcijsko odvisnost σ(E) za vsako vrsto tkiva posebej. Zato smo v okviru tega dela predlagali metodo za določitev funkcijske odvisnosti σ(E) na podlagi meritev celotnega toka.

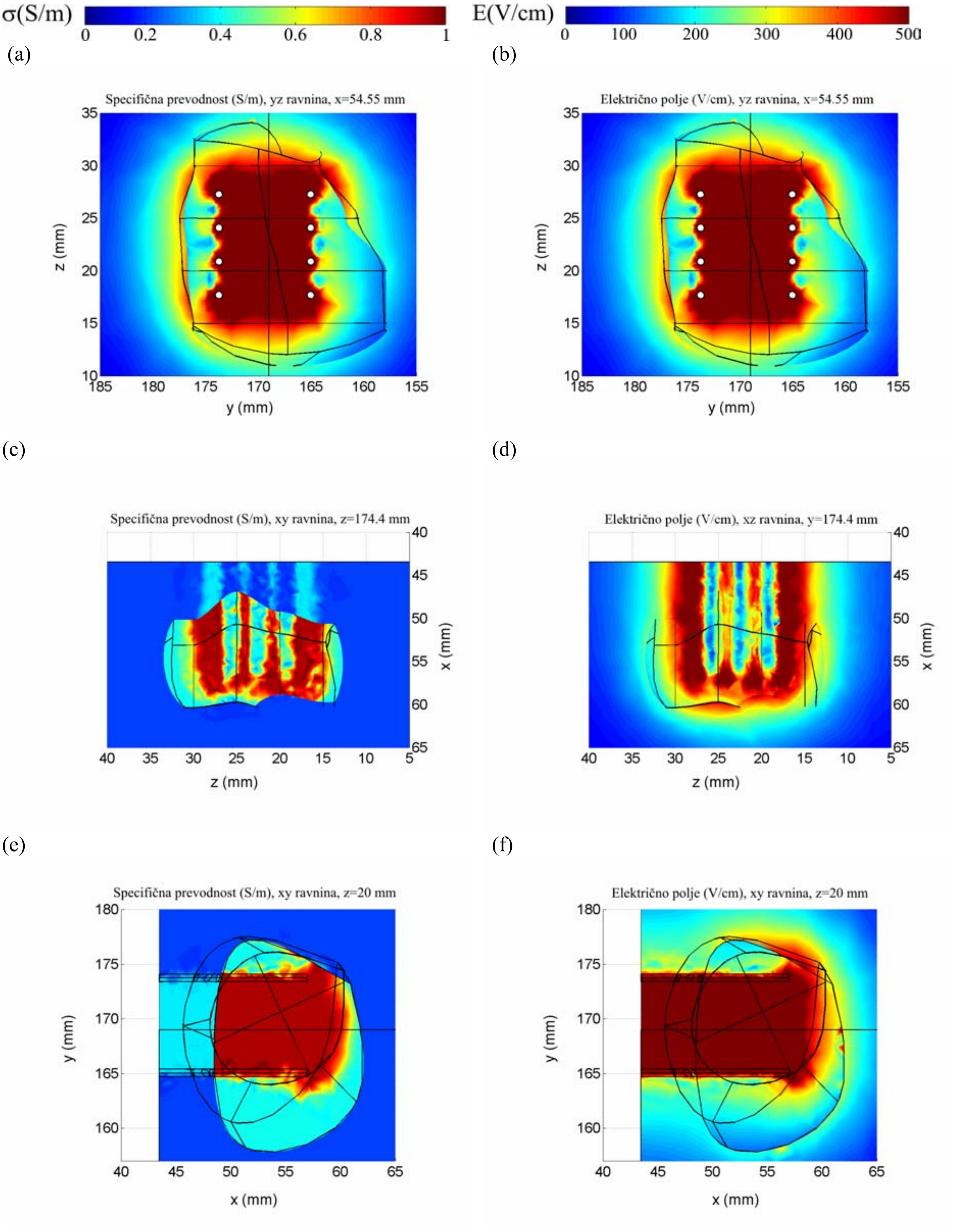

Slika xvii: Specifična prevodnost (leva stran) in porazdelitve električnega polja (desna stran) v tumorju v ustaljenem stanju; (a) in (b) presek v *yz* ravnini pri *x*=54.55 mm; (c) in (d) presek v *xz* ravnini pri *y*=174.44 mm; (e) in (f) presek v *xy* ravnini pri *z*=20 mm. Amplituda pulza, dobljena z optimizacijo, je 701 V. Pri optimizaciji je bila dosežena omejitev na maksimalni tok 16 A.

Časovno diskretni model permeabilizacije tkiva lahko pomembno prispeva k izboljšanju metod zdravljenja z elektrokemoterapijo in elektro-gensko terapijo, saj ga je mogoče uporabiti za optimizacijo parametrov električnih pulzov in razdalje med elektrodama upoštevajoč zahteve posamične terapije. Optimizacija parametrov na podlagi modela ne zahteva izvedbe poskusov in jo je mogoče opraviti vnaprej - pred samo terapijo. Na podlagi optimalnih parametrov lahko zagotovimo učinkovitost terapevtske metode, saj je cilj optimizacije približati porazdelitev poljskih jakosti v tkivu želenim pragovnim vrednostim. Obenem pa nam takšni izračuni omogočajo določitev maksimalnih tokov in napetosti pri načrtovanju elektroporatorjev in elektrod.

ABSTRACT

Electropermeabilisation of cell membranes is a phenomenon which in the last few years has been increasingly exploited for medical purposes. Namely, when exposed to an external electric field of high sufficient amplitude a cell membrane becomes permeable for molecules and even macromolecules which otherwise can not enter the cell. In this way drugs, such as some chemotherapeutics, as well as nucleic acids, proteins and dyes can enter the cell. Transport of chemotherapeutics by means of electropermeabilisation is already used in clinics. The corresponding therapeutic approach is referred to as electrochemotherapy (ECT). On the other hand the use of electropermeabilisation for transport of DNA across the cell membrane, referred to as electrogentransfer, has now entered preclinical trials.

The application of an external electric field for the purpose of electrochemotherapy and electrogenetransfer however must be done with precautions. Exposure of cells to too high electric field intensity can cause cell necrosis. On the other hand very low electric field intensities do not cause cell membrane permeabilisation at all. As an electric field is induced by applying usually rectangular electric pulses, an inappropriate pulse duration with respect to pulse amplitude can also cause cell necrosis. On the top of that, in case of electrochemotherapy, effective electropermeabilisation is achieved when the entire volume of the tumour is exposed to E intensities above reversible threshold, while in electrogenetransfer, for effective therapy, the subjected tissue should be exposed to E intensities above reversible and at the same time below the irreversible threshold. Therefore the choice of optimal electric pulse parameters for a particular application of electropermeabilisation is very important.

To date, determination of optimal pulse parameters and electrode design for ECT and electrogenetransfer has been performed experimentally. For example by utilising rapid tests [Gehl and Mir, 1999] the pulse amplitudes appropriate for cell permeabilisation were determined by measuring the uptake of dyes or drugs which can enter permeabilised cells. In some reports the rapid tests were accompanied by finite element models, used to compute the electric field intensity at optimal parameters. However those models did not consider changes in the electrical properties of tissue resulting from permeabilisation.

Thus, the aim of this thesis was to develop a time discrete model of tissue permeabilisation which can be used for determination of optimal parameters for effective tissue permeabilisation.

The time discrete model presented in this thesis is based on the fact that tissue specific conductivity changes as a result of cell membrane permeabilisation when exposed to an external electric field. The change in tissue specific conductivity (σ) due to an external electric field (E) is given by $\sigma(E)$ dependency. The latter should be obtained experimentally for each type of the tissue. As the change in tissue conductivity alters E distribution in the tissue at an applied constant pulse amplitude, the time discrete model of tissue permeabilisation consists of a sequence of static models, which describe E distribution in discrete time steps during tissue permeabilisation and thus describes the dynamics of permeabilisation. The determination of tissue conductivity in each static model in a sequence is based on E distribution from the previous step according to $\sigma(E)$ dependency. The static model that describes E distribution in tissue with particular specific conductivity can be either analytical or numerical.

In the first part of the thesis the time discrete model with analytical description of E distribution is presented. An analytical model is developed for the geometry of two concentric cylindrical electrodes with tissue placed between the electrodes. In the analytical time discrete model, different σ(E) dependencies were implemented, such as stepwise, linear, exponential and S-shaped dependency. The model was incorporated into a simulation environment which provided a means for observation of the electropermeabilisation process for different electric pulse amplitudes, electrode radii and different σ(E) dependencies at time discrete steps. The simulation environment revealed that the extent of permeabilisation i.e. radius up to which tissue is permeabilised depends on the σ(E) dependency used. The latter also influences the number of static models at which changes in E distribution are present due to permeabilisation. Similar results were obtained by a model parametric study, which lead to the conclusion that determination of σ(E) dependency is important for assessment of tissue permeabilisation with the presented time discrete model. Thus an approach for determination of σ(E) dependency was proposed which combines the experimental results and the model of E distribution. The parameter study also showed the importance of E distribution on the extent of permeabilisation, which is in agreement with previous studies [Gehl *et al.*, 1999, Miklavčič *et al.*, 1998; Miklavčič *et al.*, 2000]. While in the simulation environment the application of a rectangular pulse is assumed, investigation of the influence of the applied pulse shape on the dynamics and extent of permeabilisation is further performed. Ramp signals were tested and model results were compared with results of rectangular pulse applications.

An analytical time discrete model was also used for investigation of the feasibility of real time control of tissue permeabilisation. For that purpose a closed loop control scheme was designed which employs proportional integral (PI) controller. Based on the results it was ascertained that the major drawback of real time control is the on-line measurement of the extent of permeabilisation. To obtain such information we proposed the use of a model based control.

The analytical time discrete model of tissue permeabilisation presented was designed only for the particular geometry i.e. two concentric cylindrical electrodes. In general, analytical description of E distribution is possible when geometry, inhomogeneities and anisotropies of the tissue can be described in the same coordinate system. As biological tissue can have irregular shapes, inhomogeneities and anisotropies, the use of numerical methods is usually more appropriate for computation of the E distribution. Therefore we examined the feasibility of employing a finite element model by comparing the results of the analytical and finite element model for the same geometry. The results of both models were in close agreement, however the accuracy of the finite element model was limited when distinctive inhomogeneities or even discontinuities in the E distribution were present. This problem can be solved by generating denser mesh in such regions. Apart from this, the major drawback of the finite element model was that time spent on solving the model was significantly longer than in the case of the analytical model.

As further in the thesis, permeabilisation in biological tissue with inserted needle electrodes is examined, simplifications in finite element modelling of needle electrodes were next investigated in respect to reducing time spent on solving the finite element model. An 8-faceted needle electrode geometry was proposed to be used in the finite element model instead of a cylindrical shape. 8-faceted needle electrode geometry was determined to be superior in the model with a single needle electrode pair by means of a criteria function consisting of the weighted sum of the relative difference between measured and computed total current, the relative difference in CPU time spent on solving the model and the relative difference in the cross-section surface of electrodes. Such electrode geometry was further evaluated on physical models with needle arrays by comparison of computed total current and measured current. The agreement between modelled and measured current was good, being within 9% of measurement, except in cases with very thin gel. The reason identified was electrode polarization. This effect was incorporated in the model which reduced the difference between the model and the measurement to less than 3%.

Considering 8-faceted needle electrode geometry, a time discrete model of electropermeabilisation in liver tissue around two needle electrodes was designed by computing E distribution using the finite element model. In the time discrete model an S-shaped dependency between specific conductivity and E was considered. Parameter estimation of S-shaped dependency was performed on a set of current measurements, obtained by *in vivo* experiments. Thresholds obtained appear to be higher than previously published for rabbit liver tissue. Another set of measurements was used for model validation. All measurements were performed on rabbit liver tissue with inserted needle electrodes. Model validation was carried out in three different ways: first, through a comparison of total current at the end of pulse and computed current in the last step of the time discrete model; second, by comparing the area of irreversibly permeabilised tissue computed by the model and the area where tissue necrosis was observed in experiments; and third, by comparing reversibly permeabilised tissue in the model and the reversibly permeabilised area of tissue as obtained in the experiments. The model validation showed good agreement between modelled and measured results. The model also provided a means for better understanding processes that occur during permeabilisation. Based on the model, the permeabilised volume of tissue exposed to electrical treatment can be predicted. Therefore, the most important contribution of the model is its potential to be used as a tool for determining the electrode position and pulse amplitude needed for effective tissue permeabilisation.

Thus in the final part of the thesis a feasibility study of model based optimisation of electric pulse parameters for treatment in electrochemotherapy was performed. The feasibility of model based optimisation was first examined on a model with simple geometry, i.e. a cube representing tissue and a sphere representing a tumour inside the tissue. Electrical treatment was performed with plate electrodes positioned either on the top or placed on the sides of the cube. The parameters subject to optimisation were pulse amplitude and distance between the electrodes. A nonlinear constrained optimisation method was used, which considered constraints on voltage and current supplied by the pulse generator and the condition that E intensity must exceed reversible threshold in selected points in the tumour. The objective of optimisation was to minimize the difference between the reference value of E intensity (i.e. E reversible threshold) and the E intensity computed by the model at selected points. The points selected were where the lowest values of E intensity were computed in the non-permeabilised tumour. The application of optimal pulse amplitude and distance between electrodes resulted in E distribution in the tumour just above the reversible threshold, which was an excellent result. Thus the model based optimisation was in continuation carried on more complex geometry – i.e. the human brain with a tumour.

The human brain geometry was generated from computer tomography (CT) images. An approach for semiautomatic 3D geometry model generation from CT images was proposed and implemented. Electric treatment was applied through an array of 4 needle electrode pairs. Nonlinear constrained optimisation with the same conditions as in the case of simple geometry was used. The only parameter subject to optimisation was pulse amplitude. The distance between the electrode pairs was not optimised because problems with automatic mesh generation were encountered due to the complex geometry. Several optimisations were run, i.e. voltage was applied only to inner electrodes, only outer electrodes and to all electrodes. However in all cases the optimisation terminated by reaching constraints either on maximal voltage or maximal current supplied by the generator, without satisfying the condition that E must exceed the reference value at selected points of the tumour. That pointed to the conclusion that the treatment must be repeated by considering different positions of the electrodes or by using a different pulse generator. Additionally, another optimisation was run which assumed no constraints on generator power limitation. Optimal pulse parameters in this case gave E intensity above reversible threshold in all selected points in the tumour.

Model based optimisation showed that the time discrete model of tissue permeabilisation can be used for determination of optimal pulse parameters in a non-invasive way before therapy. The efficiency of the optimisation however depends on the accuracy of the determined σ(E) dependency and the constraints of the pulse generator. Namely, due to generator limitations on the pulse amplitude and current it is not always possible to obtain required E intensity in defined points of the tissue. Further, the optimisation of the distance between electrodes in models with a numerical description of E distribution is limited by the complexity of the geometry, because it depends on the automatic mesh generation. While in complex geometries mesh generation depends on tuning initial mesh parameters, in simple geometries automatic mesh generation can be performed without changing those parameters during optimisation. On the other hand, optimisation of pulse amplitude is not critical and thus optimal pulse amplitude can be determined regardless of the complexity of the model geometry. The optimisation of electric pulse parameters based on the time discrete model showed the importance of knowing the E distribution in the tissue to be permeabilised. Only in this way can the information be obtained if a predetermined volume of tissue is to be permeabilised. Further, model based optimisation can be extremely useful for successful electrogenetransfer, because the optimal pulse amplitude can be computed, which exposes the tissue under treatment to an E distribution just above the reversible threshold. As in most tissues, the two E threshold values – reversible and irreversible – are very close to each other, the exposure of tissue to E above irreversible threshold is minimized in this way, which is important for effective electrogenetransfer. The most important contribution of model based optimisation of pulse parameters therefore is that it yields optimal parameters with respect to the therapeutic approach intended, in a non-invasive way before the therapy. Additionally, model based optimisation can be used to establish the efficacy of the therapeutic approach considering limitations of the pulse generator and the electrode setup.

1 INTRODUCTION

Exposure of cells, either in suspension or in tissue, to the appropriate, short, intense electric pulses results in a reversible change of their membrane permeability [Tsong, 1991]. Consequently the membrane becomes permeable for molecules which otherwise cannot enter the cell, such as proteins, some drugs and nucleic acids.

This phenomenon is already exploited for clinical purposes in order to facilitate the transfer of chemotherapeutics into cells. The corresponding therapeutic method is referred to as electrochemotherapy [Mir *et al.*, 1991]. In preclinical trials another application is currently taking place, where DNA is transferred into cells by means of an applied external electric field [Jaroszeski *et al.* 1999; Neumann *et al.* 1999]. The method is termed as electrogentransfection and is currently gaining a lot of attention, because it is considered a safer method compared to other methods of gene transfer using viral vectors [Ferber, 2001].

The change in permeability of cell membrane can also result in other phenomena. When two neighbouring cells are permeabilised a fusion of the two can occur. The phenomenon is termed electrofusion [Chizmadzhev *et al.*, 1995]. It is also possible to insert molecules (proteins) into membrane of permeabilised cells, which is known as electroinsertion [Maček-Lebar *et al.*, 1998].

Theory and experiments have shown that efficacy of electropermeabilisation depends on electric field intensity across a given cell, its size and shape and also on the electric pulse parameters applied (amplitude, number, duration). In electrochemotherapy a train of short and intense rectangular electrical pulses is usually applied in order to facilitate the transfer of chemotherapeutics into cells. Such pulses have no, or minimal, cytotoxic effects by themselves. The local field experienced by the cell in tissue during electropermeabilisation is a function of applied voltage, electrode design and the conductivity of regional tissue elements and extra-cellular media.

Description of the phenomenon of the permeabilisation has been approached theoretically and by means of experimental observations and results. However exact mechanisms that occur during permeabilisation have not yet been fully elucidated. In continuation we will thus describe basic findings and different approaches towards the explanation of permeabilisation phenomena.

1.1 DEFINITION OF PERMEABILISATION AT THE CELL LEVEL

A cell membrane is a lipid bilayer which separates the interior of the cell from the exterior. The function of the cell membrane is to isolate the chemical environment inside the cell from the outside, by allowing only selected components to pass in and out of the cell.

However by applying short intense electric pulses cell membrane permeability may be changed. In such a case enhanced cell membrane permeability depends on the external electric field. The relation between superimposed transmembrane potential and the electric field intensity is for spherical cell presented with Schwan's equation:

$$\Delta V_m = fRE\cos\vartheta, \tag{1.1}$$

where V_m is the induced transmembrane potential (TMP), f numerical factor, E applied external electric field, R the cell radius and ϑ the polar angle measured from the centre of the cell with respect to the external electric field. A generalized form of Schwan's equation describing all spheroidal cells has been recently developed [Kotnik and Miklavčič, 2000].

The value of transmembrane potential at which a cell membrane is permeabilised is referred to as the critical value. Reported values of critical transmembrane potential are in the range 0.2 V – 1 V [Kinoshita and Tsong, 1997; Teissie and Rols, 1993]. As the membrane bilayer is common to eucaryotic cells the critical transmembrane potential is also similar for various types of cells. Therefore with respect to Schwan's equation the smaller the radius of the cell, the larger the external electric field is needed for membrane permeabilisation.

Cell membrane permeabilisation can be assessed through the *extent* of permeabilisation i.e. the surface of membrane permeabilised by the external electric field [Gehl, 2003] or on a large scale it can be quantified by the penetration of nonpermeant cytotohic agents [Puc *et al.*, 2003], nonpermeant dyes and fluorescent dyes that entered the cell or by measuring the leakage of the endogenous metabolite [Teisse *et al.*, 1999].

1.2 THEORETICAL MODELS OF CELL PERMEABILISATION

Although the relation between an external electric field and the induced transmembrane potential expressed by Schwan's equation is relatively simple, the molecular events at the membrane level are extremely complicated. The complexity of events caused a variety of approaches and consequent development of corresponding theoretical models aimed at description of cell membrane permeabilisation. A variety of models have been developed which describe phenomena related to permeabilisation to a different extent, however a complete model description of phenomenology of permeabilisation has not yet been provided. That is also due to the fact that molecular events which take place during permeabilisation have not been experimentally observed to a full extent. Also, as a result, none of the models could be experimentally validated.

In general the theoretical model of cell membrane permeabilisation can be divided into the following groups: electromechanical models [Crowley, 1973], denaturation model [Tsong, 1991], phase transition models [Sugar, 1991; Sugar and Neumann, 1984], and a model based on the theory of aqueous pathways [Weaver *et al.*, 1999]. The description of these models is given in [Weaver and Chizmadzhev, 1996; Kotnik, 2000]. Here we will thus just briefly present some advantages and shortcomings of each model type.

Electromechanical models describe permeabilisation as a large scale phenomenon [Kotnik, 2000] and neglect the molecular structure of the cell membrane. They fail in describing the durability of permeabilisation and dependence on pulse duration, as well as they do not distinguish between reversible membrane breakdown and irreversible rupture. With respect to this, phase transition and denaturation models are superior, because they incorporate all those phenomena and also explain permeabilisation by structural changes within the molecules. The phase transition model is based on a statistical mechanical model of lipid membrane structures, however it does not describe the permeabilised cell membrane. This phenomenon is described by the denaturation model which presents permeabilisation based on specific effects at the membrane protein level, however its drawback is that it does not incorporate the permeabilisation of the lipid bilayer. The model based on aqueous pore theory is prevalent at the moment because it represents a compromise between the above models. It describes permeabilisation as a formation of transient aqueous pores in the lipid bilayer. Recent results from molecular dynamics simulation give it additional credibility [Marrink *et al.*, 2001].

As opposed to theoretical models there are also black box models which describe events at the cell level based on RC elements. In those models the cell membrane is presented as a capacitor and intra-cellular and extra-cellular media as two resistors [Somiari *et al.*, 2000].

In general the shortcoming of all models describing permeabilisation on a cell level is that they do not apply to a tissue, where the permeabilisation phenomena is even more complicated as the number of factors that influence permeabilisation is even larger. Some attempts towards expansion of cell models to a tissue level were performed by RC black box models [Gowrishankar and Weaver, 2003]. They were expanded into a matrix, which consists of capacitors and resistors in order to describe the tissue permeabilisation. However the intricacy and variability of the model parameters was too high, preventing the use of such models for accurate modelling of tissue permeabilisation [Somiari *et al.*, 2000].

1.3 TIME COURSE OF CELL PERMEABILISATION

Permeabilisation is an extremely rapid process as it can be induced with even submicrosecond electric pulses of high enough amplitude [Kinosita and Tsong, 1977]. Direct monitoring of permeabilisation events which is usually performed by microscopic imaging methods thus require a temporal resolution lower than microseconds. The monitoring of permeabilisation is performed in different ways; for example: by observing the changes in membrane structure [Chang and Rees, 1990], by imaging changes in transmembrane potential [Hibino *et al.*, 1991; Hibino *et al.*, 1993], and by observing transmembrane transport caused by permeabilisation [Rols and Teissie, 1993]. On the other hand determination of membrane resealing is in most cases performed through current measurements [Abidor *et al.*, 1993; Chernomordik *et al.,* 1987; Hibino *et al.*, 1993], by measuring rate of swelling [Kinoshita and Tsong, 1977a] or by monitoring cell hemolysis [Neamtu *et al.*, 1999].

Chang and Rees [Chang and Rees, 1990] performed the first direct examination of structural changes in cell membrane due to electropermeabilisation. They observed volcano-shaped openings on the cell membrane of human red blood cells which were exposed to a radio frequency electric field by using rapid freezing electron microscopy. However the volcano shaped openings reported were too large and were probably resulting from the enlargement of smaller primary pores by osmotic or hydrostatic pressure [Neumann *et al.*, 1999].

Hibino *et al.* [Hibino *et al.*, 1993] visualised the transmembrane potential in sea urchin eggs with a voltage sensitive fluorescent dye. They observed that 0.5 μs after the pulse onset both sides of the egg membrane were permeabilised, however the positive electrode side had higher conductance. After that, conductivity of the membrane increased steadily, with the distinction that the conductivity increase was faster on the negative electrode side. Their study first observed the asymmetry of permeabilisation, i.e. that membrane conductance on the negative electrode side increased faster than the conductance on the positive side.

However the exact course of permeabilisation during the pulse has not been experimentally observed yet. Time dependence of permeabilisation is thus described only hypothetically by considering experimental observation and theoretical models. Teissie and Rols [Teissie and Rols, 1993] described the time course of permeabilisation by two-step kinetics: when exposed to critical electric field intensity the creation of defects in cell membrane appears in a timescale of a few nanoseconds (induction step) which is followed by an expansion on a micro second scale (expansion step). As soon as the field intensity is lower than the critical value, stabilisation of permeabilised state occurs which brings the membrane to the permeabilised state for small molecules [Teissie *et al.*, 1999].

Other hypotheses, based on the state transition model, favour the appearance of hydrophobic pores due to electrically induced entrance of water and ions. Those pores actually represent a transient state which leads to formation of hydrophilic pores [Neumann and Kakorin, 1996]. Hydrophilic pores are considered as long–lived permeation sites [Neumann *et al.*, 1999] which are responsible for transport of small molecules.

Another hypothesis explains permeabilisation with lipid rearrangements when exposed to an external electric field, which result in formation of pores, also called electropores [Weaver and Chizmadzhev, 1996]. Based on that, the phenomenon of increased cell membrane permeability under electric field exposure is referred to as electroporation.

However, the appearance of pores has not been experimentally observed and further, the mechanism of pore formation has not yet been explained. The volcano shaped openings observed in [Chang and Rees, 1990], are too large and are probably resulting from the enlargement of smaller primary pores by osmotic or hydrostatic pressure [Neumann *et al.*, 1999]. In literature it is therefore proposed to use term electropermeabilisation instead of electroporation [Mir *et al.*, 1995].

A great majority of cell membrane recovery studies were performed by applying high voltage pulse followed by a test pulse with different pauses between the two pulses. The test pulse was low voltage and therefore did not affect the membrane permeability. They revealed that the process of membrane recovery occurs in at least two stages, one in a time scale of microseconds, and the other in a range of seconds to minutes [Hibino *et al.*, 1993; Chernomordik *et al.*, 1987]. In [Abidor *et al.*, 1993] the membrane resealing was determined on cell pellets. They observed that pellet conductivity decreased in three stages. The first stage was very fast – approximately 0.5-1 μs, the second stage took approximately 10 μs, while the complete relaxation of pellet conductivity to its initial state took several minutes.

1.4 TRANSPORT MECHANISM RELATED TO CELL PERMEABILISATION

A permeabilised cell membrane is no longer a barrier for the uptake of ions and molecules. Their transport through permeabilised cell membranes can be based on different mechanisms such as diffusion, electrophoresis and osmosis which can take place at different times with respect to pulse application. During the pulse application, transport occurs by diffusion, electrophoresis and electroosmosis, while after the pulse application, transport can occur only due to diffusion provided the membrane is still permeabilised. The millisecond measurements of transport during and after the electroporation pulse are presented in [Prausnitz *et al.*, 1995].

Ion transport is electrically driven and thus occurs during the pulse application. It can be measured by increased membrane conductivity. Transport by diffusion is the predominant mechanism for transport of small molecules. It occurs due to the difference in the concentration of molecules inside and outside the cell. Similarly the osmotic transport is a consequence of the difference in osmotic pressure on both sides of a permeabilised membrane.

The transport of macromolecules, as well as DNA, is predominantly electrophoretic [Rols and Teissie, 1998] however it occurs in several temporally distinct stages [Neumann *et al.*, 1999]. Macromolecular transport is facilitated first by adsorption of the macromolecules on the membrane surface [Neumann, 1992] and then electrophoretically driven into the cell. As macromolecular transport takes place during the pulse, in order to achieve sufficient uptake, the permeabilising pulses are longer [Wolf *et al.*, 1994]. Another approach to achieving sufficient uptake is presented in [Satkauskas *et al.*, 2002], where first a short high voltage electric pulse is applied, which permeabilises cells, followed by a longer low voltage electrophoretic pulse(s) that does not affect cell permeabilisation level but facilitates DNA transfer into the cell.

There are also different models describing the transport of ions, molecules and DNA. The diffusion driven transport of small molecules is presented with a pharmacokinetic model in [Puc *et al.*, 2003], while the model of DNA uptake is given in [Neumann *et al.*, 1999]. Osmotic transport across aqueous pores is incorporated in a model presented in [Weaver and Chizmadzev, 1996]. Their model also successfully predicts ion transport by heterogeneous transient pore population by concluding that large number of metastable pores with short life-times ($t<1$ ms) can quantitatively account for significant transport of ions, charged molecules and possibly large molecules.

1.5 ASSESSMENT OF PERMEABILISATION

The first method used for the assessment of permeabilisation was electrical measurement of either the change in membrane capacitance or the change in cell conductivity when exposed to an external electric field [Abidor *et al.*, 1979; Kinoshita and Tsong, 1979; Chernomordik *et al.*, 1982]. Apart from determining values of reversible and irreversible induced transmembrane potential, those measurements revealed information about the initiation of permeabilisation and time course of resealing [Abidor *et al.*, 1979].

Another approach towards assessing cell membrane permeabilisation is the microscopic imaging method. This approach comprises observation of changes in membrane structure [Chang and Rees, 1990], imaging of changes in transmembrane potential [Hibino *et al.*, 1991; Hibino *et al.*, 1993], and monitoring of transmembrane transport caused by permeabilisation [Rols and Teissie, 1993; Gabriel and Teissie, 1999]. Those studies provided information about the onset of permeabilisation and the influence of electric pulse parameters on permeabilisation.

Finally the cell membrane permeabilisation was also assessed by measuring the uptake of nonpermeant molecules that entered a permeabilised cell. This method was used for the determination of critical transmembrane potential [Teissie and Rols, 1993], the effect of pulse parameters on permeabilisation [Teissie and Rols, 1998] and consequently for the optimisation of pulse parameters for effective permeabilisation [Gehl and Mir, 1999].

1.6 CELL AND TISSUE PERMEABILISATION

The mechanisms of cell membrane permeabilisation have been studied extensively. As opposed to a single cell, cell membrane permeabilisation in tissue might be influenced by additional factors, such as cell density, interaction and arrangement of cells in tissue as well as the properties of external medium. Several studies investigated the influence of those factors on induced transmembrane potential of the cell.

The studies of densely packed cells have shown the influence of cell density and organization on induced transmembrane potential [Susil *et al.*, 1998]. Similarly the studies of cells organized in simple cubic, body-centered cubic and face-centered cubic lattice have shown that induced transmembrane potential decreases due to interaction with neighbouring cells. At the same time the surface of the cell exposed to particular electric field intensity changes [Pavlin *et al.*, 2002]. In addition in [Pucihar *et al.*, 2001] it was shown that external medium conductivity also affects the change in transmembrane potential of the cell.

In general, the tissue properties related to electropermeabilisation can be measured by means of macroscopic parameters such as effective tissue conductivity (σ) [Davalos *et al.* 2000; Davalos *et al.,* 2002] and specific tissue permittivity (ε). The relation between effective bulk conductivity of cells and factors such as a cell's volume fraction, conductivity of medium, membrane conductivity, cell orientation and critical transmembrane potential (TMP) has been theoretically described in [Pavlin *et al.*, 2003]. This theory can be extended to more concentrated cell samples i.e. tissue. Such knowledge can be further used for monitoring of changes in membrane conductivity through the measurement of bulk effective conductivity during permeabilisation.

Therefore the relation between cell membrane permeabilisation and tissue permeabilisation is of great importance for assessment of permeabilisation. The measurement of tissue electrical properties can give information about cell membrane permeabilisation. And also in the opposite direction, if we know the value of critical transmembrane potential of the cell and its organization in tissue, we could compute the electric field intensity that needs to be applied across the tissue in order to permeabilise cells.

Still, threshold values of electric field intensity needed for tissue permeabilisation were in most cases determined by combination of experimental results and numerical models [Gehl *et al.*, 1999; Miklavčič *et al.*, 2000]. The value of electrical field intensity at which reversible permeabilisation of tissue is achieved is termed the reversible threshold, while electric field intensity at which tissue necrosis occurs is termed the irreversible electric field threshold.

1.7 ELECTRODE CONFIGURATION

Type of electrodes and their position determine the electric field distribution in tissue [Miklavčič *et al.*, 1998; Gehl *et al.*, 1999]. In *ex vivo* experiments several types of electrodes were used such as plate electrodes, needle electrodes, wire electrodes and combinations of multiple needle electrodes placed in rows or in a circle.

In *in vivo* experiments plate electrodes [Puc *et al.*, 2001] and needle electrodes are predominantly used [Gilbert *et al.*, 1997; Ramirez *et al.*, 1998; Hofmann, 2000]. The plate electrodes are employed for permeabilisation of tissue accessible from the surface, such as in cases of transdermal drug delivery. The advantages of plate electrodes are non-invasiveness and relative homogeneity of the electric field distribution produced, however their disadvantage is that they are sometimes difficult to fit to tissue and to maintain in the same position during therapy. The contact between the tissue and plate electrodes can be improved by adding conductive gel. On the other hand needle electrodes provide deep penetration of electric field in tissue and are therefore well suited for permeabilisation of deep seated tissue structures. However, needle electrodes produce an inhomogeneous field distribution. This can be minimised by using arrays of needle electrodes. Several needle electrodes can be placed either in parallel rows [Gehl *et al.*, 1999] or in a circle [Hofmann, 2000]. Two circle configurations are presented in [Gilbert *et al.*, 1997], where, in the first configuration, six needles are positioned in the circle and in the second configuration eight needles are positioned in the circle and one electrode is positioned in the centre of the circle (denoted as 8+1). For larger volumes, the so called honeycomb electrode design is used [Mir *et al.*, 1997; Ramirez *et al.*, 1998], where many needle electrodes are positioned in a honeycomb form.

1.8 ELECTRIC PULSE PARAMETERS

Since the experiments presented in [Mir *et al.*, 1991; Belehradek *et al.*, 1991] rectangular pulses have been predominantly used in *in vivo* applications of tissue permeabilisation. Compared to exponentially decaying pulses, which were used before, rectangular pulses enable independent setting of pulse amplitude and duration. Their application provides exposure of tissue to permeabilising electric field intensity for a sufficient time, by avoiding too high field strengths [Mir and Orlowski, 1999]. The latter cannot be avoided in case of exponentially decaying pulses.

Rectangular pulse parameters that influence tissue permeabilisation are, pulse amplitude (causes electric field distribution in tissue), pulse number and duration. Electric field intensity is the governing factor that controls permeabilisation, as only the area of tissue exposed to electric field intensity above reversible thresholds is permeabilised. Pulse number (N) and pulse duration (T) control the degree of flow of exchanged molecules between cell and external medium [Maček-Lebar, 1999; Puc *et al.* 2003; Teissie *et al.*, 1999]. The effect of both parameters however is not the same; at a given cumulated pulse duration (N*T=const.) a higher electropermeabilisation efficacy is obtained at higher pulse number [Rols and Teissie, 1993]. Namely, the number of pulses increases the possibility for any cell to become permeabilised and increases the number and size of membrane modifications. However in [Gabriel and Teissie 1997; Gabriel and Teissie 1999] it was also observed that the intensity of alterations increases with the pulse length. In any case, when selecting pulse duration it should be considered to select a duration longer than the time required to obtain membrane modifications and shorter than the time at which irreversible changes in cell membrane may occur [Mir and Orlowski, 1999]. The latter may be caused by excessive heating of the tissue.

Another important issue related to pulse parameters is the electrode orientation. Serša *et al.* in 1996 showed that alterations of electrode orientation during the pulse application increase the efficacy of tissue permeabilisation.

1.9 DETERMINATION OF OPTIMAL PARAMETERS FOR TISSUE PERMEABILISATION

In terms of electrochemotherapy for effective tissue permeabilisation the pre-required volume of tissue needs to be exposed to electric field intensity above the reversible threshold. When related to electrogenetransfer in addition to this requirement also the electric field intensity should be below the value which causes cell necrosis. This is a very rigorous requirement for application because the range of electric field intensities between reversible and irreversible tissue permeabilisation is often quite narrow [Mir and Orlowski, 1999].

As mentioned before, electrode configuration, electric pulse parameters (amplitude, duration, number) and the shape and type of tissue are parameters which determine the efficacy of permeabilisation. To achieve efficient permeabilisation of a given volume of specific tissue the choice of optimal pulse parameters and electrode configuration is therefore crucial.

The determination of optimal pulse duration was based on experimental work on cells in culture. Considering the requirements for the pulse length i.e. less than the time which causes irreversible cell damage and more than the time needed to permeabilise cell, the optimal pulse duration was determined to be 100 µs [Mir *et al.*, 1988; Rols and Teissie, 1989]. Latter *in vivo* experiments have also shown this pulse duration to give excellent results. Recently the same pulse parameters were systematically tried *in vivo* [Maček-Lebar *et al.*, 2002].

The number of pulses increases the number and size of membrane modification. Thus a higher number of pulses is beneficial. In [Mir *et al.*, 1988] it was shown that the application of 8 pulses gives better results than the application of 4 pulses. Therefore 8 pulses are considered as optimal for antitumour effect.

Pulse amplitude and electrode configuration are nevertheless the most important parameters responsible for tissue permeabilisation, as they control electric field distribution in tissue. Several rapid tests were proposed to determine the electric field intensity needed for *in vitro* permeabilisation of a given cell type [Mir and Orlowski, 1999]. They are based on measurement of the uptake of molecules which can not enter intact cells. Some molecules such as Cr^{51}-EDTA and Lucifer Yellow also leak out of irreversibly permeabilised cells. This provides information about the maximal pulse amplitude that can be applied without causing cell necrosis. Similar tests which were combined with numerical models of electric field distribution were performed for *in vivo* [Gehl *et al.*, 1999; Miklavčič *et al.*, 2000] determination of electric field intensities important for tissue permeabilisation. However those models assumed the electric field distribution in non-permeabilised tissue, while electric field distribution in permeabilised tissue might be different.

The electrode configurations used in *in vivo* applications are usually determined by standard electrode holders. The effect of electrode configuration on electric field distribution in tissue can be determined by means of numerical models [Miklavčič *et al.*, 1998; Gehl *et al.*, 1999; Brandinsky and Daskalov, 1999]. Despite that the choice of electrode configuration for a particular treatment is still based on empirical results. Thus for the treatment in electrochemotherapy Brandinsky and Daskalov [Brandinsky and Daskalov, 1999] addressed the importance of electrode design optimisation with respect to tumour size and location.

The optimal pulse parameters described so far are related to electrochemotherapy. In the case of electrogenetransfer those optimal pulse parameters should be slightly modified because after cell membrane permeabilisation, gene transfer is facilitated by electrophoretic forces. This requires additional low voltage pulse(s) to be added after tissue permeabilisation is achieved [Satkauskas *et al.*, 2002] or an increase of pulse length [Gehl and Mir, 1999]. The determination of optimal pulse parameters for *in vivo* gene transfer by rapid test was described by Gehl and Mir [Gehl and Mir, 1999].

In summary, the optimal number and duration of pulses have been already determined for application in electrochemotherapy, however the pulse amplitude and electrode design are the two parameters that vary depending on the type of tissue and region of tissue to be permeabilised. Despite numerous numerical models that have been developed to describe electric field distribution in tissue for different pulse amplitudes and different electrode designs, those models have not been used to determine the optimal pulse amplitude and electrode design for effective tissue permeabilisation. This was due to their inefficiency to model the electropermeabilisation process and consequently electric field distribution in permeabilised tissue.

Therefore the most important contribution of our work is development of a time discrete model that describes tissue permeabilisation and implementation of this model for the optimisation of pulse amplitude and electrode design.

1.10 APPLICATIONS OF TISSUE PERMEABILISATION

The two leading applications of tissue permeabilisation are electrochemotherapy and electrogenetransfer.

Electrochemotherapy could be defined as a local potentiation, by means of permeabilising electric pulses, of the antitumour activity of a nonpermeant anticancer drug possessing a high intrinsic cytotoxicity [Mir, 2000]. Thus electrochemotherapy is performed by administration of a cytotoxic drug and permeabilisation of the area of interest by appropriate electric pulses. The advantage of electrochemotherapy over standard chemotherapy is that it provides localized treatment, which also requires much lower drug doses than chemotherapy. The positive effect of electric pulse application in treatment was reported by Mir and Okino independently [Okino and Mohori, 1987; Mir *et al.*, 1988; Mir *et al.*, 1991]. Soon after that in 1991 the first clinical trials of electrochemotherapy were performed at The Institute Gustave-Roussy and later also in other cancer research centres. Recent clinical trials which have been performed in five cancer research centres since 1998 are summarized in [Mir *et al.*, 1998] as well as in [Heller *et al.*, 1999; Gehl, 2003; Serša *et al.*, 2003]. These clinical trials demonstrated excellent results in antitumour therapy: in [Heller *et al.*, 1998] the electrochemotherapy of basal cell carcinoma showed complete regression in 99% of the nodules; [Panje *et al.*, 1998] achieved complete regression in 50% and partial regression in the rest of oral cavity squamous cell carcinoma; further [Kubota *et al.*, 1998] obtained complete recovery in 82% of metastases of bladder transitional cell carcinoma when exposed to electrochemotherapy; and finally at The Institute of Oncology in Ljubljana they performed electrochemotherapy of malignant melanomas using cisplatinum [Serša *et al.*, 1998]. They were first to show that electrochemotherapy can also be effectively performed with cisplatinum instead of just bleomicyn as was the practice before.

In addition to electrochemoptherapy, electrogenetransfer is another promising application of electropermeabilisation. Before employing electrogenetransfer, different methods had been used to facilitate the transfer of DNA into the cell. Each of these methods was however inadequate for a particular reason, i.e. for being inefficient or non-localized. The method of gene transfer by means of viral vectors has even caused the loss of life [Ferber, 2001]. Compared to those methods, electrogenetransfer is superior because it has proven to be highly efficacious especially when exposed to longer pulses than those used in electrochemotherapy [Mir *et al.*, 1999], and also because it provides targeted gene expression due to its dependency on electric field distribution. The first demonstrations of *in vitro* gene transfection by means of electric pulses were reported in [Neumann *et al.* 1982; Wong and Neumann, 1982]. Due to its simplicity and efficacy the method of DNA electrotransfer has become a routine technique for introducing foreign genes into bacterial, plant and animal cells *in vitro* [Simon, 1993]. Successful results obtained on living cells lead to *in vivo* experiments. Electrogenetransfer has been performed *in vivo* in muscle tissue [Mir *et al.*, 1999; Aihara and Miyazaki, 1998], tumour [Rols *et al.*, 1998], skin [Zhang *et al.*, 2002], and brain tissue [Nishi *et al.*, 1996]. However no clinical trials have been performed to date. The important discovery obtained *in vivo* on muscle cells was that longer pulse durations than in electrochemotherapy increases DNA uptake [Mir *et al.*, 1999]. The most recent report [Satkauskas *et al.*, 2002] suggests the use of a short high voltage pulse that permeabilises cells followed by a longer low voltage pulse that enables electrophoretic gene transport. The successful results of electrogenetransfer obtained *in vivo* and the advantages of electrogenetransfer over other methods imply that this method will soon be put to use in clinical settings.

1.11 OBJECTIVES OF THE THESIS

The main objective of the proposed work was to develop a time discrete model of tissue electropermeabilisation which can be employed for the assessment of the extent of tissue permeabilisation. As specific conductivity changes due to cell membrane permeabilisation when exposed to an external electric field, the time discrete model has to provide information about electric field distribution in discrete time steps during permeabilisation as well as to incorporate the functional dependency $\sigma(E)$, which defines how the tissue conductivity changes when exposed to external electric field.

Another objective of the thesis was to develop a simulation environment based on the time discrete model that presents tissue permeabilisation at user supplied pulse amplitude, tissue properties and electric field thresholds. In this way the behaviour of the time discrete model could be tested against the experimental knowledge of tissue permeabilisation. Another purpose of the simulation environment was to examine the influence of different functional dependencies $\sigma(E)$, such as stepwise, liner, exponential, and S-shaped dependency on the course and the extent of permeabilisation at particular pulse amplitudes. The purpose of the time discrete model was also to establish the feasibility of real-time control of tissue permeabilisation.

Electric field distribution in a time discrete model can be described either analytically or numerically, depending on the tissue geometry and electrical properties. As numerical methods, for example, the finite element method, are computationally demanding and time consuming, a further purpose of the thesis was to determine the simplifications which can be employed to modelling of needle electrodes with the finite element method from the perspective of frequent model computation that is present in a time discrete model.

Additional objective of the thesis was to determine and validate the time discrete model of rabbit liver tissue electropermeabilisation, performed by needle electrodes. Within that model $\sigma(E)$ dependency had to be determined which also includes the determination of reversible and irreversible electric field thresholds. The model validation on experimental data is a very important part of the modelling. Thus the results of the model need to be compared to experimental currents and the areas of reversibly and irreversibly permeabilised rabbit liver tissue.

The final objective of the thesis was to examine the feasibility of model based optimisation of EP parameters for effective electrochemotherapy. The feasibility study should provide the benefits and constraints of model based optimisation of EP parameters.

Taking into account the described objectives of the thesis, the continuation of the thesis is structured as follows:

In Chapter 2 the methodology used for the development of a time discrete model is presented. Emphasis is given to the theory of volume conductor, which is a basis for the computation of electric field distribution in biological tissue. Next, the finite element method is presented, due to the fact that this method excels at modelling complex geometries with inhomogeneous and anisotropic properties, such as present in the biological tissue. As the biological tissue geometry for numerical modelling is usually acquired from computer tomography (CT) and magnetic resonance images (MRI), at the end of Chapter 2 the basics of CT and differences compared to MRI are described.

In Chapter 3 we present a time discrete model of tissue permeabilisation placed between two concentric cylindrical electrodes, within which electric field distribution is described analytically.

The model is incorporated into a simulation environment that provided means for observing the course and extent of permeabilisation at different rectangular pulse amplitudes, electrode diameters, tissue specific conductivities and different σ(E) dependencies, such as stepwise, linear, exponential and S-shaped dependency. Apart from rectangular pulse amplitude, the extent of tissue permeabilisation was further investigated for linearly increasing and linearly decreasing pulses. In continuation of Chapter 3 the feasibility of real time control was examined through the closed loop control scheme incorporating the time discrete model and proportional integral controller. At the end of Chapter 3 the comparison between the results of numerical and analytical solutions of a time discrete model for the same geometry is presented.

In Chapter 4 different approaches towards modelling of needle electrode geometry with a finite element model were examined from the perspective of frequent model computation. The optimal electrode geometry according to the defined objective function was then proposed to be employed in further numerical models.

Chapter 5 presents a time discrete model of rabbit liver tissue permeabilisation with inserted needle electrodes. Electric field distribution in the model was described numerically, due to the relatively complex geometry. Model parameter estimation i.e. the determination of σ(E) dependency was performed on current measurements, obtained from *in vivo* experiments. Parameter estimation provided also the thresholds of reversible and irreversible electric field intensity for rabbit liver tissue. Those thresholds were slightly higher than previously published values in [Miklavčič *et al.*, 2000] for the same tissue. The model validation was performed on current measurements other than those used for parameter estimation and also on measurements of the area of reversibly and irreversibly permeabilised tissue.

In Chapter 6 the feasibility of the model based optimisation of EP parameters for use in electrochemotherapy was examined. Optimisation was first performed on the simple geometry consisting of the tissue and the tumour, at which electrical treatment was performed with plate electrodes. The optimisation considered limitations in current and voltage supplied by the pulse generator and the condition that the electric field must exceed the reversible threshold value across the tumour. Considering that, nonlinear constrained optimisation was used for determination of optimal pulse amplitude and optimal position of plate electrodes. The resulting electric field distribution in the tumour exceeded reversible threshold yielding effective electrochemotherapy. Further in Chapter 6 the model based optimisation was performed on geometry representing a human brain tumour. The geometry was obtained from CT images. An approach for semiautomatic 3D geometry model generation from CT images was proposed and implemented. The array of needle electrodes was considered for electrical treatment of a brain tumour. The model based optimisation of pulse amplitude to be applied to the needle array was then performed. The complete permeabilisation of the particular tumour was not achieved with the needle array used, due to the limitation of the pulse generator. Therefore at the end of the Chapter 6 alternative solutions were proposed to achieve complete permeabilisation.

2 METHODOLOGY

This chapter comprises the methods used for the development of the time discrete model of tissue permeabilisation. At the beginning the theory of volume conductor is presented, which is used for the description of electric field distribution in biological tissue when direct constant current is applied. As the biological tissue can have anisotropies and inhomogeneities the solution yielding the electric field distribution can not always be solved analytically. In such cases the use of numerical techniques is much more appropriate. Thus, in the continuation, the numerical technique, which has proven to be very effective in numerous computations of electric field distribution in biological tissue, is presented. That is the finite element method. Further the details of finite element modelling are described with special emphasis on geometry modelling. The latter is usually acquired from computer tomography (CT) and magnetic resonance imaging (MRI). Thus at the end of the chapter the basics of computer tomography and differences compared to MRI are described.

2.1 VOLUME CONDUCTOR THEORY

The electric field problems in physiology resulting from the application of direct electric current in tissue can, in general, be considered as quasi-stationary [Plonsey, 1969; Plonsey and Heppner, 1967]. A body can be represented as a composite volume conductor comprising a number of spatially distributed tissues with differing electrical properties [Geddes and Baker, 1967; Plonsey 1984]. Thus the electric field distribution in tissue can be described by the equations for steady electric currents in volume conductor [Heringa *et al.*, 1982]. Under quasi-stationary conditions the biological tissue can be treated as purely resistive, so that current density associated with the electric field can be given by Ohm's law:

$$\vec{J} = \sigma \vec{E}\,, \tag{2.1}$$

where J is the current density, E electric field intensity and σ specific conductivity of the tissue. Specific conductivity reflects macroscopic properties of the tissue, which can also be inhomogeneous or anisotropic. Inhomogeneous tissue properties mean that tissue specific conductivity vary with space coordinates, so that different field properties prevail at different parts of the material structure. Anisotropic tissue properties mean that the field relations differ at any point for different direction of propagation. To describe such a material σ becomes a 3x3 tensor:

$$\sigma = \begin{bmatrix} \sigma_{xx} & \sigma_{xy} & \sigma_{xz} \\ \sigma_{yx} & \sigma_{yy} & \sigma_{yz} \\ \sigma_{zx} & \sigma_{zy} & \sigma_{zz} \end{bmatrix}. \tag{2.2}$$

When the tissue conductivity can be described in an orthogonal coordinate system, and both the current density and the electric field are related to the same system, the above matrix becomes diagonal:

$$\sigma = \begin{bmatrix} \sigma_{xx} & 0 & 0 \\ 0 & \sigma_{yy} & 0 \\ 0 & 0 & \sigma_{zz} \end{bmatrix}. \tag{2.3}$$

For electrostatic problems in volume conductor electric field intensity E is described as a negative gradient of scalar potential u:

$$\vec{E} = -\nabla u \, . \tag{2.4}$$

Under quasi-static conditions the total current flow is solenoidal meaning that the divergence of (2.1) is zero. Thus

$$\nabla \vec{J} = 0 \, . \tag{2.5}$$

By combining (2.5) with (2.1) we get

$$\nabla (\sigma \vec{E}) = 0 \tag{2.6}$$

and by incorporating the definition of electric field intensity we obtain

$$\nabla \left[\sigma (-\nabla u) \right] = 0 \, . \tag{2.7}$$

When the volume conductor is homogenous and isotropic specific conductivity is a scalar, the equation (2.7) becomes Laplace’s equation:

$$\nabla^2 u = 0 \, . \tag{2.8}$$

Laplace’s equation is a partial differential equation of elliptic type. Solution of the Laplace equation requires the application of boundary conditions. They can be applied either in the form of a Neumann boundary condition or a Dirichlet boundary condition.

A Neumann boundary condition is defined as the first derivative of the scalar electric potential in the normal direction to the boundary surface of the model:

$$q = \frac{\partial u}{\partial n} \qquad \text{or} \qquad q = -\frac{J_n}{\sigma} \, . \tag{2.9}$$

The latter equation denotes the current density flowing in/out of the model in the direction normal to the surface, divided by the specific conductivity of tissue.

A Dirichlet boundary condition is defined as a fixed scalar electric potential, i.e. applied voltage on the surface of the model:

$$u = \bar{u} \, . \tag{2.10}$$

The solution of Laplace’s equation can be obtained analytically or numerically. Analytical solutions can be derived when the geometry and the material properties of the volume conductor are described within the same coordinate system (Cartesian, spherical, and cylindrical). In other cases analytical models become too complex.

On the other hand numerical methods can handle complex geometries, material inhomogeneities and anisotropies. Those characteristic are also significant for biological tissue. This makes numerical methods more convenient for solving problems in physiology than analytical methods.

2.2 NUMERICAL METHODS

Numerical solutions play an important role in numerous bioelectric field problems, such as electrocardiology, cardiac defibrillation, electrical impedance tomography, therapeutic and functional electric stimulation, electromiography, electroencephalography, electromagnetic dosimetry [Johnson, 1997].

There is rich history in **electrocardiography** (ECG) of use of numerical methods and computer simulation to solve forward and inverse problems. The problem in which the source and conducting medium are known, but the field is unknown is referred to as a forward problem [Shahidi *et al.*, 1994; Klepfer *et al.*, 1997]. On the other hand when the field and conductor are known and the source is unknown we deal with an inverse problem [Nenonen, 1994].

In **cardiac defibrillation** the improvement in lead technology has progressed in two different ways. The first is to manually construct lead systems and test configurations in animals. However with increased computer power and with increased understanding of critical variables necessary for successful defibrillation the second approach in designing implantable cardioverter defibrillators is to model and test new electrode configurations on computers before testing them on animals [Sepulveda and Wikswo, 1990].

Electrical impedance tomography (EIT) is a procedure for mapping electrical conductivity properties of the internal tissue by applying electrical currents through electrodes attached to the surface of the body and measuring resulting voltage. The use of numerical modelling techniques with EIT is presented in [Kim *et al.*, 1988].

Therapeutic and functional electric stimulation (FES) of the nervous system by either external or implantable electrodes is used amongst others to treat symptoms of epilepsy, psychiatric disorders, and spinal cord injury. Here the modelling problem is to deliver a therapeutic dose of electricity to the desired region while minimizing the stimulation effect to surrounding regions. The finite element analysis of electrical stimulation of the spinal cord for example is presented in [Coburn, 1980].

Electromyography (EMG) is defined as a registration of muscle action potentials, which reflect the state of the muscle and the activity of the motor neurons in reflex and voluntary actions. Electromyography has been used mostly for diagnostic purposes, however in recent years it has also become a tool for monitoring and in conjunction with FES it is also employed for controlling the movement of artificial limbs. In [Hennenberg and Plonsey, 1993] the directional sensitivity of the concentric EMG electrode is computed by means of boundary element analysis.

The fundamental problem in computational **electroencephalography** (EEG) is the inverse EEG problem, i.e. to compute the source provided the field and the conductor are known. If an accurate solution to the inverse problem were known, a neurologist would be able to non-invasive view and interpret patient – specific cortical activity [Peters and De Munck, 1991].

Related to **electromagnetic dosimetry** the calculation of electromagnetic energy absorbed by humans in a radiation field has become important with the increased usage of electromagnetic devices. Electromagnetic analysis techniques (analytical and numerical) have been used by researchers in the field to obtain dosimetric data and understanding of absorption characteristics [Durney, 1980].

2.2.1 FINITE ELEMENT METHOD

Amongst a variety of numerical methods, that is, the finite difference (FD), finite element (FE), boundary element (BE), and multigrid (MG) methods, the finite element method excels at modelling complex inhomogeneous anisotropic materials such as are present in biological tissue. Consequently the FE method has become a powerful tool for the numerical solution of a wide range of electromagnetic field problems in physiology, such as problems related to a single cell level [Pavlin *et al.*, 2001], organs or tissue [Miklavčič *et al.*, 2000] and whole body structures [Šemrov and Miklavčič, 1998].

With the finite element method, differential equations are solved by subdividing the domain of interest into smaller elements of finite dimensions, termed as finite elements. The original domain is then considered as the assemblage of these elements connected at a finite number of joints called nodes.

The material properties and the governing relations are considered over these elements and expressed in terms of unknown values in nodes. An assembly process, duly considering the loading and constraints, results in a set of equations, the solution of which gives the approximate behaviour of the continuum [Chandrupatla and Belegundu, 1997].

An electromagnetic analysis problem is in general a problem of solving Maxwell's equations subject to certain boundary conditions. Maxwell equations state the relationship between the fundamental electromagnetic quantities [FEMLAB User Guide and Introduction, 2001]. They can be formulated either in integral or differential form. The differential form leads to differential equations which are handled by the finite element method. Thus here we present the differential form of Maxwell's equations for general time varying fields [Sinigoj, 1999]:

$$\nabla \times \vec{H} = \vec{J} + \dot{\vec{D}}, \tag{2.11}$$

$$\nabla \times \vec{E} = -\dot{\vec{B}}, \tag{2.12}$$

$$\nabla \cdot \vec{D} = \rho, \tag{2.13}$$

$$\nabla \cdot \vec{B} = 0. \tag{2.14}$$

The fundamental electromagnetic quantities within Maxwell's equations are electric field intensity $\vec{E}$, electric flux density $\vec{D}$, magnetic field intensity $\vec{H}$, magnetic flux density $\vec{B}$, current density $\vec{J}$ and electric space charge density ρ.

Equations (2.11) and (2.12) are also referred to as Maxwell-Amper's law and Faraday's law, respectively. Equation (2.13) is the electric form of Gauss' law, while equation (2.14) is a magnetic form of Gauss' law. In the system of equations (2.11) to (2.14) only two are independent. Namely equation (2.13) is included in (2.11) and equation (2.14) in (2.12).

For full description of an electromagnetic problem the boundary conditions have to be specified at material interface and physicals boundaries. Provided there are no surface charge density and no surface current density, the boundary conditions on the interface between material 1 and material 2 are expressed as

$$E_{t1} = E_{t2} \qquad \text{and consequently} \qquad J_{n1} = J_{n2}\,, \tag{2.15}$$

$$D_{n1} = D_{n2}\,, \tag{2.16}$$

$$H_{t1} = H_{t2}\,, \tag{2.17}$$

$$B_{n1} = B_{n2}\,, \tag{2.18}$$

where n denotes normal and t tangential component to the interface.

The direct solution of the system of Maxwell's equations on $\vec{E}$ and $\vec{B}$ has several disadvantages [EMAS Version 4 User's Manual, 1997]. The first disadvantage is that six unknown components can not be chosen arbitrarily because they are related through Maxwell's equations. The number of unknowns is thus larger than is actually needed. The second disadvantage is related to discontinuities in material properties. Boundary conditions in equations (2.15) to (2.18) must be met at each interface between two materials with different properties. Therefore every solution strategy, that involves $\vec{E}$ and $\vec{B}$, must enforce these conditions at every interface. This potentially means at all surfaces of each finite element. This requirement puts a huge burden on numerical computation. And third, at sharp corners of certain materials values of $\vec{E}$ and $\vec{B}$ may be infinite. Resulting singularities cause severe problems in digital computing.

To eliminate the disadvantages mentioned above the problem is formulated in terms of electric scalar potential ψ, which is related to classical potential u through the relation:

$$\psi = \int_t u dt \tag{2.19}$$

and magnetic vector potential $\vec{A}$. The new formulation is as follows:

$$\vec{B} = \nabla \times \vec{A}\,, \tag{2.20}$$

$$\vec{E} = -\nabla \dot{\psi} - \dot{\vec{A}}\,. \tag{2.21}$$

The two equations are direct consequences of the magnetic case of Gauss' law and Faraday's law respectively. Thus the three components of vector potential and the unconventional scalar potential represent the unknown quantities. Such reformulation of the problem has a profound effect on the symmetry and unity of the finite element formulation of electromagnetics [EMAS Version 4 User's Manual, 1997]. In the case of an electric field distribution within a volume conductor (quasi-stationary field), the three components of the vector potential equal 0. The solution therefore requires only the computation of unconventional scalar potential.

The system of equations to be solved by a finite element method can be derived by either Garlekin's method or by means of variation form. The former method is described in detail in [Braess, 1997; Prelog, 1975]. While here we will focus on the principle of virtual work, which is based on the variation method.

The principle of virtual work is used in the EMAS software package because unlike the Garlekin method it brings much useful information on boundary and initial conditions [EMAS Version 4 User's Manual, 1997].

In order to obtain the system of equations to be solved on finite elements the variation method is based on minimization of the functional which represents the work of generalized forces. In the case of quasi-stationary problems (current flow) the generalized work is defined by ohmic losses:

$$w = \int_t \vec{E} \cdot \vec{J} dt = -\int_t \nabla u \cdot \vec{J} dt = -\nabla(\int_t u dt) \cdot \vec{J} \tag{2.22}$$

or

$$w = -\nabla \psi \cdot \vec{J} \,. \tag{2.23}$$

The differential of virtual work is connected to unconventional scalar potential through:

$$\delta W = \int_V \delta(\nabla \psi) \cdot \vec{J} dV \,. \tag{2.24}$$

By integrating the right hand side of equation (2.24) *per partes* we obtain:

$$\int_S \delta\psi \cdot \vec{n} \cdot \vec{J} dS \,, \tag{2.25}$$

where *S* represents the surface of boundary and *n* a normal vector to that surface.

The generalized form of the upper equation can be written by adding energy, which results from prescribed constant current density $\vec{J}^*$ on a particular surface (excitation):

$$\int_S \delta\psi \cdot \vec{n} \cdot (\vec{J} - \vec{J}^*) dS \,. \tag{2.26}$$

This term equals 0 in two cases:

- if $\delta\psi$ equals 0 on the surface *S*, or if there is no change in ψ (Dirichlet boundary condition);
- if the normal component of current density *J* on the surface *S* equals prescribed value J_n^* (Neumann boundary condition).

By adding this contribution to equation (2.24) we get:

$$\delta W = \int_V \delta(\nabla \psi) \cdot \vec{J} dV - \int_S \delta\psi \cdot \vec{n} \cdot \vec{J}^* dS \,. \tag{2.27}$$

Considering the equations (2.1), (2.4) and (2.19) in the first term of the right hand side we obtain:

$$\delta W = -\int_V \delta(\nabla \psi) \cdot \sigma \cdot \nabla \dot{\psi} \, dV - \int_S \delta\psi \cdot \vec{n} \cdot \vec{J}^* dS \,. \tag{2.28}$$

This relation represents the basis for solving the problem with finite element method. The first term on the right side represents the energy of ohmic losses, while the second term represents energy due to applied boundary conditions or excitations.

Further we assume that scalar potential in each element can be represented with the low order polynomial. That is similar to the development of the function in series around a particular point. The potential in an element can therefore be described with:

$$\psi(\vec{r}) = N_1(\vec{r}) \cdot \psi_1(t) + N_2(\vec{r}) \cdot \psi_2(t) + N_3(\vec{r}) \cdot \psi_1(t) + \dots, \tag{2.29}$$

where *$N_i(r)$* are shape functions and *$\psi_i(t)$* the value of unconventional scalar potential in the *i^{th}* node. Equation (2.29) can be also written as

$$\psi = \{N\}^T \cdot \{\psi^e\}, \tag{2.30}$$

where $\{N\} = \{N_1, N_2, N_3, \ldots\}^T$ is a shape function vector and $\{\psi^e\} = \{\psi_1, \psi_2, \psi_3, \ldots\}^T$ the vector of unconventional scalar potentials. The size of both vectors equals the number of nodes *n*, corresponding to an element.

To assign the equation for virtual work to each element we have to consider the following expressions:

$$\dot{\psi} = \{N\}^T \cdot \{\dot{\psi}^e\}, \tag{2.31}$$

$$\delta\psi = \{N\}^T \cdot \delta\{\psi^e\}, \tag{2.32}$$

$$\nabla\psi = [\nabla N] \cdot \{\psi^e\}, \tag{2.33}$$

where $[\nabla N]$ is a matrix with dimensions 3 x *n*:

$$[\nabla N] = \begin{bmatrix} \frac{\partial N_1}{\partial x} & \frac{\partial N_2}{\partial x} & \cdots \\ \frac{\partial N_1}{\partial y} & \frac{\partial N_2}{\partial y} & \cdots \\ \frac{\partial N_3}{\partial z} & \frac{\partial N_3}{\partial z} & \cdots \end{bmatrix}. \tag{2.34}$$

Virtual work in an element can be therefore expressed as:

$$\delta W^e = -\int_{V^e} \left([\nabla N] \cdot \delta\{\psi^e\} \right)^T \cdot \sigma \cdot \left([\nabla N] \cdot \{\dot{\psi}^e\} \right) dV - \int_{S^e} \left(\{N\} \cdot \delta\{\psi^e\} \right)^T \cdot \left(\vec{n} \cdot \vec{J}^* \right) dS. \tag{2.35}$$

Due to independency of unconventional scalar potential $\{\psi^e\}$ on spatial coordinates we can write:

$$\delta W^e = -\delta\{\psi^e\}^T \cdot (\int_{V_e} [\nabla N]^T \cdot \gamma\sigma \cdot [\nabla N] \, dV) \cdot \{\dot{\psi}^e\} - \delta\{\psi^e\}^T \cdot \int_{S^e} \{N\}^T \cdot \left(\vec{n} \cdot \vec{J}^* \right) dS. \tag{2.36}$$

Now we can define the conductivity matrix of an element:

$$\left[B^e\right] = \int_{V^e} [\nabla N]^T \cdot \sigma \cdot [\nabla N] \, dV \tag{2.37}$$

which incorporates all information about the conductivity of an element – geometry and specific conductivity and the vector of surface current sources:

$$\left\{J^e\right\} = -\int_{S_e} \left\{N^T\right\} \cdot \left(\vec{n} \cdot \vec{J}^*\right) dS\,, \tag{2.38}$$

where (*) denotes prescribed current value (Neumann boundary condition). Considering the two equations we can express the equation (2.36) for virtual work as:

$$\delta\, W^e = -\delta\left\{\psi^e\right\}^T \cdot \left[B^e\right] \cdot \left\{\dot{\psi}^e\right\} + \delta\left\{\psi^e\right\}^T \cdot \left\{J^e\right\}. \tag{2.39}$$

By adding up all the contributions of virtual work from each element we obtain the expression for virtual work of the whole model:

$$\delta\, W = -\delta\{\psi\}^T \cdot [B] \cdot \{\dot{\psi}\} + \delta\{\psi\}^T \cdot \{J\}\,, \tag{2.40}$$

where $\{\psi\}$ consists of vectors $\left\{\psi^e\right\}$ of all elements in the model. A similar structure holds also for matrix [*B*] and vector {*J*}.

By introducing the dynamical equilibrium:

$$0 = -[B] \cdot \{\dot{\psi}\} + \{J\}_S \tag{2.41}$$

we obtain the final system of equations

$$[B] \cdot \{\dot{\psi}\} = \{J\}_S \tag{2.42}$$

or

$$[B] \cdot \{u\} = \{J\}_S\,. \tag{2.43}$$

Further we have to apply boundary conditions in equation (2.43) i.e. to assign prescribed values of potentials to nodes. The system of equation can then be transformed by putting all unknowns (potentials) on the left side:

$$\mathbf{A} \cdot \mathbf{x} = \mathbf{B} \cdot \mathbf{f}\,, \tag{2.44}$$

where **A** is a system matrix, **x** a vector of unknowns, **B** a complementary matrix and **f** the vector of boundary conditions. The matrix A is symmetric and positive definite, thus it is nonsingular and it has a unique solution. The system presented in equation (2.44) is then ready to be solved by an appropriate finite element solver.

2.2.2 FINITE ELEMENT MODELLING

Nowadays there is plenty of software packages designed for solving electromagnetic (EM) problems with numerical methods. The survey of available software packages and their capabilities as they were in 1997 is presented in [Mirotznik and Prather, 1997]. Despite the fact that this survey does not incorporate all the software packages available today, it gives directions as how to choose the EM package.

Although an EM package has to be general for different applications it also has to have specific features to adapt to the particular application. To circumvent this predicament, EM packages are usually modular. That means that the modelling process is broken down into several steps, such as: geometry modelling of the physical object, creation of an analytical mesh, the analysis proper and finally postprocessing accompanied with graphical presentation. The analysis and postprocessing modules are application specific and need to be designed for electrostatics, magnetostatics and radiation scattering problems separately.

The model construction in most EM packages is done through the graphical pre-processor, which provides similar modelling tools to those found in common computer-aided design software (CAD). Additionally, the graphical pre-processor should enable the assignment of boundary conditions, material properties, and energy sources to the geometry. Some EM packages also support the importation of geometrical models from CAD programs.

After defining the geometry, a mesh of small computational elements must be created. Finite element solvers require a mesh of non-overlapping 2D or 3D elements, such as triangles or tetrahedrons, respectively. Mesh generation is a critical step on the way to the solution. Well designed mesh produces results that are both accurate and computationally efficient. However the mesh design is usually a trade-off among accuracy, computation time, and memory requirements. The mesh generation process in most EM products is based on automated grid-meshing algorithms.

The next step performed by EM software is EM analysis. Amongst 18 EM packages presented in the survey, nine different numerical algorithms were used.

After EM analysis is performed the EM package should provide graphical visualisation of computed results. Modern EM packages can display fields in different graphical formats included 2D and 3D arrow, contour, and shaded plots. Some EM packages can also generate animated movies of EM field propagation.

EM analyses in our laboratory at the time are being performed utilising the EMAS software package (Ansoft Inc, USA), Maxwell 3-D from the same vendor and FEMLAB (Comsol AB., Sweden). The first two mentioned software tools were also presented in the survey, while the last one was developed later. All of them however meet the requirements of good EM software.

Results presented further in this work were computed either with EMAS or FEMLAB software. The software package used will be denoted next to particular solution. EMAS and FEMLAB were used because they allowed for changes in material properties based on electric field distribution across the geometry. In the EMAS software this feature was obtained by utilizing an additional programme developed within our laboratory. Similarly in FEMLAB software package the extended functionality was developed by means of Matlab functions, as FEMLAB is integrated into the MATLAB environment. MATLAB (MathWorks Inc., USA) is the software package aimed at matrix analyses, which has also an extensive set of Toolboxes for different engineering and scientific problems.

Some of the modules involved in finite element modelling will be hereafter described in more detail.

2.2.2.1 GEOMETRY MODELLING

Most of the realistic biological tissue models are based upon CT and magnetic resonance (MR) images. However despite the extensive research in the field there is still no algorithm that can automatically determine the domain boundaries from the clinically obtained medical images. Some

EM programmes, such as FEMLAB, already provide support for MR image import, however the image filtering, scaling and domain boundary definition are still performed by humans.

Further in this chapter the characteristics of CT images will be presented by focusing on issues related to geometry model generation.

2.2.2.2 MESH GENERATION

Due to complex geometries associated with bioelectric field problems and the huge number of degrees of freedom, mesh generation is a time consuming process. In 3D problems tetrahedron elements are usually used for mesh generation because they best serve for modelling of irregular 3D domains.

There are several strategies aimed at discretization of geometry into basic tetrahedron elements. In bioelectric problems two approaches to mesh generation for solving with numerical methods have become standard: the *structured partitioning* strategy and *Delayun triangulation* strategy [Johnson, 1994]. Other methods such as *mapping*, *paving* and *octree* methods are also applicable.

The structured partitioning strategy starts with a set of points which define the bounding surface. The geometry volume is then repeatedly divided into smaller regions until a satisfactory discretization level has been achieved. Usually the domain is split into eight node cubic elements, which are then subdivided into tetrahedral elements. This method is fairly simple for programming; however its main disadvantage is that it allows elements to overlap interior boundaries. This property prevents finite element method approximation to be continuous.

For a given three dimensional set of points that define the boundaries and interior regions of the domain the *Delayun* method tessellates the point cloud into an optimal mesh of tetrahedral elements. With the *Delayun* method one can create the mesh to fit any predefined geometry, including subsurfaces by starting with points which define all necessary surfaces and then adding additional points to minimize the aspect ratio. For tetrahedral elements the aspect ratio is defined:

$$D = 4\sqrt{\frac{3}{2}\frac{\rho_k}{h_k}} \tag{2.45}$$

where ρ_k denotes the diameter of the sphere circumscribed about the tetrahedron and h_k the maximum distance between the vertices. The aspect ratio equals 1 for an equilateral tetrahedron, while degenerate elements have aspect ratios close to 0. Given the available set of points the *Delayun* criterion is a method for minimizing the occurrence of obtuse angles in the mesh, yielding elements which have aspect ratios as close to 1 as possible. The primary drawback of this method is that it is very demanding for programming.

2.2.2.3 MESH QUALITY

In the FEMLAB software package mesh quality is expressed in a similar way to the aspect ratio defined above. In 3D models the element quality measure for tetrahedral element is defined as:

$$q = \frac{216}{\sqrt{3}}\frac{V}{(h_1^2 + h_2^2 + h_3^2 + h_4^2 + h_5^2 + h_6^2)^{3/2}}, \tag{2.46}$$

where V is element volume and h_1, h_2, h_3, h_4, h_5, h_6 are the side lengths of a tetrahedron. q is a number between 0 and 1. q equals 1 in an equilateral tetrahedron. A value of $q>0.6$ denotes still acceptable element quality.

In the EMAS software the mesh quality is expressed in similar way – with distortion factor [EMAS Version 4 User's Manual, 1997]. Its value is based on the smallest determinant of the Jacobian matrix of an element. The determinant is evaluated at each integration point of the element and the smallest is saved. Again the ideal distortion factor is equal to 1, however in real meshes it may vary from 0 to 1. The closer the distortion factors to 1, the better the element quality.

An additional measure of mesh quality is defined by bending of the element edges. This measure applies to elements with intermediate points only. Namely, the distance of the node on the element edge to the centre point of the edge vertices should be less than 15% of the distance of the vertices.

2.2.2.4 SOLUTION METHODS

The solution method in finite element modelling is required to solve the sparse system of linear equations of the form $Ax=b$, where A is a square matrix while solution x and b are vectors.

There are many solution techniques aimed at solving such a system. They can in general be categorized into direct and iterative solvers. Representatives of the first type are for example Gaussian Elimination and LU decomposition methods. Amongst iterative methods there are for example Jacobi, Gauss-Seidel, Conjugate Gradient (CG) methods; Good Broyden, GMRES, TFQMR [FEMLAB User Guide and Introduction, 2001]

The choice of the particular solution method depends on the size of the resulting system and also on accessible computer resources. Direct methods are usually much faster than iterative methods, however they require computer memory that suffices to the size of the system.

On the other hand iterative methods can be employed when the size of the system exceeds the memory of the machine, however they are substantially slower than direct solvers. As the iterative method solves a system by generating a sequence of approximate solutions $x^{(k)}$ that converge towards the solution $x=A^{-1}b$, an initial guess $x^{(0)}$ must be provided. The closer the initial guess is to x, the faster the method is.

Iterative solvers can be accelerated by employing for example multigrid methods. The basic idea behind this is to accelerate the convergence of a known iterative method by exploring interactions between different discretization spaces or grids. In [Polstyanko *et al.*, 2001] the iterative method is accelerated by combining the principle of a multigrid method with the decomposition property of the hierarchical finite elements.

The convergence of iterative solvers is closely related to the condition number:

$$\kappa_2 = \frac{\lambda_{\max}}{\lambda_{\min}}, \tag{2.47}$$

where λ_{max} is largest and λ_{min} the smallest eigenvalue of the matrix A. The condition number should be in an ideal example as close to unity as possible. The condition number can be improved by a method referred to as preconditioning.

The preconditioning method applies the iterative method on the transformed system $A^Tx=b^T$, where $A^T=M^{-1}A$ and $b^T= M^{-1}b$ [FEMLAB User Guide and Introduction, 2001]. The matrix M is referred to as a preconditioner and it should approximate A to some degree. The better the approximation, the closer A^T to identity matrix, making A^T well conditioned with clustered values. The preconditioned iterative method involves the solution of linear systems $My=z$, which should be easy to compute. Thus the preconditioner should have an easily computed inverse while $\kappa^2(A^T)$ is close to unity. Preconditioning methods used in the Femlab software are Diagonal scaling, SSOR (Symetric Succesive Over-Relaxation), Incomplete LU, Geometric Multigrid and Algebraic Multigrid.

2.2.2.5 DISCRETIZATION ERROR

The quality of solution approximation is affected by discretization error for the following reasons [Grosz *et al.*, 1994]:

- the ***interpolation error*** is produced by the approximation of the solution by picewise polynomials;
- due to the fact that integration over the domain is subdivided into integrations over the elements, numerical integration schemes are applied; however in general the evaluation of weak partial differential equations does not deliver a true value which produces an ***integration error*** for the returned solution approximation;
- the Dirichlet boundary condition can not be fulfilled on the total boundary of a certain domain, but only at those global nodes which are on the boundary of that domain; the resulting error is referred to as ***interpolation of the Dirichlet conditions;***
- when having curved boundaries of the domain, the representation of the domain with basic elements is only an approximation of the true domain; this occurs if the boundary of the domain is different than the polynomial used for the representation of the curved element edge; the error produced is due to ***representation of the domain***;
- as iterative solutions are terminated by a ***stopping criterion***, the returned solution is not the exact solution of the discretized problem.

2.3 COMPUTERISED TOMOGRAPHY (CT)

CT is a method for generating cross-sectional X-ray images using a narrow X-ray beam directed through the target at many different angles. As X-rays pass through the various tissues of the body, a portion of the beam is absorbed. The loss of the X-ray from the beam is referred to as attenuation and differs between various tissues. Absorption properties of any tissue are represented by a linear attenuation coefficient. The attenuation measurement of each ray is referred to as a ray sum [Reddinger, 1997]. A complete set of ray sums is termed projection. The task of CT imaging is to reconstruct an image from its projections. That is mathematically performed by convolution of beams and series of attenuation profiles obtained at different angles of view [Kak and Slaney, 1988].

The mathematical solution of the reconstruction problem from its projections was given by Radon in 1917. However its usage in CT imaging began in 1972 when Hounsfield invented the CT scanner, for which he received the Nobel Prize in medicine in 1979.

2.3.1 CT IMAGE QUALITY

There are several characteristics that influence the quality of CT images such as spatial resolution, contrast resolution, linearity, noise and artefacts. Those characteristics can be either enhanced or suppressed in order to improve the quality of a CT image of a particular body region of interest [Reddinger, 1998]. Therefore CT image quality is dependent upon balancing these characteristics and parameters to produce the best possible image for the anatomical region and at the same time to reduce the risk of increasing the patient dose.

Spatial resolution is the ability to differentiate small neighbouring objects. The edge between two small objects with different densities is considered to be a region of high frequency. However, the problem is that CT blurs those edges to a certain degree, which sometimes results in non differentiation between the two objects. There are methods (such as use of high pass algorithms) that reduce structural blurring, however they increase image noise, which consequently decreases contrast or soft tissue resolution. Another way of increasing spatial resolution is to decrease section thickness or to manipulate other factors such as pixel size, width of the detector, spacing between detectors, number of projections obtained in focal spot size.

Contrast resolution or **tissue resolution** describes the ability of a CT scanner to differentiate the small attenuation differences on the image. Tissue absorption which is expressed with a linear attenuation coefficient depends on the thickness of the material, its density, atomic number and photon energy. Contrast resolution is also limited by noise; as noise increases, the contrast resolution decreases. During the reconstruction process the standard or smoothing algorithm can be used to enhance contrast resolution.

Linearity describes the accuracy between the linear attenuation coefficient and the computer assigned CT number (a number assigned to each pixel).

2.3.2 GEOMETRIC DISTORTIONS

In addition to the characteristics mentioned above the outcome of a CT image is also affected by geometric distortions. Those are scaling distortion and shearing distortion. The first can be introduced by, for example, incorrectly reported scanner table speed, while the latter can be caused by, for example, incorrectly reported gantry tilt or table bending due to patient's weight [Breeuwer *et al.*, 1999; Zylka and Wischmann, 1996].

2.3.3 CT VS MRI

Different imaging modes associated with MRI enhance the sensitivity and specificity of MRI. As a result the MRI is able to differentiate to a greater degree between soft tissues than CT [Hagemann and Cummins, 1983]. This is especially significant with respect to pathological lesions and tumours. Therefore MRI has become the preferred method for use in neuroimaging. However, MRI is usually not widely available as a diagnostic tool and it is considerably more expensive than CT. On the other hand CT continues to advance technologically which means that it is unlikely to be totally superseded by MRI in the near future.

2.3.4 NEUROIMAGING

A 2D picture obtained for example by CT scanning consists of pixels. The 3D equivalent to the pixel, which usually has the shape of a cube, is referred to as voxel. When imaging a slice, it is supposed to be one voxel thick, so that each voxel is represented by one pixel in the resulting image. Typical brain images are, for instance, 256 x 256 pixels. In a CT greyscale image, attenuation values determine the pixel brightness. The latter has values between 0 (black) and 1 (white). This range is divided into 256 grades of grey, which is approximately the range that can be distinguished by a typical human vision.

The quantification of attenuation values is expressed by a CT number. When the CT number is given in the Hounsfield unit it is expressed as:

$$CTnumber = 1000\frac{\mu_{tissue} - \mu_{water}}{\mu_{water}}, \tag{2.48}$$

where μ is linear attenuation coefficient [Duliu, 1999]. The linear attenuation coefficient of water is 0.21. The CT number assigned to water has value 0, the bone and contrast agents have value 1000, white matter has value 15 and grey matter 18, while fat has -100 and air -1000 [Goodwin and Tan, 2003]. A conversion factor relates the range of CT numbers to 0-255 graded greyscale represented in CT image. The conversion factor can be varied for display purposes, by a procedure called windowing.

3 SIMULATION ENVIRONMENT FOR MONITORING PERMEABILISATION BASED ON TIME DISCRETE MODEL OF TISSUE PERMEABILISATION

Permeability of cell membrane changes due to exposure to external electric field (E) above threshold value and consequently, the conductivity of the corresponding tissue changes. Changes in bulk tissue conductivity could be then considered as an indicator of tissue permeabilisation [Abidor *et al*., 1993]. However the change in bulk tissue conductivity does not provide enough information by itself to determine the efficacy of permeabilisation. In clinical applications of permeabilisation, such as electrochemotherapy, permeabilisation is efficient when all parts of the tumour are exposed to E intensities above reversible threshold. The tumour is then permeabilised and the passage of the chemotherapeutic is enabled. Similarly for *in vivo* electrogenetransfer the whole volume of tissue of interest must be exposed to E intensities above reversible threshold but at the same time remain below irreversible threshold. In this way the entrance of DNA is facilitated and cells are preserved against irreversible damage which can be caused by too high E intensities. Thus for efficient tissue permeabilisation we need to know for each point of tissue whether it was exposed to E intensities which correspond to the particular purpose of the treatment. Such information however can not be obtained by measuring the change in bulk tissue conductivity.

The efficacy of permeabilisation can be determined by means of a permeabilisation model. Having a model that describes E distribution by considering the change in tissue specific conductivity due to permeabilisation in the whole volume of tissue at the applied pulse amplitude is important not only for estimating the efficacy of permeabilisation after the therapy but above all to determine the pulse amplitude before the therapy for effective tissue permeabilisation.

In this chapter we present an analytical model of tissue permeabilisation, which describes E distribution in tissue at discrete time steps during permeabilisation. The model geometry consists of two concentric cylindrical electrodes and tissue placed in between. Such geometry was chosen because E distribution between two concentric electrodes can be described analytically. Another reason for choosing such geometry was that it provides inhomogeneous E distribution similar to the distribution around needle electrodes, which are used for clinical treatment of deeply seated tissue. In this respect the presented analytical model could assist in determination of optimal pulse amplitude for effective tissue permeabilisation in a non-invasive way before the treatment.

The idea behind the time discrete permeabilisation model is to compute changes in specific tissue conductivity at discrete time steps due to exposure to E intensities according to a given dependency between specific conductivity and E intensity - $\sigma(E)$. The E distribution computed having considered changed specific tissue conductivity is then used to determine the extent of tissue permeabilisation. In the model we assumed different $\sigma(E)$ dependencies such as stepwise, linear, exponential and S-shaped.

The time discrete model is incorporated into a simulation environment that enables monitoring of permeabilisation by displaying E distribution, specific conductivity, and the area (volume) of permeabilised tissue influenced by different pulse amplitudes, distances between electrodes and tissue electric properties (conductivities of non-permeabilised and permeabilised tissue). The influence of those parameters as well as different functional dependencies on the course of permeabilisation was also systematically examined by performing a model parameteric study. As the impact of functional dependency σ(E) on tissue permeabilisation was established to be important, an approach towards determination of σ(E) dependency was proposed later in this chapter. The approach combines the experimental data, which should be obtained by *in vivo* experiments and the model of E distribution.

While in the simulation environment we assumed the application of rectangular pulses, we further investigated the influence of the shape of the pulse applied (ramp signals) on the dynamics and extent of permeabilisation.

As the objective of effective tissue permeabilisation is to expose a predefined volume of tissue to adequate E intensities, we also examined the possibility of real time control of the extent of permeabilisation. Thus we incorporated the model in a closed loop control scheme with a proportional integral controller, which was required to manipulate the extent of permeabilisation by changing pulse amplitude to be as close as possible to the goal of effective tissue permeabilisation.

We also compared the results of the time discrete permeabilisation model with analytical description of E distribution for different functional dependencies σ(E) with results computed by the time discrete model where E distribution was computed by means of a numerical model (finite element model) on the same geometry. The methodology of the latter is described in detail in Chapter 5. By comparing the two models we tested the results and examined the advantages and disadvantages of numerical modelling for use in the time discrete model.

Hereafter we will refer to the extent of permeabilisation on tissue level as the volume of tissue that was exposed to E intensities above the reversible threshold.

3.1 ANALYTICAL MODEL OF E DISTRIBUTION BETWEEN TWO CONCENTRIC CYLINDRICAL ELECTRODES

Our goal was to design an analytical model which describes changes in tissue conductivity due to applied external E as present during permeabilisation. For that purpose we selected simple geometry which allows for an analytical description of E distribution and at the same time gives a similar E distribution as experienced near needle electrodes used in clinics.

The geometry consists of two concentric cylindrical electrodes and conductive material, which represents tissue, placed between the electrodes. We assigned the inner electrode with radius R_0 potential u and the outer electrode with radius R_1 potential 0 V. A cross section of the electrodes is shown in Figure 3.1.

Electric potential between the cylindrical electrodes as a function of radius r satisfies Laplace's equation:

$$\Delta\varphi(r) = 0 \quad \text{or} \qquad \frac{1}{r}\frac{\partial}{\partial r}\left(r\frac{\partial\varphi}{\partial r}\right) = 0\,. \tag{3.1}$$

The general solution of Laplace equation is expressed as:

$$\varphi(r) = A \ln r + B\,, \tag{3.2}$$

where parameters *A* and *B* are derived from boundary conditions. We set boundary conditions by taking into account potentials on the electrodes. Considering homogenous tissue conductivity between the electrodes and by applying boundary conditions we obtain the solution for potential and E respectively:

$$\varphi(r) = \frac{u(t)}{\ln\left(\frac{R_1}{R_0}\right)} \ln\left(\frac{r}{R_0}\right) \tag{3.3}$$

and

$$E = -\frac{u(t)}{\ln\left(\frac{R_1}{R_0}\right)} \frac{1}{r}\,. \tag{3.4}$$

During permeabilisation however the conductivity of tissue changes once the applied E intensity exceeds reversible threshold value. For further model derivation we assume that in the whole area where E intensity exceeds reversible threshold E_0 the conductivity increases to a constant value σ_1, while in the area where E intensity is still below E_0 tissue conductivity remains equal to σ_0 i.e. the conductivity of a non-permeabilised tissue. Such dependency between specific conductivity and the electric field σ(E) was termed a stepwise dependency.

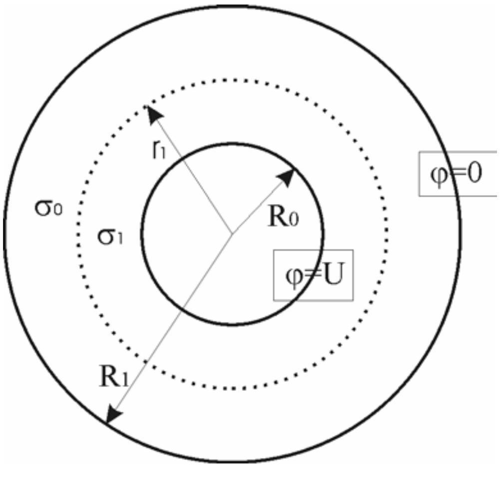

Figure 3.1: Cross section of two concentric cylindrical electrodes. The area with increased conductivity is denoted with r_1.

Where a given value of reversible threshold E_0 is higher than $E(R_0)$ and lower than $E(R_1)$ the conductivity of the material where $E>E_0$ changes to σ_1. As a consequence we obtain material with two different conductivities as shown in Figure 3.1.

The potential in material with two different conductivities is then described by:

$$\varphi_1(r) = A \ln r + B \qquad \text{for} \qquad R_0 \le r \le r_1\,, \tag{3.5}$$

$$\varphi_0(r) = C\ln r + D \qquad \text{for} \qquad r_1 \le r \le R_1\,. \tag{3.6}$$

By considering the following boundary conditions:

$$\varphi_1(R_0) = u(t)\,, \quad \varphi_0(R_1) = 0\,, \quad \varphi_1(r_1) = \varphi_0(r_1)\,, \quad \sigma_1\frac{\partial\varphi_1(r_1)}{\partial r} = \sigma_0\frac{\partial\varphi_0(r_1)}{\partial r}\,, \tag{3.7}$$

we obtain parameters A, B, C and D:

$$A = -\frac{u(t)}{\ln\left(\frac{r_1}{R_0}\right) + \frac{\sigma_1}{\sigma_0}\ln\left(\frac{R_1}{r_1}\right)}\,, \tag{3.8}$$

$$B = u(t)\left[1 + \frac{\ln R_0}{\ln\left(\frac{r_1}{R_0}\right) + \frac{\sigma_1}{\sigma_0}\ln\left(\frac{R_1}{r_1}\right)}\right], \tag{3.9}$$

$$C = -\frac{\sigma_1}{\sigma_0}\frac{u(t)}{\ln\left(\frac{r_1}{R_0}\right) + \frac{\sigma_1}{\sigma_0}\ln\left(\frac{R_1}{r_1}\right)} \quad \text{and} \tag{3.10}$$

$$D = \frac{\sigma_1}{\sigma_0}\frac{u(t)\ln R_1}{\ln\left(\frac{r_1}{R_0}\right) + \frac{\sigma_1}{\sigma_0}\ln\left(\frac{R_1}{r_1}\right)}\,. \tag{3.11}$$

E intensity in the area with non-permeabilised tissue is then expressed as:

$$E(r) = -\frac{C}{r} = \frac{\sigma_1}{\sigma_0}\frac{u(t)}{\frac{\sigma_1}{\sigma_0}\ln\left(\frac{R_1}{r_1}\right) + \ln\left(\frac{r_1}{R_0}\right)}\frac{1}{r} \qquad \text{for} \qquad r_1 \le r \le R_1 \tag{3.12}$$

and in the area with permeabilised tissue as:

$$E(r) = -\frac{A}{r} = \frac{u(t)}{\frac{\sigma_1}{\sigma_0}\ln\left(\frac{R_1}{r_1}\right) + \ln\left(\frac{r_1}{R_0}\right)}\frac{1}{r} \qquad \text{for} \qquad R_0 \le r \le r_1\,. \tag{3.13}$$

The presented model describes E distribution between two concentric electrodes for the case when conductivity was increased in the part of tissue exposed to E above E_0 i.e. between R_0 and r_1. The subsequently computed E distribution could again exceed E_0 in the remaining part of the tissue with conductivity σ_0. We described the propagation of these changes within a time discrete model of tissue permeabilisation, which is described in continuation.

3.2 TIME DISCRETE MODEL OF TISSUE PERMEABILISATION WITH STEPWISE σ(E) DEPENDENCY

In the time discrete model, permeabilisation is modelled as a time discrete process, where E distribution is computed by an analytical model at time discrete steps k=0, 1 ,..N. At k=1 electric field distribution is equal to the distribution in completely non-permeabilised tissue. If E distribution at k=1 exceeds reversible threshold E_0 in part of the tissue, the conductivity of that part of the tissue is changed according to σ(E) dependency to value σ_1. In such a way the tissue specific conductivity at step k=2 is computed. Based on changed tissue conductivity, E distribution in partially permeabilised tissue at k=2 is computed analytically considering the equations presented in Chapter 3.1. Again, E distribution at k=2, provided above E_0, causes further changes in tissue conductivity at k=3. In that manner E distribution at discrete time steps is computed, until no further change in tissue conductivity due to exposure to E intensities above E_0 is obtained.

The calculation of E distribution at discrete time steps that considers the change in tissue conductivity during permeabilisation is shown in Figure 3.2.

Conductivity determination at step k from E distribution at $k-1$ is presented in Equation (3.14). The term $\sigma(r,k-1)$ is included in Equation (3.14) because the conductivity calculation also takes into account that once conductivity is increased at a particular point in tissue it can not decrease during constant pulse application. This corresponds to experimental observations that once the tissue is permeabilised it remains permeabilised at least for the duration of constant pulse application.

$$\sigma(r,k) = f(E(r,k-1),\sigma(r,k-1)) \quad \text{for} \qquad k \geq 2 \tag{3.14}$$

The functional dependency between specific conductivity and E used in the simulation environment was stepwise, as described in Chapter 3.1.

The described time discrete model simulates the propagation of tissue permeabilisation, due to exposure of tissue to E intensities above E_0. After the pulse application, reversibly permeabilised tissue reseals in two distinct stages, referred to as fast and slow resealing [Abidor *et al.*, 1993, Hibino *et al.*, 1993]. Modelling of tissue resealing was however outside the scope of this model.

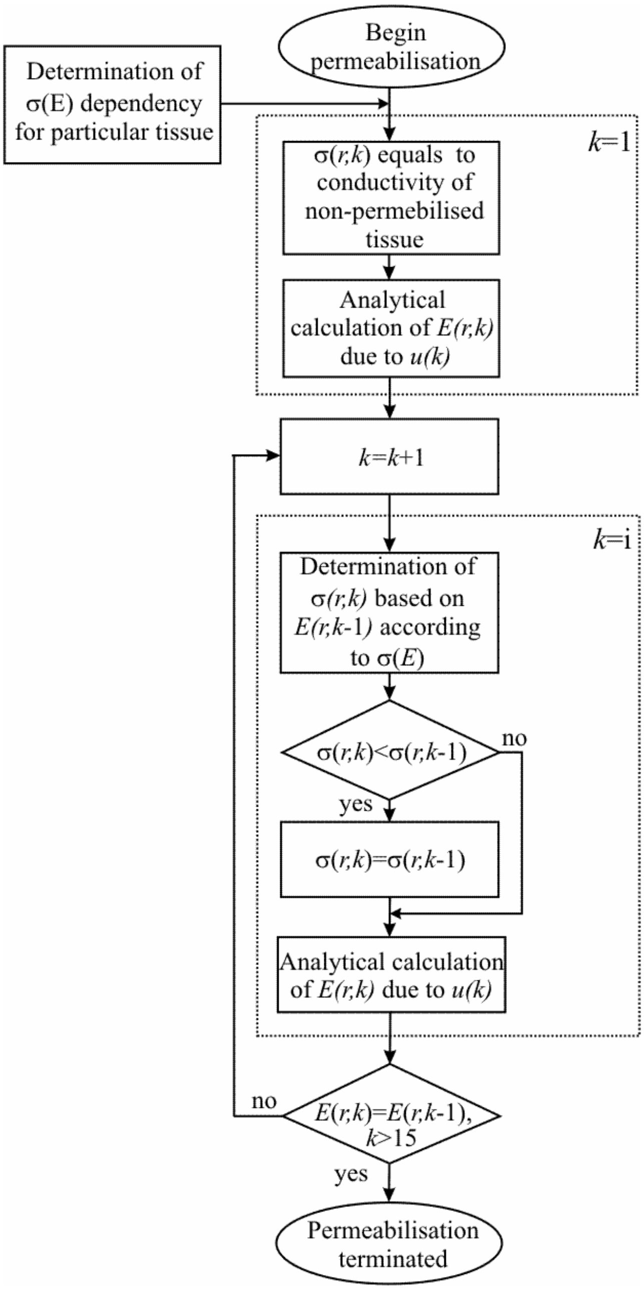

Figure 3.2: Time discrete model of tissue permeabilisation – schematic presentation.

3.2.1 SIMULATION ENVIRONMENT OF TISSUE PERMEABILISATION

The simulation environment is based on the time discrete model of tissue permeabilisation with analytical description of E distribution between two concentric electrodes. By means of the simulation environment we wanted to investigate the extent of permeabilisation in tissue at a particular pulse amplitude i.e. to determine the radius between concentric electrodes up to which tissue is permeabilised. As pulse parameters, electrode geometry and tissue electrical properties influence the course of tissue permeabilisation, a further purpose of the simulation environment was to enable monitoring of the course of tissue permeabilisation as influenced by changes in pulse amplitude, tissue geometry (distance between electrodes) and tissue electric properties (conductivity of non-permeabilised and permeabilised tissue).

3.2.1.1 GRAPHICAL INTERFACE OF SIMULATION ENVIRONMENT

We developed the graphical interface of the simulation environment presented in Figure 3.3 by means of the Matlab software (MathWorks Inc., USA). Before starting a simulation, entering of simulation parameters presented in Table 3.1 is required into the lower left window (*Parameter window*) of the graphical interface. Then the actuation of permeabilisation follows by pressing the *START permeabilisation* button. After starting the simulation, the propagation of permeabilisation is computed for 15 time discrete steps. We had determined in previous testing that this number of steps was sufficient to terminate the propagation of permeabilisation.

Table 3.1: Meaning of simulation parameters to be entered by means of the graphical interface.

Parameter	*Meaning*
R_0	Radius of inner electrode
R_1	Radius of outer electrode
Sigma0	Specific conductivity of non permeabilised tissue
Sigma1	Specific conductivity of permeabilised tissue
E0	Electric field reversible threshold
E1	Electric field irreversible threshold*
l	Cylinder electrode length
u	Pulse amplitude

**does not apply for stepwise dependency σ(E)*

The upper right window of the graphical interface displays E intensity at each time discrete step in the simulation sequence for the particular set of simulation parameters displayed in the *Parameter window*. The red line presents E distribution in non permeabilised tissue i.e. E intensity at k=1, which is used to compute conductivity at k=2. Conductivity at k=1 is equal to conductivity of non-permeabilised tissue. The green line denotes the reversible threshold E_0 and blue lines present E distribution at k=2 to k=15. We can see that at k=1 the part of tissue up to a radius of 1.6 units was exposed to E intensity above E_0 thus the conductivity there increased to σ_1. Consequently at k=2 E intensity changed at that radius according to the transient condition of a normal component of E, at the boundary of two materials with different conductivities. E distribution at k=2 caused permeabilisation of tissue up to radius 1.9 units. Following the same principle, E distribution in the next time discrete step was computed and displayed.

The upper left window shows the tissue conductivity during permeabilisation used to compute E distribution for each of 15 time discrete steps. The red line presents tissue conductivity at k=14 and blue lines present tissue conductivity at k=2 to k=13. The blue line at the top left corresponds to tissue conductivity computed from E distribution in non-permeabilised tissue. We can see that at k=2 tissue up to radius 1.6 units has increased conductivity σ_1.

The window at the lower right presents the radius at which reversible threshold is attained for each of 15 time discrete steps. Again we can observe that at k=2 the radius of permeabilised tissue was 1.6 units, at k=3 it was 1.9 units and that at the end of permeabilisation, tissue was permeabilised up to radius of approximately 2.25 units.

In the parameter window of the graphical interface, the maximum voltage denoted as *umax* is also displayed. Maximum voltage represents the pulse amplitude that can be applied to electrodes in order to not exceed irreversible threshold value anywhere between the electrodes as far as non permeabilised tissue is concerned. We can see that the selected pulse amplitude in Figure 3.3 was higher than *umax* which means that part of the tissue was exposed to E intensities above E_1. However at the end of permeabilisation E intensities in the entire area between the electrodes were below E_1. Therefore the value of *umax* is only of an informative nature and gives orientation for setting up the pulse amplitude in cases when E_1 must not be exceeded at anytime during permeabilisation. The parameter window also displays total computed current before (*i before*) and after permeabilisation (*i after*), which was computed considering equations (3.15) and (3.16) respectively:

$$i_{before} = -\frac{2\pi L \sigma_0}{\ln\left(\frac{R_1}{R_0}\right)} u(t)\,, \tag{3.15}$$

$$i_{after} = -\frac{2\pi L \sigma_1}{\ln\left(\frac{r_1}{R_0}\right) + \frac{\sigma_1}{\sigma_0}\ln\left(\frac{R_1}{r_1}\right)} u(t)\,. \tag{3.16}$$

The simulation environment revealed that for the particular set of parameters (pulse amplitude, distance between electrodes, and conductivity of permeabilised and non permeabilised tissue) only part of the area between the electrodes (up to radius 2.25 units) was permeabilised. The permeabilisation of the entire area between electrodes would therefore require a higher pulse amplitude.

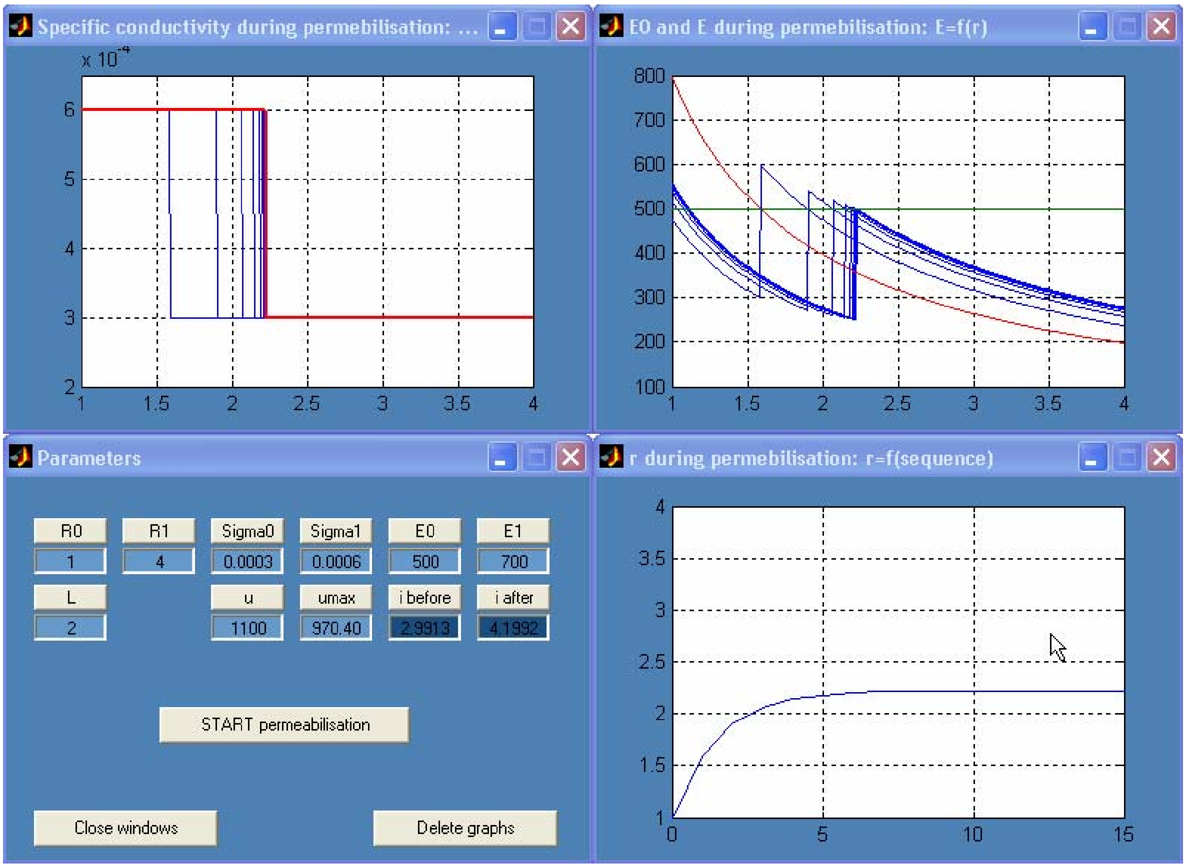

R0: 1
R1: 4
Sigma0: 0.0003
Sigma1: 0.0006
E0: 500
E1: 700
L: 2
u: 1100
umax: 970.40
i before: 2.9913
i after: 4.1992

Figure 3.3: Graphical interface of simulation environment of tissue permeabilisation between two concentric electrodes. Stepwise σ(E) dependency was employed.

3.3 TIME DISCRETE MODEL OF TISSUE PERMEABILISATION WITH ARBITRARY σ(E) DEPENDENCY

Up to this point we have considered the stepwise functional dependency σ(E). However in biological tissue it is very unlikely that such a dependency occurs. Considering differences in cell size, shape and their interaction we can expect some cells to be permeabilised before others when E above E_0 is applied. This was also observed in experiments with bleomicyn [Miklavčič *et al.*, 2000], where at the reversible threshold E_0 both normal and altered nuclei were found adjacent to each other in the middle region between the electrodes. By increasing E above E_1 the loss of viability of some cells was expected and later of all cells which lead into saturation of the σ(E) curve at increased tissue conductivity σ_1. This implies that σ(E) dependency could have a different profile than that described by a stepwise function.

For this reason we extended the simulation environment presented in Chapter 3.2.1 by adding different functional dependencies σ(E), such as linear, exponential and an S-shaped function. This however required modification of the analytical description of E distribution within the time discrete model. Thus the analytical model was modified in order to describe an arbitrary functional dependency between specific conductivity and applied E.

Modification of the analytical model was performed by dividing the region between the inner and outer electrodes into a large number of intervals denoted with *n* instead of just two as in the model previously described in Chapter 3.1. To each interval we assigned homogenous conductivity. Conductivity within each interval was changed according to a defined σ(E) function which can have an arbitrary profile.

Similar to the previous model derivation (Chapter 3.1) the electric potential in i^{th} interval out of *n* is given by

$$\varphi_i(r) = A_i \ln r + B_i \qquad \text{for} \qquad i = 1 \to n \ \text{ and } \ r_{i-1} \le r \le r_i , \tag{3.17}$$

$$\text{where} \quad r_0 = R_0 \qquad \text{and} \qquad r_n = R_1 .$$

On boundaries between two neighbouring intervals the following boundary conditions apply:

$$\begin{aligned} \varphi_1(R_0) &= u(t), \\ \varphi_i(r_i) &= \varphi_{i+1}(r_i) \qquad \text{for } i = 1 \to n-1 \ , \\ \varphi_n(R_1) &= 0, \end{aligned} \tag{3.18}$$

and

$$\sigma_i \frac{\partial \varphi_i(r_i)}{\partial r} = \sigma_{i+1} \frac{\partial \varphi_{i+1}(r_i)}{\partial r} \qquad \text{or} \qquad \sigma_i A_i = \sigma_{i+1} A_{i+1} . \tag{3.19}$$

We can derive constant *B* by writing equations (3.18) as :

$$A_1 \ln R_0 + B_1 = u(t) \Rightarrow \quad B_1 = u(t) - A_1 \ln R_0 , \tag{3.20}$$

$$A_{i+1} \ln r_i + B_{i+1} = A_i \ln r_i + B_i \ \Rightarrow \quad B_{i+1} = (A_i - A_{i+1}) \ln r_i + B_i , \tag{3.21}$$

$$A_n \ln R_1 + B_n = 0 \ \Rightarrow \quad B_n = -A_n \ln R_1 . \tag{3.22}$$

By taking into account equations (3.20) and (3.21) we can express B_{i+1} recursively:

$$B_{i+1} = -A_{i+1} \ln r_i + A_i \ln \frac{r_i}{r_{i-1}} + A_{i-1} \ln \frac{r_{i-1}}{r_{i-2}} + ... + A_1 \frac{\ln r_1}{R_0} + u(t) \quad . \tag{3.23}$$

Considering equation (3.23) for *i=n,* and the boundary condition in equation (3.22) we can express *u(t)*:

$$-u(t) = A_n \ln \frac{R_1}{r_{n-1}} + ... + A_i \ln \frac{r_i}{r_{i-1}} + ... + A_1 \ln \frac{r_1}{R_0} \qquad \text{for } i = 2 \to n-1 \, . \tag{3.24}$$

Parameter A_i can be substituted by parameter A_1 based on equation (3.20), which gives:

$$u(t) = -A_1 \left[\frac{\sigma_1}{\sigma_n} \ln \frac{R_1}{r_{n-1}} + ... + \frac{\sigma_1}{\sigma_i} \ln \frac{r_i}{r_{i-1}} + ... + \ln \frac{r_1}{R_0} \right] \text{ for } i = 2 \to n-1 \, . \tag{3.25}$$

Therefore E intensity in the first interval can be expressed as:

$$E_1 = -\frac{A_1}{r} = \frac{u(t)}{\frac{\sigma_1}{\sigma_n} \ln \frac{R_1}{r_{n-1}} + .. + \frac{\sigma_1}{\sigma_j} \ln \frac{r_j}{r_{j-1}} + ... + \ln \frac{r_1}{R_0}} \frac{1}{r} \tag{3.26}$$

and E intensity in i^{th} interval between the electrodes can be consequently expressed as:

$$E_i = -\frac{A_i}{r} = -\frac{\sigma_1}{\sigma_i} \frac{A_1}{r} = \frac{\sigma_1}{\sigma_i} \frac{u}{\frac{\sigma_1}{\sigma_n} \ln \frac{R_1}{r_{n-1}} + .. + \frac{\sigma_1}{\sigma_j} \ln \frac{r_j}{r_{j-1}} + ... + \ln \frac{r_1}{R_0}} \frac{1}{r} \, ,$$

$$\text{for} \qquad r_{i-1} \le r \le r_i \text{ and } j = 2 \to n-1 \, . \tag{3.27}$$

3.3.1 EXTENDED SIMULATION ENVIRONMENT

In addition to stepwise dependency we added linear, exponential, and S-shaped functional dependencies σ(E) into simulation environment in order to investigate the influence of different σ(E) dependencies on the course of permeabilisation. The programme code of the extended simulation environment is given in Appendix. The selection of a particular functional dependency could be performed through the *Parameter window* in the simulation environment (Figure 3.4) by pressing the corresponding button.

In the *Parameter window* we set values for reversible threshold to 300 V/unit and for irreversible threshold to 700 V/unit for all subsequent functional dependencies because we wanted to have the major part of non-permeabilised tissue exposed to E-intensities between the two threshold values. In this way we emphasised the influence of the shape of σ(E) dependency between two thresholds on the course of permeabilisation. The rest of the parameters were the same as when employing a stepwise dependency, except for parameter *B*, which was set for exponential and S-shaped dependency σ(E) separately.

Figure 3.4 presents permeabilisation propagation when linear σ(E) dependency was chosen The linear σ(E) dependency was defined as:

$$\sigma(E) = k_2 * E - n_2\,, \tag{3.28}$$

where

$$n_2 = k_2 * E_0 - \sigma_0 \tag{3.29}$$

and

$$k_2 = \frac{\sigma_1 - \sigma_0}{E_1 - E_0}\,. \tag{3.30}$$

Another reason for setting a lower value of E_0 in the *Parameter window* than for the stepwise dependency was to have with linear dependency 50 % increase in conductivity below reversible threshold used in stepwise dependency. We can see that tissue permeabilisation propagated up to a radius of 3.5 units. Change in tissue conductivity was observed only in the first three time discrete steps.

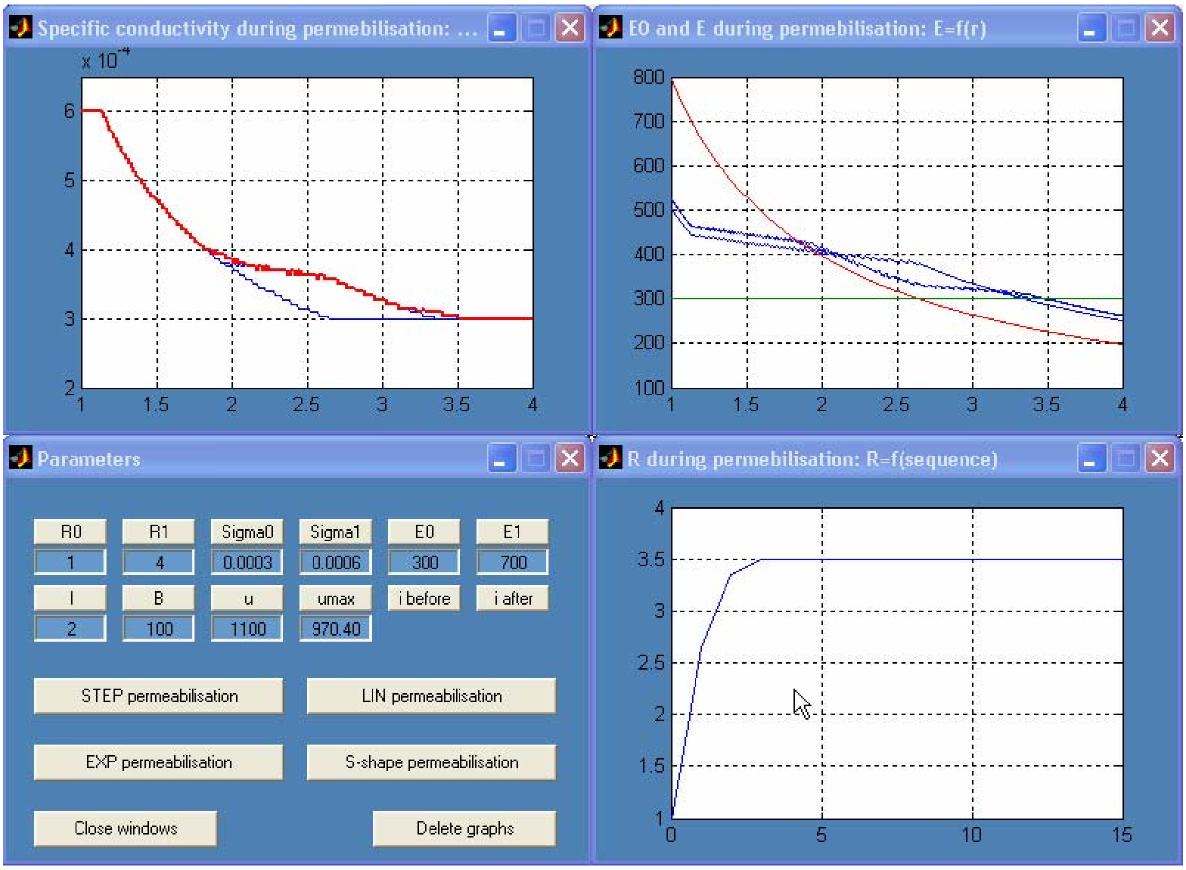

R0	R1	Sigma0	Sigma1	E0	E1
1	4	0.0003	0.0006	300	700

I	B	u	umax	i before	i after
2	100	1100	970.40		

Figure 3.4: Graphical interface of simulation environment of tissue permeabilisation between two concentric electrodes. Linear σ(E) dependency was employed.

Further, we selected exponential dependency in the simulation environment. Exponential dependency was defined as:

$$\sigma(E) = A * e^{\frac{E - E_1}{B_E} - 1} + \sigma_1\,, \tag{3.31}$$

where,

$$A = \frac{\sigma_0 - \sigma_1}{e^{\frac{E_0 - E_1}{B_E}} - 1} \tag{3.32}$$

and B_E was set to 100. Again we can observe (Figure 3.5) that permeabilisation propagation terminated rapidly. The radius of permeabilised tissue was lower than when employing linear dependency due to the gradual increase in conductivity at lower E intensities compared to linear σ(E) dependency.

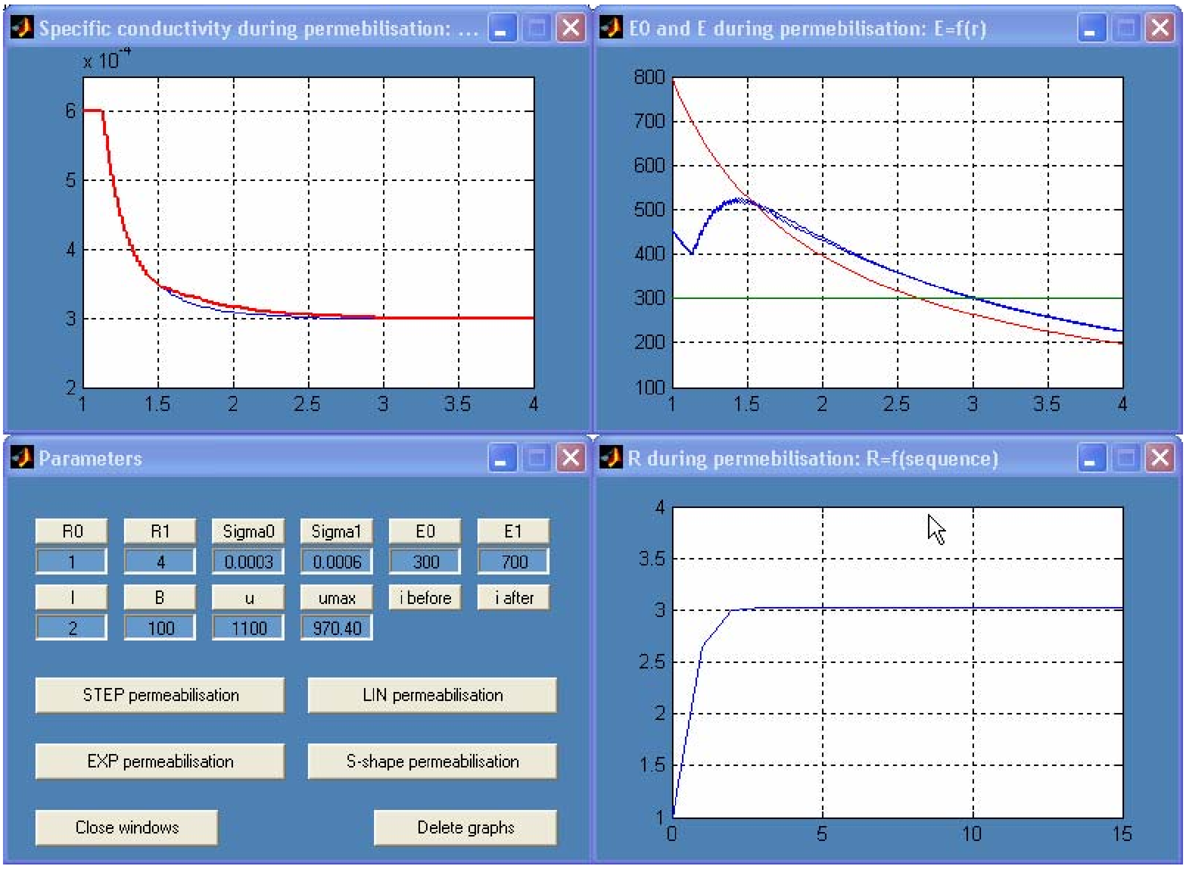

R0	R1	Sigma0	Sigma1	E0	E1
1	4	0.0003	0.0006	300	700

I	B	u	umax	i before	i after
2	100	1100	970.40		

Figure 3.5: Graphical interface of simulation environment of tissue permeabilisation between two concentric electrodes. Exponential σ(E) dependency was used.

Finally we tested the influence of S-shaped dependency (Figure 3.6). The latter was expressed as:

$$\sigma(E) = \frac{\sigma_1 - \sigma_0}{1 + De^{-\frac{E-A}{B_S}}} + \sigma_0 \,, \tag{3.33}$$

where

$$A = \frac{E_0 + E_1}{2} \,, \tag{3.34}$$

B_S=30 and D=1. The tissue was permeabilised up to a radius of 3.4 units.

Figure 3.7 presents all functional dependencies σ(E) used within the simulation environment. Based on results shown in Figure 3.3 to Figure 3.6can conclude that the extent of permeabilisation i.e. radius of permeabilisation depends on the selected functional dependency σ(E). In inhomogeneous E the impact of different functional dependencies σ(E) also depends on the volume of tissue exposed to E intensities between the two threshold values and the E field distribution between those thresholds. The important difference between stepwise dependency and other dependencies used was also that the stepwise dependency causes discontinuities in E distribution during permeabilisation, while the other dependencies produce continuous or at least piecewise continuous

E distribution. This results in smaller differences in E field distributions between the steps, which terminates propagation of permeabilisation earlier compared to the stepwise dependency.

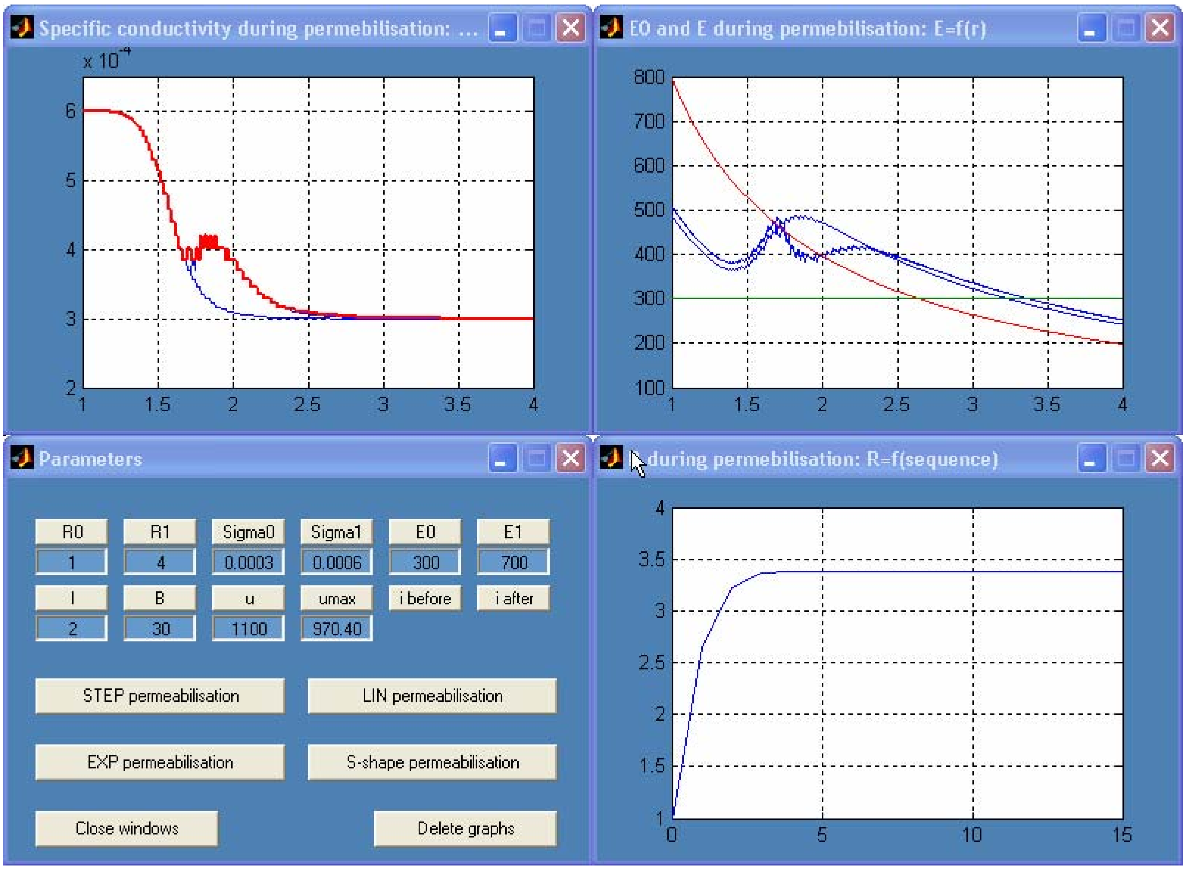

R0	R1	Sigma0	Sigma1	E0	E1
1	4	0.0003	0.0006	300	700

l	B	u	umax	i before	i after
2	30	1100	970.40		

Figure 3.6: Graphical interface of the simulation environment of tissue permeabilisation between two concentric electrodes. S-shaped σ(E) dependency was employed.

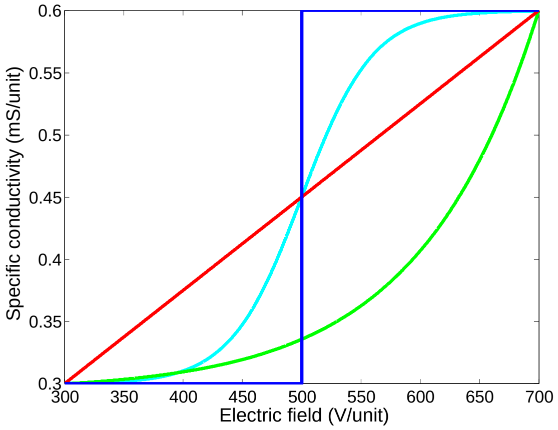

Figure 3.7: Stepwise, linear, exponential and S-shaped σ(E) dependencies used within the simulation environment.

3.4 PARAMETRIC STUDY

The purpose of the parametric study was to verify the time discrete model and to analyse the effect of tissue parameters and E distribution on the radius of permeabilisation and specific conductivity between the two concentric cylindrical electrodes at the end of permeabilisation propagation. In addition we wanted to investigate the influence of different functional dependencies σ(E) on the course of permeabilisation.

The parametric study was carried out on the time discrete model of tissue permeabilisation presented in Chapter 3.1 to Chapter 3.3. In the model we changed one parameter at a time, preserving the rest of the parameters as constants. We examined changes in tissue parameters (E_0, E_1, σ_1, B), and the parameters that influenced E distribution between the cylindrical electrodes (R_1, u). Initial values of the parameters were E_0=300 V/unit (except for stepwise σ(E) where E_0=500 V/unit), E_1=700 V/unit, σ_1=0.6 mS/unit, B_E=100, B_s=30, R_1=4 units and u=1100 V.

3.4.1 INFLUENCE OF REVERSIBLE THRESHOLD E$_0$

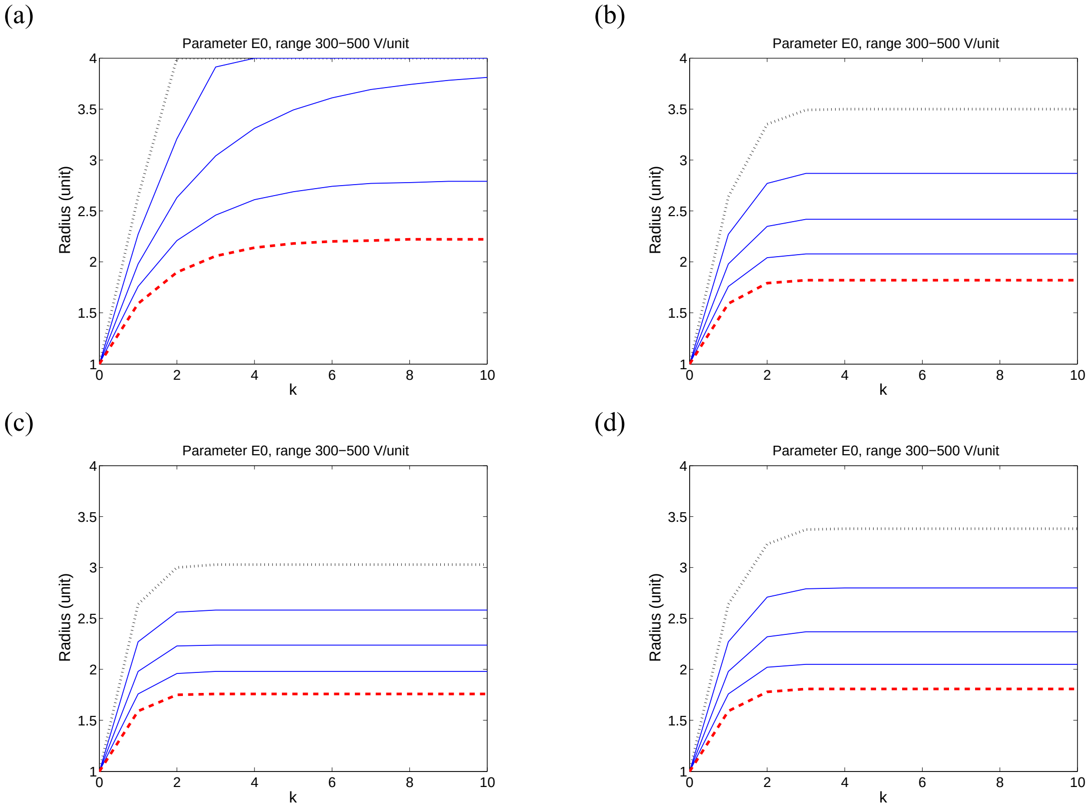

Figure 3.8: Influence of E_0 on the radius of permeabilisation for (a) stepwise, (b) linear, (c) exponential and (d) S-shaped σ(E) dependency. E_0 was changed in the range of 300 V/unit (…) to 500 V/unit (---) in increments of 50 V/unit (-).

Reversible threshold E_0 is a tissue parameter, usually referred to as key parameter for electropermeabilisation. It denotes the E intensity at which an increase in cell membrane permeability is observed and a consequent increase in tissue conductivity. Parameter E_0 is usually determined by means of rapid tests [Belehradek *et al.*, 1994; Gehl and Mir, 1999], which are sometimes combined with numerical models. The combination of rapid test and numerical model for determination of reversible threshold for muscle tissue is presented in [Gehl *et al.*, 1999] and for rabbit liver tissue in [Miklavčič *et al.*, 2000]. However, the quantitative value of reversible threshold E_0 is still unavailable for most tissues. Therefore we examined the influence of E_0 on permeabilisation.

In the analytical model we parameterized E_0 in the range 300 V/unit to 500 V/unit in increments of 50 V/unit. Figure 3.8 presents the influence of E_0 on the radius of permeabilisation between two concentric electrodes. No matter whether a stepwise, linear, exponential or S-shaped functional dependency was employed, in all cases the lower the E_0, the higher the radius of permeabilisation was obtained, as expected. In the case of stepwise dependency the whole area between the electrodes was permeabilised provided E_0 was lower than 350 V/unit, while with linear, exponential and sigmoid dependency even at E_0=300 V/unit permeabilisation did not reach the outer radius. This is due to the gradual increase of those dependencies at E_0 compared to stepwise dependency.

Figure 3.9 shows the effect of E_0 on E distribution and specific conductivity at the end of permeabilisation. The horizontal lines present parameterised reversible thresholds $E_{0.}$ We can observe discontinuities in E distribution for stepwise dependency which reflected in a higher average number of time discrete steps (6) required for termination of permeabilisation than in the case of other dependencies (3). In general at lower E_0 we obtained lower E intensities and higher specific conductivities in regions where tissue was reversibly permeabilised.

Specific conductivity at the end of permeabilisation also differed for different dependencies σ(E). Linear, exponential and S-shaped dependencies had a small area of tissue irreversibly permeabilised compared to stepwise dependency. Despite similar radii of permeabilisation and irreversibly permeabilised tissue obtained by the linear and S-shaped dependency, the specific conductivity differed in the area between the two thresholds. This difference would reflect in the total current between electrodes which is how it could be measured.

Based on the fact that at lower E_0 a larger area of tissue was permeabilised and also that specific conductivity between electrodes at the end of permeabilisation depended on E_0, we have to emphasise again the importance of knowing E_0 in advance for effective tissue permeabilisation.

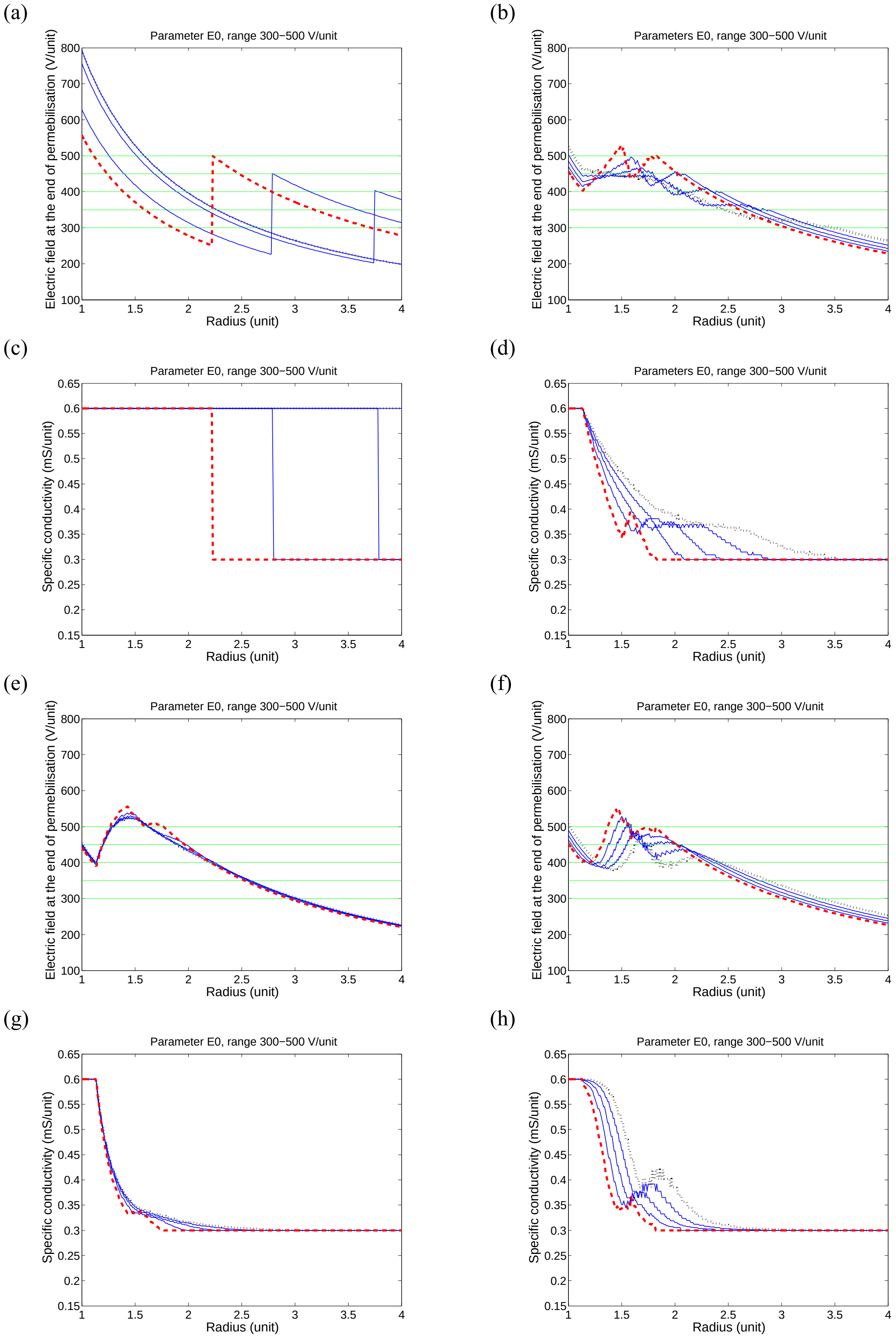

Figure 3.9: Influence of E_0 on E distribution and specific conductivity at the end of permeabilisation respectively for (a) and c) stepwise, (b) and (d) linear, (e) and g) exponential and (f) and (h) S-shaped σ(E) dependency. E_0 was changed in the range of 300 V/unit (…) to 500 V/unit (---) in increments of 50 V/unit (-). Horizontal lines present permeabilisation threshold E_0.

3.4.2 INFLUENCE OF IRREVERSIBLE THRESHOLD E_1

Apart from the reversible threshold E_0, the irreversible threshold E_1 also plays an important role in tissue permeabilisation, especially for the case of electro gene transfer. Namely, E_1 is a tissue parameter at which cell necrosis occurs which is to be avoided in electro gene transfer. Values of E_1 are even more rarely reported in literature than values of E_0. Determination of E_1 for rabbit liver tissue is presented in [Miklavčič *et al.*, 2000]. We examined the influence of E_1 by changing its value in the range of 700 V/unit to 900 V/unit in increments of 50 V/unit.

Figure 3.10 presents the radii of reversible permeabilisation for different values of E_1. As expected in the case of stepwise dependency E_1 does not influence the radius of permeabilisation. However, in the case of other dependencies as E_1 increases, the radius of permeabilisation decreases.

Specific conductivity at the end of permeabilisation (Figure 3.11) reveals that by increasing E_1 the area of irreversibly permeabilised tissue decreases, which was expected. That was clearly visible in the case of linear and exponential dependency; while in the case of S-shaped dependency it was not so pronounced. The reason was in the quite flat shape of the S-shaped dependency near E_1. Further, with all dependencies, excluding stepwise, when increasing E_1, we obtained lower values of specific conductivity in the area between the two thresholds.

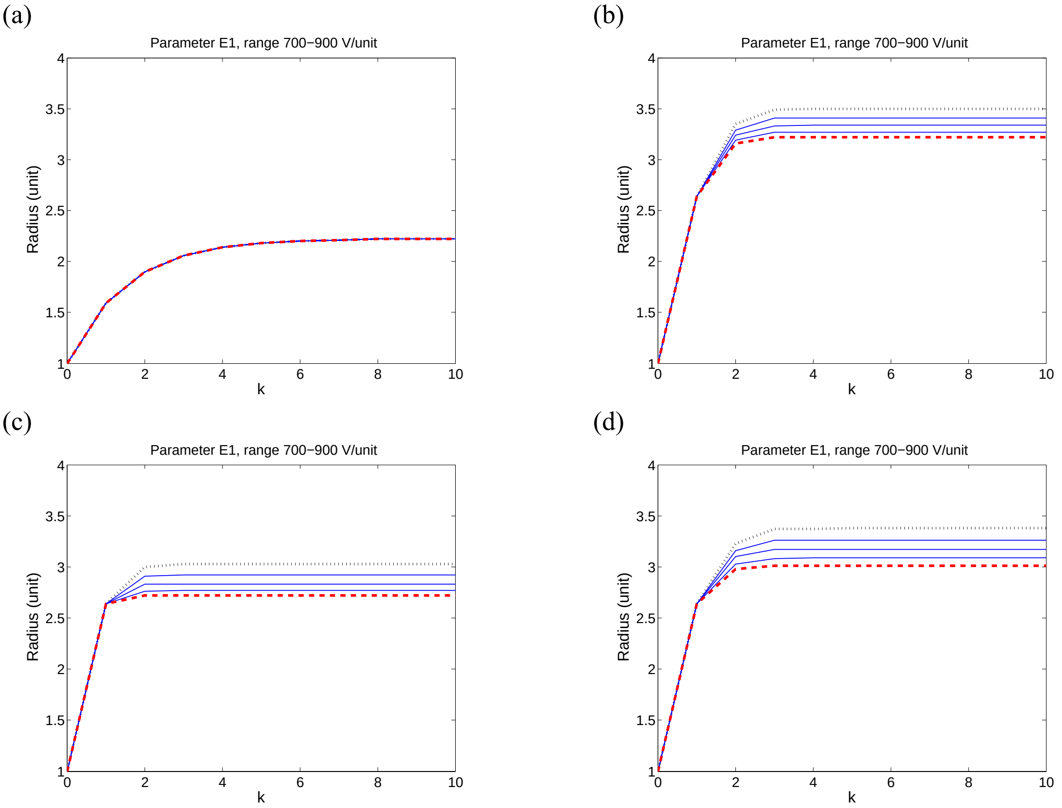

Figure 3.10: Influence of E_1 on radius of permeabilisation for (a) stepwise, (b) linear, (c) exponential and (d) S-shaped σ(E) dependency. E_1 was changed in the range of 700 V/unit (…) to 900 V/unit (---) in increments of 50 V/unit (-).

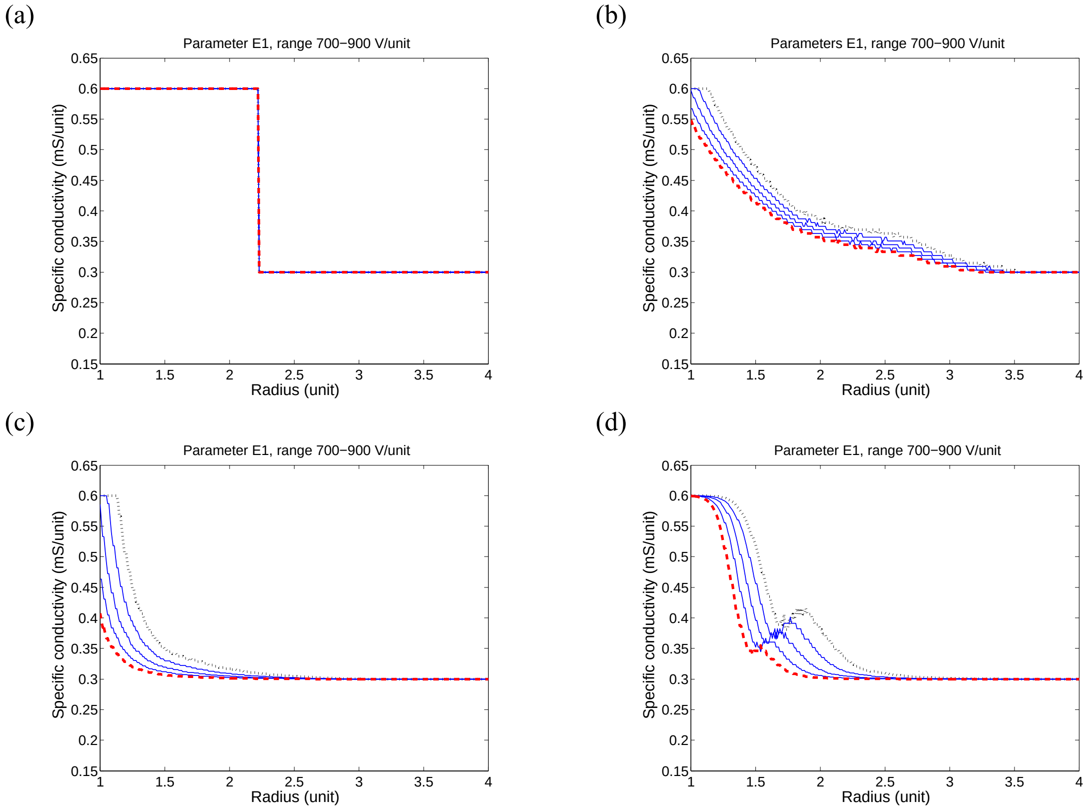

Figure 3.11: Influence of E_1 on specific conductivity at the end of permeabilisation for (a) stepwise, (b) linear, (c) exponential and (d) S-shaped σ(E) dependency. E_1 was changed in the range of 700 V/unit (…) to 900 V/unit (---) in increments of 50 V/unit (-).

3.4.3 INFLUENCE OF MAXIMUM CONDUCTIVITY OF PERMEABILISED TISSUE σ_1

Specific conductivity is a tissue electrical parameter. For most biological tissues, values of specific conductivity can be found in literature [Rush *et al.*, 1963; Schwan, 1963; Gedded and Baker, 1967; Faes *et al.*, 1999], but there are not many reports in literature about maximum conductivity of permeabilised tissue. Therefore we examined how the maximum conductivity of permeabilised tissue σ_1 affects permeabilisation. We parameterized σ_1 in the range of 0.4 mS/unit to 0.75 mS/unit.

In Figure 3.12 we can see that the higher the maximum conductivity of permeabilised tissue, the larger the radius of permeabilisation. We can also observe a difference in radius of permeabilisation obtained with various σ(E) dependencies. The largest radius was attained with the linear dependency, while the smallest was obtained with the stepwise dependency. However at k=1 the tissue was permeabilised up to the same radius no matter which functional dependency was used, because it depended solely on the E distribution in non-permeabilised tissue and E_0.

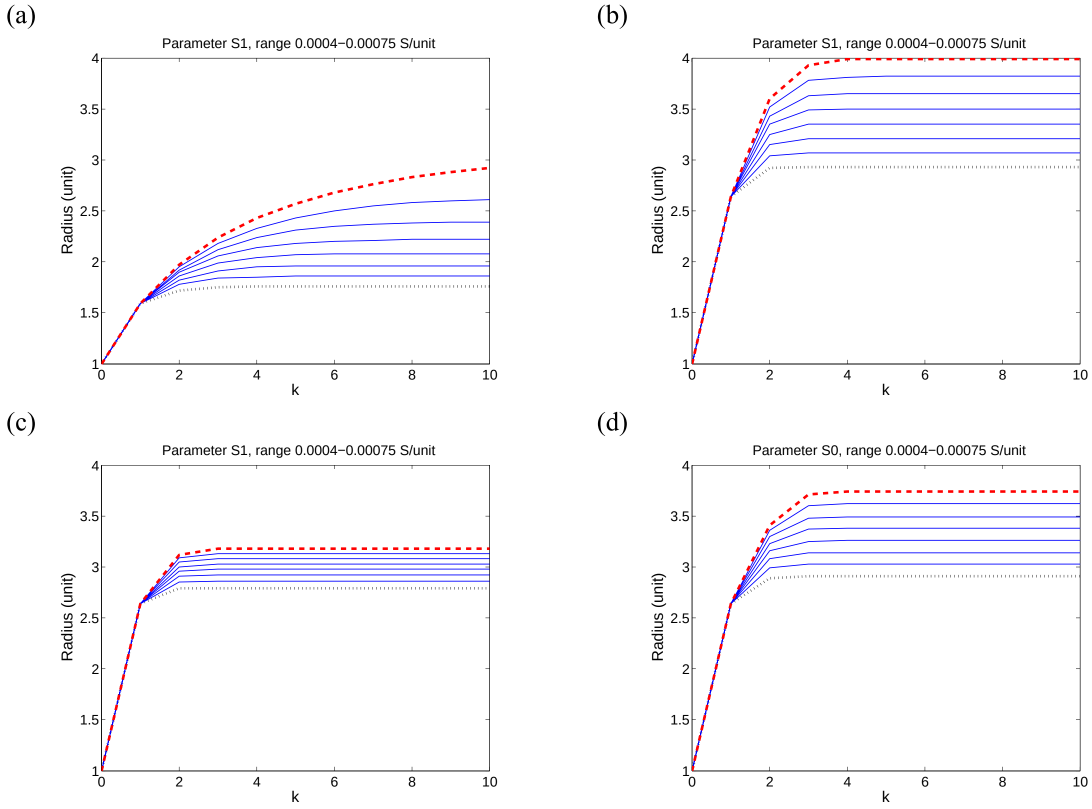

Figure 3.12: Influence of σ_l on radius of permeabilisation for (a) stepwise, (b) linear, (c) exponential and (d) S-shaped σ(E) dependency. σ_l was changed in the range of 0.4 mS/unit (…) to 0.75 mS/unit (---) in increments of 0.05 mS/unit (-).

Figure 3.13 presents specific conductivity at the end of permeabilisation. We can see that areas of irreversibly permeabilised tissue differ among the various dependencies. The largest was obtained with stepwise dependency. Further we observed that by increasing σ_l, conductivity between the two thresholds also increased, which would in turn give higher currents.

3.4.4 INFLUENCE OF OUTER CYLINDER DIAMETER R_1

The diameter of electrodes influences the E distribution between the electrodes as described in Equation (3.27). The effect of the change in distance between cylindrical electrodes is also similar to the effect of the change in distance between two needle electrodes inserted in tissue. To examine the influence of inter-electrode distance on tissue permeabilisation, we parameterised the diameter of the outer electrode from 4 units to 6 units in increments of 0.4 units.

According to equation (3.4) E distribution in non-permeabilised tissue at a particular radius depends on the natural logarithm of ratio between the outer and the inner electrode. The smaller the distance between the electrodes, the larger E intensity at a particular point between the electrodes. Therefore by increasing R_1, E intensities were lower in the area between the electrodes and consequently less tissue permeabilised as shown in Figure 3.14. On top of that, with larger R_1, lower E intensities were present near the inner electrode, which resulted in a smaller area of permeabilised tissue with maximal conductivity (Figure 3.15).

Therefore by changing the position of the electrodes we can influence the amplitude and degree of inhomogeneity of E distribution. Consequently we can control the area of reversibly permeabilised tissue.

Such information is very important in electrochemotherapy and for gene transfer when determining the position of needle electrodes, which produce a similar inhomogeneous E distribution.

Comparison of results in Figure 3.14 and Figure 3.15 between different functional dependencies revealed that the largest radius of permeabilisation was obtained with the linear dependancy followed by the sigmoid, exponential and finally stepwise dependency.

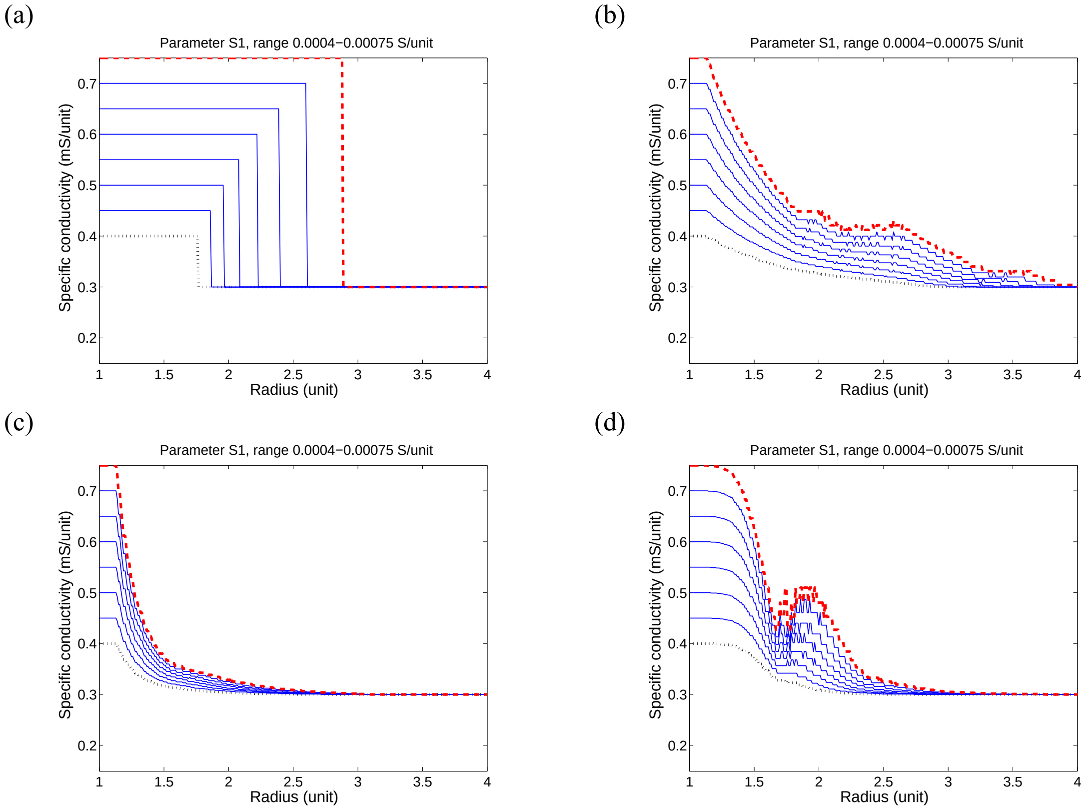

Figure 3.13: Influence of σ_l on specific conductivity at the end of permeabilisation for (a) stepwise, (b) linear, (c) exponential and (d) S-shaped σ(E) dependency. σ_l was changed in the range of 0.4 mS/unit (…) to 0.5 mS/unit (---) in increments of 0.75 mS/unit (-).

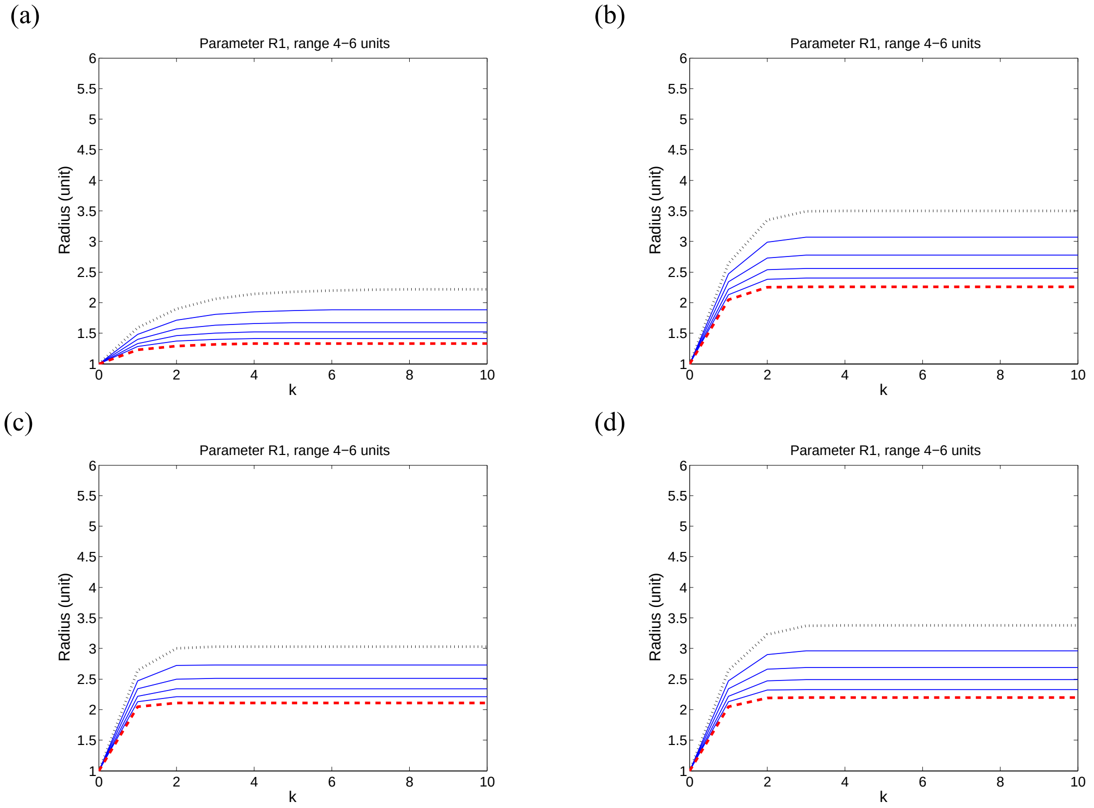

Figure 3.14: Influence of R_1 on radius of permeabilisation for (a) stepwise, (b) linear, (c) exponential and (d) S-shaped σ(E) dependency. R_1 was changed in the range 4 units (…) to 6 units (---) in increments of 0.4 unit (-).

3.4.5 INFLUENCE OF PULSE AMPLITUDE U

Pulse amplitude *u* is the parameter usually used to control the extent of permeabilisation. By increasing pulse amplitude, E intensity at a particular point in tissue increases. The effect is similar to the previously described influence of changes in cylinder diameter.

For illustration of the impact of *u* on permeabilisation we parameterised *u* in the range of 900 V to 1150 V. As expected at higher *u* the radius of permeabilisation was larger (Figure 3.16). Further, we observed that amongst the different functional dependencies linear dependency resulted in a larger radius, then sigmoid, exponential and stepwise dependency followed.

Specific conductivity in the area between the two threshold values was higher when higher pulse amplitudes were applied (Figure 3.17), which was also in accordance with experimental observations.

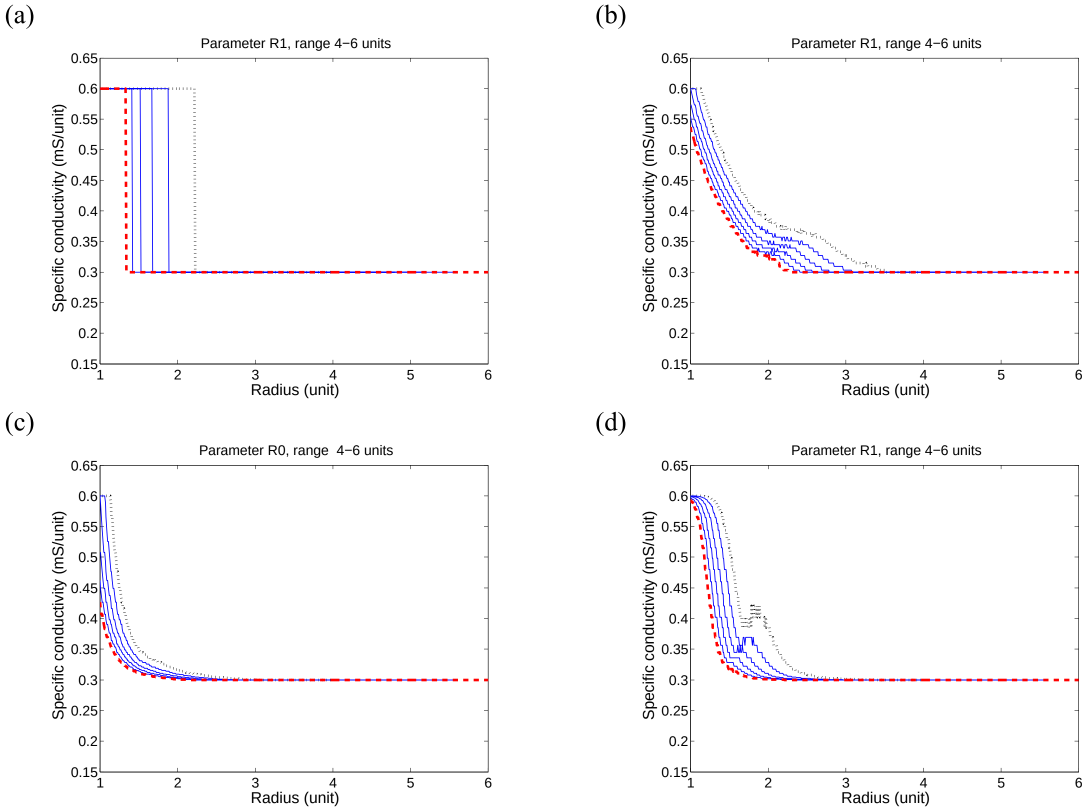

Figure 3.15: Influence of R_1 on specific conductivity at the end of permeabilisation for (a) stepwise, (b) linear, (c) exponential and (d) S-shaped σ(E) dependency. R_1 was changed in the range of 4 units (…) to 6 units (---) in increments of 0.4 unit (-).

3.4.6 INFLUENCE OF PARAMETER B_S IN S-SHAPED FUNCTIONAL DEPENDENCY

We can consider parameter B_S as a tissue parameter, provided specific conductivity in tissue follows an S-shaped dependency. Namely, parameter B_S in an S-shaped dependency defines the steepness of the function: the smaller the value of B_S the steeper the S-shaped dependency. We parameterised B_S in the range 20 to 50, to observe its impact on the course of permeabilisation between two concentric electrodes.

In Figure 3.18 we can see that the steepness of the S-shaped dependency did not significantly influence the radius of permeabilisation, with lower B_S values the decrease in radius was hardly visible. However it had some impact on specific conductivity at the end of permeabilisation between the two threshold values. At higher E intensities (close to the inner electrode) the lower the B_S the higher the specific conductivity, while at lower E intensities (closer to the outer electrode) the lower the B_S the lower the specific conductivity.

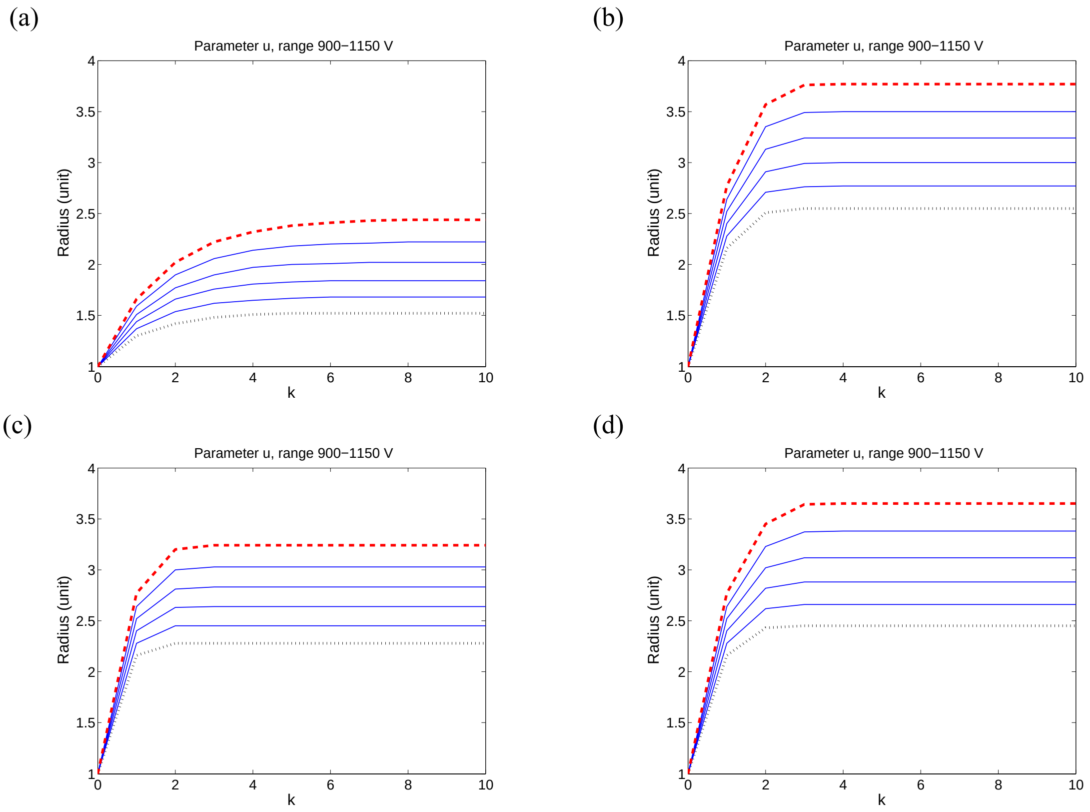

Figure 3.16: Influence of pulse amplitude *u* on the radius of permeabilisation for (a) stepwise, (b) linear, (c) exponential and (d) S-shaped σ(E) dependency. *u* was changed in the range of 900 V (…) to 1150 V (---) in increments of 50 V (-).

3.4.7 INFLUENCE OF PARAMETER B_E IN EXPONENTIAL FUNCTIONAL DEPENDENCY

Similarly to the S-shaped dependency, in exponential dependency, parameter B_E also reflects tissue properties: the smaller the parameter B_E, the steeper the exponential dependency. We were changing parameter B_E in the range of 60 to 160 in increments of 20. As shown in Figure 3.19 a steeper exponential dependency σ(E) resulted in a smaller radius of permeabilisation. A steeper dependency σ(E) also caused lower specific conductivity between the two thresholds.

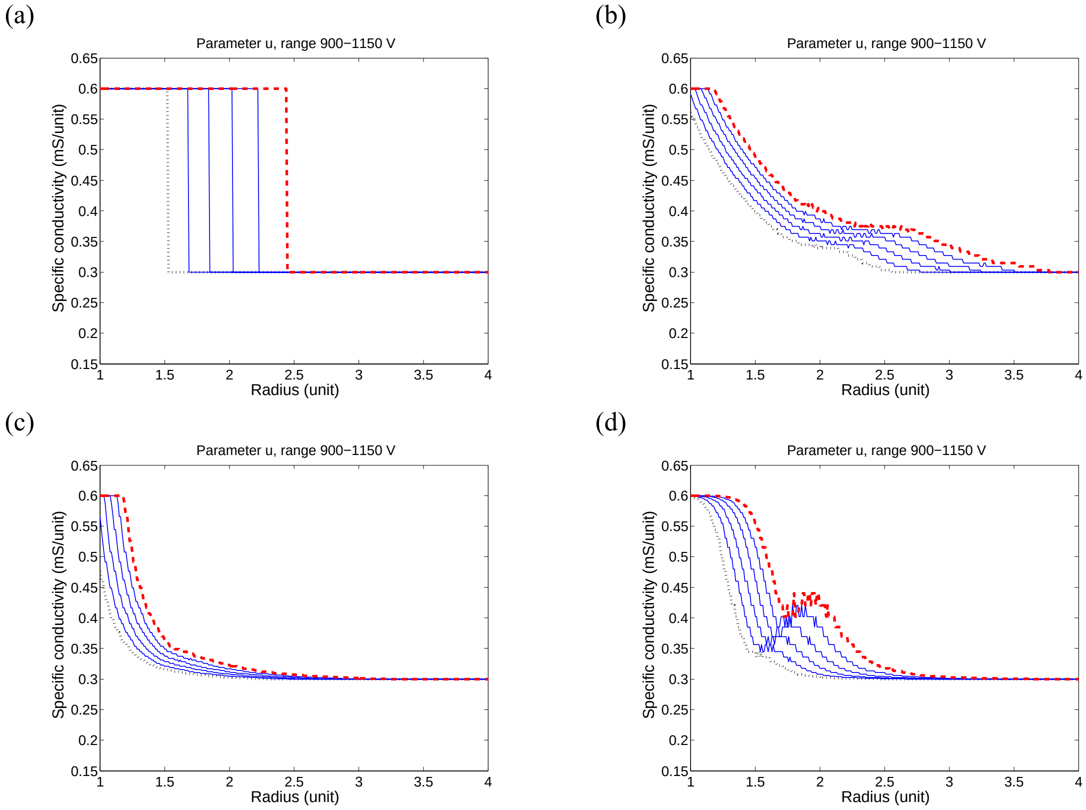

Figure 3.17: Influence of pulse amplitude *u* on specific conductivity at the end of permeabilisation for (a) stepwise, (b) linear, (c) exponential and (d) S-shaped σ(E) dependency. *u* was changed in the range of 900 V (…) to 1150 V (---) in increments of 50 V (-).

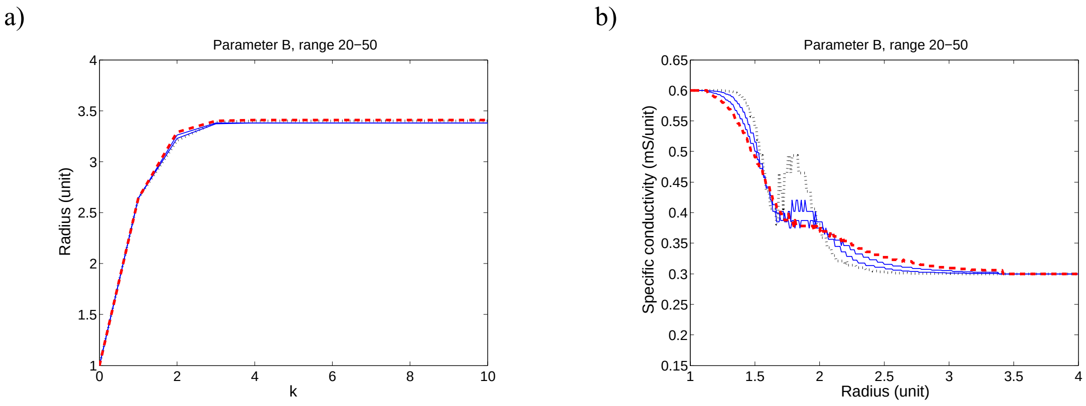

Figure 3.18: Influence of parameter B_S in S-shaped functional dependency σ(E) on (a) radius and (b) E distribution at the end of permeabilisation. Parameter B_S was changed in the range of 5 (…) to 55 (---) in increments of 10 (-).

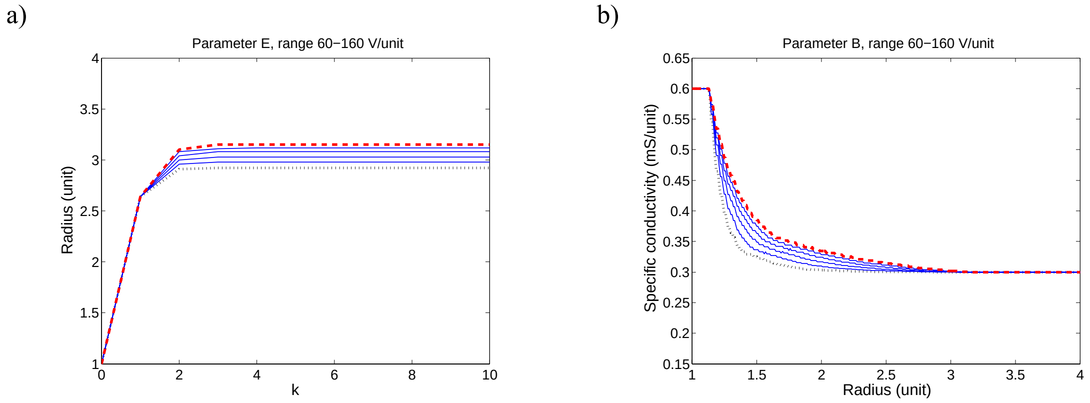

Figure 3.19: Influence of parameter B_E in exponential functional dependency σ(E) on (a) radius and (b) E distribution at the end of permeabilisation. Parameter B_E was changed in the range of 60 (…) to 160 (---) in increments of 20 (-).

3.5 INFLUENCE OF THE SHAPE OF INPUT SIGNAL

Within the simulation environment and parameteric study we assumed the application of rectangular pulses due to the fact that the use of rectangular pulses has been found to have many advantages over other pulse shapes as described in Chapter 1.8. These advantages are the reason that rectangular pulses are predominantly used in *in vivo* applications of tissue permeabilisation.

Having a time discrete model of tissue permeabilisation we can however examine tissue permeabilisation for other pulse shapes, including shapes which have not been tested experimentally yet. In this chapter we therefore examined the influence of ramped signals i.e. linearly decreasing and linearly increasing pulses on the course of tissue permeabilisation.

Figure 3.20 to Figure 3.23 present tissue permeabilisation when stepwise, linear, exponential and S-shaped σ(E) dependencies were used in the model, respectively. The left hand side of each figure presents the input signal and results computed by the time discrete model when a linearly increasing input signal was applied. Equivalently, the right hand side presents the input signal and results for the case of linearly decreasing input signal application. On each side, in the first row the input signal of duration 15 time units is displayed. The minimum amplitude of the input signal was 500 V, while the maximum was 1000 V. Below the input signal, the E distribution at time discrete steps during permeabilisation is shown, followed by the specific conductivity in the line below. At the bottom, the radius of tissue permeabilisation for each time discrete step is presented.

In Figure 3.20 to Figure 3.23 we can see that when a linearly increasing input signal is applied E distribution in permeabilised tissue is actually higher than when a linearly decreasing input signal is applied. This is due to the fact that with a linearly increasing input signal, at the beginning of pulse application less tissue is permeabilised at the particular time discrete step than with a linearly decreasing signal. The tissue permeabilisation with the latter signal is already complete after the first two or three time discrete steps. Also in case of σ(E) dependencies other than stepwise, the change in tissue conductivity at the beginning of a linearly increasing pulse application is smaller than in the case of a linearly decreasing signal. The latter maximally increases the tissue conductivity at the beginning of pulse application. Considering all the cited reasons, the voltage drop in permeabilised tissue is thus smaller in the case of a linearly increasing input signal, resulting in higher E intensity in permeabilised tissue than in the case of a linearly decreasing signal.

The comparison of radii of permeabilised tissue in Figure 3.20 to Figure 3.23 shows that the extent of tissue permeabilisation (radius up to which tissue was permeabilised) was similar no matter whether a linearly increasing or a linearly decreasing input signal was applied. However, when a linearly decreasing input signal was applied the maximal radius of permeabilisation was already obtained at the beginning of pulse application, while in the case of a linearly increasing input signal, the maximal radius of tissue permeabilisation was obtained just before the end of pulse application.

We further compared the radius of permeabilisation shown in Figure 3.20 to Figure 3.23 with the radius obtained by application of a rectangular pulse with amplitude 750 V – the average amplitude of the ramped signals. The comparison performed for all σ(E) dependencies (Table 3.2) showed that the radius of permeabilisation obtained by constant pulse amplitude was significantly smaller than the radius obtained when the ramped signals were applied. Thus we can conclude that maximal amplitude in the pulse affects the extent of permeabilisation.

Table 3.2: Extent of permeabilisation for different shapes of input signal and different dependencies σ(E).

	Linearly increasing pulse	Linearly decreasing pulse	Rectangular pulse
σ(E)	Radius of permeabilisation (unit)		
Stepwise	1.75	1.61	1.12
Linear	2.77	2.81	1.97
Exponential	2.52	2.53	1.83
S-shaped	2.63	2.72	1.89

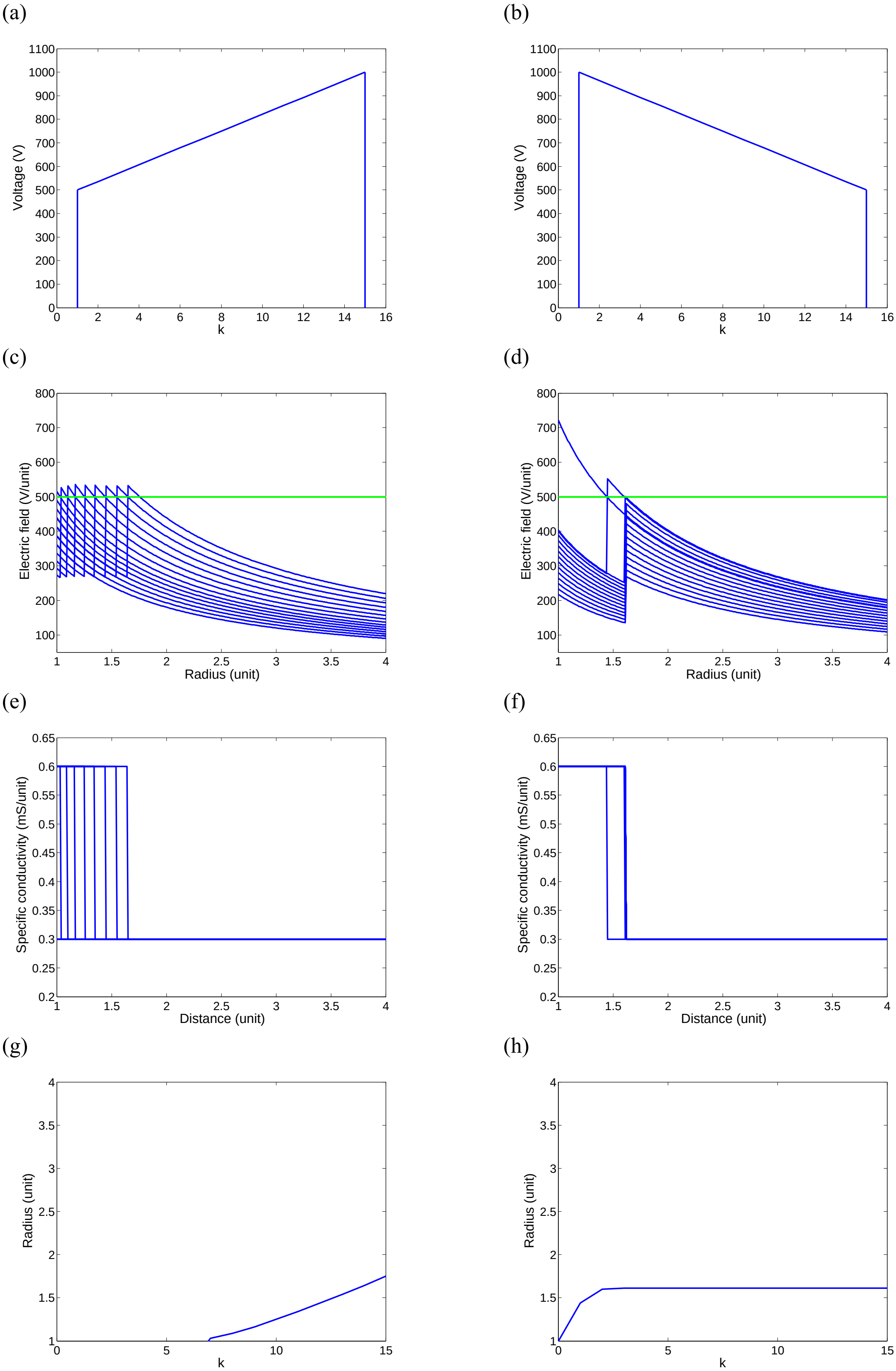

Figure 3.20: The left hand side presents the shape of a linearly increasing input signal (a) and corresponding E distribution (c), specific conductivity (e) and radius of permeabilisation (g), computed by the time discrete model. Equivalently the right hand side presents E distribution (d), specific conductivity (f) and radius of permeabilisation (h) for a linearly decreasing input signal (b). The stepwise σ(E) dependency was used.

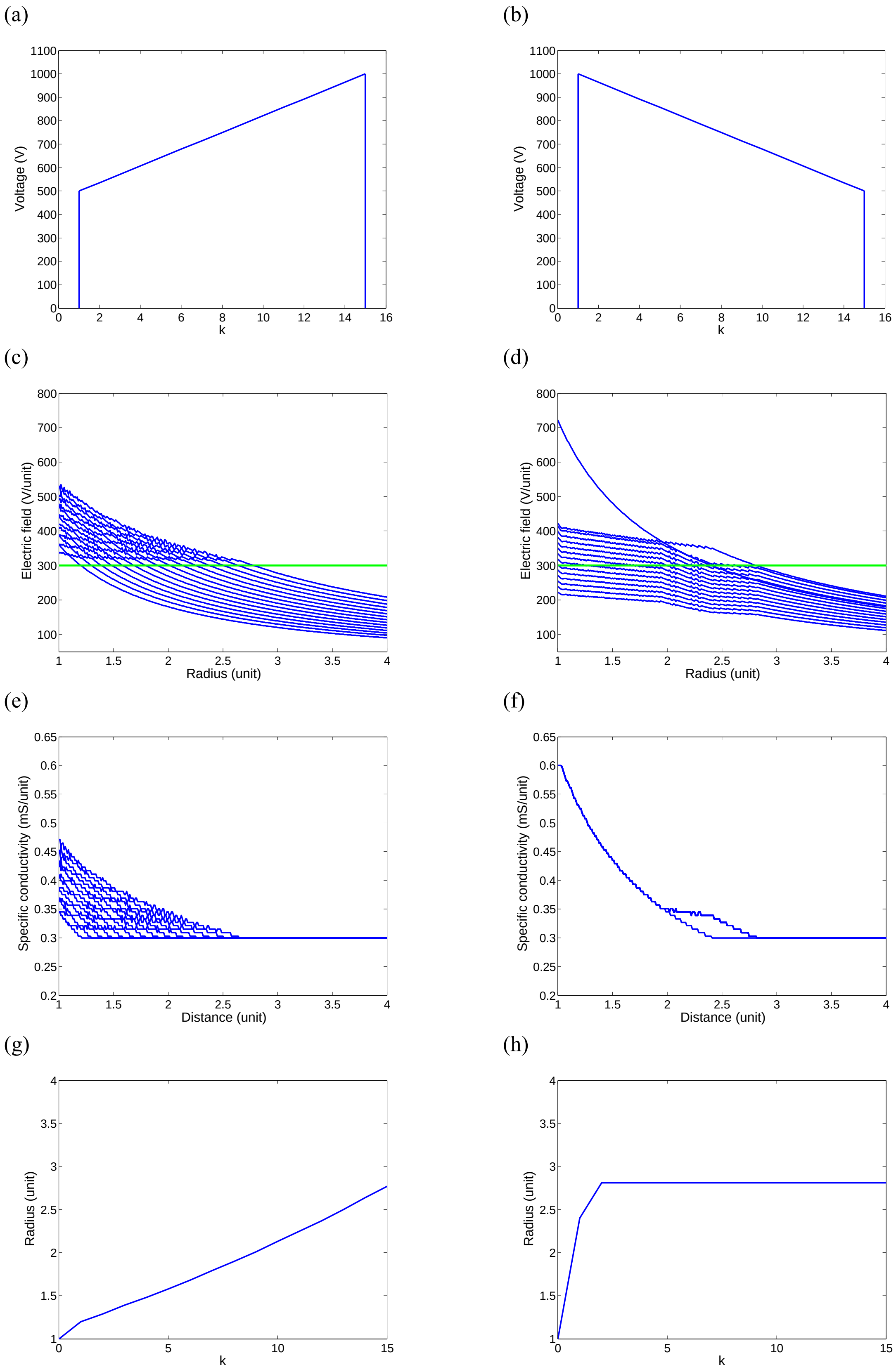

Figure 3.21: The left hand side presents the shape of a linearly increasing input signal (a) and corresponding E distribution (c), specific conductivity (e) and radius of permeabilisation (g), computed by the time discrete model. Equivalently the right hand side presents E distribution (d), specific conductivity (f) and radius of permeabilisation (h) for a linearly decreasing input signal (b).The linear σ(E) dependency was used.

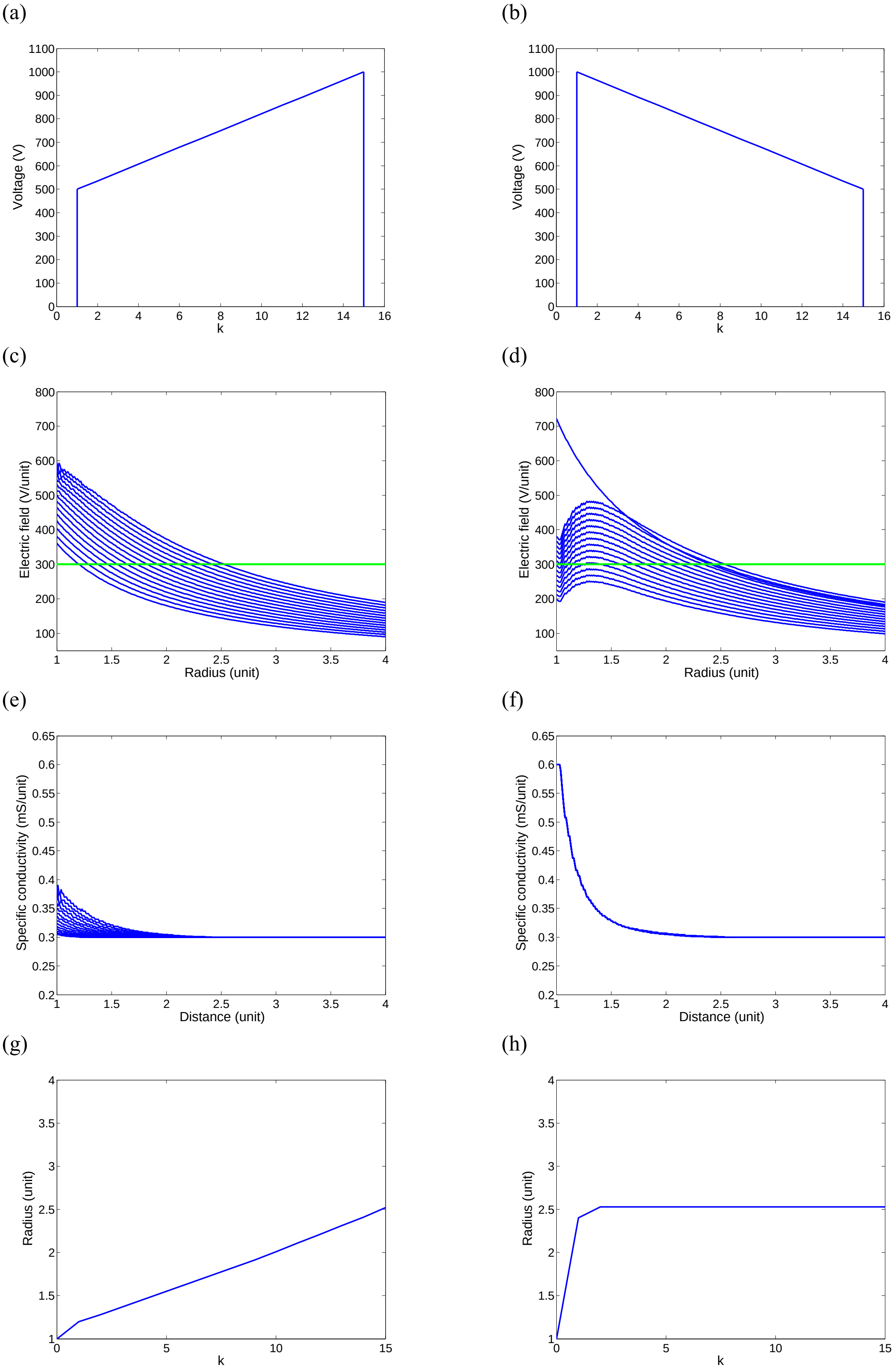

Figure 3.22: The left hand side presents the shape of a linearly increasing input signal (a) and corresponding E distribution (c), specific conductivity (e) and radius of permeabilisation (g), computed by the time discrete model. Equivalently, the right hand side presents E distribution (d), specific conductivity (f) and radius of permeabilisation (h) for a linearly decreasing input signal (b).The exponential σ(E) dependency was used.

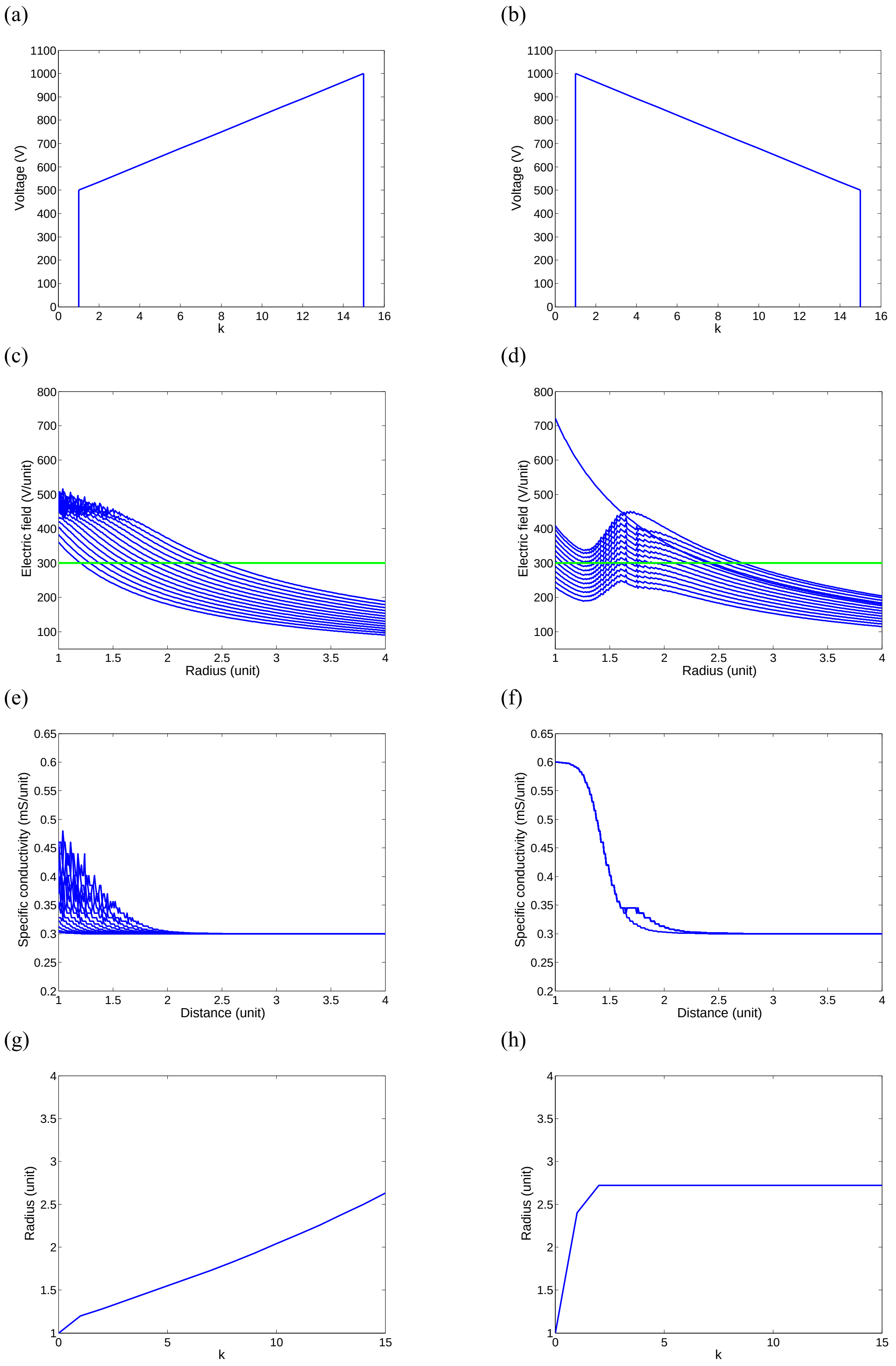

Figure 3.23: The left hand side presents the shape of a linearly increasing input signal (a) and corresponding E distribution (c), specific conductivity (e) and radius of permeabilisation (g), computed by the time discrete model. Equivalently, the right hand side presents E distribution (d), specific conductivity (f) and radius of permeabilisation (h) for a linearly decreasing input signal (b).The S-shaped σ(E) dependency was used.

3.6 REAL TIME CONTROL OF TISSUE PERMEABILISATION

In the previous chapter it was shown that the extent of permeabilisation as well as the dynamics of permeabilisation can be manipulated by the electric pulse shape. As for effective tissue permeabilisation the electric pulse amplitude which permeabilises the desired volume of tissue has to be defined, within this chapter we investigated the feasibility of real time control of tissue permeabilisation. Feasibility of real time control was examined by means of the time discrete model of tissue permeabilisation with stepwise dependency σ(E) presented in Chapter 3.1 to Chapter 3.3. Considering the model presented, the control task was to provide the electric pulse amplitude that permeabilises tissue up to a predefined radius which represents the goal of effective tissue permeabilisation. The radius of permeabilised tissue was controlled by a closed loop control algorithm, which defines pulse amplitude according to the reference radius and the current radius of permeabilisation.

The corresponding control scheme is shown in Figure 3.24. The permeabilisation process is described by the time discrete permeabilisation model denoted as *permeabilisation* in the control scheme. The reference value for the control algorithm R_{ref} is the radius of tissue to be permeabilised. The control variable (the model input) is the pulse amplitude u. The manipulated value is the radius of permeabilised tissue r. A proportional integral (PI) controller was implemented to control the model output r. The use of a PI controller is justified by the fact that it is capable of steady-state control error elimination and it gives sufficient transient response in the case of a first order system. In time domain the PI controller has the following form:

$$u(t) = K_P e + K_I \int e(t)dt \, , \tag{3.35}$$

where e is the difference between R_{ref} and r, K_p is the proportional gain and K_I the constant of the integral part. The transfer function of the PI controller, which is denoted as the Laplace transform of the system unit impulse response, is the following:

$$G_{PI}(s) = K_P + \frac{K_I}{s} \, . \tag{3.36}$$

The parameters of the PI controller were derived by means of a cancellation controller design (Isermann *et al.*, 1992). The latter is designed by prescribing the desired input-output relation to the closed loop system. The transfer function of the closed loop system is given by:

$$G_w(s) = \frac{G_R(s)G_P(s)}{1 + G_R(s)G_P(s)} \tag{3.37}$$

where G_R and G_P are controller and process transfer functions, respectively. From equation (3.37) the controller transfer function follows:

$$G_R(s) = \frac{1}{G_P(s)} \frac{G_w(s)}{1 - G_w(s)} \, . \tag{3.38}$$

Considering the step response of our model (Figure 3.25), permeabilisation can be approximately described by a first order model. The transfer function of a first order model is given by

$$G_P(s) = \frac{K}{Ts + 1} \, , \tag{3.39}$$

where *K* denotes the gain and *T* the time constant of the model. Our goal was to force the closed loop model to behave like the model described by the desired transfer function:

$$G_w(s) = \frac{1}{nTs+1}, \tag{3.40}$$

where *nT* denotes the time constant of the closed loop model. If the closed loop time constant is to be shorter than the model time constant, parameter *n* should be in the range between 0 and 1.

Considering equations (3.38), (3.39) and (3.40) we can express the transfer function of the controller as:

$$G_R(s) = \frac{1}{nK} + \frac{1}{nTKs}. \tag{3.41}$$

By comparing equation (3.41) with (3.36) we can obtain parameters of the PI controller:

$$K_P = \frac{1}{nK} \qquad \text{and} \qquad K_I = \frac{1}{nTK}. \tag{3.42}$$

The gain of the model $K=216$ was computed from the model step response. The time constant of the model was also derived from the model step response shown in Figure 3.25, where step responses were given for pulse amplitudes in the range of 900 V to 1300 V, in increments of 50 V. For each time discrete step we assumed a time unit of 1 µs. That was speculative and could be determined only by comparison with the step response of a corresponding experimental system. In Figure 3.25 we can see that due to the nonlinearity of the system, time constants differ according to the input signal. For use in transfer function the shortest time constant was selected i.e. T=1 µs, in order to satisfactorily control the dynamics at lower pulse amplitudes also.

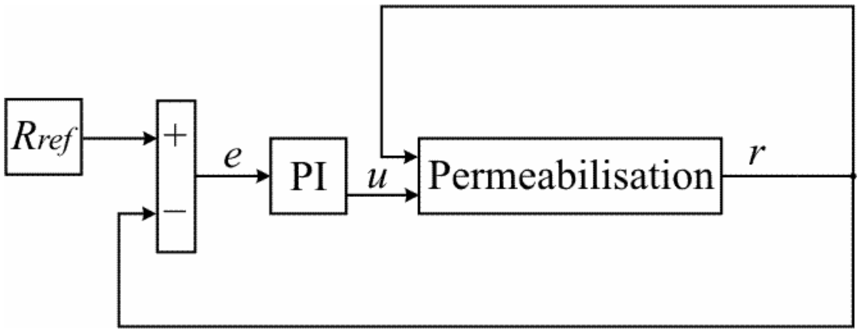

Figure 3.24: Control scheme.

Parameter *n* was selected to obtain a shorter time constant of the closed loop model compared to the model time constant (n=0.3). The resulting parameters of the PI controller were therefore K_P=720 and K_I=720.

Figure 3.26 presents simulation results of control i.e. the controlled variable *r* and the control signal *u* when different reference values R_{ref} were set in the control scheme. For example, if R_{ref} is equal to 3.5 units, the control variable value in a steady state reached u=1329.8 V (Figure 3.26 (a) and (b)). When the reference was set to R_{ref}=3 units, the corresponding pulse amplitude in a steady state was u=1255.5 V (Figure 3.26 (c) and (d)), similarly for R_{ref}=2.5 units and R_{ref}=2 units, in a steady state the pulse amplitudes obtained were u= 1160.2 V and u=1039.7, respectively (Figure 3.26 (e) to (h)).

As observed from the results in Figure 3.26, despite using the shortest time constant *T* in computation of PI controller parameters, the model control gave satisfactory results in the presented range of reference values. However for better performance at a particular set point, parameter tuning should be redefined or a gain-scheduling PI controller can be implemented.

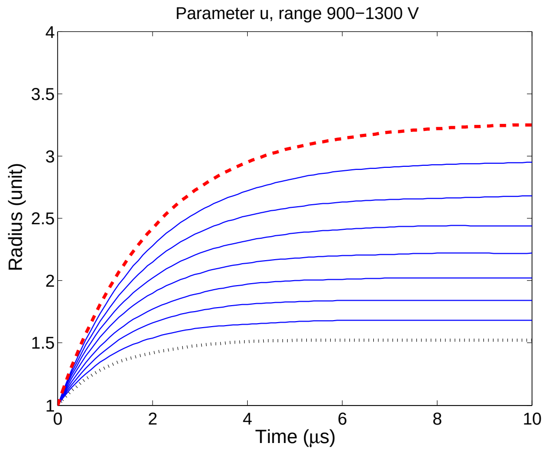

Figure 3.25: Model step response at different pulse amplitudes.

3.7 COMPARISON OF ANALYTICAL MODEL AND FINITE ELEMENT MODEL

For the same geometry of two concentric cylindrical electrodes we designed a time discrete model of tissue permeabilisation where E was computed by a finite element method. The methodology of the time discrete finite element (FE) model will be explained later in Chapter 5. At this point we wanted to compare results obtained by the analytical and FE model for different dependencies σ(E). We used the same parameters in the analytical model and FE model when comparing results for a particular σ(E) dependency.

The left hand side of Figure 3.27 presents conductivities at the end of permeabilisation computed by the analytical model, while the right hand side presents conductivities computed with the FE model for different dependencies σ(E). The distance on the *x* axis is denoted as the distance between the inner and outer radius of concentric cylindrical electrodes. We can see that in the case of stepwise dependency the FE model gives distorted results at permeabilisation radii obtained in discrete time steps – the points of discontinuity of E distribution. This is due to FE interpolation between nodes. This problem can be minimised by generating very dense mesh in the whole region where we expect discontinuities in E distribution to occur. For stepwise dependency σ(E) we also calculated the total current before and at the end of permeabilisation. With the analytical model we computed current before permeabilisation i_{before}=2.99 A and after permeabilisation i_{after}=4.19 A, while the FE model gave i_{before}=2.88 A and i_{after}=3.79 A. The difference was small and resulted from the discretisation of evaluation points inherent to FE modelling.

Further comparison of the analytical and FE model for linear, exponential and S-shaped σ(E) dependency showed that there were no such differences between the models as occurred with stepwise dependency. The reason was the smoother E distribution obtained when employing those dependencies. Namely, a smoother distribution is not as sensitive to the mesh density.

The major difference between the analytical and FE model was the time spent on solving the model, which in the case of FE model was significantly longer.

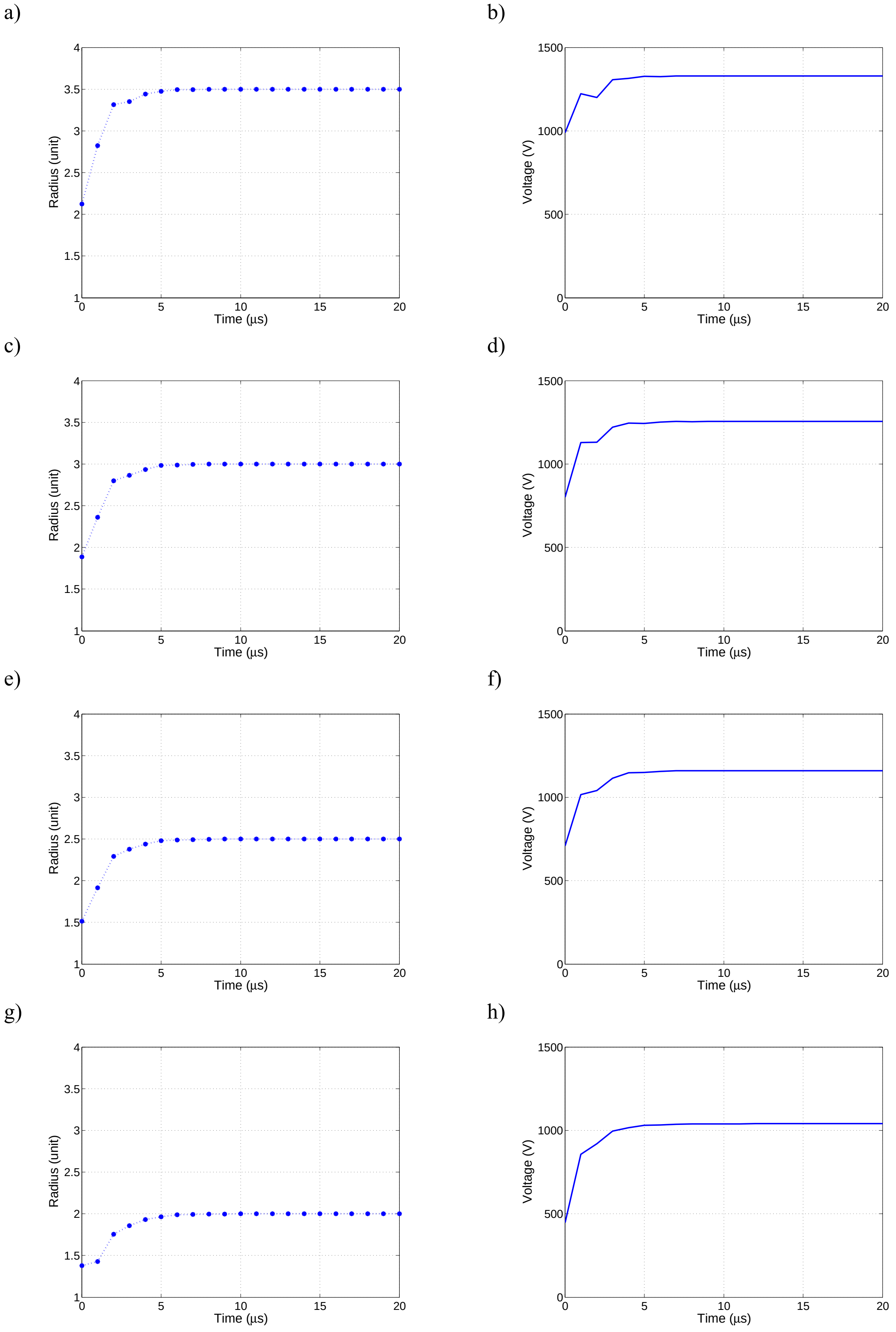

Figure 3.26: Controlled variable - model response (radius) and control variable (voltage) for different reference values: R_{ref}=3.5 units (a) and (b); R_{ref}=3 units (c) and (d); R_{ref}=2.5 units (e) and (f); R_{ref}=2 units (g) and (h).

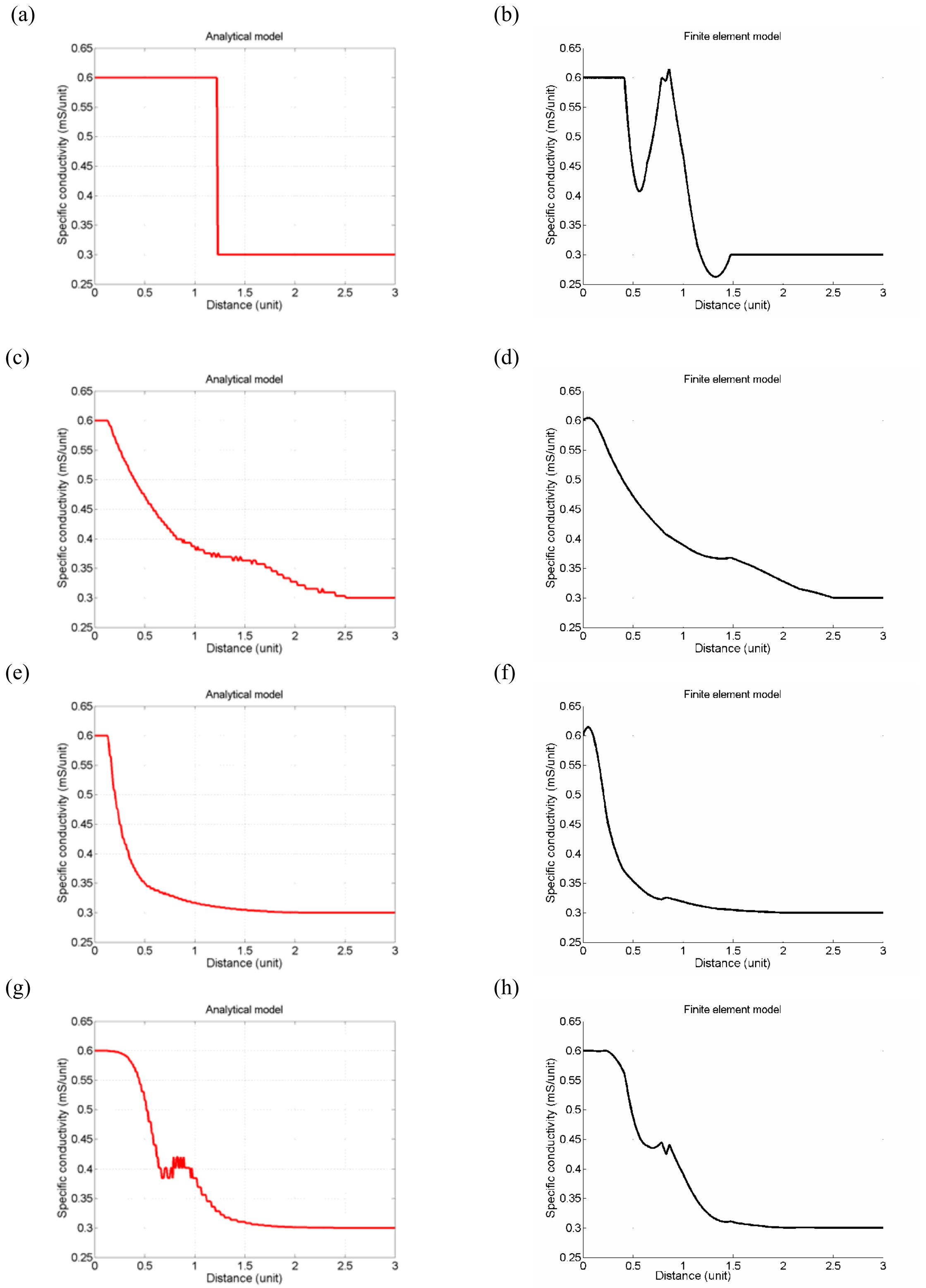

Figure 3.27: Comparison of specific conductivity at the end of permeabilisation computed by analytical model (left) and FE model (right) for different functional dependencies σ(E). Stepwise dependency: (a) analytical model, (b) FE model; linear dependency: (c) analytical model, (d) FE model; exponential dependency: (e) analytical model, (f) FE model; S-shaped dependency: (g) analytical model, (h) FE model.

3.8 DETERMINATION OF σ(E) DEPENDENCY

With the model parametric study we confirmed that parameters of σ(E) dependency play an important role in tissue permeabilisation. Their impact of course is related to the distribution of the E in tissue. For use in permeabilisation models σ(E) dependency has to be determined for each tissue, which requires specially designed experiments and corresponding models of tissue permeabilisation. Therefore in this chapter we present one approach towards determination of σ(E) dependency from experiments on rat liver tissue.

The approach is based on determination of approximate threshold values by measuring Cr^{51}-EDTA uptake. Namely Cr^{51}-EDTA can only enter permeabilised cells, and it leaks out from necrotic cells. Therefore Cr^{51}-EDTA can be considered as an indicator of the volume of reversibly permeabilised tissue.

As the total current reflects the specific conductivity of the tissue we optimized the precise thresholds and the shape of σ(E) dependency by minimizing the difference between modelled current and current measured in experiments.

3.8.1 EXPERIMENTS

In vivo experiments were performed at the Institute Gustave-Roussy, France on rat liver tissue in accordance with European Council directives and French legislation regarding animal welfare and care. Rats were kept anaesthetised for the duration of the experiment. At the beginning of the experiment the Cr^{51}-EDTA was injected intravenously and after a few minutes the rat liver was isolated from the abdomen by surgical intervention. The tissue was then placed between two plate electrodes as shown in Figure 3.28 and exposed to electrical treatment i.e. a sequence of eight square wave pulses of duration 100 μs and repetition frequency of 1 Hz. The amplitude of pulses was in the range between 50 to 500 V i.e. an electric field in the range 110 V/cm to 1100 V/cm. Pulses were delivered by Jouan GHT 1287B, France pulse generator. The applied voltage and resulting current were acquired by high voltage and current probes respectively and stored on-line by oscilloscope (LeCroy, France). Animals were sacrificed after 24 hours. Blocks of liver tissue exposed to the electric treatment and blocks of non-exposed tissue of the same size were then taken out. Both blocks were weighted and gamma counted. The difference in measured activity per gram between the two blocks indicated the net uptake of Cr^{51}-EDTA caused by electropermeabilisation.

Another set of experiments was performed under the same electrical treatment, however without Cr^{51}-EDTA injection, thus the number of experiments with voltage and current measurements was higher than the number of experiments where Cr^{51}-EDTA measurement was included.

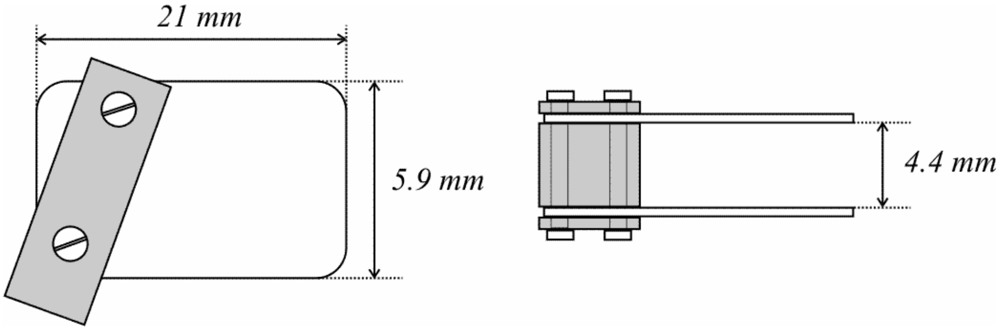

Figure 3.28: Plate electrodes used in experiments.

3.8.2 OPTIMISATION OF PARAMETERS OF σ(E) DEPENDENCY

We assumed homogenous E distribution in the area between the two plate electrodes. This was also confirmed by the FE model, where slightly increased E distribution was found only at the electrode edges. Due to the negligible difference in E we used the simple analytical model based on equations for steady electric current in a volume conductor instead of the FE model in order to determine σ(E) dependency. Specific conductivity in homogenous E between two plate electrodes is denoted as:

$$\sigma = \frac{i}{u}\frac{d}{A}, \tag{3.43}$$

where i is measured total current, u pulse amplitude, A the tissue surface in contact with electrodes and d the distance between the electrode.

The average tissue surface in contact with the electrodes in our experiments was estimated to be 88.5 mm^2 - smaller than the surface of the electrodes. The distance between the electrodes was 4.4 mm as shown in Figure 3.28. We determined specific conductivity of non-permeabilised tissue as the mean value of measured specific conductivity at E intensities where no Cr^{51}-EDTA uptake was observed. Similarly we defined specific conductivity of irreversibly permeabilised tissue by averaging measured specific conductivities computed at higher E intensities than the E intensity at which Cr^{51}-EDTA uptake decreased significantly (above 680 V/cm). In this way we obtained σ_0=1.41 mS/cm and σ_1=3.10 mS/cm.

The approximate E thresholds were also determined by means of Cr^{51}-EDTA uptake. Between two neighbouring E intensities i.e. where no Cr^{51}-EDTA uptake was measured and where the first increase in Cr^{51}-EDTA uptake was found we set the range for E_0. Further, between two E intensities where Cr^{51}-EDTA uptake was still increased and where Cr^{51}-EDTA uptake dropped we defined the range for E_1. The measured Cr^{51}-EDTA uptake and determined ranges for E_0 and E_1 are shown in Figure 3.29.

In continuation we assumed an S-shaped dependency between specific conductivity and E intensity. Such a dependency was used because it best describes experimental observations. Those observations revealed that at reversible threshold, at first some cells are permeabilised, and then by increasing the E intensity neighbouring cells are also permeabilised, while when E exceeds irreversible threshold the death of some cells is observed yielding to tissue necrosis with further increases in E.

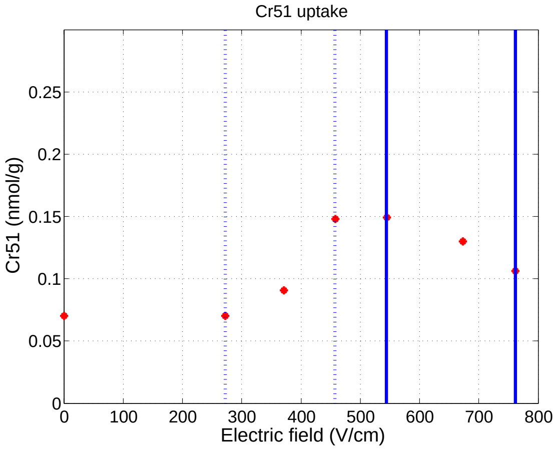

Figure 3.29: Average Cr^{51}-EDTA uptake (*) and range of E_0 (dashed lines) and E_1 (full lines).

Thus electropermeabilisation parameters subject to optimisation were E_0, E_1 and parameters B_S and D of S-shaped dependency presented in Equation (3.33). The constraints on E_0 and E_1 were set according to the range determined by Cr^{51}-EDTA uptake i.e. 272 V/cm $<E_0<$ 457 V/cm and 544 V/cm $<E_1<$ 762 V/cm. The optimisation goal was to minimise the objective function f representing the difference between measured (i) and modelled (i_m) total current:

$$\min_{E_0, E_1, B, D} f(i, i_m)\,. \tag{3.44}$$

The objective function $f(i,i_m)$ was expressed as:

$$f(i,i_m) = \frac{\sqrt{\sum_j \left(i_j - i_{m\,j}\right)^2}}{\sqrt{\sum_j i_j^{\,2}} + \sqrt{\sum_j i_{m\,j}^{\,2}}}\,, \tag{3.45}$$

where j denoted measurement at applied voltage u_j.

A constrained nonlinear optimisation method was used. The minimum of the objective function was found at $f(i,i_m)=0.129$. Optimal parameters were E_0=272 V/cm, E_1=762 V/cm, B_S=61, D=1.1. We can see that optimized threshold values reached bounds, which could mean that lower reversible and higher irreversible threshold would give even better results of the objective function. However, as the S-shaped dependency is very flat at the threshold values, the determination of threshold values is very sensitive to the accuracy of current measurements used to compute the objective function. We believe that current measurements were subjected to measurement error because surface of tissue in contact with electrodes differed amongst experiments. On the other hand Cr^{51}-EDTA measurements were performed in the region of tissue in the middle between the electrodes, thus they should be more accurate. The combination of the current and Cr^{51}-EDTA measurements for determination of $\sigma(E)$ dependency was therefore sensible in case of plate electrodes, where the current measurements are affected by the alteration in surface of tissue in contact with electrodes. On the other hand in case of, for example needle electrodes, the surface of tissue in contact with electrodes could be determined more accurately.

Figure 3.30 presents measured and modelled current by using optimised parameters in $\sigma(E)$ dependency.

Figure 3.31 presents the shape of functional dependency σ(E) and specific conductivity computed from *u* and *i* measurements.

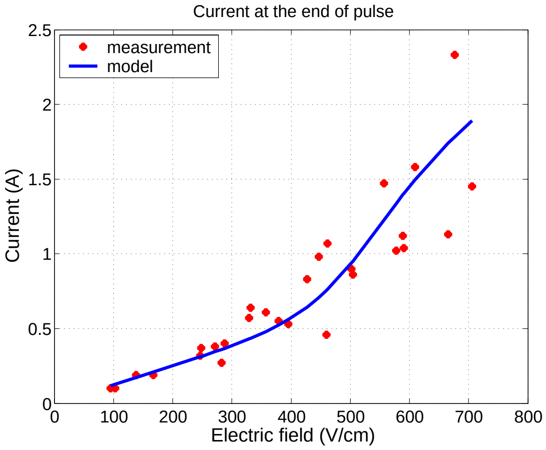

Figure 3.30: Total current measured by experiments (*) and total current computed by model (full line).

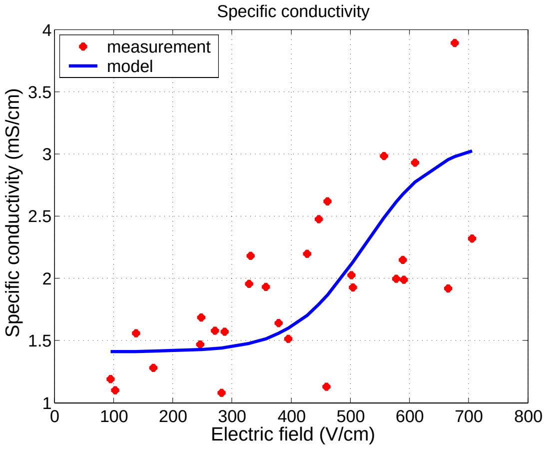

Figure 3.31: Specific conductivity computed from measurements (*) and specific conductivity obtained by model (full line).

3.9 DISCUSSION

A time discrete model of tissue permeabilisation with an analytical description of E distribution was designed for the geometry of two concentric cylindrical electrodes. The methodology proposed could also be used for other geometries which allow for an analytical description of E distribution. The important contribution of the geometry used was that such geometry provides an inhomogeneous E distribution similar to the distribution around needle electrodes as used for treatment of deeply seated tissue in clinics. In this respect the presented model could assist in determination of optimal pulse amplitude for effective tissue permeabilisation in a non-invasive way before the treatment (see Chapter 6).

The time discrete model was incorporated into a simulation environment that presents the course of permeabilisation by displaying E distribution, specific conductivity, and radius of permeabilised tissue. As pulse parameters, the geometry and tissue electrical properties influence the course of tissue permeabilisation, a further purpose of the simulation environment was to provide monitoring of tissue permeabilisation as influenced by changes in those parameters. The time discrete simulation of tissue permeabilisation revealed that at constant pulse amplitude and stepwise σ(E) dependency, permeabilisation propagation terminated after a few time discrete steps. The number of time discrete steps at which changes in E distribution due to permeabilisation were present depended on E intensity and tissue parameters. As stepwise σ(E) dependency was not very likely to occur in biological tissue, we extended the time discrete model to describe arbitrary functional dependency σ(E). Based on such a model the time discrete simulation of tissue permeabilisation when linear, exponential and S-shaped dependencies were used was presented within the simulation environment.

The influence of E distribution and different functional dependencies σ(E) on the course of permeabilisation was systematically examined by performing a model parameteric study afterwards. The parameteric study revealed that tissue parameters (E_0, E_1, S_1, B) influence the radius of permeabilisation and specific conductivity at the end of permeabilisation. It also confirmed that the distribution of external E defined by parameters R_0 and u, controls permeabilisation. This yielded the conclusion that pulse amplitude and electrode position should be very carefully determined in order to permeabilise the pre-required volume of tissue with given σ(E) dependency.

Based on the parametric study we also inferred that when continuous (S-shaped) or at least piecewise continuous (linear, exponential) functional dependencies σ(E) were used, permeabilisation propagation was terminated even earlier than in the case of stepwise dependency σ(E). Those dependencies namely smoothed the effect of the transition condition on the border between two materials with different conductivities, which in the case of stepwise dependency caused discontinuities in E distribution and prolonged propagation of permeabilisation.

Further, the differences caused by the shape of functional dependencies σ(E) depended on E distribution in tissue. The more tissue exposed to E intensity between the two thresholds, the more pronounced the differences caused by the shape of functional dependencies σ(E). Considering E distribution between two concentric electrodes, the largest radius of permeabilised tissue was obtained with a linear dependency. Such dependency σ(E) assumed a proportional increase in conductivity due to E intensity in the whole area between the two threshold values. Exponential dependency σ(E) however assumed that at lower E intensities a gradual increase in conductivity was present and that it increased exponentially with higher E intensities. The S-shaped dependency caused a gradual increase at lower intensities, then a steep increase around the inflection point and later again, a gradual increase just below E_1. Because E intensity in non-permeabilised tissue between the electrodes dropped with 1/r, less tissue was exposed to higher intensities than lower. This was the reason why the linear dependency, which caused the largest increase at lower E intensities, resulted in a larger radius of permeabilisation than the other dependencies.

Linear and exponential dependencies are piecewise continuous at both threshold values, which could hardly be justified in biological tissue. It is only the S-shaped dependency which is continuous in the whole range. The S-shaped dependency also better fits the permeabilisation process which was observed experimentally in [Miklavčič *et al.*, 2000] to be at E_0 present in some cells, then with higher E-intensities it expanded to other cells. After reaching E_1 the first necrotic cells were observed leading to a whole tissue necrosis at higher E intensities. Based on the above results and experimental observations further in this work we used the S-shaped dependency. The constant D in equation (3.33) in the S-shaped dependency enables the translation of inflection point at other E intensities than the mean value between the two thresholds. In this way by changing either of parameters B_S or D we can transform the S-shaped dependency to resemble a more linear or more exponential dependency in the area between the two thresholds.

While within the simulation environment and parametric study we assumed the application of a rectangular pulse, it was a further question of interest to investigate the influence of pulse shape (linearly decreasing and linearly increasing or ramp signal) on the dynamics and extent of permeabilisation. Modelled tissue permeabilisation at applied ramp signals showed that similar radii of permeabilised tissue were obtained no matter whether a linearly increasing or linearly decreasing input signal was applied. However, when a linearly decreasing input signal was applied, the maximal radius of permeabilisation was obtained in the beginning of the pulse application, while in the case of a linearly increasing input signal the maximal radius of tissue permeabilisation was obtained just before the end of pulse application. The comparison of ramp signals with a rectangular pulse of amplitude equal to the average amplitude of the ramp signals showed that the radius of permeabilisation obtained by a rectangular pulse was significantly smaller than the radii obtained when the ramp signals were applied. It seems that the maximal amplitude in the pulse greatly affects the extent of permeabilisation.

Thus, as the radius of permeabilisation can be manipulated by adequate pulse shape, we further examined the possibility of real time control of tissue permeabilisation on the time discrete model. The permeabilisation control, performed by a closed loop control algorithm with proportional integral controller showed that such an approach could be used to control the effectiveness of permeabilisation. However, tuning of controller parameters which was based on the model step response would in real applications require specially designed experiments to obtain the step response. To avoid this, model based determination of the controller parameter could be used, which of course requires an accurate and reliable model of tissue permeabilisation. In the presented control scheme we considered the radius of the permeabilised tissue as the controlled variable. In case of *in vivo* permeabilisation control it is difficult to measure the radius or the volume of permeabilised tissue (in real geometries the volume of permeabilised tissue would be the equivalent to the radius used in presented analytical model). Measurement of bulk tissue conductivity, which is usually performed, could not be used for assessment of the volume of permeabilised tissue, as it does not provide information about whether a specific point of tissue was permeabilised. A possible approach for determining the volume of permeabilised tissue could be electric impedance tomography, but this method does not provide on-line data. Another approach would be model based control, i.e. to determine the volume of permeabilised tissue by means of a time discrete model. However, analytical description of E distribution is possible only for simple geometries, while in the case of complex geometries, numerical methods should be considered.

Thus we performed a comparison of analytical and numerical models to test the feasibility of employing a numerical model in a time discrete simulation of tissue permeabilisation. Both models predicted a similar change in specific conductivity at the end of permeabilisation for different dependencies $\sigma(E)$. The comparison showed that computation of the numerical model is time consuming and that the accuracy of the time discrete model is limited due to discretisation of the solution in evaluation points. The latter has a significant impact when distinctive inhomogeneities or even discontinuities are present in the solution. Such a problem however can be reduced by generating denser mesh in that region. Therefore the use of a numerical model in a time discrete simulation of tissue permeabilisation is feasible. Even more, when modelling complex geometries it represents the only possible solution. However, a numerical model can not be used for model based control as it is time consuming and thus can not provide the on-line data needed for real time control.

On the other hand the application of the controller is reasonable when we also want to control the dynamics of tissue permeabilisation. Considering the problems mentioned above and the fact that rectangular pulses have been found experimentally to be effective, as well as when applied they provide sufficient dynamics of permeabilisation the determination of the rectangular pulse amplitude that would permeabilise a given volume of tissue in a steady state is more important than the control of the dynamics of phenomenon. The determination of rectangular pulse amplitude for effective permeabilisation could be performed by other means, such as for example the model based optimisation.

For determination of optimal pulse amplitude based on the proposed time discrete model, the $\sigma(E)$ dependency should be known in advance. Therefore at the end we proposed an approach for determination of $\sigma(E)$ dependency. The approach combined experimental results and a model of E distribution. Experimental results comprised measured uptake of Cr^{51}-EDTA and total current. The former was used to determine the approximate range of thresholds for reversible and irreversible tissue permeabilisation, while the latter was used for model based optimisation of $\sigma(E)$ dependency, where the approximate threshold range was considered as a constraint. The combination of measurements of Cr^{51}-EDTA and total current minimized the influence of measurement errors, as Cr^{51}-EDTA and current are measured by different measurement methods. However model based optimization of $\sigma(E)$ dependency on current only could also be used, provided a reliable model of tissue permeabilisation is employed and satisfactorily accurate current measurements are available.

4 FINITE ELEMENT MODELLING OF NEEDLE ELECTRODES IN TISSUE FROM THE PERSPECTIVE OF FREQUENT MODEL COMPUTATION

Electric field (E) distribution in tissue is a key factor influencing the effectiveness of electropermeabilisation. In the previous chapter the E distribution in tissue between two concentric electrodes was computed by means of an analytical model. The analytical model of E distribution was also used to determine σ(E) dependency in rat liver tissue between two plate electrodes. The development of both analytical models was feasible because tissue and electrodes formed simple geometry.

However for tissue permeabilisation other electrode configurations are also used such as needle electrodes, needle arrays, wire electrodes, etc. [Gilbert *et al.*, 1997; Mir *et al.*, 1997; Ramirez *et al.*, 1998; Hofmann, 2000]. In such cases the use of numerical methods is almost unavoidable for calculation of E distribution in tissue. Widely used numerical methods for that purpose are the finite element (FE) and the finite difference (FD) methods [Gehl *et al.*, 1999; Miklavčič *et al.*, 2000].

In the previous chapter we also presented that a time discrete model of tissue permeabilisation requires several calculations of E distribution to determine the extent of permeabilisation at applied pulse amplitude. Analytical calculations of electric fields were not time consuming and thus the influence of several calculations was negligible. However if we want to use numerical methods instead of analytical to describe E distribution within a permeabilisation model we have to be aware that numerical methods are in general computationally demanding and thus time consuming.

Therefore, simplifications in the modelling process which can decrease computational efforts and at the same time preserve the accuracy of the result i.e. E distribution in our case are more than welcome.

In this chapter we focused on simplifications, which can be employed to modelling of needle electrodes with the FE method. Needle electrodes, compared to other electrodes mentioned above, are routinely used in *in vivo* experiments, because deep penetration of the field is obtained. Needle electrodes also present a very complex task for FE modelling, due to their curved shape and usually large disproportions in terms of size with respect to the surrounding tissue dimensions.

We have therefore investigated how to model needle electrodes in FE model in order to hasten the solution process. Different needle geometries (4, 8 and 12 faceted) were tested on an FE model with one pair of needle electrodes. The results were evaluated by comparing computed total current and measured current in tissue phantoms. Proposed needle electrode geometry was then examined in needle arrays with 2, 3 and 4 pairs of needle electrodes. The results of all examples were validated by comparison of computed total current and measured current on phantom tissue.

4.1 EXPERIMENTS

4.1.1 SAMPLE

Experiments were performed at The Institute of Pharmacology and Structural Biology in Toulouse, France. Tissue phantom was used instead of real tissue in all experiments, with electrical parameters and characteristics close to real tissue. Tissue phantom was made from gelatine (2.4% w/v) in phosphate buffer (concentration 20 mM, pH = 7.4) and NaCl (concentration 150 mM). This is actually a gel with some rigidity when cooled. Due to the moisture of the gel a good electrical contact is obtained with electrodes inserted in the gel. Tissue phantom conductivity was 1.5 S/m. Fresh gel was prepared in a buffer before each experiment and its conductivity was measured.

The phantom tissue was prepared in a petri dish of 35 mm diameter. The thickness of the gel used in experiments was either 2, 4 or 6 mm and it was controlled by pouring a given volume of hot liquid gel in the dish.

4.1.2 ELECTRICAL MEASUREMENTS

Needle electrodes were placed in a holder as described in [Gehl *et al.*, 1999] and shown in Figure 4.1, i.e. non conductive material with needles in the array placed 2 mm apart. The two arrays were 6.5 mm apart. The arrays had place for up to 4 needles. Needle diameter was 0.5 mm. The tip of the needle was always in contact with the bottom of the dish. Therefore the length of the needle in contact with the gel was equal to the thickness of the gel. Needle tips were oriented towards each other as shown in Figure 4.4, left.

The voltage pulse was delivered by a high voltage square wave pulse generator (Jouan PS 10, France). A resistor R (about 1 ohm) was inserted in series with the electrode array to monitor the current. Both the voltage pulse delivered by the generator and the voltage across the resistor R were digitized (8 bit resolution) and stored on line with a transient recorder (Data Lab DL 905, UK). The stored signals were observed on an oscilloscope and analyzed on a MacIntosh LCIII microcomputer (Apple, USA) by using an ADA4 interface with an Excel subroutine. The system as shown in Figure 4.2 was calibrated for the current by using an ohmic calibrated high power resistor in place of the needle array. A linear current response of the system was observed for increasing values of the applied voltage (100 to 1000 V). Lower applied voltages (0 to 100 V) were studied with increments of 25 V. In experiments, applied voltage was up to 500 V, in increments of 100 V. The pulse duration was 0.1 ms. By plotting current by voltage (U/I) ratio during the pulse delivery, material conductivity was observed to be constant. Under our experimental condition (sampling rate 1 μs), no delay between voltage and current signals was observed and negligible transient response of current comparing to pulse length was detected, which indicated pure ohmic behaviour of the gel.

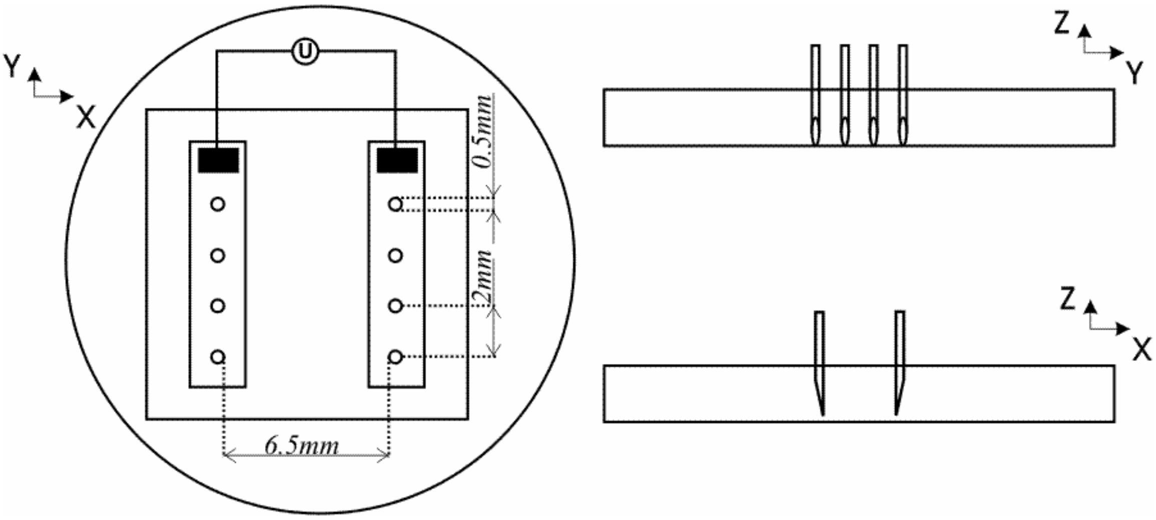

Figure 4.1: Position of needle electrodes and holder in petri dish, view in *xy* plane (left); *yz* and *zx* plane (right).

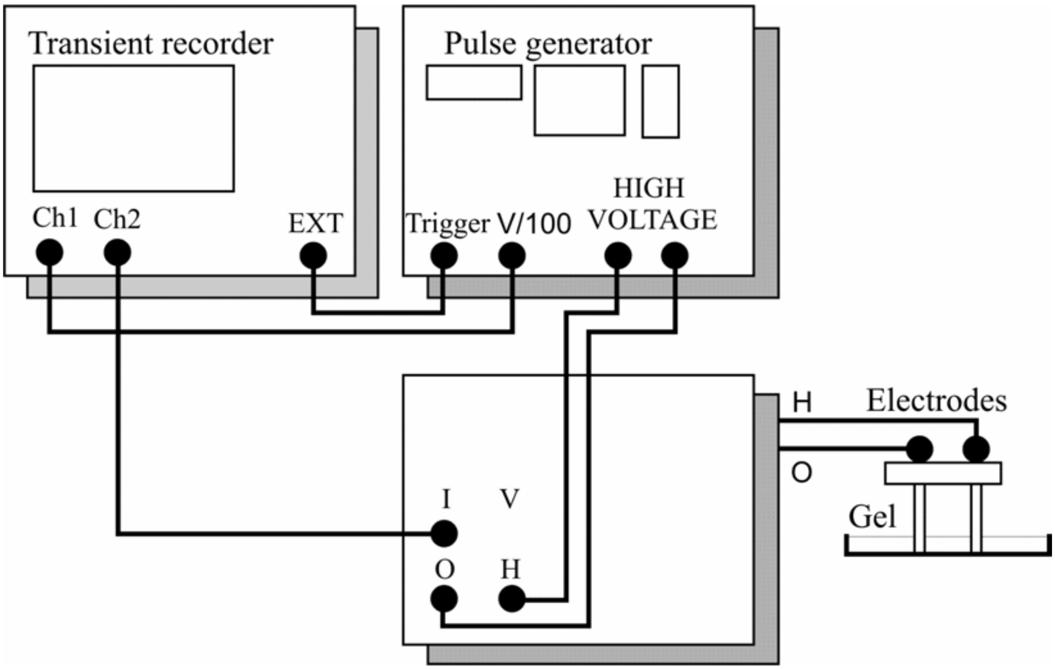

Figure 4.2: Pulse generator and acquisition unit.

Several experiments with needle electrodes differing in the number of needles, distance between the needles and also gel thickness (2 mm, 4 mm and 6 mm) were carried out. Each experiment was performed in three replicates, which all together sum up to 50 experiments. Reproducibility of replicate accuracy in each experiment was high, which was the reason to conclude three replicates per experiment were enough.

4.2 MODELLING

A three dimensional FE model of a gel in petri dish with inserted needle electrodes was designed using EMAS software.

The geometry under the study was moderately complex, involving few physical objects (gel, needles) with specific geometrical and material properties. To simplify the modelling and solution process the basis of FE approach is to divide volume into many finite elements, each with much simpler properties. In the EMAS software, when automatic mesh generation was selected, finite elements had the shape of tetrahedrons. Finite elements with an additional mid-side node on each element edge are referred to as quadratic elements. The curved element edge option enabled mid-side nodes to be placed outside the straight line connecting corner nodes. In such a way a curved element edge was obtained, which lead to a better representation of curved geometries.

Mesh was denser in regions around the electrodes than at the edge of a petri dish. The reason for such meshing was a steep change in E distribution expected close to electrodes. Another reason to create denser mesh around the electrodes was that the dimension of the electrodes was significantly smaller than dimensions of the surrounding gel.

4.2.1 NEEDLE ELECTRODES

Modelling of cylindrical shapes with FE method is a demanding task. Namely, such a shape has to be approximated with a huge number of basic elements such as bricks or tetrahedrons. This problem is usually solved by allowing a certain deviation between geometry edge and finite element edge, using elements with curved boundaries and by generating very dense mesh in the curved region (at the edge of the electrodes). However, very dense mesh results in computational complexity of models.

Needle electrodes in our model represented a problem of such type. Due to the fact that their size was 70 times smaller than the size of the surrounding gel, very dense mesh had to be generated in the region around the electrodes. Despite using quadratic tetrahedron elements with curved edges the modelling of cylindrical electrodes was inadequate. For generating a better solution, very dense mesh was required. Therefore in order to simplify the modelling process we approximated cylindrical electrodes with 4, 8 and 12 faceted shapes. Needle tips of 2 mm length were modelled in all needle approximations. Another point was to investigate whether electrodes could be modelled as hollow, solid or they had to be approximated as tubes having a certain wall thickness, like the needles used in experiments. Figure 4.3 shows the 4, 8 and 12 faceted electrodes in plane perpendicular to their length, as well as the solid and tube electrode.

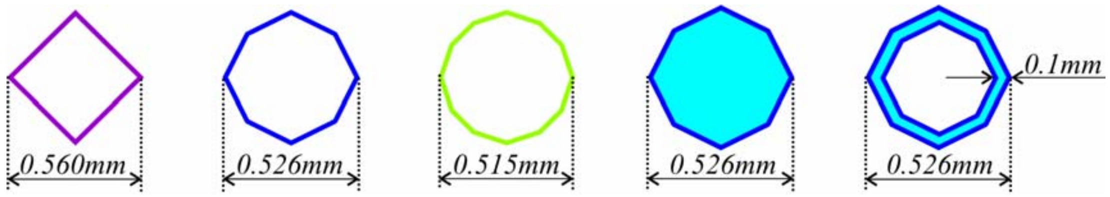

Figure 4.3: Cross section of 4, 8 and 12 faceted, solid and tube electrodes.

Another issue of interest was to determine if modelling of needle tips can be ignored, as shown in the middle of Figure 4.4, or they have to be modelled in such a way as to correspond to real tips, as shown in Figure 4.4, left and to investigate the influence of the tip orientation as shown in Figure 4.4, right.

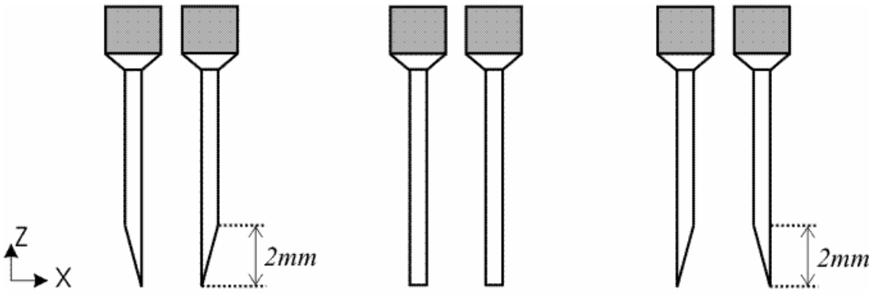

Figure 4.4: Modelling needle electrodes. Left: tips-in; centre: no tips; right: tips-out.

In order to determine which simplifications can be employed without seriously affecting modelling results, we designed all needle geometries mentioned above, computed total current and compared the result with current measurements from the experiments. These comparisons were performed on the experiments with a single needle pair. Based on validation of results on a single needle pair the most adequate needle geometry was selected and used in models with 2, 3 and 4 needle pairs. In all models E amplitude was observed in two planes, i.e. *xy* plane, perpendicular to electrode lengths, 1 mm below the surface and *yz* plane crossing in the middle between the electrodes.

4.2.2 TISSUE WITH A SINGLE PAIR OF NEEDLE ELECTRODES

Needle electrode geometries used for simplified representation of cylindrical electrodes were hollow 4, 8, 12 faceted, solid (stainless steel) and tube electrodes with modelled tips and 8-faceted needles without modelled tips. Due to the fact that in the FE model constant voltage was applied to the surface of the electrodes (Dirichlet boundary condition), we preserved the same electrode surface in cases of 4, 8 and 12 faceted electrodes, as for cylindrical electrodes ($o=2\pi r=1.57$ mm). The inner distance between electrodes was kept constant at 6.5 mm for all electrode geometries. Total currents computed for all types of electrodes and different gel thicknesses are summarized in Table 4.1.

Table 4.1: Measured currents and total currents computed by models with different needle geometries.

Thickness of gel (mm)	Current (A)							
	Measurement	4-facet, tips in	8-facet, tips in	8-facet, tips out	12-facet, tips in	Solid, tips in	Tube, tips in	8-facet, no tips
2	1.00	1.23	1.25	1.25	1.26	1.25	1.26	1.38
4	2.60	2.60	2.64	2.63	2.64	2.63	2.64	2.76
6	4.00	3.98	4.02	4.01	4.02	4.01	4.02	4.13

Relative difference between measured (y_o) and modelled (y_m) current was expressed as:

$$e = \frac{y_o - y_m}{y_o} 100\% \,. \tag{4.1}$$

The relative difference computed by considering currents from Table 4.1 showed that different electrode geometries used in FE models did not differ significantly among each other. The maximal difference in relative error amongst models was 3%, except for needles without modelled tips where it was 15%. However, we observed that computed total current significantly differed from the measurement for all experiments with gel thickness equal to 2 mm. In experiments with gel thickness equal to 4 and 6 mm, computed total current with the FE model did not differ from the measured one by more than 2%, except for needles without modelled tips, where it was 6%.

In FE models the number of finite elements or nodes in the model affects the time spent on solving the model [Polstyanko *et al.*, 2001], because the differential equation is discretized into a series of finite element equations, which form a system of linear equations to be solved. Models with needle electrode geometries examined in our study also differed in the number of finite elements. Default finite element size, which had to be determined according to EMAS software at the beginning of automatic mesh generation, was the same in all cases. The programme itself then generated denser mesh in critical regions, i.e. around curved or smaller objects. The difference in CPU time spent on solving model with the smallest mesh ($CPUtime_4$) - according to the number of elements that was the mesh in model with 4 faceted needle electrodes and CPU time spent for solving other models ($CPUtime_m$) - was expressed in relative terms as

$$R_t = \frac{CPUtime_m - CPUtime_4}{CPUtime_4} 100\% . \tag{4.2}$$

The largest relative difference was obtained in the model with solid needle electrodes (57%) and the smallest in the model with hollow 8 faceted electrodes (7%), while models with 12 faceted and tube electrodes differed by about 15% and the model with untipped electrodes by 20%, from the model with 4 faceted needle electrodes. CPU time was measured on the same computer with the same applications running at the time of the FE model computations.

Due to the fact that the distance between the inner edges of electrodes was kept constant in all models no matter if they were 4, 8 or 12 faceted, the gel volume between them was not the same, because needle electrodes differed in cross-section surface. The relative difference between the cross-section surface of a cylindrical electrode and faceted electrodes was expressed as:

$$R_S = \frac{S_o - S_m}{S_o} 100\% , \tag{4.3}$$

where S_o denotes the cross-section surface of a cylindrical electrode and S_m the cross-section surface of either 4, 8 or 12 faceted electrodes. The relative difference R_S was the highest for 4-faceted electrodes (22%) and the smallest with 12 faceted electrodes (2%), while with 8 faceted electrodes it was 5%.

Based on information gathered on all needle electrode models, and the validation of corresponding models with current measurements, we defined a criteria function in order to determine which electrodes were the most suitable for implementation in further models. The criteria function was expressed as a weighted sum of absolute values of relative difference between model and measurement e, relative difference in CPU time spent on solving model R_t and relative difference in cross-section surface R_S:

$$J = w_1 \left| e \right| + w_2 \left| R_t \right| + w_3 \left| R_S \right| . \tag{4.4}$$

Table 4.2 shows the value of criteria function for all needle electrode geometries used in models. The smaller the value of the criteria function the better the electrode geometry used. All weights used in the criteria function represented in Table 4.2 were equal to 1. However, if a certain factor in the criteria function needs to be exposed, the corresponding weight in the criteria function can be changed.

Table 4.2: Value of criteria function *J* for all needle electrode geometries used.

Thickness of gel (mm)	Criteria function *J*						
	4-facet, tips in	8-facet, tips in	8-facet, tips out	12-facet, tips in	Solid, tips in	Tube, tips in	8-facet, no tips
2	45	36	34	42	63	42	53
4	22	9	9	5	58	20	22
6	22	12	21	18	62	22	29
Σ	90	57	64	65	183	84	104

According to the results of criteria function in Table 4.2 the best supplement for cylindrical needle electrodes in the FE model were 8 faceted needle electrodes with modelled tips. Furthermore we observed that tip modelling played a very important role, especially in models with thin gel, where the length of needle tip was equal to gel thickness, which was the case with 2 mm gel. No significant difference in current was observed between the tip out and tip in configurations presented in Figure 4.4 left and right.

4.3 CURRENT BASED MODEL VALIDATION

Figure 4.5 shows E distribution computed by the model with 8-faceted needle electrodes in *xy*, *yz* and *xz* plane, respectively. Due to the lack of measured E distribution we cannot evaluate the E distribution obtained by models in details. However in [Miklavčič *et al.*, 1998; Miklavčič *et al.*, 2000] it was shown that FE models can be efficiently used for computing E distribution in tissue around needle electrodes.

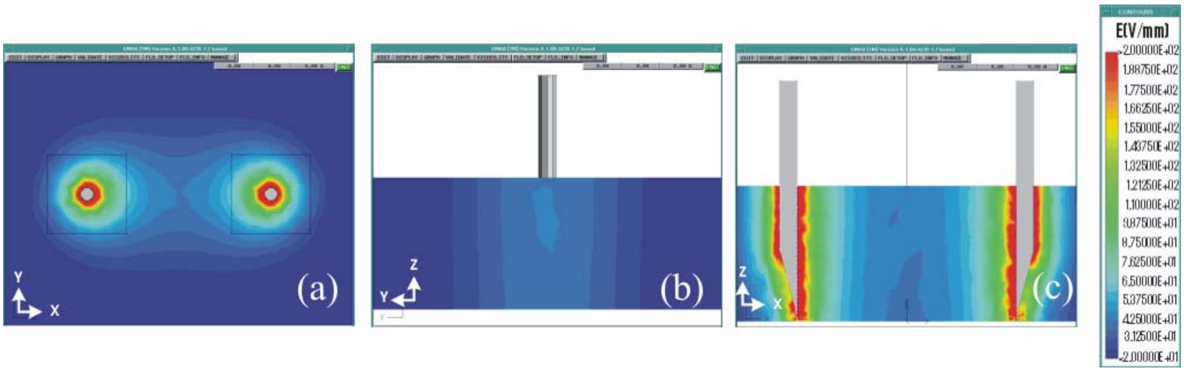

Figure 4.5: Amplitude of E computed by model with 8-faceted needle electrodes. Gel thickness was 4 mm. Voltage applied was 500 V. (a): *xy* plane, depth 1 mm below surface; (b): *yz* plane crossing in the middle between the electrodes; (c): *xz* plane.

We therefore performed current based model validation by comparing total computed and total measured current in experiments. This method is much faster than imaging methods used to validate E distribution in tissue. The applicability of the method was demonstrated in [Miklavčič *et al.*, 1998] where experimental current density obtained by Current Density Imaging (CDI) method [Serša *et al.*, 1997] was qualitatively compared with current density obtained by an FE model. The comparison was performed for two different needle electrode sets producing different current densities and E distributions. Modelled and measured current densities showed strong correlation for both electrode sets. Also, total current measured during CDI was very similar to total current obtained by the FE model for both electrode sets. Therefore FE model validation with experimental current measurements can be used as a fast method of rough model validation, provided material properties and geometry are properly described in the model.

We performed current based model validation on models with 8 faceted needle electrodes. The first group of measurements used for model validation consisted of needle arrays with 2, 3 and 4 needle pairs. The two arrays were 6.5 mm apart and the distance between needles in array was always 2 mm. In the second group of measurements used for model validation only 2 needle pairs were used. The two arrays were again separated by 6.5 mm, however the distance between neighbouring needles in the array was either 2, 4 or 6 mm.

4.3.1 NEEDLE ARRAYS WITH 2, 3 OR 4 NEEDLES IN ARRAY

The results obtained by the FE model for the first group of measurements are shown in Table 4.3. Figure 4.6 gives the E distribution obtained by the FE model with 8-faceted needle electrodes for the arrays with 2, 3 and 4 needle electrode pairs respectively (in all cases the gel thickness was 4 mm and voltage applied was 500 V).

Table 4.3: Measured and modelled current and relative difference between them for needle arrays. Voltage applied was 500 V.

No. of electrode pairs	Thickness of gel (mm)	Measurement, Current (A)	Model, Current (A)	Relative error (%)
2	2	1.33	1.86	-40
	4	3.56	3.88	-9
3	2	1.78	2.36	-33
	4	4.45	4.90	-10
4	2	2.44	2.83	-16
	4	5.33	5.78	-8

Based on the results in Table 4.3 the problem with the discrepancy between the model and measurement persisted in cases with 2 and 3 needle pairs for gel thickness equal to 2 mm. However, in the case with 4 needle electrode pairs and gel thickness of 2 mm the discrepancy between the model and the measurement decreased. Furthermore, the relative difference between the model and the measurement increased to 9% ±1% for all experiments with gel thickness equal to 4 mm, which was about 7% higher than in the model with a single needle pair used to determine needle geometry for FE modelling. Measurements with 6 mm gel thickness were not performed, due to safety limitations of the generator.

The degree of electroporation and E distribution using needle arrays with four needle pairs were investigated in [Gehl *et al.*, 1999]. The E distribution shown in Figure 4.6(c) is comparable to their results. In Figure 4.6 the change in E distribution around the electrodes can be observed when additional needle pairs were added. This information is of great importance in cases of electrochemotherapy or gene transfer when a predefined volume of tissue needs to be exposed to an E greater than the threshold value. As seen in Figure 4.6, as the number of needles in the array increases, the E between electrodes turns out to be more homogenous and a higher value of E can be obtained between the electrodes. A more homogenous E distribution with 3 electrode pairs can be also seen in Figure 4.7(a), where comparison of the E along the x and along the y axis in the region between the electrodes is shown for 1 electrode pair and 3 electrode pairs. In Figure 4.7(b) the comparison of E distribution between 1, 2, 3 and 4 electrode pairs is shown along the y-axis.

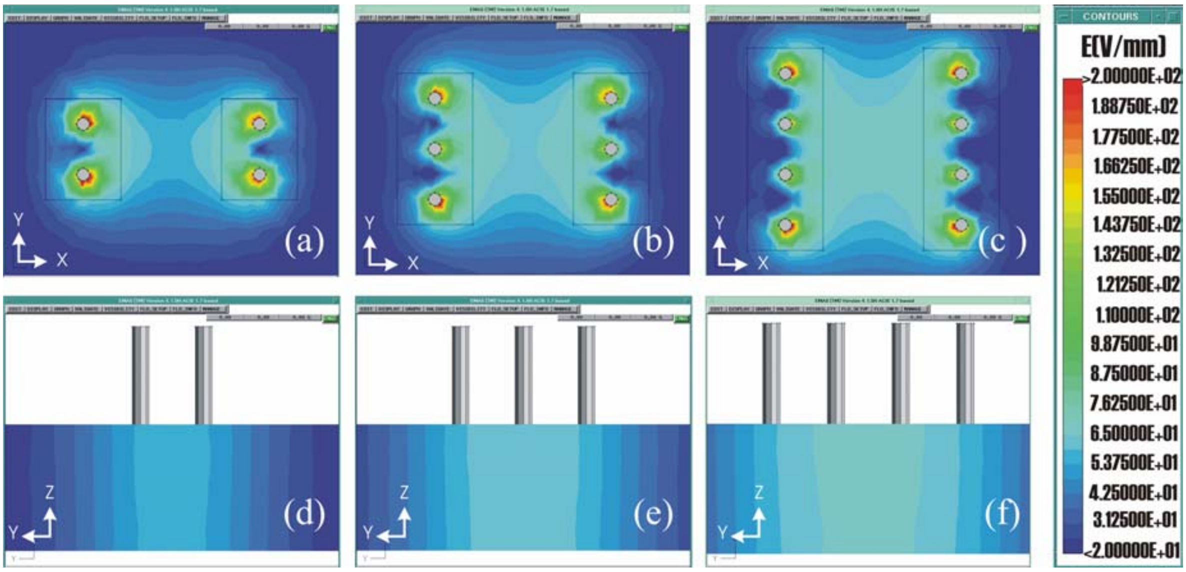

Figure 4.6: Amplitude of E around 2, 3 and 4 needle pairs approximated by 8-faceted needle electrodes in FE model in *xy* plane, i.e. plane perpendicular to the electrodes, depth 1 mm below surface: (a) 2 needle pairs; (b) 3 needle pairs; and (c) 4 needle pairs and in a *yz* plane, crossing in the middle between arrays: (d) 2 needle pairs; (e) 3 needle pairs; and (f) 4 needle pairs. Voltage applied was 500V.

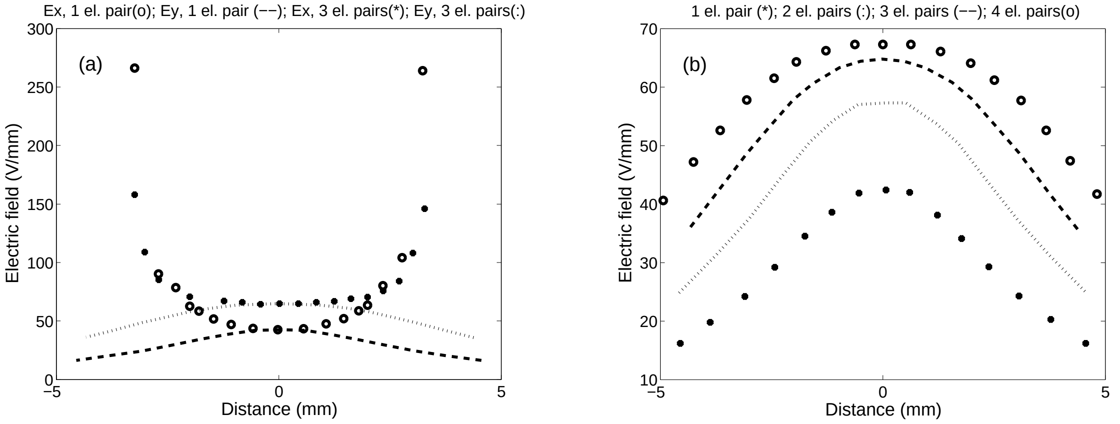

Figure 4.7: (a): Comparison E(*x*) at *y*=0 and E(*y*) at *x*=0 for 1 electrode pair and 3 electrode pairs. (b): Comparison E(*y*) for 1, 2, 3, and 4 electrode pairs. *x*-axis represents the distance from the centre between electrodes i.e. at *x*=0 when E(*y*) is shown and at y=0 when E(*x*) is shown. Electrodes placed at *x*=-3.5 and *x*=3.5 have different polarities.

4.3.2 DISTANCE BETWEEN NEEDLES IN ARRAYS

Modelling results, i.e. the total current and the relative difference between the model and the measurement for the second group of measurements used for model validation are shown in Table 4.4. All measurements from the second group were performed only with 4 mm gel thickness. Figure 4.8 presents E distribution for the cases where two electrode pairs were placed at distances of 2, 4 and 6 mm.

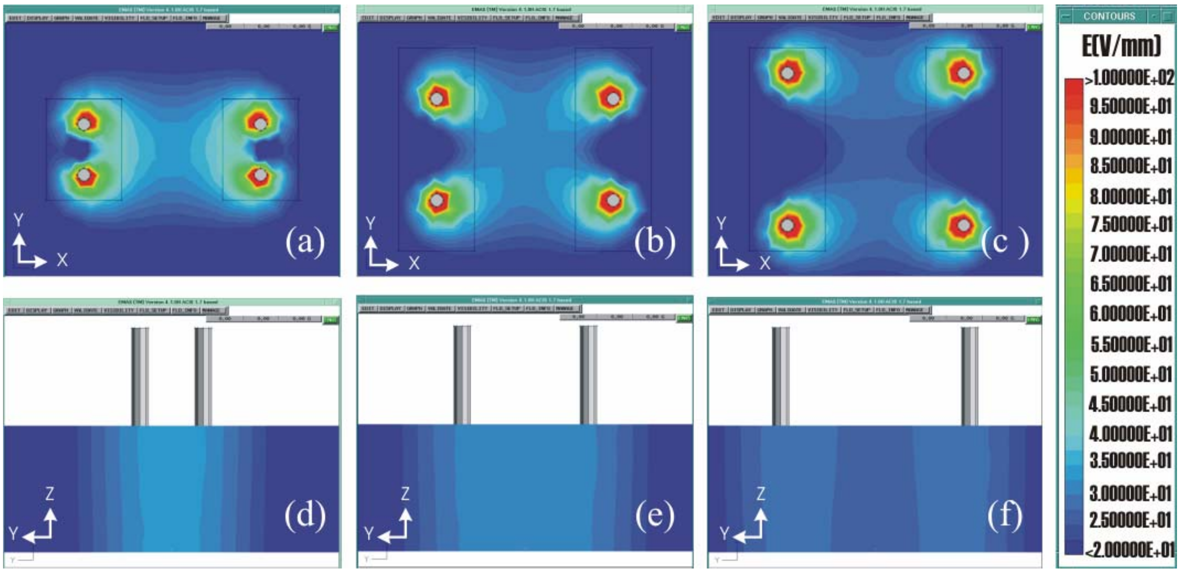

Figure 4.8: Amplitude of E around two electrode pairs in *xy* plane, i.e. perpendicular to the electrodes, depth 1 mm below surface: (a) d=2 mm; (b) d=4 mm; and (c) d=6 mm, and in *yz* plane, crossing in the middle between arrays: (d) d=2 mm; (e) d=4 mm; and (f) d=6 mm. Voltage applied was 300 V.

Table 4.4: Measured and modelled current and relative difference between them for needle arrays with 2 needle pairs and gel thickness 4 mm. Voltage applied was 300 V.

Distance between needle pairs (mm)	Measurement, Current (A)	Model, Current (A)	Relative error (%)
2	2.30	2.33	-1
4	2.70	2.63	3
6	2.70	2.81	-4

Results in Table 4.4 show that the current computed by the model fit the measurement very well. Figure 4.8 displays the change in E distribution as a result of increments in distance between the two neighbouring needle pairs. By increasing the distance between the needle pairs, the E in the middle of the arrays decreases. This result is also observed in Figure 4.9, where E distribution along the *x* and *y* axis is shown, in the area between electrodes (distance 0 denotes centre between electrodes). If the two needle pairs were placed far apart, interaction between both pairs decreased and finally the two pairs behaved as two independent pairs. This is also shown in Figure 4.9(b), where the curve representing E(*y*) for 2 electrode pairs at distance 6 mm already has bimodal distribution. Figure 4.10 shows the volume of gel exposed to E above the value indicated on the *x* axis. Information in Figure 4.8 to Figure 4.10 can be used to determine optimal distance between electrodes to achieve the objective of electropermeabilisation – required permeabilised volume of tissue.

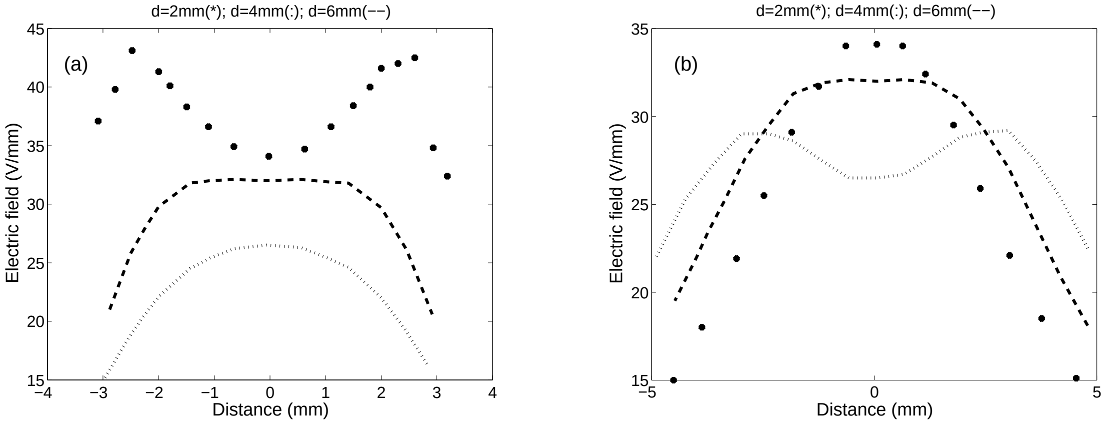

Figure 4.9: (a) E(*x*) at *y*=0; and (b) E(*y*) at *x*=0 for 2 needle pairs, with distance between needles with the same polarity as parameter. *x*-axis represents distance from the centre between electrodes i.e. at *x*=0 when E(*y*) is shown and at *y*=0 when E(*x*) is shown. Electrodes placed at *x*=-3.5 and *x*=3.5 have different polarities.

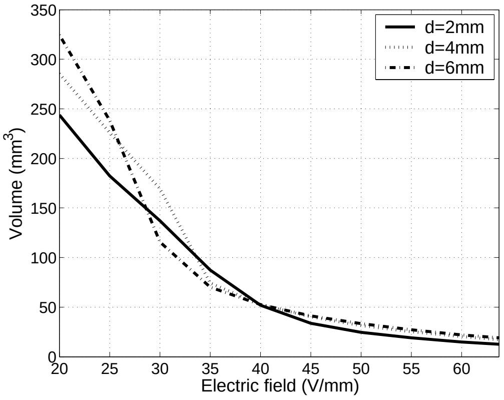

Figure 4.10: Volume of gel exposed to E above the amplitude indicated on *x* axis, with distance between the needle pairs *d* as parameter. Voltage applied was 300 V. Total volume of gel observed was 2450 mm^3 - the volume of a cube with the diagonal equal to the diameter of the petri dish.

4.4 ANALYSIS OF DIFFERENCES BETWEEN MODEL AND MEASUREMENT

As found during the model validation phase, measured current and current computed by the FE model differed in cases with gel thickness of 2 mm.

In order to obtain deeper insight into the reasons for such deviations we plotted graphs with all current measurements (for all voltages and each gel thickness), along with currents computed by the FE model. Due to the linear character of the model, results for other voltages than those presented in Table 4.1, Table 4.3 and Table 4.4 were obtained by scaling.

Figure 4.11 shows approximation of measured and modelled current with the first order polynomial - line for the experiments with 1, 2, 3 and 4 needle electrode pairs. In the legend corresponding polynomial coefficients are displayed. Comparison of both polynomials shows that they have similar slope in all cases. This is also confirmed by equations representing the first order polynomial:

$$y = k_1 x + n_1 , \tag{4.5}$$

where k_1 represents the line slope. The polynomial representing the model always intercepts zero crossing, as expected, while the polynomial representing the measurement always had certain bias, which was the same as constant n_1 in the corresponding linear equation. Furthermore we analyzed possible elements that could cause bias such as influence of a change in gel thickness, deviations in electrode diameter, effect of change in distance between arrays and change in distance between two electrode pairs due to possible inaccuracies in experimental setup.

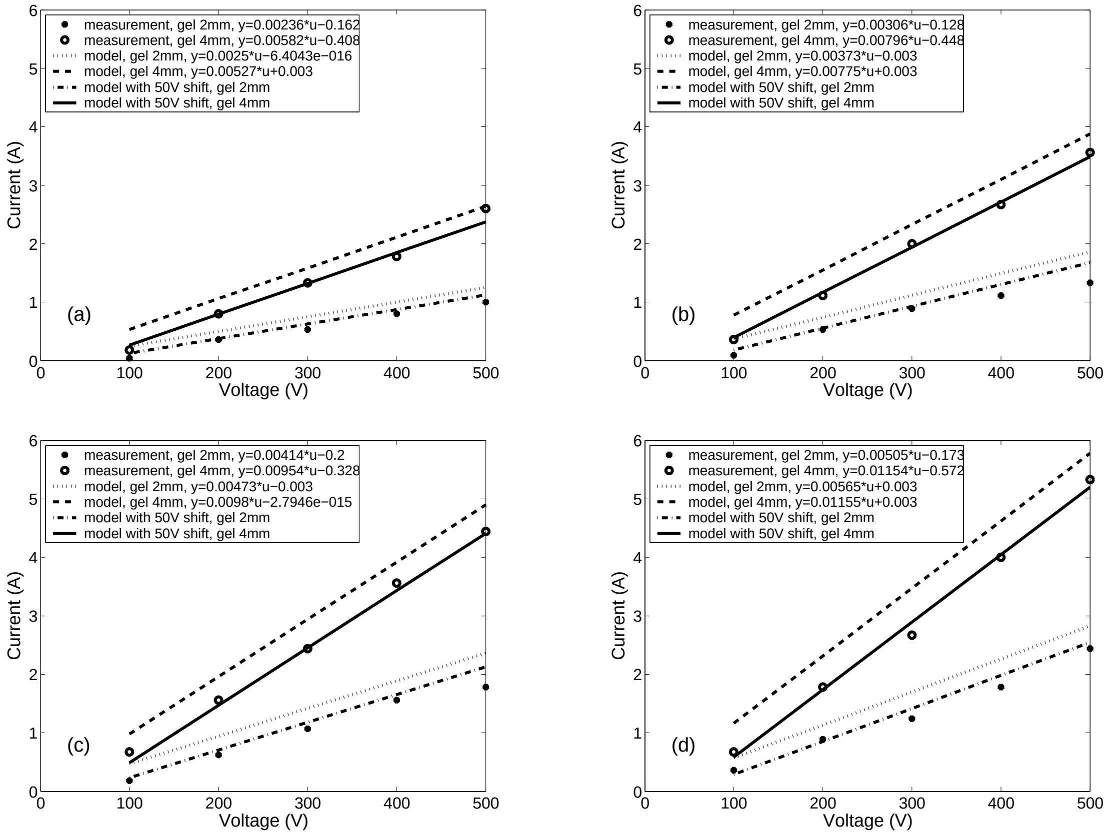

Figure 4.11: Measured, computed current and computed current with 50V shift added to model (a) 1 needle pair; (b) 2 needle pairs; (c) 3 needle pairs; (d) 4 needle pairs. Gel thickness was either 2 mm or 4 mm. Measurements are fitted with first order polynomial, whereas modelled currents are computed by scaling modelled current obtained at 500 V.

4.4.1 ANALYSIS OF MEASUREMENTS ON PHANTOMS

When performing measurements, special attention was paid to several factors in order to provide precise current results. Such factors were, for example, the conductance of the gel, thickness of the gel in the petri dish, angle between needle electrodes and the gel, and local heating close to the electrodes where the current density is high.

The conductance of gel was controlled by conductometer in a vessel where gel was stored. Before each experiment a fresh gel was poured into a petri dish from the vessel. During the pulse application, plotting of U/I ratio was observed in order to determine if conductance changed during the pulse. The temperature in the laboratory where the experiments were performed was kept constant, which could otherwise affect the conductivity of the gel. Another possible source of measurement error would also be the angle between electrode position and the gel. The angle was adjusted mechanically, which was coarse and therefore it is possible that needle position was not precisely perpendicular to the gel in all experiments.

The change in conductance and deviations in angle between electrodes and gel (i.e. the length of the contact between the gel and the electrodes) contributed mostly to random measurement error, which was determined to be negligible. In that respect the comparison of measurements and model in Figure 4.11 also showed influence of bias greater than random error. Namely, slopes of measurement and model polynomials being parallel to each other confirmed that the conductivity used in the model was close to that used in experiments. There were also very small deviations around the measurement line which, if they existed, could indicate random measurement error. And finally, based on the fact that replicate results in all experiments were very close to each other we can conclude that the random measurement error was negligible. The total measurement error, which consists of bias and random error, was therefore equal to bias error.

A possible source of bias error could be small deviations in gel thickness, deviations in distance between electrodes and in distance between arrays which depended on the accuracy of holder dimensions. Another possible source of bias error could be electrode polarization [Plonsey, 1969], which could have decreased measured current compared to modelled current. All the potential contributions were checked systematically.

4.4.1.1 THICKNESS OF GEL

A critical control was to check the thickness of the phantom. As described in the Chapter 4.1.2, the thickness of the gel was obtained from the values of the volume of the liquid gel. This was measured at 37°C. Due to the temperature dilatation coefficient of the gel and of the pipette, some inaccuracies might be present in the effective values of the volume and as such in the gel thickness after cooling to 20°C. This was checked by mechanical means with a precision of 0.2 mm. All thicknesses were correct in the central part of the dish within this precision. But due to the meniscus effect, the gel was thicker along the edge of the dish. Therefore all electrical measurements were run by inserting the electrodes only in the central part of the gel. We checked the effect of small changes in the thickness (±0.2 mm) on the computed current for a 500 V pulse using the two needle electrode set-up. As shown in Table 4.5, a good improvement in the fit between measurements and simulations, provided the thickness decreased was obtained with the thin gel (2 mm), while it increased the difference with thicker gel (4 mm and 6 mm).

Table 4.5: Simulated variations in thickness of gel.

Thickness of gel (mm)	Current (A)		Thickness of gel (mm)	Current (A)	Thickness of gel (mm)	Current (A)
	Measurement	8-facet		8-facet		8-facet
2	1.00	1.25	1.8	1.13	2.2	1.37
4	2.60	2.64	3.8	2.51	4.2	2.76
6	4.00	4.02	5.8	3.89	6.2	4.14

4.4.1.2 ELECTRODE DIAMETER

Simulations were run under the assumption that the electrode diameter was different than declared. No significant change in the relative difference between experiments and simulation (up to 3%) was obtained for the three different gel thicknesses, provided that relative change in electrode diameter was within ±10%.

4.4.1.3 DISTANCE BETWEEN ARRAYS

As the electrode holder was mechanically drilled, some imperfections were present in the distance between the two electrodes. This was introduced in the model but was observed not to improve the relative differences significantly (improvement up to 2%) provided the distance between arrays was changed by ±5%.

4.4.1.4 DISTANCE BETWEEN TWO ELECTRODE PAIRS

For the same technical reason, whether the distance between electrodes in an array might alter the simulated current, the influence of change in distance was checked. The distance between two electrode pairs was altered up to ±5%. Again no significant improvement in the relative difference was detected (improvement up to 1%).

4.4.1.5 LOW VOLTAGE RESULTS AND VOLTAGE SHIFT

A 0.1 ms pulse with different low voltages was applied to a two needle electrode set-up inserted in a 6 mm gel. As shown in Figure 4.12, a non linear dependence of the current on the applied voltage, when less than 50 V, was observed. No current flowed between the electrodes when 25 V were applied. A sharp increase was only observed when the voltage was above 50 V. Nonlinear current - voltage dependency indicated an electrode polarization effect. Based on the results at low voltages shown in Figure 4.12, a 50 V shift (simulating electrochemical effects at tissue – electrode interface) was added to the model. A significant improvement in the fit between the model and the measurement in the current – voltage plot was obtained whatever the electrode array or the gel thickness as shown in Figure 4.11. The 50 V shift was introduced in the models only when voltage above the nonlinear part of current - voltage dependency was used.

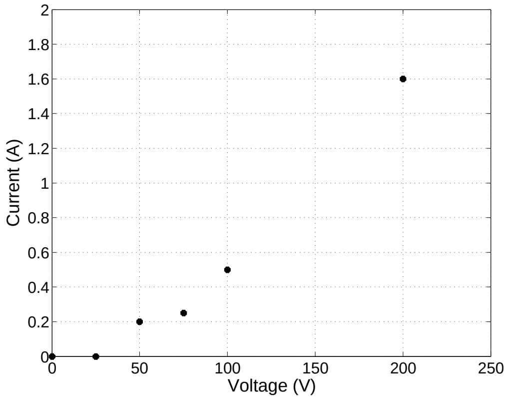

Figure 4.12: Current under low voltage pulse conditions. Thickness of gel was 6 mm.

Electrochemical effects at the electrode – tissue interface are in general influenced by electrode chemical nature, sample composition and electrical parameters. In [Pliquett *et al.*, 1996] it was shown for aluminium electrodes that the calculated E using electrode voltages and geometries alone could be significantly higher than the real E present in the tissue. In [Loste *et al.*, 1998] it was also presented that aluminium electrodes demonstrate higher electrochemical effects than stainless steel electrodes. Thus the voltage drop at the electrode - tissue interface needs to be evaluated and correction for electrochemical effects needs to be taken into account in models, which in our model was introduced with a 50 V shift.

4.4.2 ANALYSIS OF REASON OF MODELLING ERROR

In our FE models cylindrical needle electrodes were simplified by 8 faceted electrodes. Our analysis of optimal needle electrode geometry has shown that 12 faceted electrodes, which were closer to cylindrical electrodes, did not perform better than 8 faceted electrodes regarding relative current difference. Therefore we assumed that this approximation did not introduce a significant part in the modelling error.

On the other hand comparison of 8-faceted needles with modelled tips and without modelled tips has shown, that tip modelling significantly affected current at 2 mm gel thickness. Tip modelling could therefore be one of the reasons for the discrepancy in modelled and measured current at 2 mm gel thickness. However, further improvement in tip modelling would not have brought additional improvement because tip-in and tip-out orientation did not give significantly different results.

Another source of modelling error could also be the mesh density. Namely scarce mesh could give distorted results. In FE modelling it was therefore important to recompute the same model with different mesh densities. Our results with different mesh densities did not differ significantly, so we assumed that mesh densities used were sufficiently high.

4.5 DISCUSSION

The method of modelling needle electrodes in the FE model, which hastened the solution process was proposed and validated by measurements on a phantom tissue. Based on the results of criteria function, 8 faceted needle electrodes were proposed as a substitute for cylindrical needles. Results showed that such a simplification could be used without serious impact on model results.

The model relative difference in total current, which was evaluated during model validation on measurements, was 9% for gel thickness of 4 mm. This difference was not due to approximation of needles with faceted shape nor could it be explained by geometrical inaccuracies (gel thickness, tip modelling, and inter electrode distance) between the model and the real system. The bias was due to the low voltage behaviour which was non-ohmic. This could not be predicted by the simulation. However, based on low voltage measurements, a 50 V voltage shift was introduced in the model and bias error was sharply decreased for applied voltages above 100 V. The relative difference between modelled and measured current decreased from 9% to 3% for gel thickness of 4 mm.

Current measurement was also examined as a means of FE model validation [Miklavčič *et al.*, 1998]. Provided model geometry and material properties are known and properly modelled, an FE model producing current results which correspond to measured results could be used for at least rough estimation of E distribution in tissue. This information is of great importance for effective tissue electroporation in electrochemotherapy and *in vivo* tissue gene transfection. Based on known

E distribution, pulse parameters (especially amplitude) and needle electrode positions could also be optimized.

Additionally, such an FE model could be used for estimation of maximal current, for different needle electrode geometries and given tissue properties (geometry, conductivity). Maximal current could be determined and preset in the electroporator in order to protect tissue against damage. Maximal current and required voltage for effective tissue electropermeabilisation at given electrode geometry are also important in designing power supply and capacity of elctroporators.

5 VALIDATION OF TIME DISCRETE MODEL OF TISSUE PERMEABILISATION

Modelling of electric field (E) distribution in tissue is complex and demanding due to the sometimes inhomogeneous and anisotropic tissue electrical properties and usually complex tissue geometry. Analytical models can be employed only for simple geometries and under the condition that tissue geometry, anisotropies and inhomogeneities can be described within the same coordinate system. For example Dev *et al.* in [Dev *et al.*, 2003] developed the analytical model of potential and E distribution around six needle electrodes. Their model is applicable only to 2D problems and tissue with homogenous electrical properties. In Chapter 3 we also presented a time discrete model of tissue permeabilisation with an analytical description of E distribution. However despite the ability of our model to describe inhomogeneous tissue properties, it is designed only for a geometry consisting of two concentric cylindrical electrodes.

Therefore for modelling E distribution in tissue in most cases numerical modelling techniques are still the only techniques applicable. Predominantly finite element (FE) method and finite difference (FD) methods are applied. Both numerical methods have been successfully used and also validated by comparison of computed and measured E distribution [Miklavčič *et al.*, 1998; Gehl *et al.*, 1999; Miklavčič *et al.*, 2000].

There are several software products available for numerical modelling of electromagnetic problems. Sophisticated finite element software products provide support for 3D analysis and handle time domain and frequency domain problems [Mirotznik and Prather, 1997]. However most of the products do not provide possibility to dynamically change material properties (e.g. specific conductivity, permittivity) based on computed output variables (e.g. E intensity) in the material. This feature is needed to describe the course of electropermeabilisation, in the manner described in Chapter 3 on analytical model. Our group tested three software packages for finite element modelling (introduced in Chapter 2) and found two packages suitable for the development of a time discrete permeabilisation model. Those were the EMAS (Ansoft Inc., USA) and FEMLAB (Comsol Inc., Sweden) software packages. Both of them however required substantial efforts for development of additional programme codes that enabled dynamical changes of material properties.

In this chapter we therefore present a time discrete model of rabbit liver tissue permeabilisation with inserted needle electrodes. E distribution around the needle electrodes is computed numerically with a finite element method. The model consists of a sequence of static models, which describe E distribution at discrete time steps during permeabilisation. In this way the model presents the dynamics of electropermeabilisation since, according to distribution of E intensities from the preceding time discrete step, tissue conductivity is changed in the next step. The functional dependency between specific conductivity and E intensity was S-shaped as introduced in Chapter 3. Estimation of the S-shape function parameters was based on *in vivo* current measurements. The model was then validated on experimentally obtained total current measurements and areas of reversibly and irreversibly permeabilised rabbit liver tissue. Measurements of reversibly and irreversibly permeabilised tissue were used from published work of Miklavčič *et al.* [Miklavčič *et al.*, 2000] which were performed on the same tissue geometry and electrode design.

5.1 EXPERIMENTS

In vivo experiments were performed at the Institute Gustave-Roussy, France on rabbit liver tissue in accordance with European Commission Directives and French legislation concerning animal welfare. Three rabbits were used in the experiments. Animals were kept anaesthetised for the entire duration of the experiments. A subxypoid incision was made and the liver was gently exteriorised and exposed to electrical treatment. Electrical treatment was performed through two parallel needle electrodes (Figure 5.1) inserted perpendicularly to the tissue surface approximately 7 mm in depth. In the experiments, three different needle diameters were used: ϕ=0.3 mm, ϕ=0.7 mm and ϕ=1. 1 mm. The inner distance between the needles was always 8 mm as in Miklavčič *et al.*, 2000. Eight rectangular monophasic pulses of 100 µs duration and 1 Hz repetition frequency were applied. Pulses were delivered by pulse generator Jouan GHT 1287B, St.Herblain, France. Applied pulse amplitudes were in the range of 200 V - 1200 V. The applied voltage and resulting current were acquired by high voltage and current probes respectively and stored on-line by a digital oscilloscope (LT344, LeCroy Corporation, USA). Altogether 13 experiments were performed with needles of diameter 0.3 mm and again with needles of 1.1 mm diameter, whereas 43 experiments were performed with 0.7 mm diameter needles. These experiments were performed in the same way as in the previous work of our group [Miklavčič *et al.*, 2000], with the difference that in previous experiments reversibly and irreversibly permeabilised areas of tissue were determined, while the current was not measured. In the present experiments total current was measured. Therefore the results of both experiment sets were used in the present study for the purpose of the model parameter estimation and model validation.

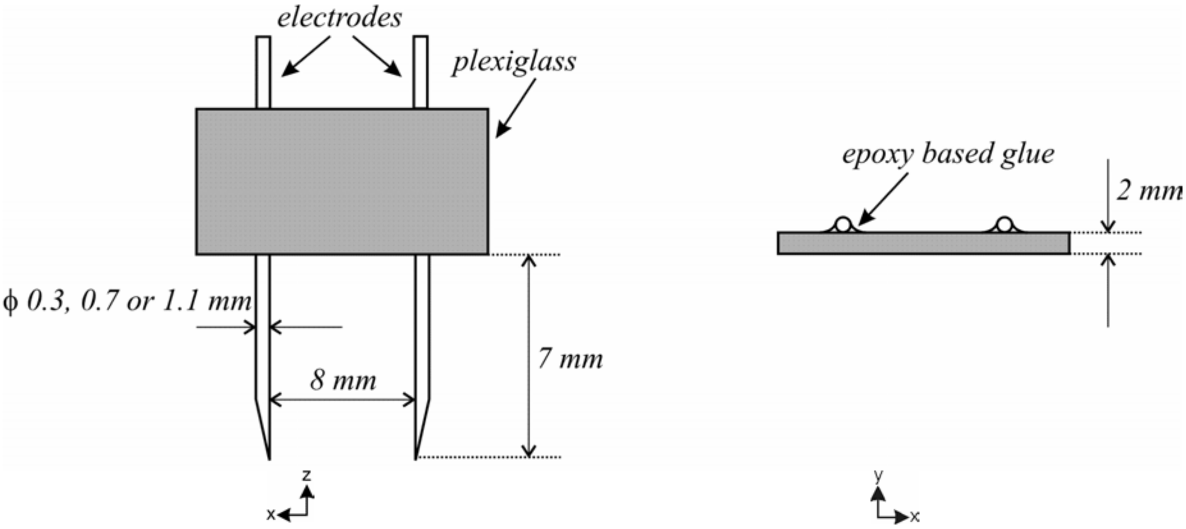

Figure 5.1: Needle electrodes used in experiments. Left: side view; right: top view.

5.2 TIME DISCRETE PERMEABILISATION MODEL WITH NUMERICAL CALCULATION OF E DISTRIBUTION

The time discrete model is based on the hypothesis that the change in tissue conductivity caused by E intensity follows $\sigma(E)$ dependency. When a constant voltage is applied to tissue with inserted needle electrodes, it results in inhomogeneous E distribution in tissue. According to σ(E) dependency and as a result of the tissue exposure to inhomogeneous E distribution, the tissue conductivity becomes heterogeneous. Namely in the volume of tissue exposed to E intensity above reversible threshold the tissue conductivity increases, while in the rest of the tissue the conductivity remains unchanged.

Having tissue with conductivity increased in such a way still exposed to constant voltage, we obtain an E distribution which differs from the distribution in completely non-permeabilised tissue. In part of the tissue with increased conductivity the potential drop is lower than in part of still non-permeabilised tissue. As a consequence E intensities are higher in part of still non-permeabilised tissue compared to the previous distribution of E intensities. Consequently, increased E intensities cause a change of conductivity according to σ(E) dependency in that part, too. The process continues in this manner until the increase in E intensity in part of non-permeabilised tissue is not high enough to further change conductivity. The propagation of tissue permeabilisation is then terminated.

Following this idea a sequence of static finite element (FE) models was designed in order to describe the electroporation process at time discrete intervals. In each static model (step) tissue conductivity was determined based on the E distribution and specific conductivity from the previous step in the sequence, as described in equation (5.1):

$$\sigma(x,y,z,k) = f(E(x,y,z,k-1),\sigma(x,y,z,k-1)), \qquad \text{for} \qquad k \geq 2 \tag{5.1}$$

where E denotes electric field intensity, σ denotes tissue conductivity and k the step in the modelling sequence. In equation 5.1, the conductivity computation takes into account that once the conductivity is increased at a particular point in tissue during step $k-1$ it can not drop even though in step k electric field E_{k-1} would imply that. In the first step (k=1) we assume homogenous tissue conductivity i.e. conductivity of completely non-permeabilised tissue.

A three dimensional FE model was built using FEMLAB software produced by Comsol, Sweden. The model geometry is shown in Figure 5.2.

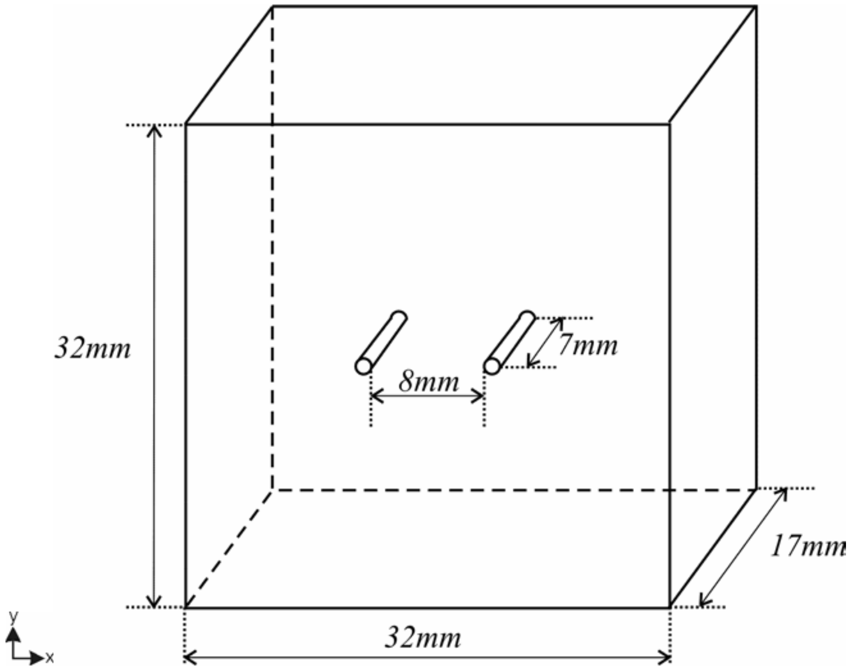

Figure 5.2: Model geometry.

The E distribution in a FE model was described with equations for steady electric currents in volume conductor. Voltage was applied as a Dirichlet boundary condition to the surface of the needles. The needle electrodes were modelled as 8 faceted hollow shapes [Šel *et al.*, 2003] instead of cylinders, which we described in Chapter 4, to give proper results and at the same time spend less computing power. Due to the fact that needles were significantly smaller than the surrounding tissue, a FE mesh was designed to be much denser in regions around electrodes than at the edge of the parallelepiped.

5.3 PARAMETER ESTIMATION

In our experimental condition (sampling rate was 25 MS/s), no significant delay between voltage and current was observed and also negligible transient response was detected with respect to the pulse length, which was the reason to consider only the ohmic behaviour of the tissue in the model. For the illustration the voltage and the current during the first pulse are presented in Figure 5.3.

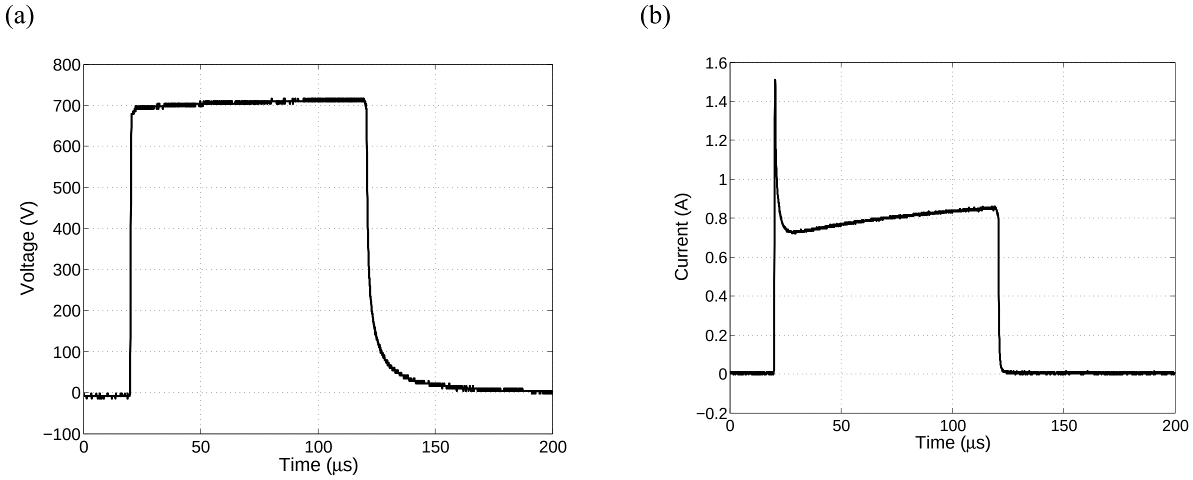

Figure 5.3: Voltage (a) and current (b) during the first pulse.

Parameter estimation of σ(E) dependency was carried out on a subset of experiments with current measurements. For each needle electrode diameter, we selected measurements at three different voltages, i.e. around reversible threshold, above irreversible threshold and in the middle between the two thresholds. Threshold voltages were chosen according to published values for rabbit liver tissue in [Miklavčič *et al.*, 2000]. The conductivity of non-permeabilised tissue (σ_0) was determined at low voltages, far below reversible threshold. The obtained value for rabbit liver (σ_0=0.067 S/m) was smaller than the mean values for human liver tissue reported in the literature [Faes *et al.*, 1999; Geddes and Baker, 1967; Rush *et al.*, 1963; Schwan and Key, 1957]. However in [Geddes and Baker, 1967], the lack of agreement between the measurements in the low frequency region and at body temperature is reported for the liver conductivities of other mammals – for example the range of liver conductivity for a guinea pig was between 0.025 and 0.440 S/m. The value of non permeabilised rabbit liver conductivity obtained in our experiments is well within this range.

The σ(E) dependency was described by following an S-shape function:

$$\sigma(E) = \frac{\sigma_1 - \sigma_0}{1 + De^{-\frac{E-A}{B_S}}} + \sigma_0 \,. \tag{5.2}$$

The electropermeabilisation tissue parameters subject to estimation were thus E_0, E_1, σ_1 and S-shape function parameters B_S and D. Parameters were estimated by optimising modelled current to be close to the measured current, obtained in experiments. Current measurement was used to determine the extent of membrane permeabilisation in pellets [Abidor *et al.*, 1993]. It was also suggested that current can be used for *in vivo* measurement of the change in conductance due to permeabilisation [Davalos *et al.*, 2002]. Therefore current measurement was also used in our study to determine the change in tissue conductivity resulting from membrane permeabilisation.

Estimated parameter values were E_0=460 V/cm, E_1=700 V/cm, σ_1=0.2412 S/m, B_S=30 and D=10. Figure 5.4 presents σ(E) dependency based on these estimated parameters. Comparison of measured and modelled current is presented in Table 5.1.

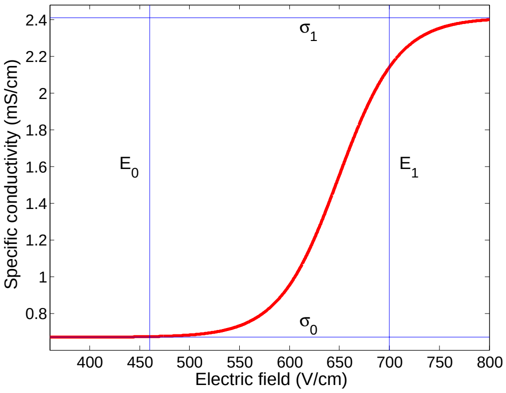

Figure 5.4: Optimised dependency σ(E).

As already explained in Chapter 3.8 the reason for choosing the S-shape function to describe σ(E) dependency was that by considering differences in cell size, shape and their interaction we can expect some cells to be permeabilised before others when E above E_0 is applied. That could result in a gradual increase in tissue conductivity at E_0 described by the σ(E) curve. By increasing E above E_1 the loss of viability of some cells is expected and later of all cells which again leads into gradual saturation of σ(E) curve. Similarly, Teissie *et al.* [Teissie *et al.*, 1999] described the influence of cell size on electropermeabilisation. They stated that the population of permeabilised cells increases with an increase in field intensity.

Table 5.1: Modelled current computed on estimated parameters at three different voltages for needle diameters 0.3, 0.7 and 1.1 mm. The relative error is expressed as the difference between measured and modelled current, divided by measured current.

ϕ (mm)	Up (V)	Measured I (A)	Modelled I (A)	Rel. error (%)
0.3	617	0.58	0.62	-7
0.3	815	0.90	0.92	-3
0.3	1023	1.11	1.23	-11
0.7	507	0.54	0.55	-1
0.7	704	0.87	0.90	-3
0.7	909	1.20	1.28	-7
1.1	508	0.49	0.60	-23
1.1	707	1.04	1.02	2
1.1	911	1.46	1.43	2

Another reason for choosing the S-shape dependency was that in electrooptical and conductometrical relaxation measurements during electropermeabilisation in the suspension of the salt filled vesicles [Neumann and Kakorin, 1996; Neumann *et al.*, 1999] it was observed that a massive conductivity increase as a function of E intensity had similar shape.

5.4 MODEL VALIDATION

The time discrete permeabilisation model with S-shape $\sigma(E)$ dependency was validated in the presence of inhomogeneous E distribution. Validation was based on experiments where electrical treatment was performed with needle electrodes inserted in liver tissue.

The observed outputs at each step in the time discrete model, which represented values at discrete time intervals of electropermeabilisation, were E distribution and total current. During simulations it was ascertained that under the conditions used in experiments (applied voltages, number and pulse duration), a sequence of five time discrete steps sufficed for termination of electropermeabilisation process, which in other words meant that no change in conductivity was obtained with further steps. This was also in agreement with results of the analytical model presented in Chapter 3.3.1.

5.4.1 VALIDATION OF THE E INTENSITY OBTAINED IN THE LAST STEP OF THE TIME DISCRETE MODEL ON THE AREA OF REVERSIBLY PERMEABILISED TISSUE

The area of reversibly permeabilised tissue was determined by means of the bleomycin method in experiments on rabbit liver tissue. Experiment description and details of the method are given in [Miklavčič *et al.*, 2000]. Experiments with a needle diameter of 0.7 mm revealed that when increasing voltages were applied to the needles, at 527 ±30 V the nuclei started to become altered in the middle region between the two electrode insertions, which reflected the permeabilisation of the cell membranes and entrance of bleomycin in that region of the tissue. Therefore, we ran simulations of the time discrete permeabilisation model at 520 V in order to compare the computed E distribution with experimental results.

Figure 5.5 presents E distribution and total current in five consecutive steps computed by the model. Figure 5.5(a) shows E intensity in non-permeabilised tissue, while Figure 5.5(e) shows E intensity at the end of the permeabilisation process. During the propagation of permeabilisation, as shown in Figure 5.5(b) and Figure 5.5(c), intensity of E exceeds reversible threshold value in the whole area between electrodes; even more, in some parts it also exceeds irreversible threshold value. However, at the end of the permeabilisation propagation, modelled E distribution corresponds to the situation as observed in experiments. During pulse application, E intensity causes a change in membrane permeability which allows for transfer of ions - current carriers. Consequently tissue conductivity increases, which does not however bring the same increase in membrane permeability for molecules such as bleomycin. Namely, molecule transport occurs predominantly after the pulse [Puc *et al.*, 2003]. Total current in each of 5 time discrete steps is shown in Figure 5.5(f).

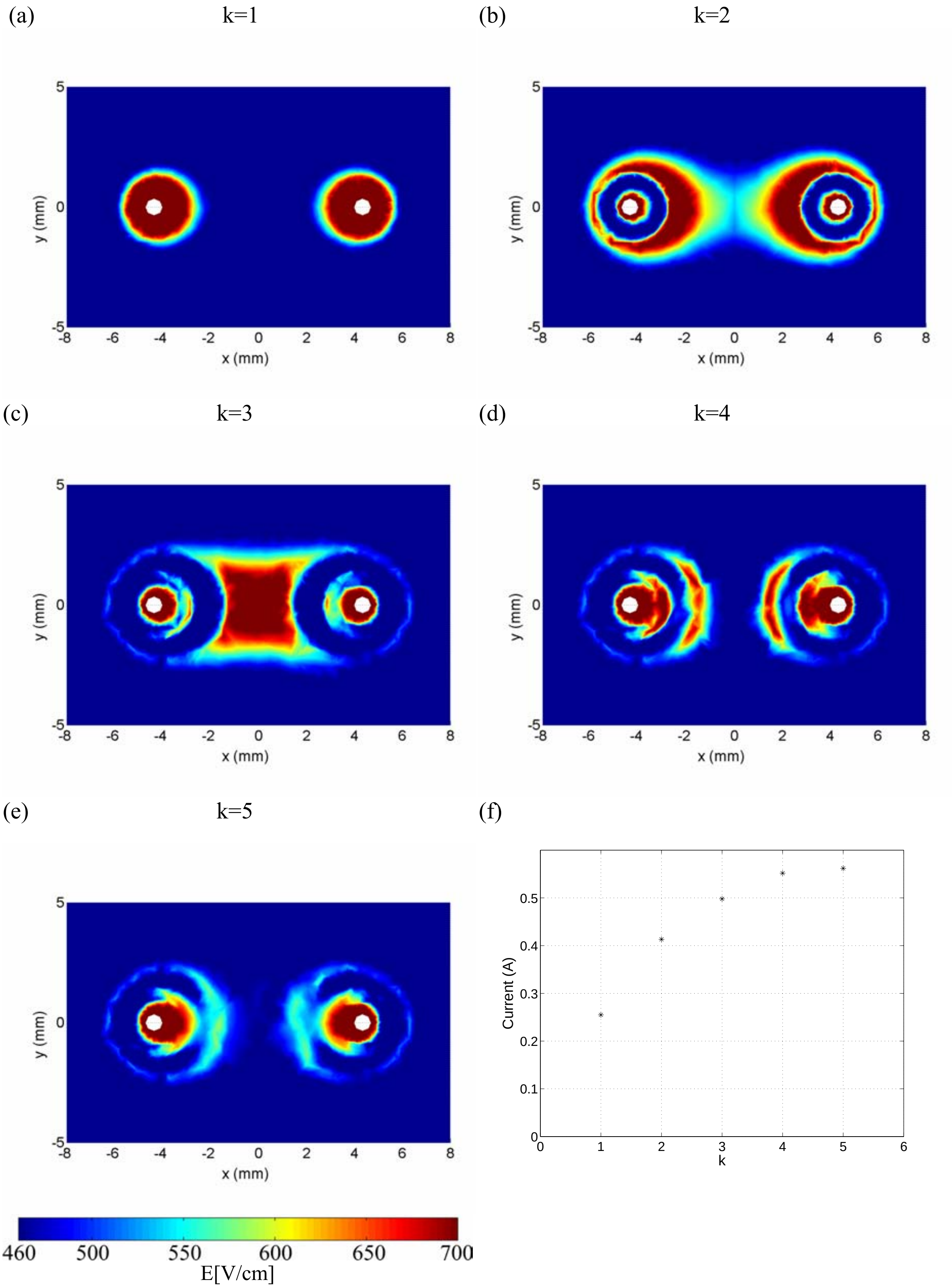

Figure 5.5: E intensity during electropermeabilisation as obtained in five consecutive steps of the time discrete electropermeabilisation model. (a): 1st step, (b): 2nd step, (c): 3rd step, (d): 4th step and (e): 5th step and total current at each step (f). Needle diameter was ϕ=0.7 mm. Voltage applied was 520 V.

Increase in tissue conductivity caused a modification in E distribution, which consequently caused another change in tissue conductivity and propagation of permeabilisation. This was a dynamic process, during which E intensity was changing very fast in the region between and around electrodes. Consequently we presumed that E intensity above irreversible threshold value did not persist in the region between electrodes long enough to cause irreversible changes in cell membranes. We can also observe this in Figure 5.8(b), where the current computed in each step of the permeabilisation model was compared to the current measured during the first pulse. At 500 V the first three steps occurred in less than half the duration of the pulse length. In that first half, E intensity was permanently changing as was the current. After the third step, the E intensity stabilised, and consequently the current. The steady E intensity could then influence the increased membrane permeability for bleomicyn through the formation of long lived stable pores, which enabled the diffusive transport of bleomycin across the permeabilised cell membrane after the pulse application. Subsequently, we compared E distribution of the fifth step with the reversibly permeabilised area obtained in experiments. In Figure 5.5(e) we can observe that in the middle between the electrodes, E intensity is just around the reversible threshold E_0=460 V/cm, which is in accordance with experimental results.

5.4.2 VALIDATION OF E INTENSITY OBTAINED IN THE LAST STEP OF THE TIME DISCRETE MODEL ON THE AREA OF IRREVERSIBLY PERMEABILISED TISSUE

In previous work of our group [Miklavčič *et al.*, 2000] experiments were performed on rabbit liver tissue with needle electrodes in order to determine the area of tissue necrosis at different pulse amplitudes. In Figure 5.6 the black line presents the contour of tissue necrosis as determined during those experiments. The contour is compared to E intensity computed in the last step of the model presented in Chapter 5.2. The dark red area presents the area of tissue exposed to E above irreversible threshold (E_0=700 V/cm) which corresponds very well to the necrosis contours (black contours) obtained in experiments.

5.4.3 VALIDATION OF THE CURRENT OBTAINED IN THE LAST STEP OF THE TIME DISCRETE MODEL ON TOTAL CURRENT AT THE END OF THE PULSE

The total current obtained in the fifth step and the measured current at the end of the first pulse in rabbit liver tissue are compared in Figure 5.7 for needle diameters of ϕ=0.3 mm, ϕ=0.7 mm and ϕ=1.1 mm. In Figure 5.7 the root mean square error (RMSE) and Theil's inequality criteria (TIC) measures are given, which illustrate the agreement between modelled and measured current. RMSE and TIC measure for current are expressed as:

$$RMSE = \sqrt{\frac{\sum_j (i_j - im_j)}{N}}\ , \tag{5.3}$$

$$TIC = \frac{\sqrt{\sum_j \left(i_j - im_j\right)^2}}{\sqrt{\sum_j i_j^2} + \sqrt{\sum_j im_j^2}}\ , \tag{5.4}$$

respectively. In Equations (5.3) and (5.4) *N* denotes the number of measurements, *im* denotes modelled current and *i* measured current in j^{th} measurement out of *N*. With respect to results

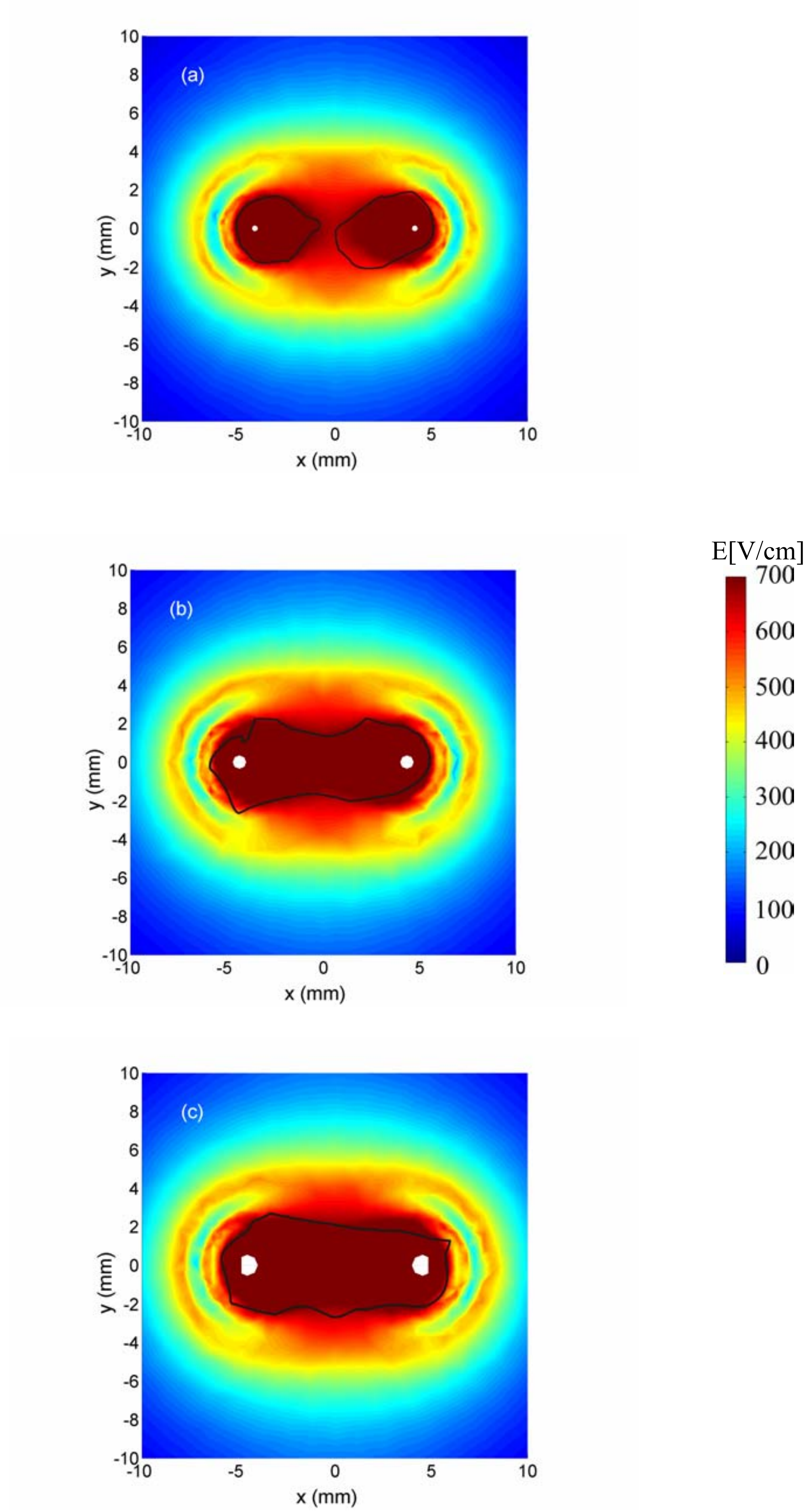

Figure 5.6: Comparison of irreversibly permeabilised tissue computed by model (dark red area) and area of tissue necrosis determined in experiments (black contour). Needle diameter and applied voltage were (a): ϕ=0.3 mm, U=960 V, (b): ϕ=0.7 mm, U=960 V and (c):ϕ=1.1 mm, U=952 V.

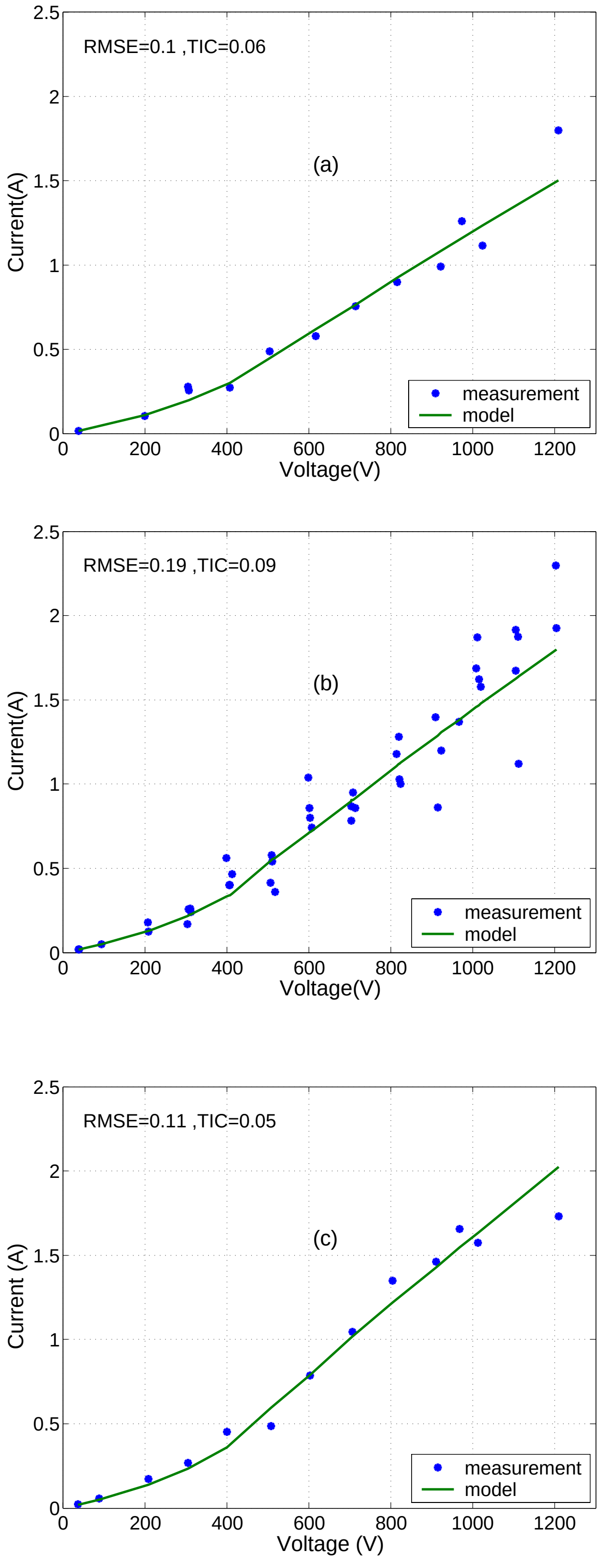

Figure 5.7: Total current at the end of pulse. Comparison of computed (full line) and measured current (asterisk) at different voltages for needles with diameter (a): ϕ=0.3 mm, (b): ϕ=0.7 mm and (c):ϕ=1.1 mm.

presented in Figure 5.7, TIC for needle electrodes with diameter 0.3, 0.7 and 1.1 mm was 0.06, 0.09 and 0.05, respectively. As the TIC value can be in the range between 0 and 1, and considering the fact that values below 0.3 indicate good agreement [Murray-Smith, 1995], we can say with confidence that excellent agreement between the modelled and the measured current was obtained.

5.4.4 VALIDATION OF THE CURRENT OBTAINED AT TIME DISCRETE STEPS COMPUTED BY THE MODEL ON TIME COURSE OF MEASURED TOTAL CURRENT DURING THE FIRST PULSE

The total currents for each of five time discrete steps of electropermeabilisation model at different voltages for all needle diameters and measurement of current obtained during the first pulse are shown in Figure 5.8. The discrete time intervals, at which the model results are presented, were determined by calibrating the kinetics of the model to the measurements and by assuming independency of time intervals on pulse amplitude.

Comparisons of measurements showed nonlinear increases in current when different voltages are applied, which was significant for all needle diameters. In principle, an increase in current which is not proportional to the increase in voltage reflects the increase in tissue conductivity. It was observed that the model also predicted this increase in amplitude, for all needle diameters.

We further observed (Figure 5.8) that at low voltages, below permeabilisation threshold, the current remained constant after the pulse rise time. This was also predicted by our model. However, at higher voltages, above reversible threshold, the current increased during the whole pulse length, while modelled current increase was moderate. The difference could result from tissue heating and a consequent increase in conductivity [Duck, 1990]. Another reason for increased tissue conductivity could be also ion dissociation. Both effects could have occurred in tissue but were not incorporated into the model at this stage.

The comparison of modelled current results with the current dynamics of the first pulse is a preliminary result. Further investigations have to be carried out in order to determine how tissue conductivity depends on the duration of exposure to E intensity and increases in temperature T at higher pulse amplitudes, i.e. to determine $\sigma(E,T,t)$ dependency.

Results of the time discrete permeabilisation model, presenting permeabilisation at discrete time intervals were compared only to the first pulse. Namely, the first pulse had a similar time course to the others in the train of pulses, as shown in Figure 5.9(b), where the applied pulse amplitude was 700 V (Figure 5.9(a)). In Figure 5.8(b) we can observe that at 700 V in non permeabilised tissue (circle symbol at t=0.2 μs) the current response would be 0.35 A. However the current at the end of pulse was 0.82 A, which was a result of increased conductivity due to tissue permeabilisation (the same was predicted by the model). That is evidence of tissue permeabilisation already during the first pulse. As current responses had similar shapes when the following pulses were applied we presume that during pauses between the pulses the tissue resealed, at least concerning the small pores that contribute to current conductance [Chang and Reese, 1990]. Note that in Figure 5.9 the pauses between pulses (1 s) were skipped, by employing the segmentation feature of the oscilloscope which enabled acquisition of pulses only.

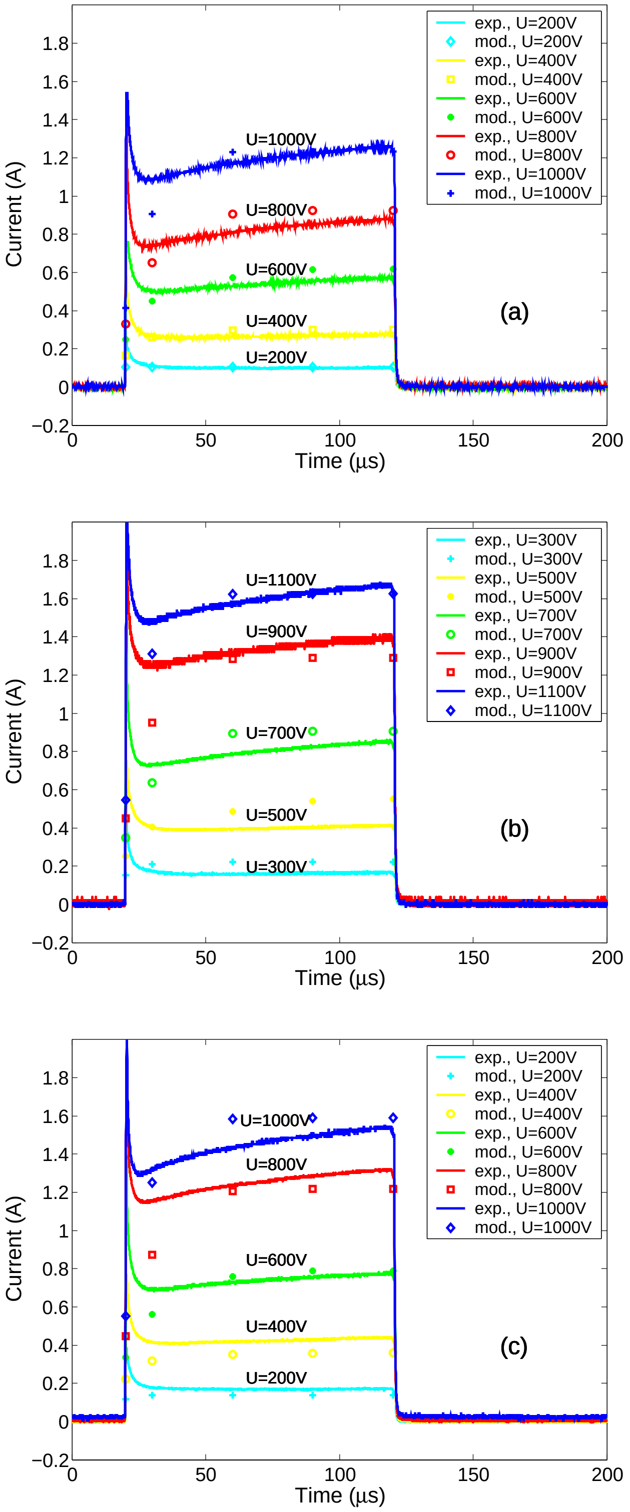

Figure 5.8: Current for five consecutive time discrete steps of the electropermeabilisation model (open symbols) and measured current during the first pulse (full line) at different applied voltages (expressed as parameter) and needles with diameter (a): ϕ=0.3 mm, (b): ϕ=0.7 mm and (c):ϕ=1.1 mm.

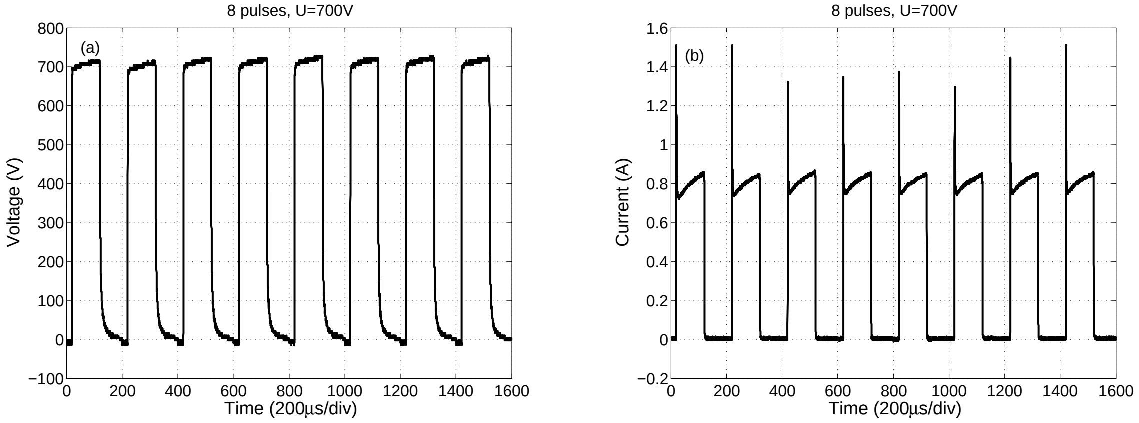

Figure 5.9: Train of 8 pulses: (a) applied voltage, (b) resulting current. Needle diameter was 0.7 mm. Pulses were acquired using the segmentation feature of the oscilloscope, which enabled the acquisition of pulses only.

5.5 DISCUSSION

We presented the development and validation of the time discrete model of tissue permeabilisation. In the model we first assumed S-shaped σ(E) dependency and then estimated its parameters by means of experimental current results. Amongst estimated parameters we also obtained values of reversible and irreversible E thresholds. Estimated E thresholds were: 460 V/cm for reversible and 700 V/cm for irreversible threshold. Those values appeared to be higher than values previously published by our group [Miklavčič *et al.*, 2000]. As the new thresholds are higher we can also expect the calculated induced TMP to be higher from previously published. Therefore we examined the reasons for the difference between previously published and presently obtained thresholds in detail. The results are presented in the following two subchapters. At the end of this chapter the mechanisms that occur during permeabilisation are described as revealed by means of the time discrete permeabilisation model.

5.5.1 COMPARISON WITH PREVIOUSLY PUBLISHED E THRESHOLD VALUES

Permeabilisation threshold values as obtained in Chapter 5.3 (E_0=460 V/cm, E_1=700 V/cm) differ from values previously published by our group [Miklavčič *et al.*, 2000] (E_0=362 V/cm, E_1=637 V/cm). The reason being that previous permeabilisation thresholds were determined based on E distribution in non-permeabilised tissue. Here we will explain why they differ.

As E distribution around needle electrodes resembles an E distribution between two cylindrical concentric electrodes we based the explanation of the difference between thresholds on the analytical model of E distribution with S-shaped σ(E) dependency, presented in Chapter 3.3.1.

Figure 5.10 explains the influence of E distribution on the reversible threshold determination. The full red line in Figure 5.10 presents E intensity in non-permeabilised tissue as a function of distance between two concentric cylindrical electrodes (*k*=1). E_0*-real* denotes the real E threshold value in the tissue. The dashed blue lines present E distribution, computed by the analytical time discrete permeabilisation model in steps two and three. According to E intensity of non-permeabilised tissue, permeabilisation in the first step of the analytical permeabilisation model occurs in tissue somewhere up to a distance of approximately 2 units (where the red line crosses green line denoted as E_0*-real*). The permeabilisation model takes into consideration the increased conductivity obtained in that part to compute E distribution in the second time discrete step by the analytical model. The resulting E distribution (second step) crosses the green line E_0*-real* at a distance of approximately 2.45 units, meaning that tissue was permeabilised up to that distance in the second step. In the next step, tissue was permeabilised up to a distance of 2.6 units indicated on the x axis. In further steps, E-intensity in part of non-permeabilised tissue did not exceed E_0*-real* meaning that at the end of the permeabilisation propagation tissue was permeabilised up to a distance of 2.6 units

However if we consider E distribution in completely non-permeabilised tissue and the fact that tissue was permeabilised up to 2.6 units to determine reversible E threshold, we would obtain reversible threshold at E intensity where the vertical blue line crosses the E distribution of completely non-permeabilised tissue (red line). This threshold is shown in the green line denoted E_{00}. The difference between E_0-real and E_{00} explains why the thresholds obtained by our sequential model are higher than the thresholds previously published in [Miklavčič *et al.*, 2000].

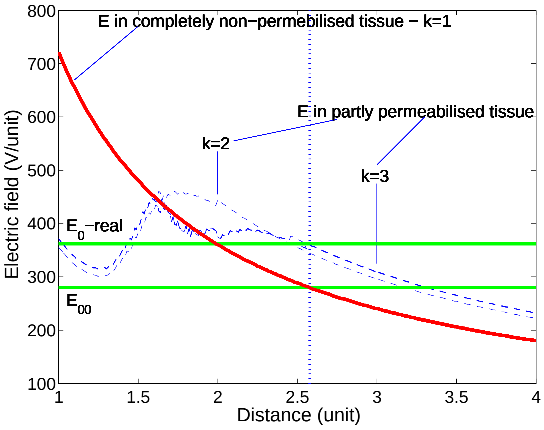

Figure 5.10: E distribution during electropermeabilisation, compared to the E distribution of non-permeabilised tissue.

Taking into account that molecules, which differ in size, shape and in electrical properties use different transport mechanisms (diffusion, electroosmosis, electrophoresis) [Puc *et al.*, 2003] to cross the cell membrane during permeabilisation, different transfer rate coefficients and time courses can be related to their transport. The dependence of transport of ions and small molecules on an applied external E is schematically shown in Figure 5.11. According to that, the reversible threshold presented in Chapter 5.3 reflects the threshold for ion conduction and possibly small molecules which enter by diffusion. The transport kinetics of larger molecules is more complicated and occurs in several temporally distinct stages [Neumann et al., 1999; Wolf et al., 1994]. It also appears that transport of larger molecules requires either long-lived stable pores or, according to [Neumann and Kakorin, 1996], it requires critical pore density for DNA translocation through permeabilised membrane patches following a cooperative scheme. Considering the fact that membrane permeabilisation for ions is fast, it causes rapid changes in E intensities across the tissue and consequently the propagation of permeabilisation. After this process is terminated the steady distribution of E intensities is present for longer period of pulse duration. We presume that steady E intensities influence the appearance of long lived stable pores enabling the transfer of molecules such as bleomycin which occurs predominantly after the pulse by diffusion. Steady E intensities could also be responsible for the state of membrane permeabilisation which enables transport of DNA across the cell membrane by electrophoresis. Additionally, the steady E intensity can be used for assessment of E thresholds related to permanent cell membrane damage, such as the irreversible E threshold value 700 V/cm, at which cell necrosis was observed.

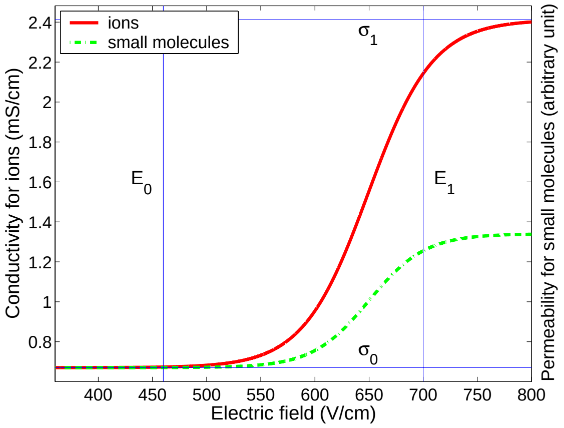

Figure 5.11: Hypothetical presentation of the transport of ions and small molecules due to permeabilisation as functions of applied E intensity.

5.5.2 COMPARISON WITH PREVIOUSLY PUBLISHED INDUCED CRITICAL TRANSMEMBRANE POTENTIAL

When exposing cells to an external E, transmembrane potential (*TMP*) is induced. At critical *TMP* value (TMP_c) cell membrane permeabilisation occurs. Reported values of TMP_c at room temperature are between 0.2 to 1 V [Hibino *et al.*, 1993, Teissie and Rols, 1993, Tsong, 1991]. The relation between the external E and *TMP* for spherical cells is expressed by Schwan's equation:

$$TMP = fRE\cos\vartheta \tag{5.6}$$

where *R* is a cell diameter, *f* a numerical factor and ϑ the angle between cell radius vector and *E* vector. By taking into account the average diameter of hepatocytes being 21.8 ±2.7 µm and by using the value of factor f=1 which corresponds to densely packed cells – such as in tissue, we computed the value of TMP_c. Considering E threshold values E_0=460 V/cm and E_1=700 V/cm, we obtained TMP_c=0.50 V and *TMP* for irreversible threshold equal to 0.76 V. As expected, computed *TMPc* is slightly higher than our previously published value [Miklavčič *et al.*, 2000], however it is still well within the range of reported values in the literature.

5.5.3 PERMEABILISATION PROCESS AS REVEALED BY MEANS OF MODEL VALIDATION

The development and validation of the time discrete permeabilisation model provided means for better understanding mechanisms which occur during permeabilisation. When comparing modelled and simulated total currents and the areas of reversibly and irreversibly permeabilised tissue several hypotheses arose aimed at explaining the permeabilisation process.

First, the basis for accurate presentation of permeabilisation with a time discrete model is to have σ(E) dependency known in advance.

Second, the comparison of current computed by the model at time discrete steps and the current measured during 8 pulses showed that after each pulse, ion conductivity is the same as before the pulse. However during the pulse, conductivity increases significantly due to permeabilisation.

According to one of the commonly accepted theories of cell electropermeabilisation [Neumann *et al.*, 1999; Weaver and Chizmadzev, 1996] which explains the electropermeabilisation phenomena by the formation of a large number of metastable pores and reduced number of stable long lived pores, the metastable pores (provided already hidrophilic pores) could be responsible for increased current conduction during the pulse application. While the small number of stable pores does not contribute a significant part in current conduction, they do however enable the transfer of small molecules after the end of the pulse. After the end of the pulse application, metastable pores reseal in the time range of microseconds [Abidor *et al.*, 1993; Hibino *et al.*, 1993] (fast resealing). Therefore, the situation concerning current conductance is repeated after the first pulse. When several pulses are applied, more of stable long-lived pores are formed with cooperative effect [Marrink *et al.*, 2001]. Those pores reseal in the second stage of membrane resealing which can take as long as a few minutes [Abidor *et al.*, 1993; Hibino *et al.*, 1993].

Another explanation could be based on the model of pore formation energy [Abidor *et al.*, 1993; Weaver and Chizmadzev, 1996]. In the presence of an E the free energy of pore formation is lower than after the pulse application. This means, that the pulse reduces the free pore energy, therefore easing pore formation and consequently current flow. After pulse application, the pore radii decreases and free energy is increased. Such a situation needs to be overcome with the following pulse, which results in a similar current response as in the first pulse.

Third, the comparison of current in five sequential steps of the model and the measured current in the first pulse showed that at higher pulse amplitudes a permanent, however moderate increase in measured current is present after the current rise time, which was not observed in modelled current. We assume that the measured current increase was due to ion dissociation or it resulted from tissue heating and consequent increase in conductivity. That implies that $\sigma(E)$ dependency should also incorporate the influence of temperature T. For future work that requires determination of $\sigma(E,T)$ dependency.

Fourth, fast dynamic changes of E intensity during tissue permeabilisation influence the change in tissue conductivity, however even if E intensities are higher than the irreversible threshold value they do not necessarily cause cell necrosis. Only when steady E intensities are present for a certain period of pulse length and if higher than irreversible threshold, they can cause cell necrosis. Model validation has therefore shown presence of a time component in $\sigma(E)$ dependency, which has to be incorporated, i.e. $\sigma(E,T,t)$ dependency needs to be defined in future work.

Fifth, during permeabilisation, two transport mechanisms were present: fast ion transport, which is reflected in the change of tissue conductivity and the slow transport, which indicates the transport of small molecules (bleomycin…). Both transports are presumably initiated at the same threshold value, however their dynamics are different. Due to the fact that ion transport is very fast, the consequent change in tissue conductivity causes further rapid changes in E distribution which propagates permeabilisation. The final result is distribution of decreased E intensities across the permeabilised tissue than at the beginning of pulse application. The system behaves as if it had a specific negative feedback, which preserve cells from irreversible damage [Abidor *et al.*, 1993]. After this process is terminated it seems to be only final steady E distribution that influences the origination of long lived stable pores, enabling transport of small molecules across the cell membrane.

Model validation also showed that the model predicted the change in total current in accordance with measurements as well as estimating the reversibly and irreversibly permeabilised volume of tissue. Therefore, a validated time discrete permeabilisation model can be used for simulation of the permeabilisation process. That could be very important in clinics where electrode set-up (position) and electrode parameters (amplitude only) can be estimated by means of simulation before the treatment in order to achieve effective permeabilisation of a particular tissue volume.

6 MODEL BASED OPTIMISATION OF ELECTROPERMEABILISATION PARAMETERS

As electric field (E) distribution in tissue can be controlled by the applied pulse amplitude and electrode design, determination of optimal electropermeabilisation parameters (EP) is crucial for effective tissue permeabilisation. In the case of electrochemotherapy, effective electropermeabilisation is achieved when the entire volume of the tumour is exposed to E intensities above reversible threshold, while in electrogenetransfer, for effective permeabilisation, the subjected tissue should be exposed to E intensities above reversible and at the same time below the irreversible threshold. The determination of optimal EP parameters (amplitude, electrode design) should therefore consider the requirements of the particular application of permeabilisation.

There are different approaches towards optimisation of EP parameters. Usually they are based on information of *in vitro* [Rols and Teissie, 1990] and also *in vivo* [Gehl and Mir, 1999] tests used to determine the E intensity needed for tissue permeabilisation. Model based approaches to optimisation of EP parameters however have not been used so far, due to the lack of models describing tissue permeabilisation.

Thus within this chapter we investigated the feasibility of model based optimisation of EP parameters. We conducted the optimisation on the time discrete model of tissue permeabilisation presented in the previous chapters. We considered pulse amplitude and distance between the electrodes (where applicable) as EP parameters subject to optimisation. In that respect we designed several models with different electrodes (plate and needle electrodes) to investigate the feasibility of model based optimisation of EP parameters. We first examined the optimisation of EP parameters on models with simple geometry and ultimately we extended the optimisation to the complex geometry of a human brain with a tumour. The goal of the optimisation in all models was to permeabilise the whole tumour, i.e. to expose the entire area of the tumour to E intensity values above reversible threshold as used in electrochemotherapy, assuming this leads to 100% effectiveness of electrochemotherapy.

At the beginning of this chapter the optimisation problem in electrochemotherapy is defined and a model based optimisation of EP parameters is presented on simple geometries. In continuation the generation of the 3D geometry model of a brain with a tumour from CT images of a head is described. This is followed by optimisation of EP parameters for electrochemotherapy of this particular brain tumour.

6.1 DEFINITION OF THE OPTIMISATION PROBLEM

6.1.1 NONLINEAR CONSTRAINED OPTIMISATION

In general, the minimization of an objective function can be subject to different constraints. In most real life optimisation applications the values of the parameters to be optimised are limited within a certain interval. When the parameters to be optimised are constrained with linear (in)equalities, the constraints are referred to as linear constraints, while where the parameters to be optimised have to satisfy nonlinear (in)equalities the constraints are denoted as nonlinear.

Thus a nonlinear constrained optimisation problem has the form:

$$\min_{x \in \Re^n} f(x) \tag{6.1}$$

subject to

$$l \le \begin{pmatrix} x \\ c(x) \\ Ax \end{pmatrix} \le u \, , \tag{6.2}$$

where $f : \Re^n \to \Re$ is a linear or nonlinear objective function, $c : \Re^n \to \Re^m$ is a vector of constraint functions, *A* is a matrix, and *l* an *u* are vectors of bounds. *Ax* thus presents a set of linear constraints, while *c(x)* presents nonlinear constraints [Friedlander, 2002; Optimisation Toolbox for use with Matlab, 1999].

6.1.2 OPTIMISATION PROBLEM IN ELECTROCHEMOTHERAPY

The goal of the optimisation of EP parameters for application in electrochemotherapy is to have in a steady state the entire volume of the tumour exposed to E intensities just above the reversible threshold. In general, parameters subject to optimisation could be pulse parameters (shape, amplitude, frequency, pulse duration) and electrode parameters (shape and position of the electrodes). Optimisation of all the stated parameters requires a permeabilisation model comprising all those parameters. The development of such a model however is too complex and probably would result in a model describing only a narrow range of input parameters.

Within our work we focused on the optimisation of two parameters: pulse amplitude *u* and the distance between electrodes *d* based on the time discrete model of tissue permeabilisation.

Considering that the objective function has the following form:

$$\min_{u,d} f(E_r, E(u,d)) \, . \tag{6.3}$$

The function to be minimized is defined with TIC measure:

$$f(E_{r,}E(u,d)) = \frac{\sqrt{\sum_j \left(E_r - E_j\left(u,d\right)\right)^2}}{\sqrt{\sum_j E_r^2} + \sqrt{\sum_j E_j^2(u.d)}} \tag{6.4}$$

where E_r denotes reference value i.e. the reversible threshold to be reached by optimisation and $E_j(u,d)$ the E intensity at j^{th} point in the tumour. Those points represent parts of the tumour where the lowest E intensity is expected.

For electric pulse application we assumed the use of the Cliniporator prototype. This is an electroporation device, developed within the Cliniporator project, supported by The European Commission within the 5th framework programme (grant QLK3-1999-00484). Taking into account the technical limitations of the Cliniporator, which can supply maximal voltage u_{max}=1000 V and maximal current i_{max}=16 A, we defined constraints on voltage (*u),* subject to optimisation:

$$0 < u < u_{\max} \tag{6.5}$$

and we set a limitation on current as a nonlinear constraint of the following form:

$$c_1\left(u,d\right) = \left(i\left(u,d\right) - i_{\max}\right) \leq 0 \,, \tag{6.6}$$

where *i(u,d)* denotes the total current computed by the model. In addition we wanted to ensure that E in predetermined points *j* of the tumour exceeds reversible threshold. Thus we set additional nonlinear constraints for each evaluation point *j*:

$$c_{2j}\left(u,d\right) = \left(E_r - E_j(u,d)\right) \leq 0 \,. \tag{6.7}$$

Constraints on the second optimisation parameter – distance *d* were set considering the characteristic of each particular geometry model and by considering the electrode holder dimensions. Thus they will be described next for each model.

6.2 TISSUE SPECIFIC CONDUCTIVITIES USED IN MODELS

With respect to the final goal i.e. to optimise EP parameters aimed at electrochemotherapy of a brain tumour based on real geometry extracted from CT images, we used tissue electric parameters which correspond to brain and tumour tissue in all further models.

The specific conductivity of brain tissue reported in literature for animals (cow, pig, and rabbit) at low frequency and at body temperature was 0.17 S/m, with grey matter conductivity 0.35 S/m and white matter 0.15 S/m [Geddes and Baker, 1967]. The same value i.e. 0.17 S/m was reported for average human brain conductivity in [Barber and Brown, 1984], while the measurement at 1kHz reported in [Schwan, 1963] estimated specific human brain conductivity in the range between 0.20-0.22 S/m. Considering a possible increase in conductivity at 1 kHz, we used the lower value of human brain conductivity (0.17 S/m) in this work.

There were no reported values of brain tumour conductivity in literature available to us. Thus we based the value of brain tumour conductivity on the fact, that tumour tissue has higher conductivity than surrounding tissue [Surowiec *et al.*, 1988; William *et al.*, 1994; Smith *et al.*, 1986]. The increased value of tumour conductivity compared to surrounding tissue was reported to be between 2-4 times higher for breast tissue [Surowiec *et al.*, 1988] and 6-7 higher for liver tissue at 1 kHz [Smith *et al.*, 1986]. Considering this in all subsequent models we set the conductivity of brain tumour tissue to be 2.23 times larger than the conductivity of non-permeabilised brain tissue, which corresponds to 0.38 S/m.

We approximated σ(E) dependency of both brain and tumour tissue with an S-shaped function for the reasons presented in Chapter 3. Figure 6.1 displays both σ(E) dependencies of brain and tumour tissue, respectively. Parameters of both σ(E) dependencies are shown in Table 6.1. The reversible and irreversible E thresholds of tumour tissue were based on estimated values for a subcutaneous tumour presented in [Pavšelj, 2002]. The rest of the values except for specific conductivity of non-permeabilised brain and tumour tissue were defined hypothetically. This is not questionable for use in feasibility study, however for application on real tissue, σ(E) dependency should be exactly defined, for example by the method proposed in Chapter 3.8 or Chapter 5.3.

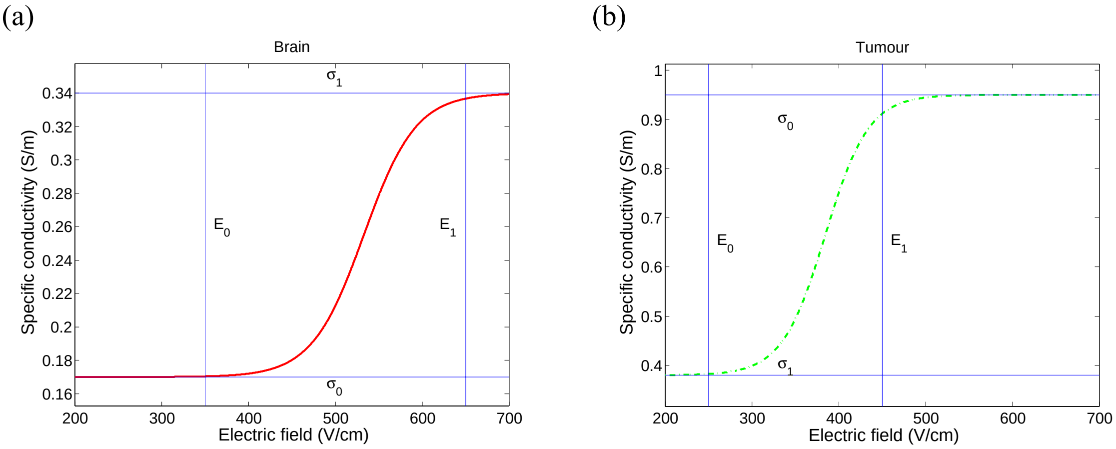

Figure 6.1: σ(E) dependency of brain tissue (a), tumour tissue (b).

Table 6.1: Parameters of S-shape dependency σ(E) for brain and tumour tissue.

Tissue	σ_0(S/m)	σ_1(S/m)	E_0(V/cm)	E_1(V/cm)	B_S	D
Brain	0.17	0.35	350	650	30	3
Tumour	0.38	0.95	250	450	25	4

6.3 OPTIMISATION OF EP PARAMETERS ON DIFFERENT GEOMETRIES

Optimisation of EP parameters was performed on models with plate electrodes and needle electrodes. In models with plate electrodes the geometry of the tissue was chosen to satisfy the dimensions of Cliniporator plate electrodes with respect to the distance between the electrodes, while in the case of needle electrodes we used real geometry of a brain with a tumour. The needle electrode geometry was also designed to take into account the dimensions of Cliniporator needle electrode holder.

Optimisation was carried out on the following models:

- tissue with the tumour between two plate electrodes,
- tissue with the tumour and two plate electrodes positioned on the top,
- brain with the tumour having a needle electrode array inserted.

6.3.1 MODEL OF TISSUE WITH THE TUMOUR BETWEEN TWO PLATE ELECTRODES

The tissue was modelled as a block with dimensions 8 mm x 16 mm x 10 mm, with a sphere representing a tumour of radius 2 mm in the centre of the block. The tissue was positioned between two plate electrodes that were 8 mm apart. The surface of each electrode in touch with the tissue was 10 mm x 7 mm. The geometry and its mesh consisting of 1378 nodes are shown in Figure 6.2.

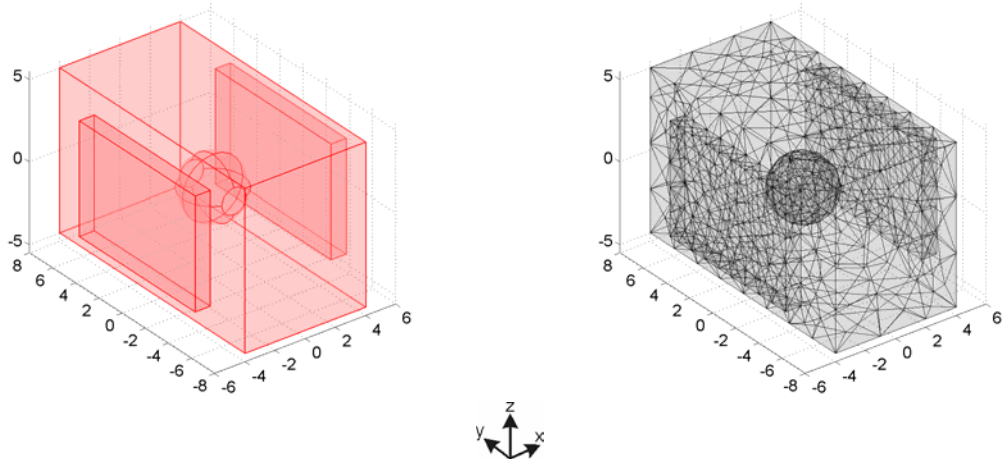
(a) (b)

Figure 6.2: Geometry of tissue between two plate electrodes (a), meshed geometry (b).

6.3.1.1 PULSE AMPLITUDE OPTIMISATION

With the particular geometry, the relevant parameter subject to optimisation was pulse amplitude *u*, because the distance between two plate electrodes was determined by the thickness of the tissue.

The optimisation procedure is shown schematically in Figure 6.3. We set the initial value for *u* at u_0=100 V which represented the starting point for the optimisation. Linear and nonlinear constraints on *u*, *i(u),* and *E(u)* were as defined in Chapter 6.1.2. The objective function evaluation is based on computing E_1 in the last step of the time discrete permeabilisation model in a selected point of the geometry. The point with coordinates x_1=0, y_1=2, z_1=0 was selected at the edge of the tumour. As plate electrodes should provide homogeneous E, we could also have selected this point to be in other parts of the tumour. However we were interested in the E intensity at the point on the edge of the tumour which is most distant to the electrodes, thus we selected this point. Considering the threshold parameter for reversible permeabilisation of the tumour E_0=250 V/cm we used a slightly higher reference value E_r=255 V/cm in the objective function (defined in equation (6.4)) to ensure the field in the selected point to be above reversible threshold. During optimisation based on the time discrete permeabilisation model, E and current were evaluated in three time discrete steps. The reason was that prior to optimisation we evaluated that three steps were sufficient for the termination of permeabilisation propagation.

The minimum of the objective function obtained by optimisation was *f(u)*=0.0002 and the optimal parameter value *u*=286.5 V. There were no constraints reached such as bounds on *u* as evident in Table 6.2. Also, nonlinear constraints i.e. $i(u)<16$ A and $E(u)>E_r$ were satisfied.

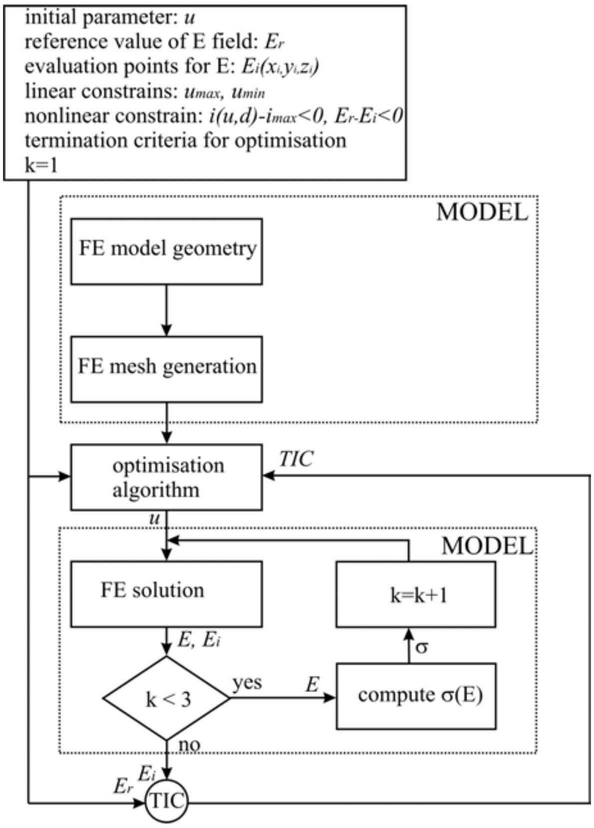

Figure 6.3: Schematic presentation of optimisation procedure.

Table 6.2: Optimisation parameters and results.

E_r	u_0	u	$f(u)$	$E_i(u)$	$i(u)$
255 V/cm	100 V	286.5 V	0.0002	255.1 V/cm	0.80 A

Figure 6.4, Figure 6.5, and Figure 6.6 present specific conductivity and E distribution in *yz*, *xz* and *xy* planes respectively at applied voltage u=286.5 V. Electric field and specific conductivity are shown at three consecutive steps of the time discrete permeabilisation model. We can observe that in the third step the whole volume of the tumour was permeabilised i.e. exposed to E intensities just above 255 V/cm. This resulted in a moderate, almost unobservable, increase in conductivity of the tumour compared to the conductivity of the non-permeabilised tumour with respect to σ(E) dependency shown in Figure 6.1. From the optimisation point of view this is an excellent result, however for effective electrochemotherapy it depends on the accuracy of the reversible threshold determination. Thus for effective electrochemotherapy it would be better to define reference value E_r to be higher i.e. in between the reversible and irreversible thresholds. On the other hand, this excellent result is advantageous for electrogene transfer, because we can determine the optimal pulse amplitude to be applied to plate electrodes which can reversibly permeabilise cells, without causing cell death.

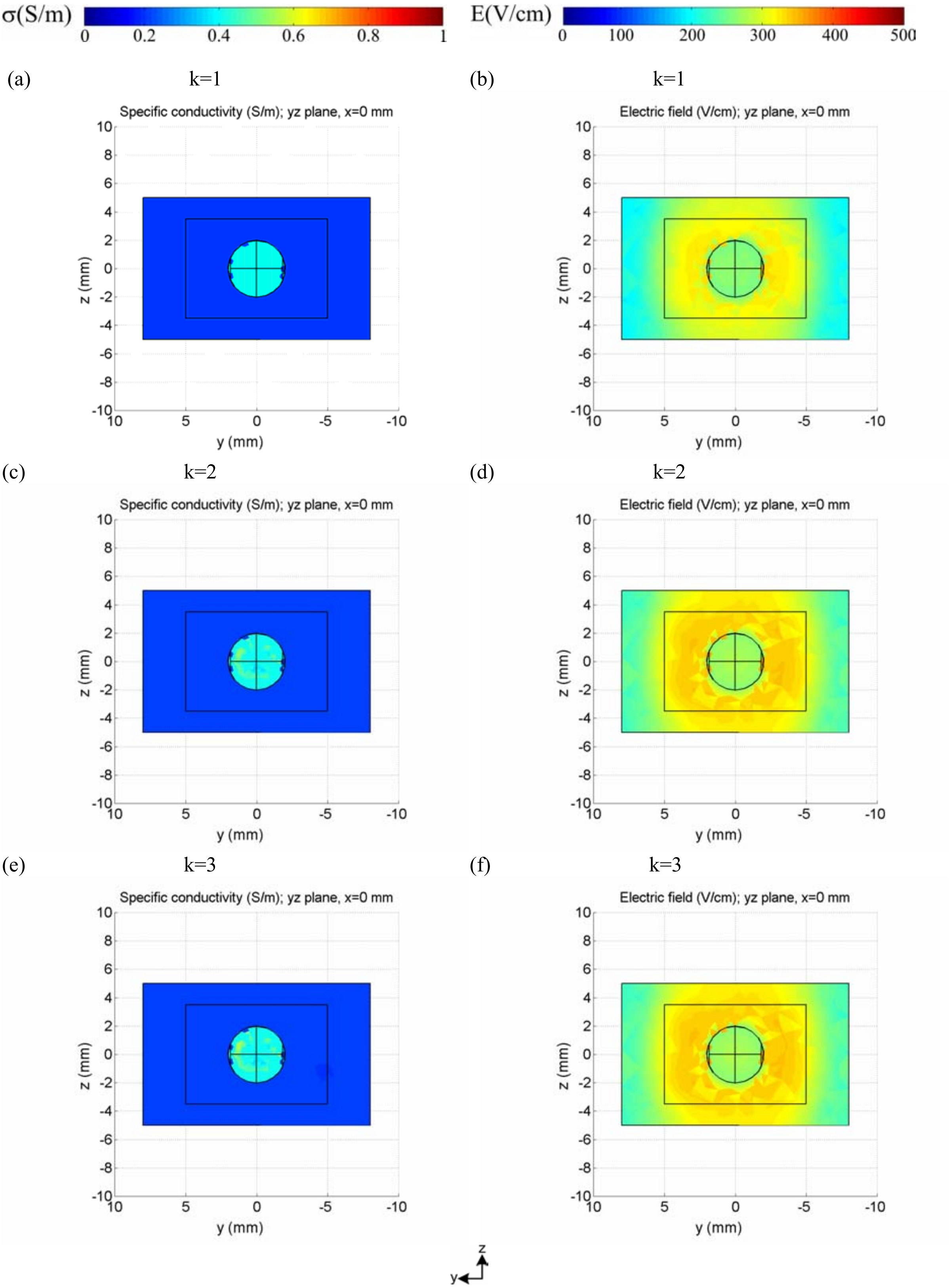

Figure 6.4: Three consecutive steps computed by the model at u=286.5 V in *yz* plane at *x*=0: (a) and (b) specific conductivity and E, respectively in the first step; (c) and (d) specific conductivity and E, respectively in the second step; (e) and (f) specific conductivity and E, respectively in the third step.

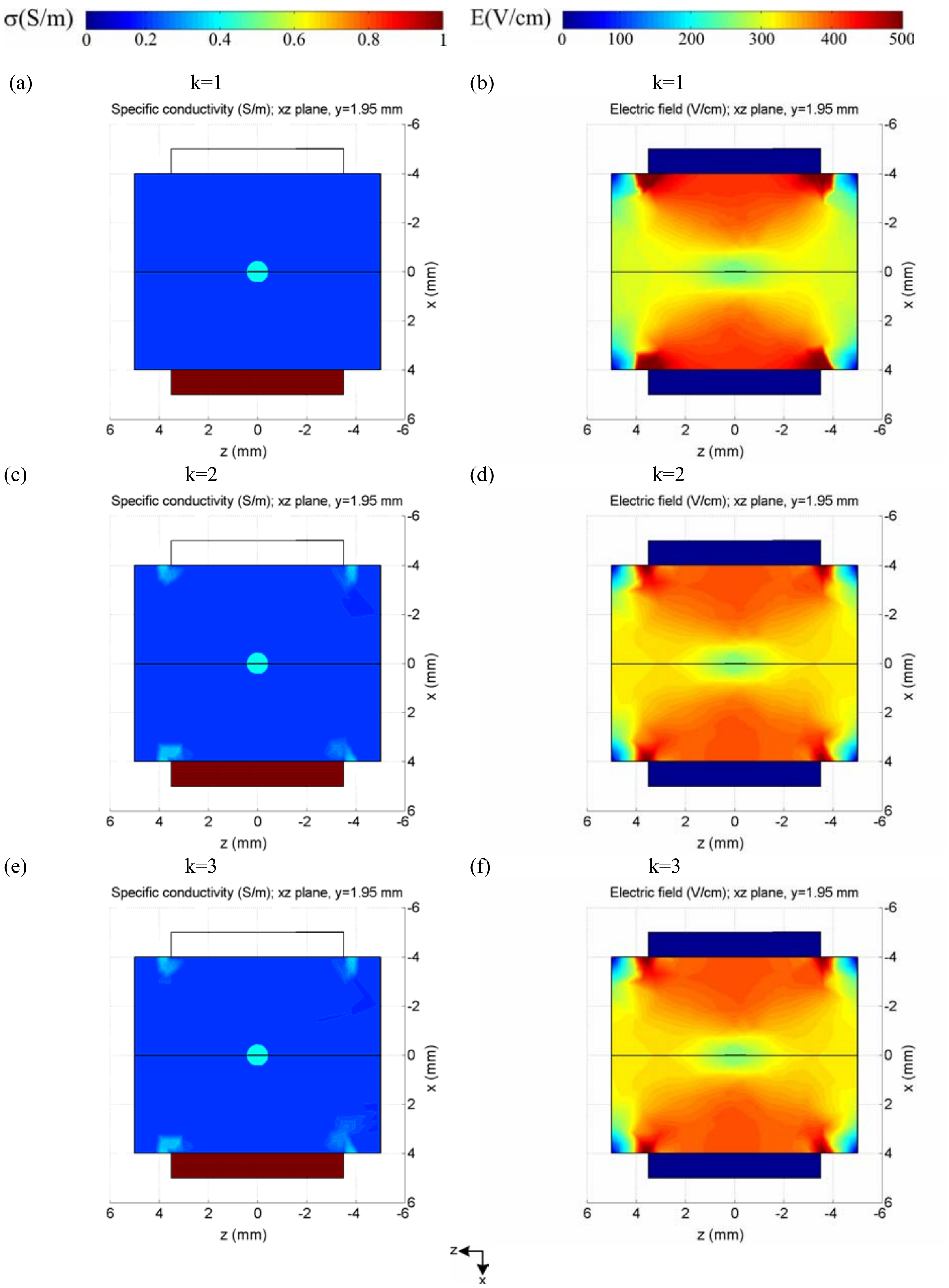

Figure 6.5: Three consecutive steps computed by the model at u=286.5 V in *xz* plane at *y*=1.95: (a) and (b) specific conductivity and E respectively in the first step; (c) and (d) specific conductivity and E respectively in the second step (e) and (f) specific conductivity and E respectively in the third step.

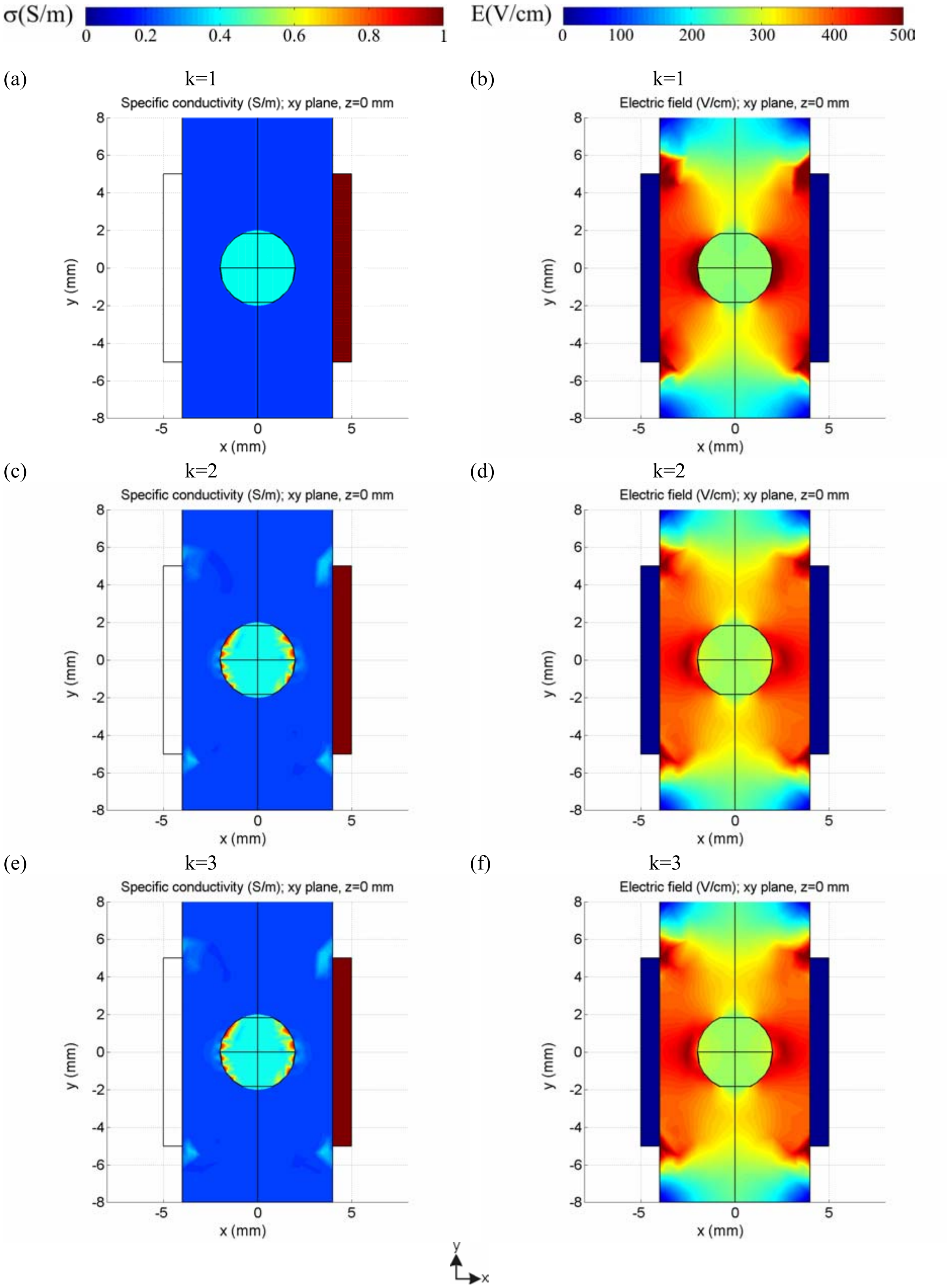

Figure 6.6: Three consecutive steps computed by the model at u=286.5 V in *xy* plane at *z*=0: (a) and (b) specific conductivity and E respectively in the first step; (c) and (d) specific conductivity and E respectively in the second step (e) and (f) specific conductivity and E respectively in the third step.

6.3.2 MODEL OF TISSUE WITH TWO PLATE ELECTRODES ON TOP

The model presented in this chapter was designed with the purpose of investigating the optimisation of two parameters at a time, i.e. pulse amplitude *u* and the distance between the electrodes *d*. Considering this, we positioned two plate electrodes on the top of the tissue with dimensions of 20 mm x 8 mm x 12 mm. The surface of each electrode in contact with the tissue was 1 mm x 7 mm. The centre of the sphere representing the tumour of radius 2 mm was 3 mm below the surface where electrodes were placed. The model geometry and corresponding finite element mesh are shown in Figure 6.7. The mesh consisted of 759 nodes.

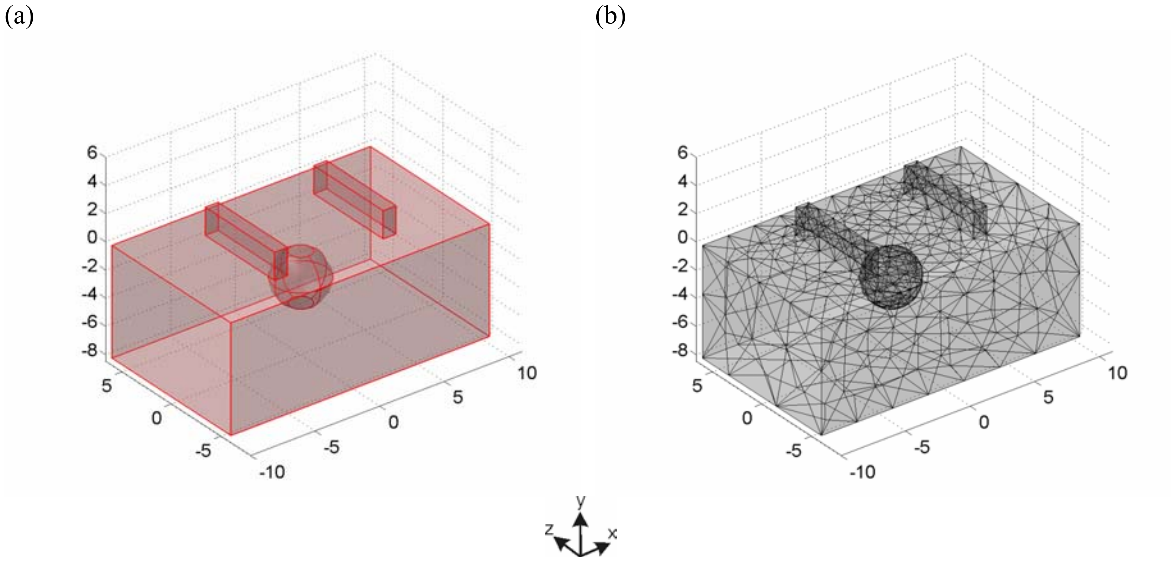

Figure 6.7: Geometry of tissue with two electrodes on top (a), meshed geometry (b).

6.3.2.1 PULSE AMPLITUDE AND ELECTRODE DISTANCE OPTIMISATION

E_1 was computed in the third time discrete step of the model at a point with coordinates $x_1=0$, $y_1=-5$, $z_1=0$ where the lowest value of E in the tumour was present. As in the previous model E_r was 255 V/cm, due to the same electrical tissue properties. Also the same were the bounds on *u* and nonlinear constraints for *i(u,d)* and *E(u,d)*. We set the initial value for *u* at $u_0=100$ V and for *d* at $d_0=9$ mm. The bounds for *d* were $d_{min}=5$ mm and $d_{max}=18$ mm.

During optimisation based on the time discrete permeabilisation model, three steps were computed for the same reason as in the previous model. The difference from the previous model however was that this model required a new geometry definition and consequently new mesh generation in each iteration of the optimisation (Figure 6.8). The reason was the change in distance between the electrodes during optimisation which caused a change of model geometry. In each optimisation iteration new geometry and new mesh were generated automatically. Due to the fairly simple model geometry we did not encounter any problems with mesh generation.

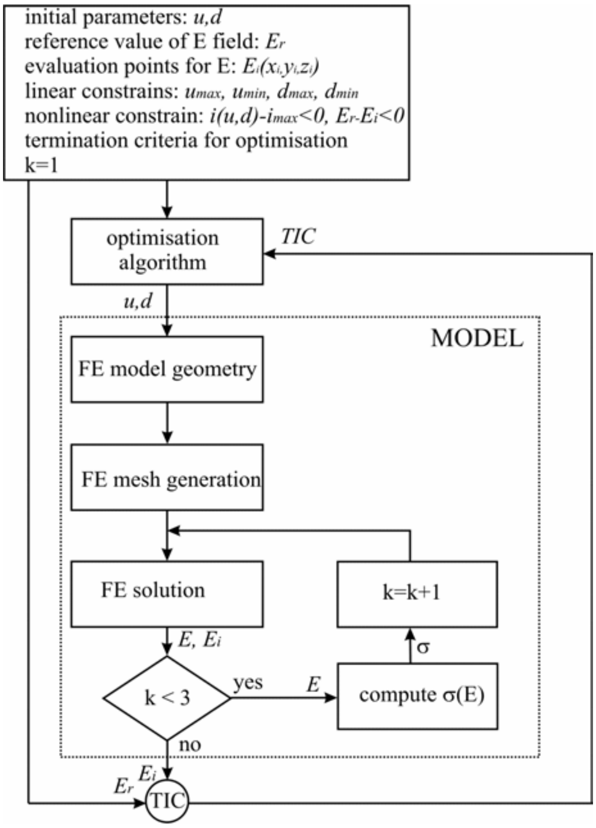

Figure 6.8: Schematic presentation of the optimisation procedure.

Optimisation terminated with an active constraint on *d*. Therefore the optimal value of *d* was 5 mm, while the optimal value for *u* was *u*=958.4 V. The obtained minimum value of the objective function was *f(u,d)*=0.0007. Initial parameter and optimisation results are summarized in Table 6.3.

Table 6.3: Initial parameters and optimisation results.

E_r	u_0	d_0	u	d	$f(u,d)$	$E_1(u)$	$i(u)$
255 V/cm	100 V	9 mm	958.4 V	5 mm	0.0007	255.3 V/cm	0.78 A

Figure 6.9, Figure 6.10, and Figure 6.11 present the specific conductivity and E distribution in *yz*, *xz* and *xy* planes respectively for the three consecutive steps where plate electrodes were positioned at distance *d*=5 mm and the voltage applied was *u*=958.4 V. We can observe that in the third step the entire volume of the tumour was permeabilised i.e. exposed to an E intensity above 255 V/cm. Plate electrodes positioned on top of the tissue produce inhomogeneous E distribution in tissue. Therefore the region of the tumour close to the electrodes was irreversibly permeabilised, while the most distant region of the tumour i.e. the deepest, was exposed to E intensities just above reversible threshold. This sufficed for complete permeabilisation of the tumour, provided the reversible threshold is accurately determined. In this model we could also have increased reference value E_r distincly above the reversible threshold (and still below irreversible threshold) to ensure permeabilisation. However this would require a higher pulse amplitude, which could yield to irreversible permeabilisation of healthy tissue situated just below the electrodes where the highest E intensities are present. Therefore when inhomogeneous E distribution is present the reference value for optimisation should be determined just above reversible threshold.

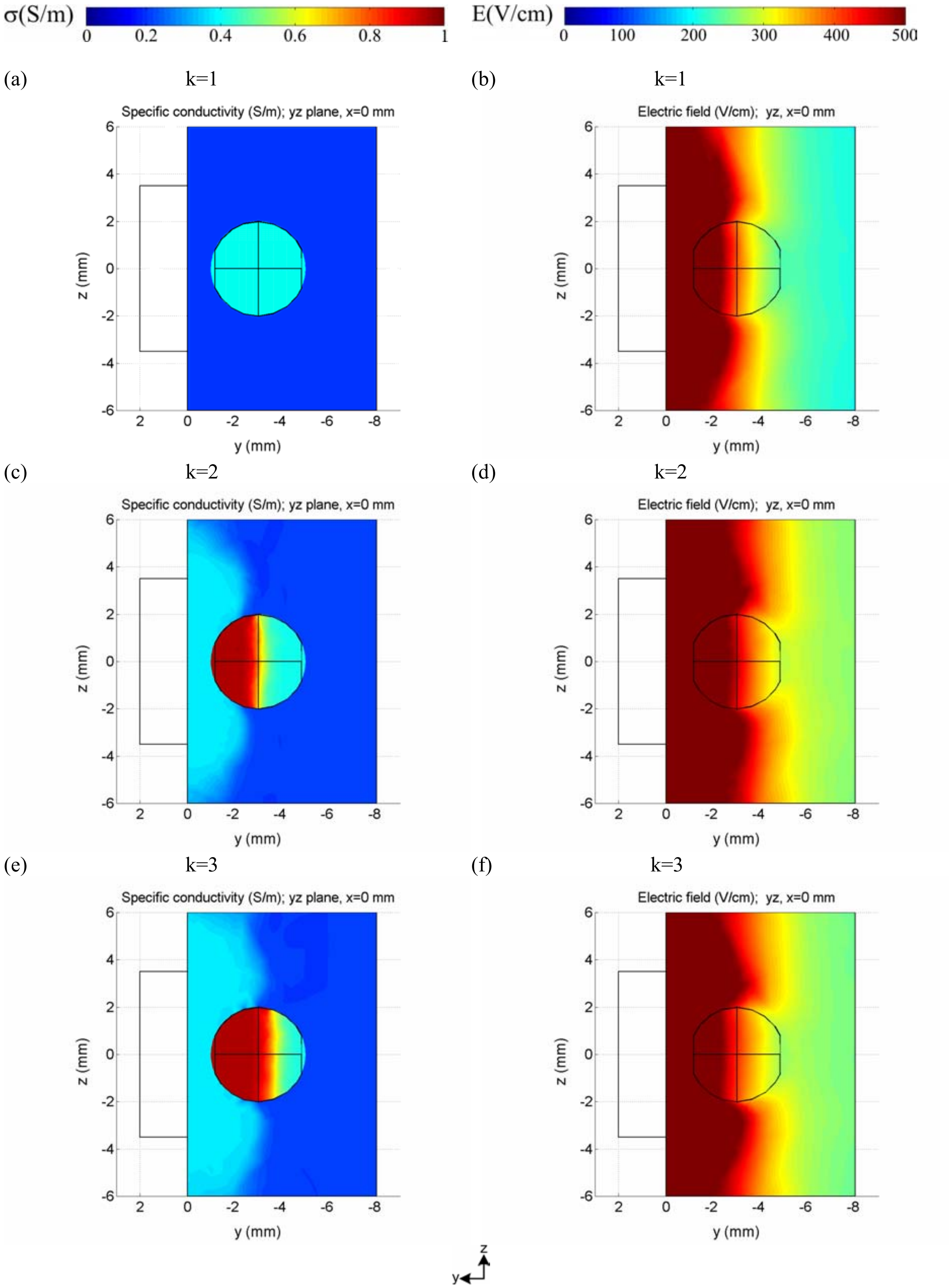

Figure 6.9: Three consecutive steps computed by the model at *d*=5 mm and *u*=958.4 V in *zy* plane (*x*=0): (a) and (b) specific conductivity and E respectively in the first step; (c) and (d) specific conductivity and E respectively in the second step (e) and (f) specific conductivity and E respectively in the third step.

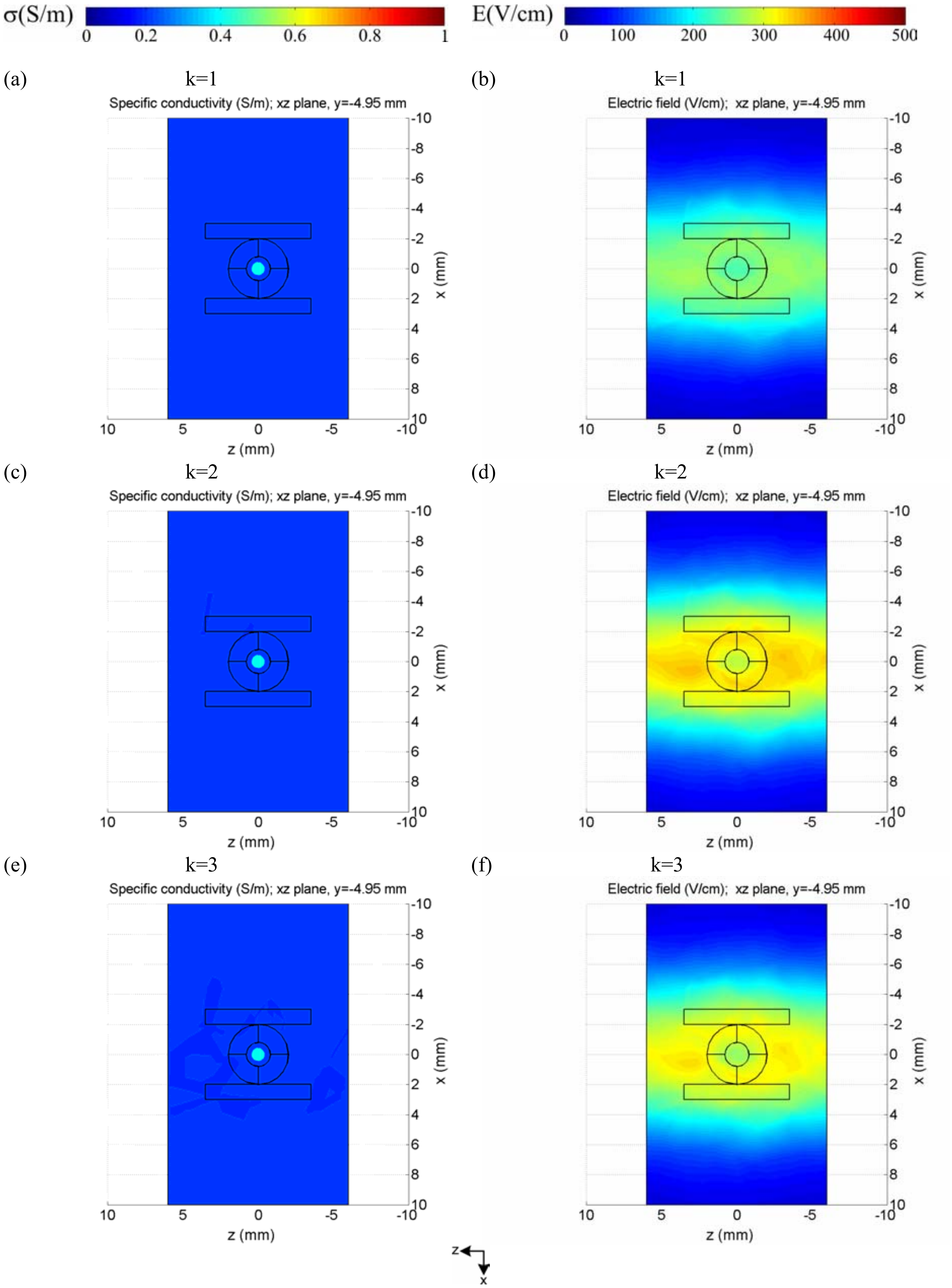

Figure 6.10: Three consecutive steps computed by the model at *d*=5 mm and *u*=958.4 V in *xz* plane (*y*=-4.95): (a) and (b) specific conductivity and E respectively in the first step; (c) and (d) specific conductivity and E respectively in the second step (e) and (f) specific conductivity and E respectively in the third step.

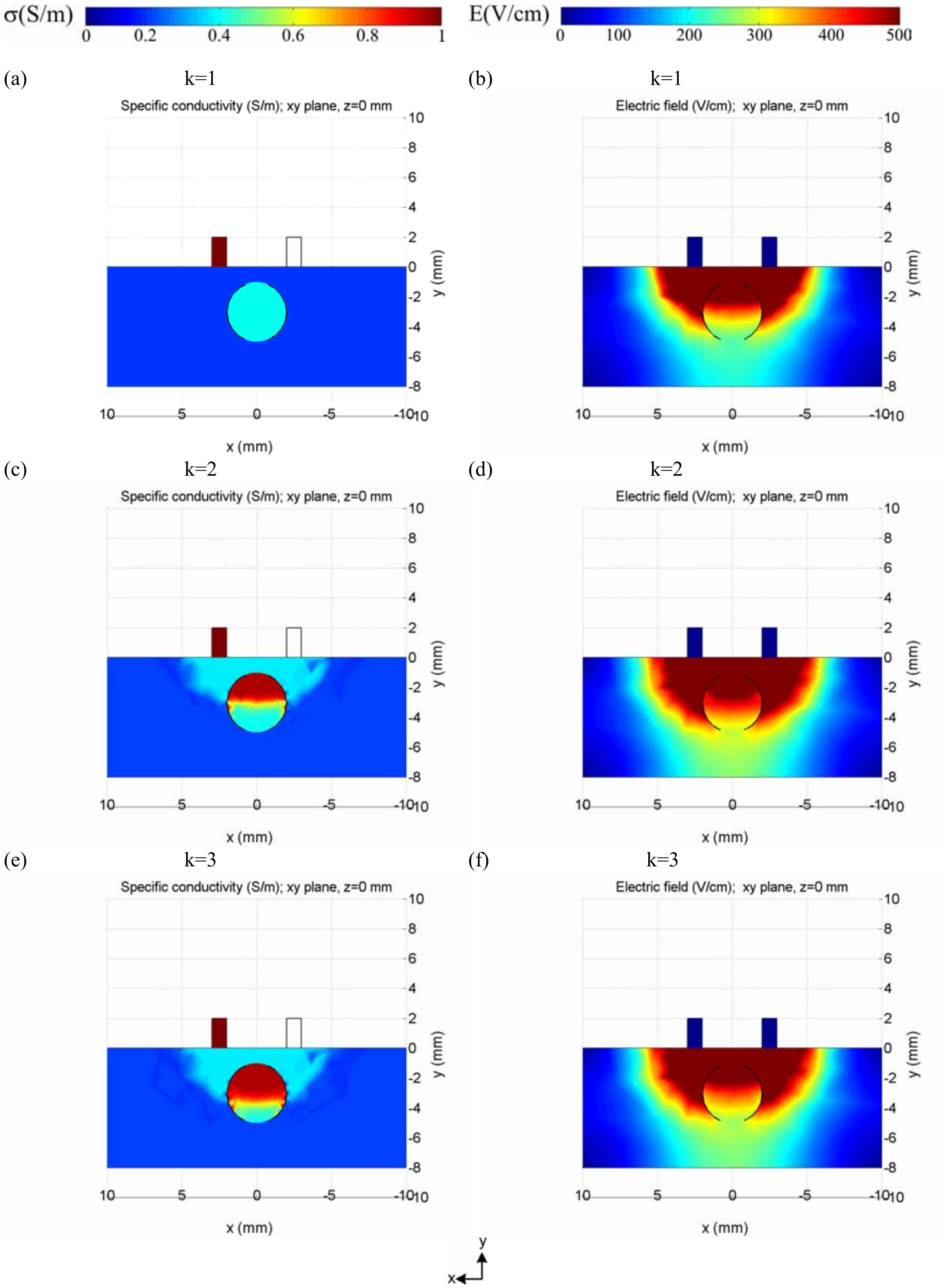

Figure 6.11: Three consecutive steps computed by the model at *d*=5 mm and *u*=958.4 V in *xy* plane (*z*=0): (a) and (b) specific conductivity and E respectively in the first step; (c) and (d) specific conductivity and E respectively in the second step (e) and (f) specific conductivity and E respectively in the third step.

6.3.3 MODEL OF THE BRAIN TUMOUR WITH INSERTED NEEDLE ELECTRODES

A substantial part of the model based optimisation of EP parameters for electrochemotherapy of a brain tumour was the generation of brain model geometry from CT images. Therefore we will first describe the geometry model generation and then present the results of model based optimisation of EP parameters.

6.3.3.1 IMAGE PROCESSING OF THE BRAIN CT IMAGES

Brain CT images of a patient with a brain tumour were scanned at the Institute of Oncology, Ljubljana, Slovenia. The brain scan consisted of 22 slices, each 5 mm thick. The imaging plane was rotated by 24 degrees with respect to the horizontal plane (tilt: -24 degrees). The CT images were stored in Digital Imaging and Communications in Medicine (DICOM) file format. Information about the image data is given in DICOM metadata structure.

For the purpose of 3D brain geometry reconstruction from CT brain images, we used every second slice to avoid generating too complex geometry for subsequent mesh generation. Figure 6.12 presents the original CT images obtained from the Institute of Oncology. As seen in Figure 6.12, the bone (skull) is represented in white, while the liquid and the air are represented in black colour. Considering the wide range of attenuation values, it is hard to expect to differentiate between the white and the grey matter on CT images in Figure 6.12.

Our goal was to design a 3D geometry model representing a brain and a brain tumour. We performed CT brain image processing using Matlab software and 3D geometry generation from processed images with Femlab software. Our goal also was to design a process of 3D model generation which requires the least amount of human interaction possible.

6.3.3.2 3D BRAIN GEOMETRY MODEL GENERATION

As our primary interest was investigation of the feasibility of optimising the positioning of electrodes and pulse amplitude for electrochemotherapy of a brain tumour and due to the lack in differentiation between soft tissues, we decided to model the brain as a homogenous tissue for the purpose of 3D brain geometry model generation. In addition we also modelled the 3D geometry of the brain tumour.

The first step in 3D brain geometry model generation was to determine the edge of the brain from CT images. CT images were imported into Matlab using the *dicomread* function [Image Processing Toolbox for use with Matlab, 2002] which is a special purpose function aimed at reading DICOM files. The output of the *dicomread* function, provided the CT slice image in the DICOM file consists of a single frame greyscale image, is an *m* by *n* array of greyscale values representing pixel values. In our specific case we obtained an array of 512 x 512 pixel values for each of 22 CT images.

We determined the edge of the brain by means of a greyscale threshold value, which we detected on the border between the brain and the skull, and a *contour* function, which creates contour curves of the image at a predefined threshold value. The contour curves of imported CT images are given in Figure 6.13. We can see that the same threshold value was also found in other locations of the image. In addition to the brain edge, the skull edge and the CT pillow edge, were also found, which resulted in several contour curves of a single CT image.

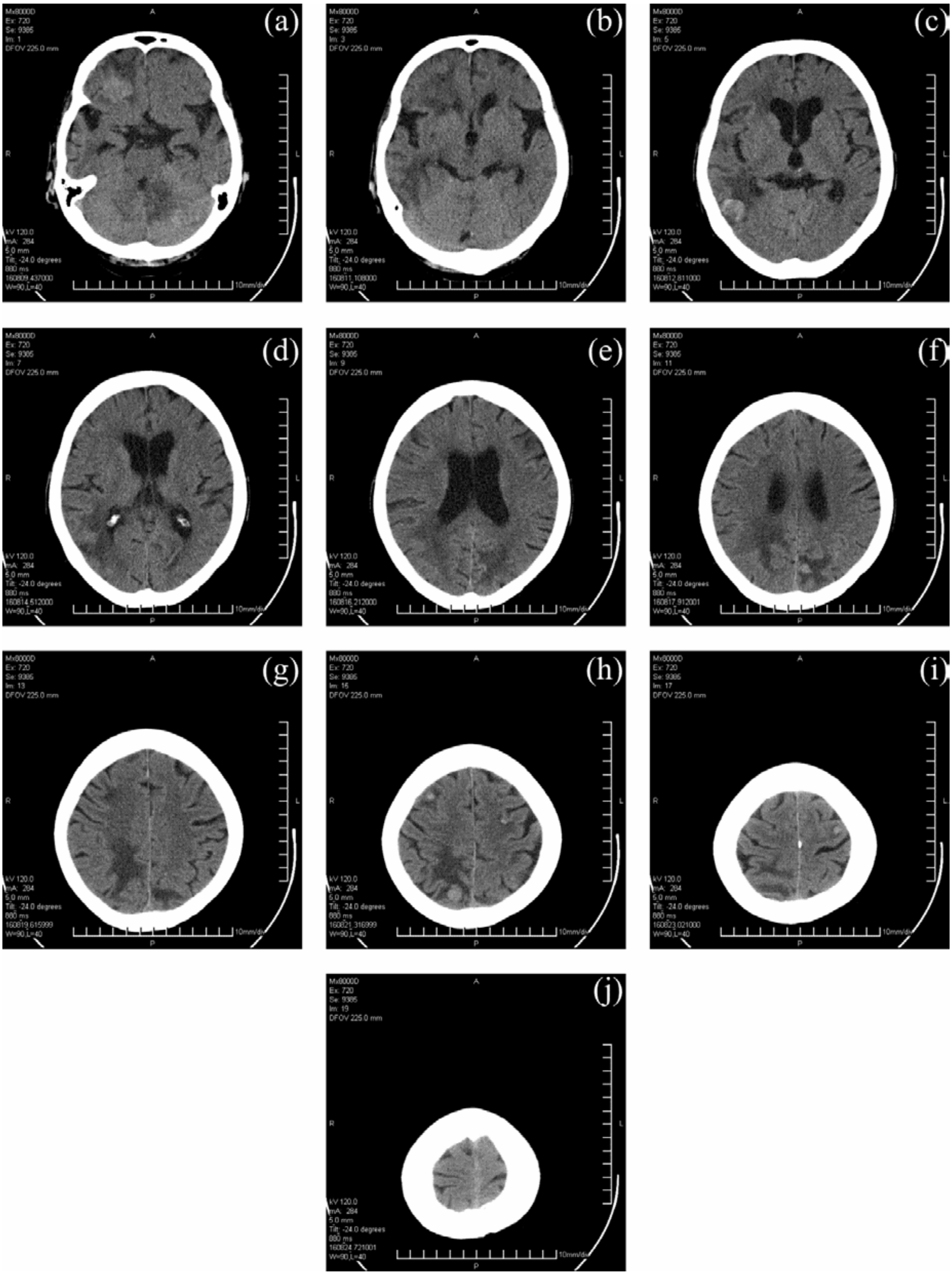

Figure 6.12: Original CT images obtained from the Institute of Oncology. Figures (a) to (j) represent every second slice, from the 1st to 19th image scanned at the Institute, i.e. (a) represents 1st slice, (b) represents 3rd slice, etc. The tumour is visible on image (c) and (d).

Therefore we programmed a special function to automatically extract the brain edge curve from the contour curves shown in Figure 6.13. The function detects the brain edge curve by computing the difference between the maximum and minimum distance in the direction from back to front of each contour curve. The largest difference was always obtained with the skull contour and the second largest with the brain contour curve, which is how the brain edge contour was detected.

In Figure 6.14 the brain edge contour curves are shown in red on the top of the imported CT images. We can see that they match brain edges very well.

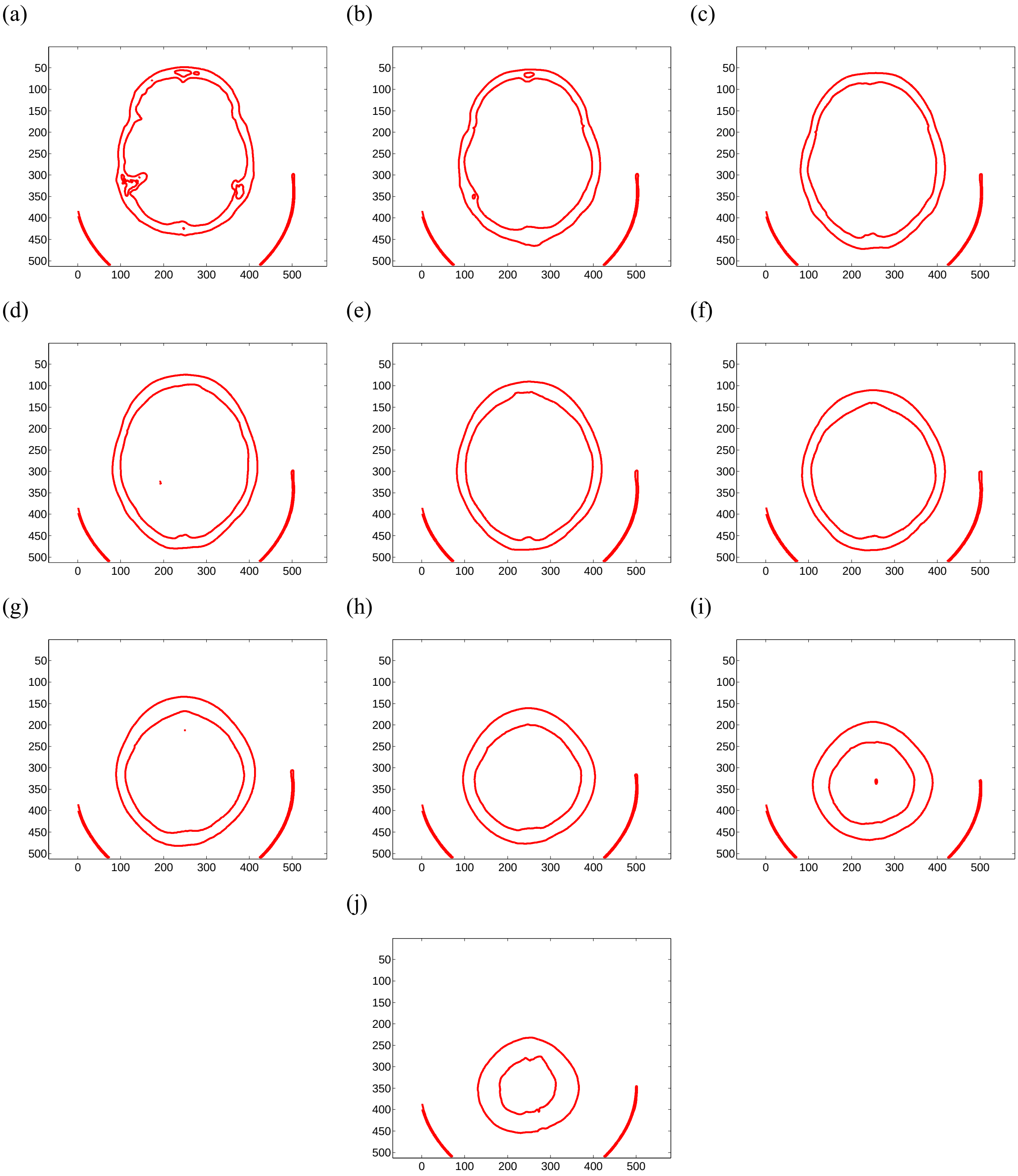

Figure 6.13: Contour curves obtained on imported CT images at the predefined threshold value determined on the border between the brain and the skull. Contours in figures (a) to (j) correspond to CT images in Figure 6.12 (a) to (j).

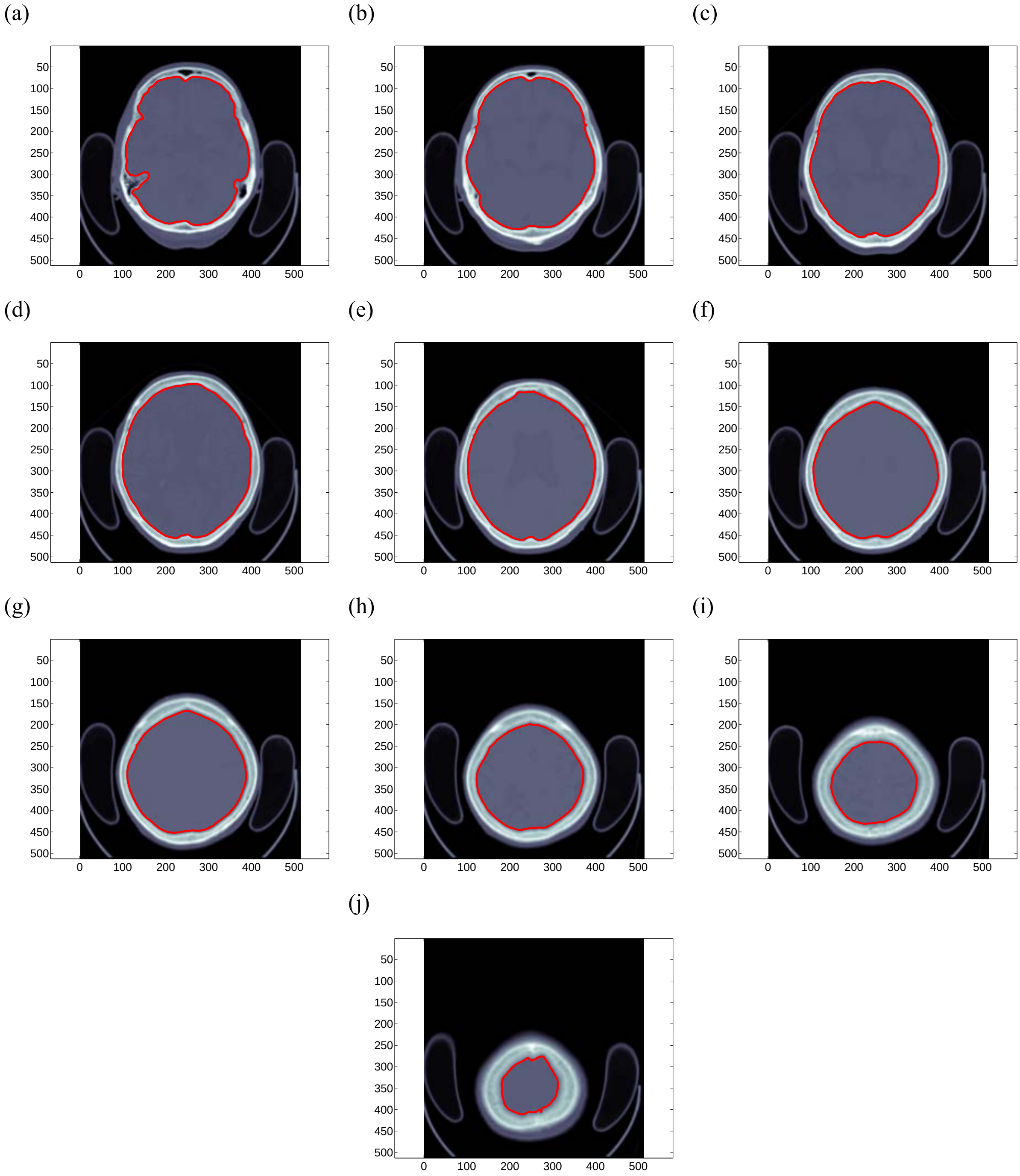

Figure 6.14: Brain edge contour curves (red) on top of the imported CT images. Figures (a) to (j) correspond to CT images in Figure 6.12 (a) to (j).

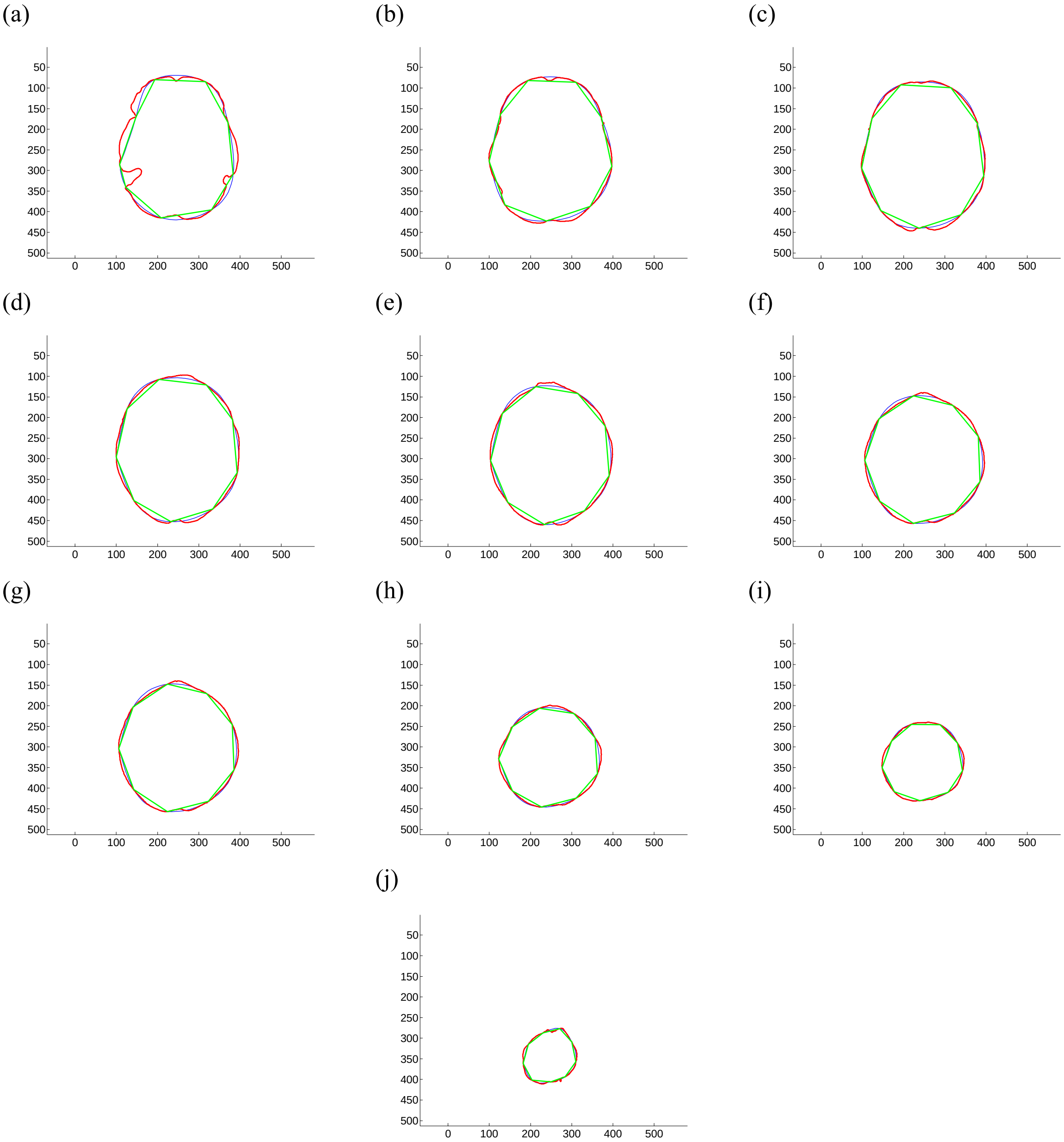

Figure 6.15: Contour curves (red), equidistant points with linear interpolation (green), equidistant points with spline interpolation (blue). Figures (a) to (j) correspond to CT images in Figure 6.12 (a) to (j).

For further 3D brain geometry model generation from the sequence of brain contour curves we had to define the same number of points on each contour curve that split each curve object into the same number of edges. Those edges are then mapped with curve edges of precedent and subsequent slice to form the 3D brain geometry model. For that purpose we designed a function that automatically inserts a predefined number of equidistant points on the contour curve of each CT image as shown in Figure 6.15, green line. We created edges between the equidistant points on the contour curve (Figure 6.15, red line) by *spline* interpolation (Figure 6.15, blue line). We used the latter contours for 3D geometry model generation by using cubic lofting.

When lofting, the distance between CT slices had to be defined. We derived the distance by counting the number of pixels which represent 10 mm on the scale at the bottom of the CT image (Figure 6.12) and determined 10 mm to be equal to 22 pixels. Thus by taking every second slice, which were 5 mm apart, we used 22 pixels distance between slices for lofting. The resultant 3D brain geometry model is presented later in this chapter.

The described process of 3D brain geometry model generation is almost fully automatic. From the user it requires only to set the greyscale threshold value of the brain edge, which is needed for the generation of brain contour curve. However if other organs (parts of body) are to be modelled in such a way, their edges need to be unambiguously differentiated from the rest of the body or in other words CT images must have high spatial resolution and in the case of soft tissue the images must also have high contrast resolution. Apart from this the possibility remains that several contours are obtained at the same threshold value, which requires the user to determine which of the contour curves represent the organ of interest by aid of the special function we programmed and presented earlier in this chapter.

6.3.3.3 3D TUMOUR GEOMETRY MODEL GENERATION

The problem of low spatial resolution and low contrast resolution were present in CT images under our study therefore preventing unambiguous differentiation of the tumour from the rest of the brain. Consequently, the 3D geometry model generation described above required modification.

Instead of automatically determining the edge of the tumour, we defined the edge manually. For that purpose we enlarged the area where the tumour was observed and used pixel mapping in order to increase the intensity of the enlarged part of CT image. The pixel mapping process assigns new values from the user defined output interval (*lowOUT – highOUT*) to input pixel values from the user defined input interval (*lowIN* to *highIN*). The remainder of the values are clipped.

On the enlarged part of the CT image with increased intensity we manually selected a polygonal region just on the edge of tumour and in this manner acquired the coordinates for the edge of the tumour. The selected polygonal region is superimposed on the CT scans in Figure 6.16.

Due to the fact that the tumour was visible in the 4th, 5th, 6th and 7th CT image, we used each of these images for the 3D tumour geometry model generation, not only every second as in the case of the 3D brain geometry model generation.

The rest of the 3D tumour geometry model generation was the same as with the brain: from creating equidistant points on the edge curve shown in Figure 6.17 in green, spline interpolation between the points (Figure 6.17, blue) and lofting the latter by taking into account the distance 11 pixels between the slices.

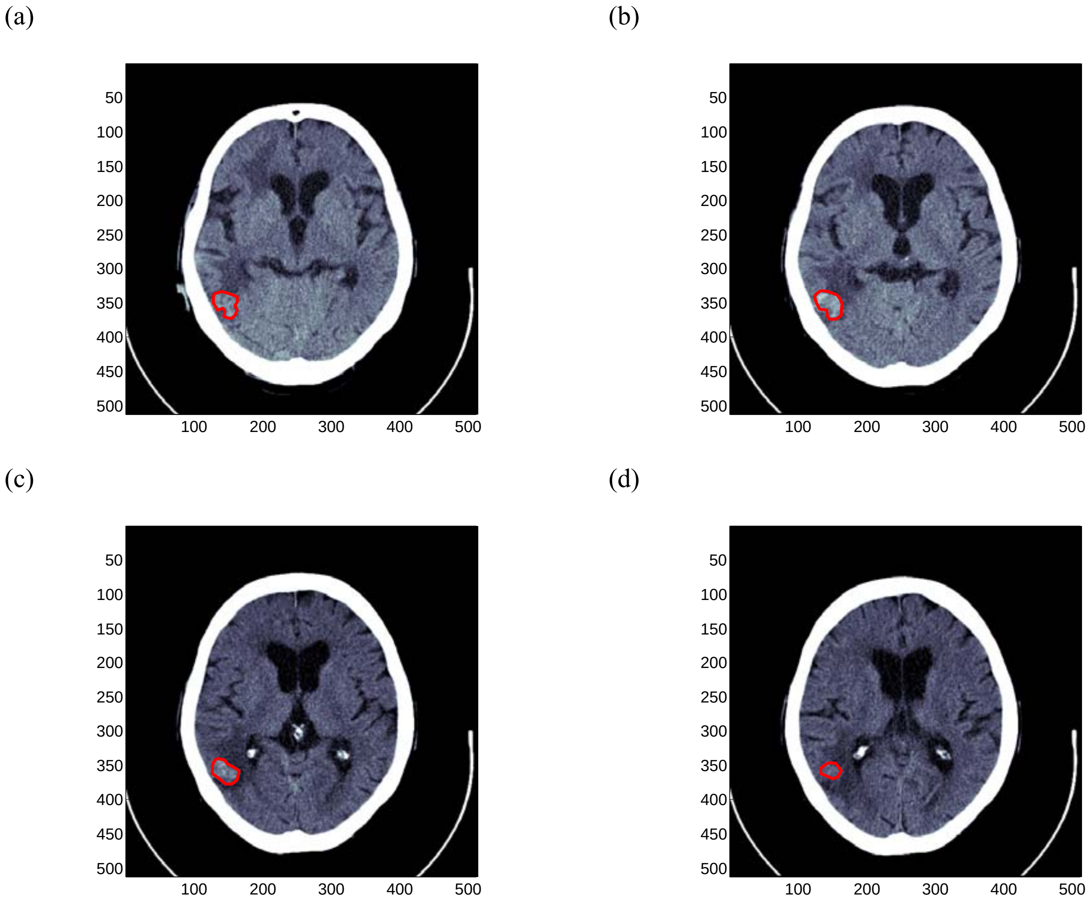

Figure 6.16: Manually selected polygonal region (red), which defines the edge of the tumour on top of imported brain CT images. Figures (a) to (d) represent CT images 4-7 consecutively.

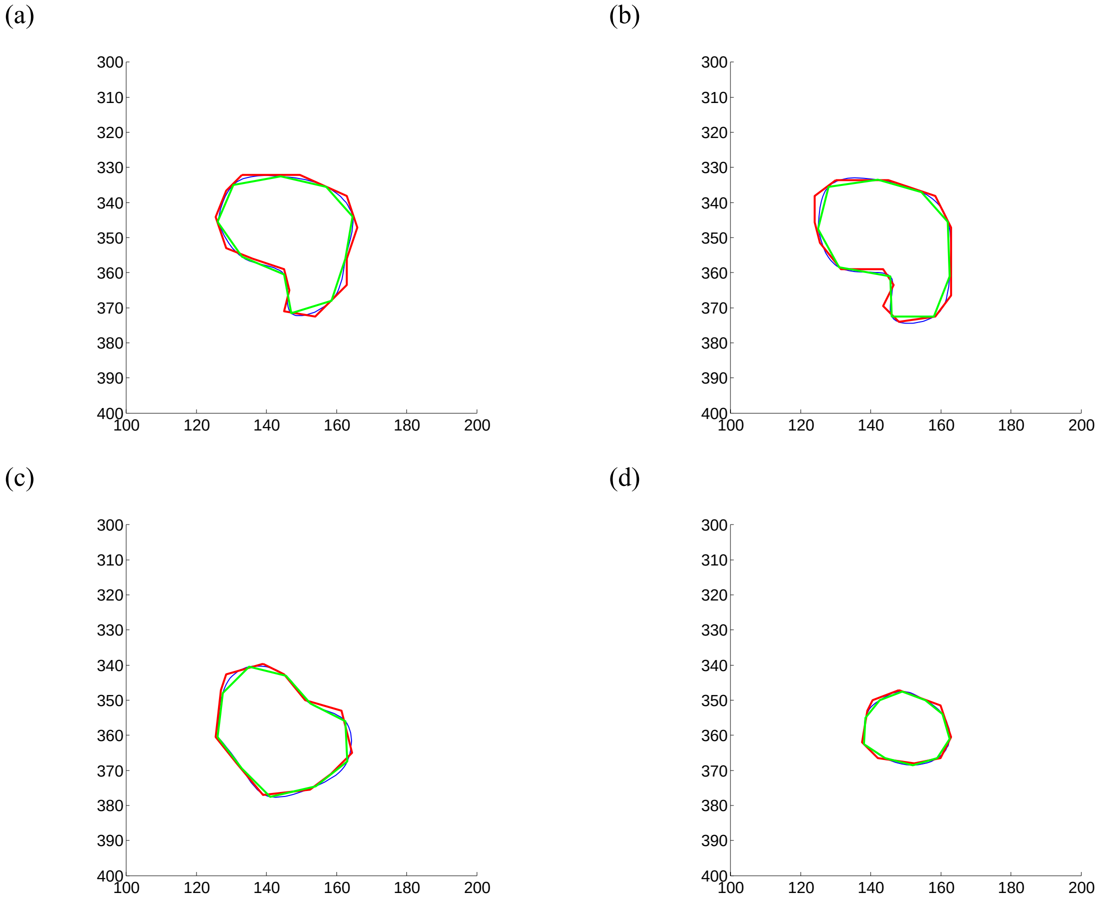

Figure 6.17: Manually determined tumour edge (red), equidistant points with linear (green) and spline interpolation (blue). Figures (a) to (d) correspond to CT images in Figure 6.16 (a) to (d).

6.3.3.4 3D GEOMETRY MODEL PRESENTATION

The generated 3D geometry model of the brain, tumour and skull (obtained in the same way as for the brain geometry) is shown in Figure 6.18. We rotated the combined 3D geometry by -24 degrees (tilt -24 degrees) with respect to the horizontal plane (*xy* plane) in order to obtain a real position as in a standing human.

We designed the 3D geometry model of the head exactly by following the procedure described above. If the obtained geometry does not represent the realistic object, it is because of inherent problems in CT imaging as described in Chapter 2.3.2. Another reason could also be patient movement during the CT scan.

Further, we displayed the *yz* projection of the combined geometry on the CT image of the patient head scanned in *sagital* plane (Figure 6.19). However in order to compare the *yz* model projection with the CT image in *sagital* plane we had to adjust the model to fit the proportions of the head.

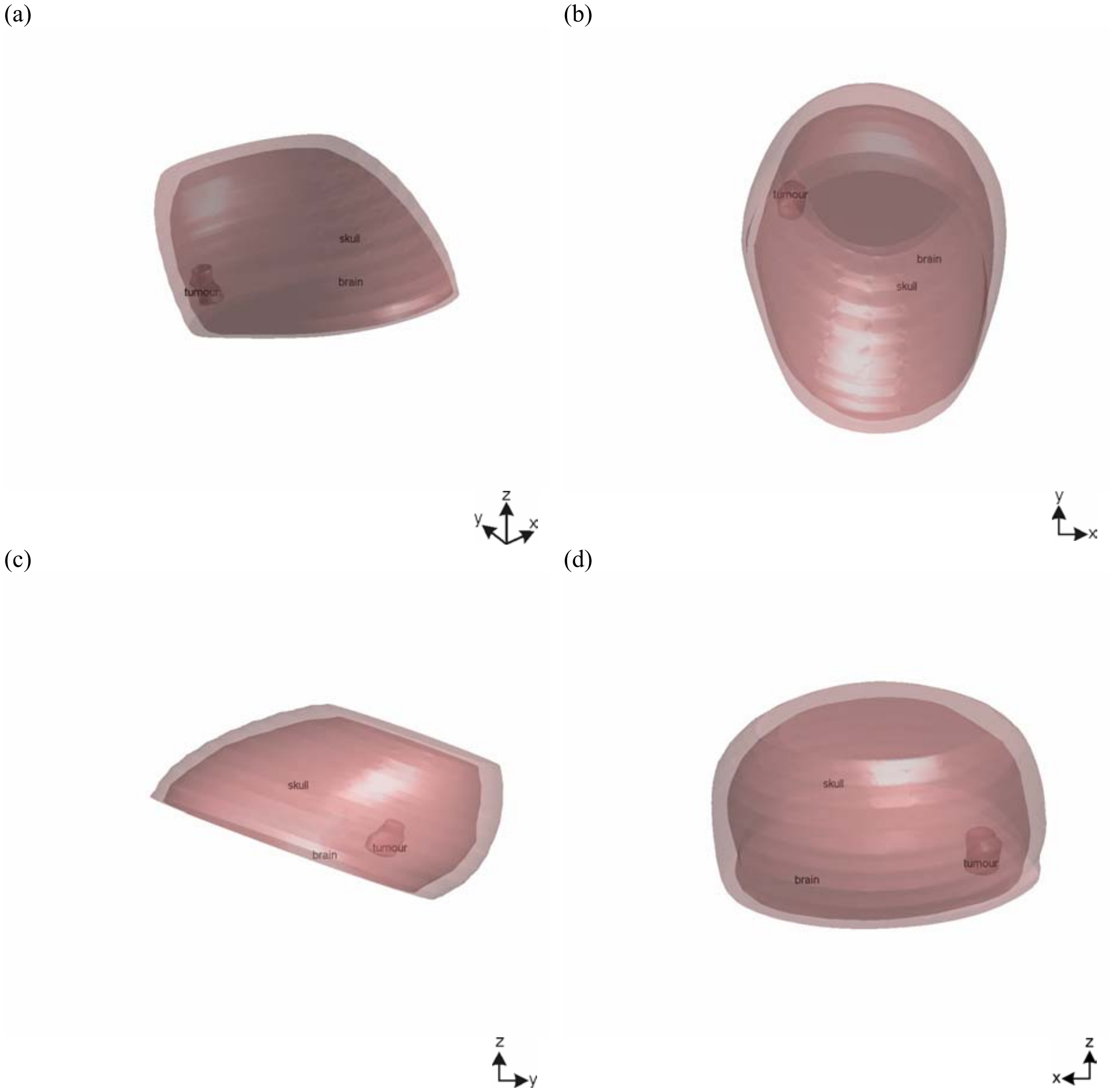

Figure 6.18: Generated 3D geometry model of the skull, brain and tumour: (a) 3D perspective, (b) *xy* projection, (c) *yz* projection and (d) *xz* projection.

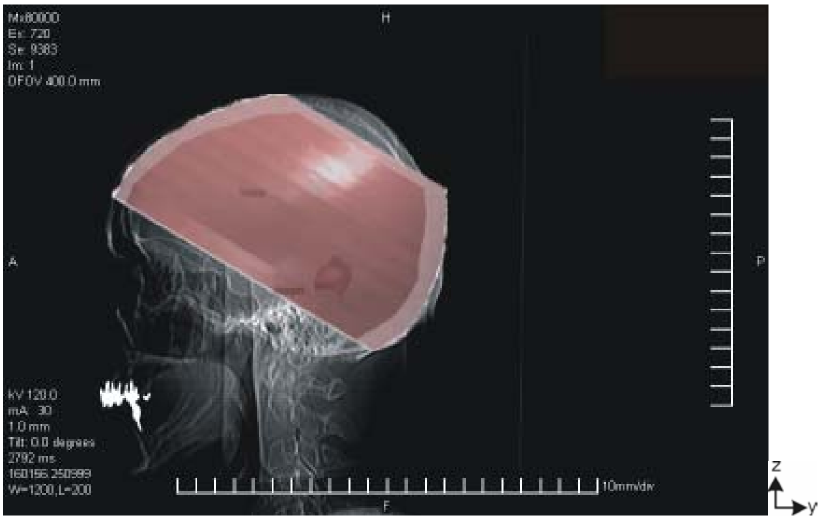

Figure 6.19: CT image in sagital plane with *yz* projection of the modelled 3D geometry.

6.3.3.5 NEEDLE ELECTRODE INSERTION AND MESH GENERATION

Before inserting an array of needle electrodes, we scaled the 3D brain geometry to correspond to real dimensions of the head i.e. divided the geometry by the number of pixels that correspond to 1 mm. Then we rotated the geometry to have the scanning plane parallel to the *xy* plane for better visualisation of results.

The array of needle electrodes was designed to correspond to the Cliniporator holder. Needles of 0.7 mm in diameter were placed in two rows with different polarities. The rows were 8.7 mm apart (centre of needles). The distance between the centres of neighbouring needles in the row was 3.2 mm.

We inserted the needle electrode array in the brain geometry through the area where the tumour was closest to the edge of the brain. The depth of needle penetration (14 mm) was chosen not to exceed the dimension of the tumour in the direction towards the centre of the brain, which would otherwise damage healthy brain tissue. We also took care when inserting needle electrodes that the resulting E distribution will cover the greatest area of tumour possible. Figure 6.20 presents the position of the needle array with respect to the brain and tumour. On the right hand side of the same figure the close up is shown. Details of the needle array insertion in the tumour are shown in Figure 6.21. We can see that the tumour has a very irregular shape and that certain needles are placed very close to the edge of tumour.

The described geometry is very demanding for automatic mesh generation for the following reasons:

- the geometry consists of many curved objects;
- curved objects significantly differ in dimensions (dimension ratio, brain to needles was 140 to 0.7);
- the distance between the boundaries of two curved objects is very small (the tumour is near the edge of the brain).

Even though employing automatic meshing, the mesh generation was a long process subject to initial mesh parameter tuning. The obtained mesh is presented in Figure 6.22. We can see that the mesh was very dense in the region around the electrode insertion and inside the tumour. The mesh consisted of 8916 nodes.

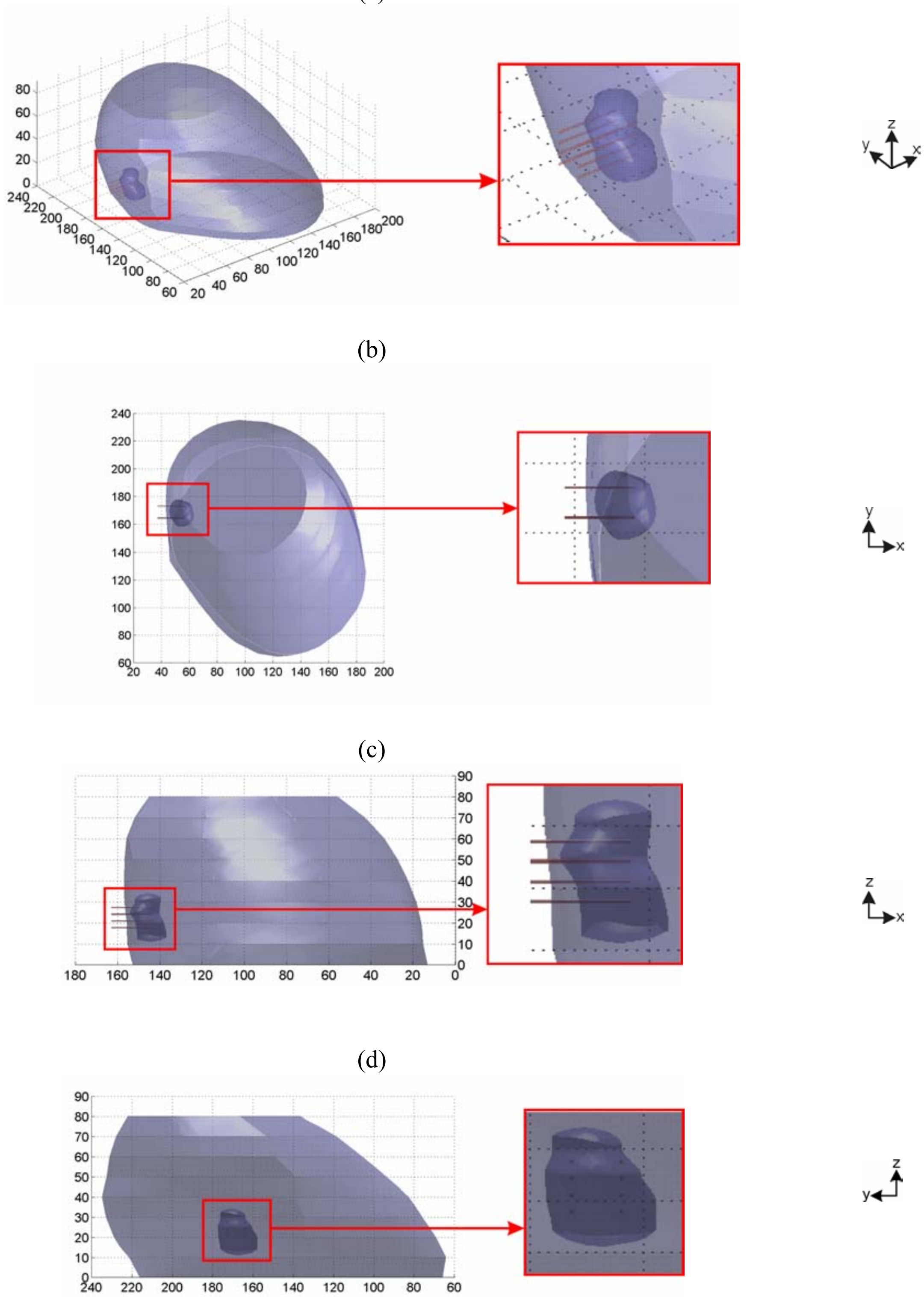
(a)

(b)

(c)

(d)

Figure 6.20: Insertion of the needle electrode array in the brain geometry with a close up of the tumour. (a) 3D perspective, (b) *xy* plane, (c) *xz* plane, (d) *yz* plane.

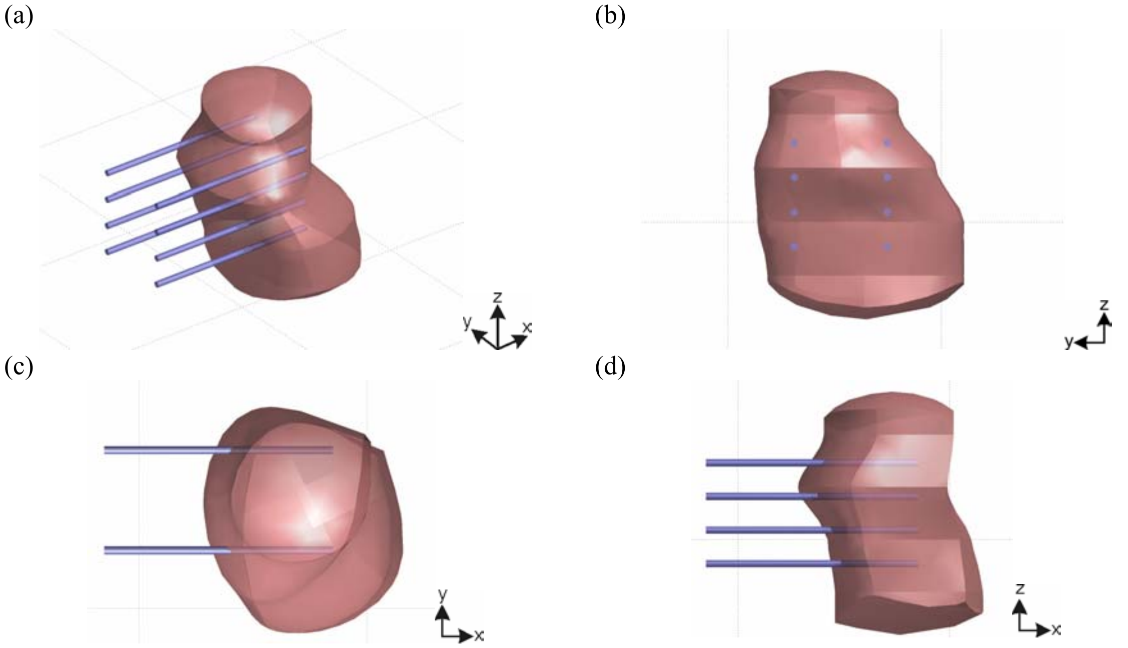

Figure 6.21: Details of needle array insertion in tumour: (a) 3D perspective, (b) *yz* plane, (c) *xy* plane, (d) *xz* plane.

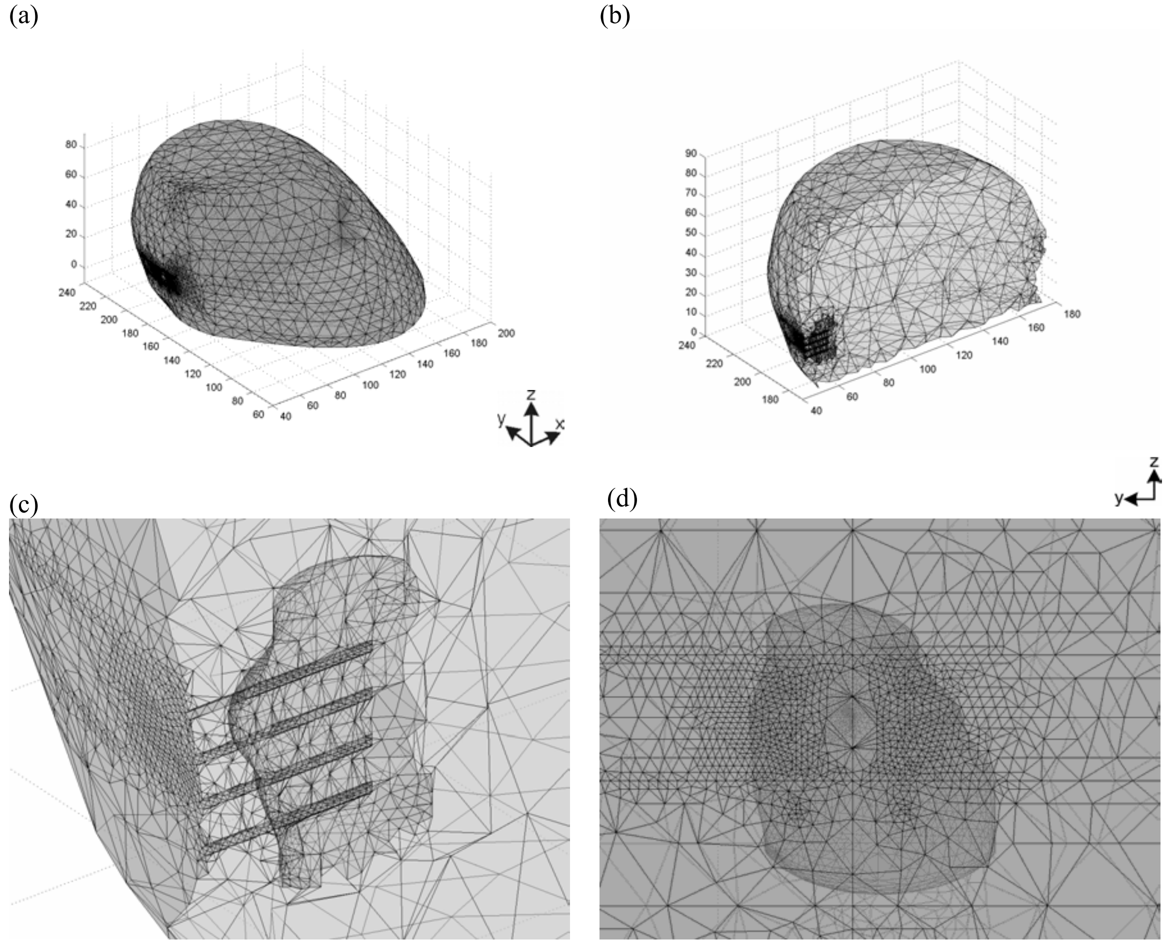

Figure 6.22: Finite element mesh of the brain with a tumour and inserted needle electrode array: (a) 3D perspective, (b) 3D mesh in cross section parallel to needle length, (c) 3D close up of tumour in cross section parallel to needle length, (d) close up of tumour in *yz* plane.

6.3.3.6 SIMPLIFYING BRAIN GEOMETRY FOR THE OPTIMISATION PURPOSE

Optimisation itself is time consuming because it requires several model evaluations. Each evaluation of the FE brain model takes tens of minutes. On top of that the part of the brain far from electrodes does not influence E distribution in the tumour, yet it adds to the time required for solving the model. Therefore we simplified the 3D brain geometry by substituting the brain with a block and preserving the same position of the tumour and electrodes. The block was positioned as to correspond to the edge of the brain close to the tumour (Figure 6.23). The FE mesh of the block with a tumour and needle electrodes had 6165 nodes (30% fewer than the mesh of the brain geometry).

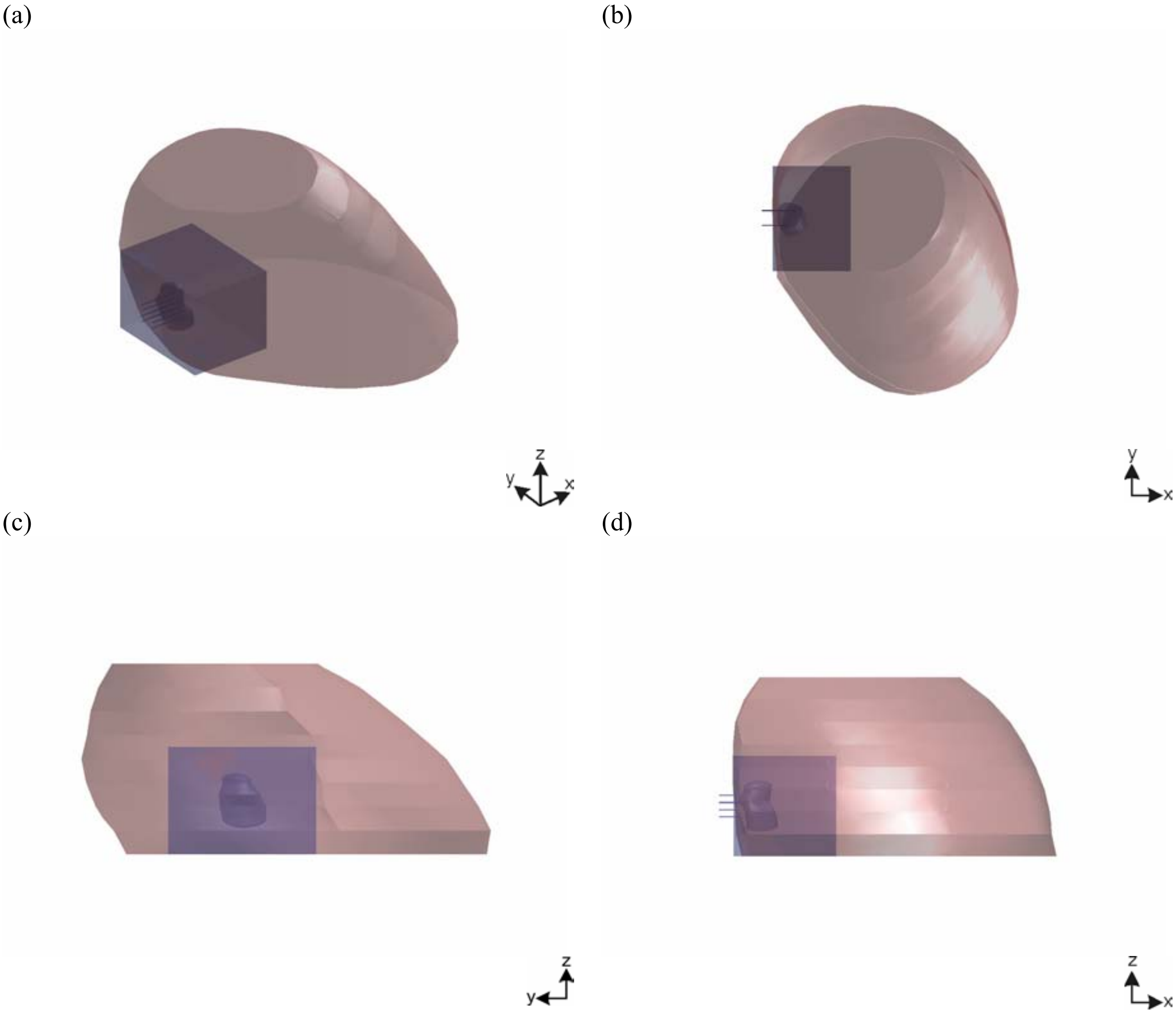

Figure 6.23: Position of the block aimed at substituting brain geometry with respect to the brain: (a) 3D view, (b) *xy* plane, (c) *yz* plane, (d) *xz* plane.

6.3.3.7 OPTIMISATION OF EP PARAMETERS BASED ON MODEL OF BRAIN WITH TUMOUR

Five points were selected for assessment of E intensity at the end of permeabilisation propagation and computation of the objective function during optimisation: $E_1(x_1=60.34$ mm, $y_1=174.4$ mm, $z_1=30$ mm), $E_2(x_2=54.55$ mm, $y_2=170.7$ mm, $z_2=34$ mm), $E_3(x_3=55.26$ mm, $y_3=167$ mm, $z_3=11.06$ mm), $E_4(x_4=53$ mm, $y_4=158.5$ mm, $z_4=20$ mm), and $E_5(x_5=54.55$ mm, $y_5=159$ mm, $z_5=15$ mm). They are critical as they represent points on the edge of the tumour where the lowest E intensities could be present. Those points are shown in Figure 6.24 (a), Figure 6.25 (a) and Figure 6.26 (a). The reference value of E to be reached in each of those points was E_r=255 V/cm.

The parameters subject to optimisation were either pulse amplitude *u* or a combination of *u* and distance *d* between two electrode pairs. We first used the same constraints on *u, i(u,d),* and *E(u,d)* as described in Chapter 6.1.2.

When incorporating the distance between electrodes as a parameter for optimisation we utilized two electrode pairs in an electrode holder instead of four and defined *d* as the distance between two electrode pairs with different polarity. Optimisation of the distance between electrodes required new mesh generation for each distance as shown in Figure 6.8. Therefore we tested mesh generation for different distances between electrodes in advance and found it impossible to build the mesh at certain distances. Therefore we transformed the problem of distance optimisation into a problem of optimisation of discrete distances at which mesh generation succeeded. The transformed optimisation problem was required to find the minimum of the objective function subject to one continuous parameter *u* and one discrete parameter *d*. This is a so called mixed integer programming problem [Fletcher and Leyffer, 1994], which can be solved either by optimising continuous parameter at each value of discrete parameter or by using special purpose algorithms, such as Tree-search algorithm for mixed integer programming problems [Dakin, 1965].

We used the first approach, because only two discrete distance values applied to our problem. Even more with increased distances between electrode pairs the mesh generation failed. Thus we used geometry with 4 needle pairs and then simulated the change in distance by applying voltage to two needle pairs with different polarity distanced either at 3.2 mm or 9.6 mm. Therefore the optimisation procedure as shown schematically in Figure 6.3 was employed in all further models. However if several discrete values of *d* were present we would consider optimisation based on a Tree-search algorithm.

6.3.3.7.1 PULSE AMPLITUDE OPTIMISATION OF TWO NEEDLE PAIRS 3.2 MM APART

We applied voltage to two electrode pairs at distance d_1=3.2 mm and set the initial value for *u* at u_0=200 V. During optimisation in each model evaluation, three time discrete steps were computed in the permeabilisation model. However the optimisation provided no feasible solution. The reason was that nonlinear constraints were in contradiction. Namely, the constraint which required E intensity in selected points of the tumour to be above the reference value of E intensity i.e. $E_j > E_r$ could be satisfied only if total current was higher than 16 A. As the latter is the objective limitation of the Cliniporator, we omitted the nonlinear constraint on E intensity in further optimisations of this model because it can not be achieved with such a generator.

The minimum of the objective function obtained by optimisation without considering the nonlinear constraint on E was $f(u,d_1)$= 0.1907. The constraint on *u* was active, which means that the resulting optimal voltage was *u*=1000 V at d_1=3.2 mm. Total current was 15.07 A. In evaluation points the electric field reached the following values: E_1=200.3 V/cm, E_2=173.6 V/cm, E_3=169.3 V/cm, E_4=196.6V/cm, and E_5=138.6 V/cm. E intensity did not exceed reversible threshold in any of those points, which means that the tumour was not completely permeabilised. The reason for the discrepancy was reached boundary on pulse amplitude *u* which if higher would give E intensities closer to reversible threshold value in points of interest.

Figure 6.24, Figure 6.25, and Figure 6.26 present E distribution and specific conductivity in three time discrete steps of permeabilisation in *yz*, *xz* and *xy* plane respectively at applied voltage *u*=1000 V. We can see that some parts of the tumour were permeabilised while others were not. As a consequence, in order to achieve complete permeabilisation of the tumour the treatment should be repeated considering a new position of electrodes that would permeabilise areas of the tumour which remained non-permeabilised in the first treatment. This, however, is outside the scope of this work.

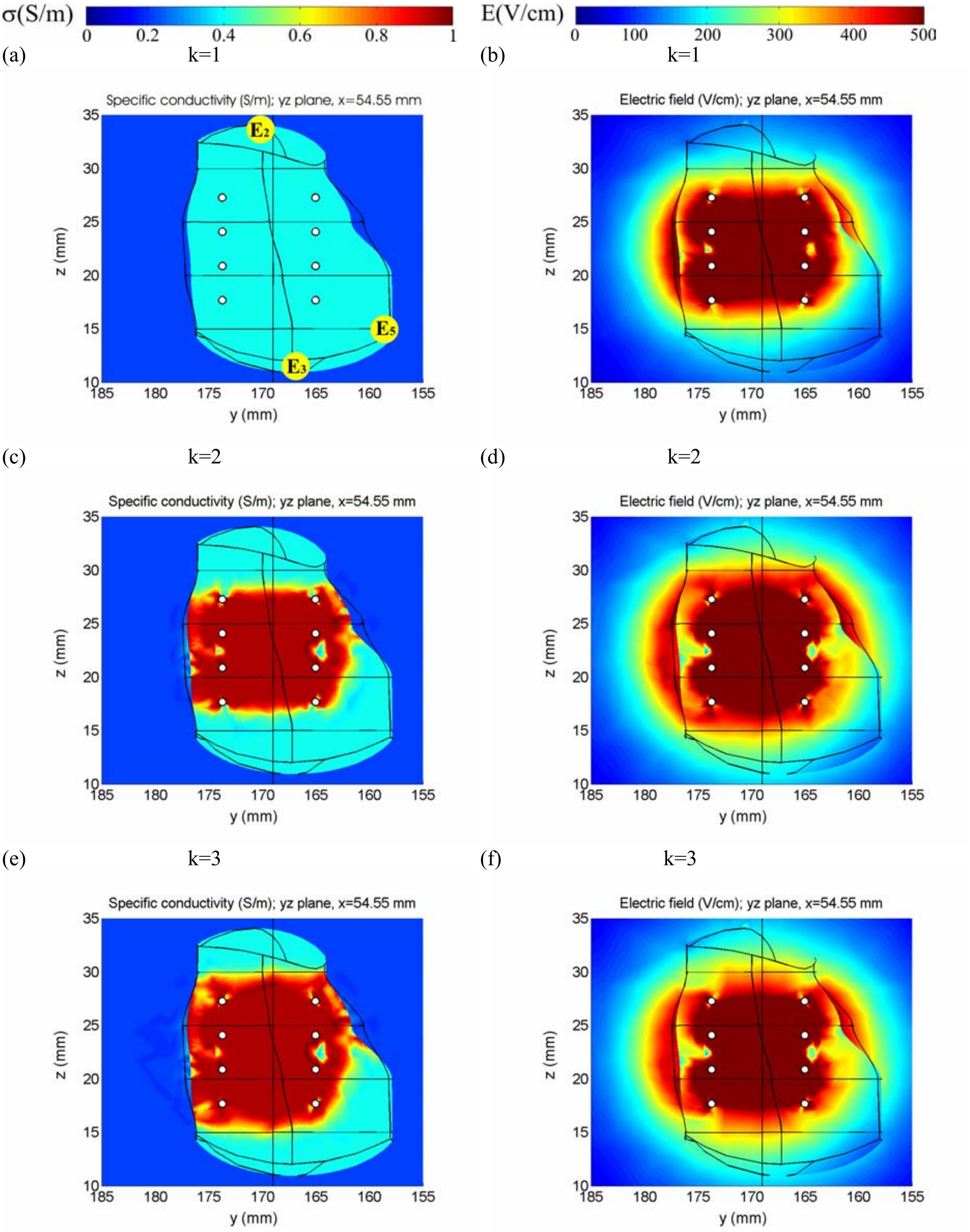
(a) k=1 (b) k=1

(c) k=2 (d) k=2

(e) k=3 (f) k=3

Figure 6.24: Three consecutive steps computed by the model at u=1000.0 V in yz plane (x=54.44 mm): (a) and (b) specific conductivity and E respectively in the first step; (c) and (d) specific conductivity and E respectively in the second step (e) and (f) specific conductivity and E respectively in the third step. The distance between two needle pairs with different polarity was d_l=3.2 mm.

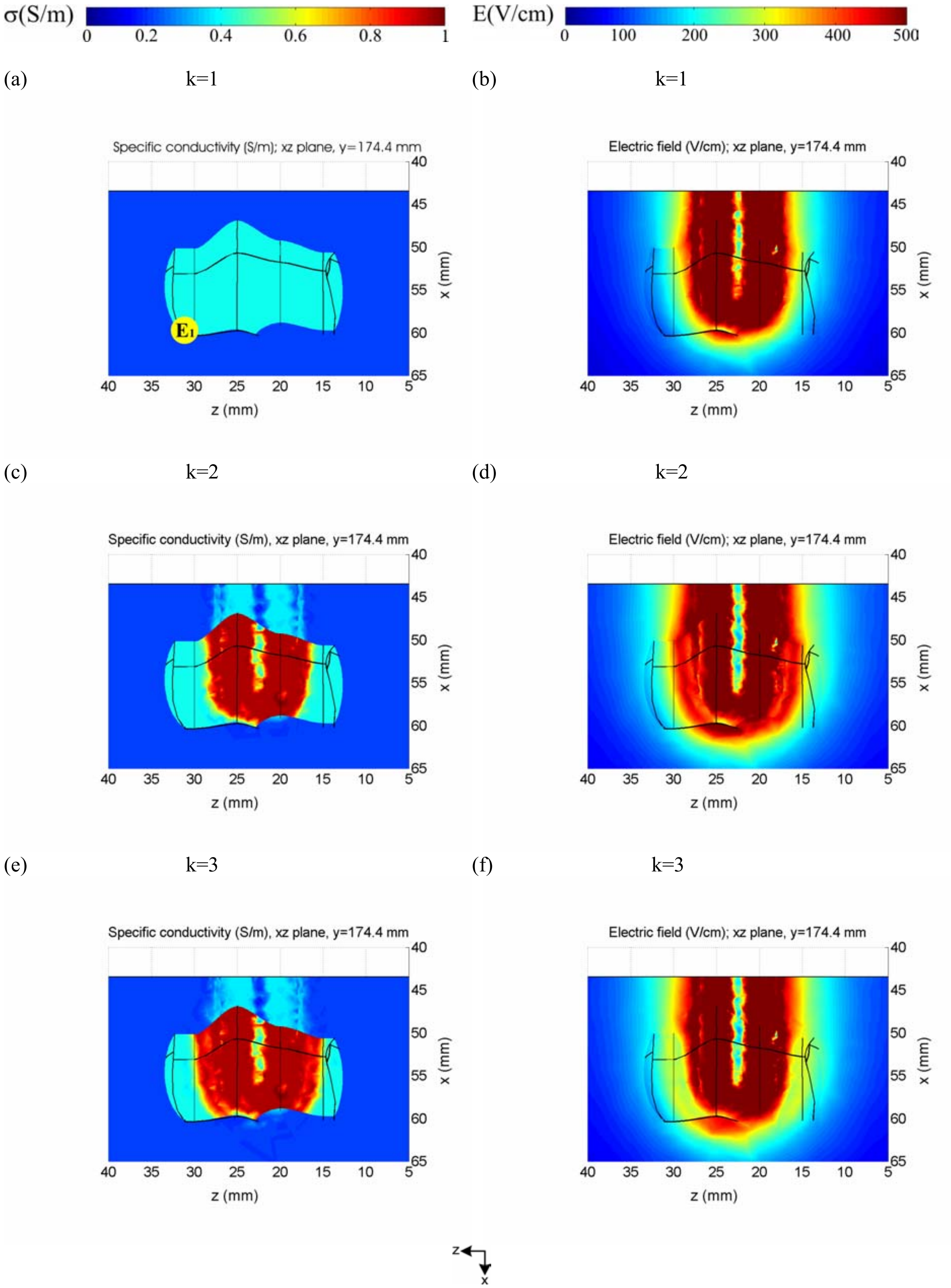

Figure 6.25: Three consecutive steps computed by the model at u=1000.0 V in xz plane (y=174.4 mm): (a) and (b) specific conductivity and E respectively in the first step; (c) and (d) specific conductivity and E respectively in the second step; (e) and (f) specific conductivity and E respectively in the third step. The distance between two needle pairs with different polarity was d_1=3.2 mm.

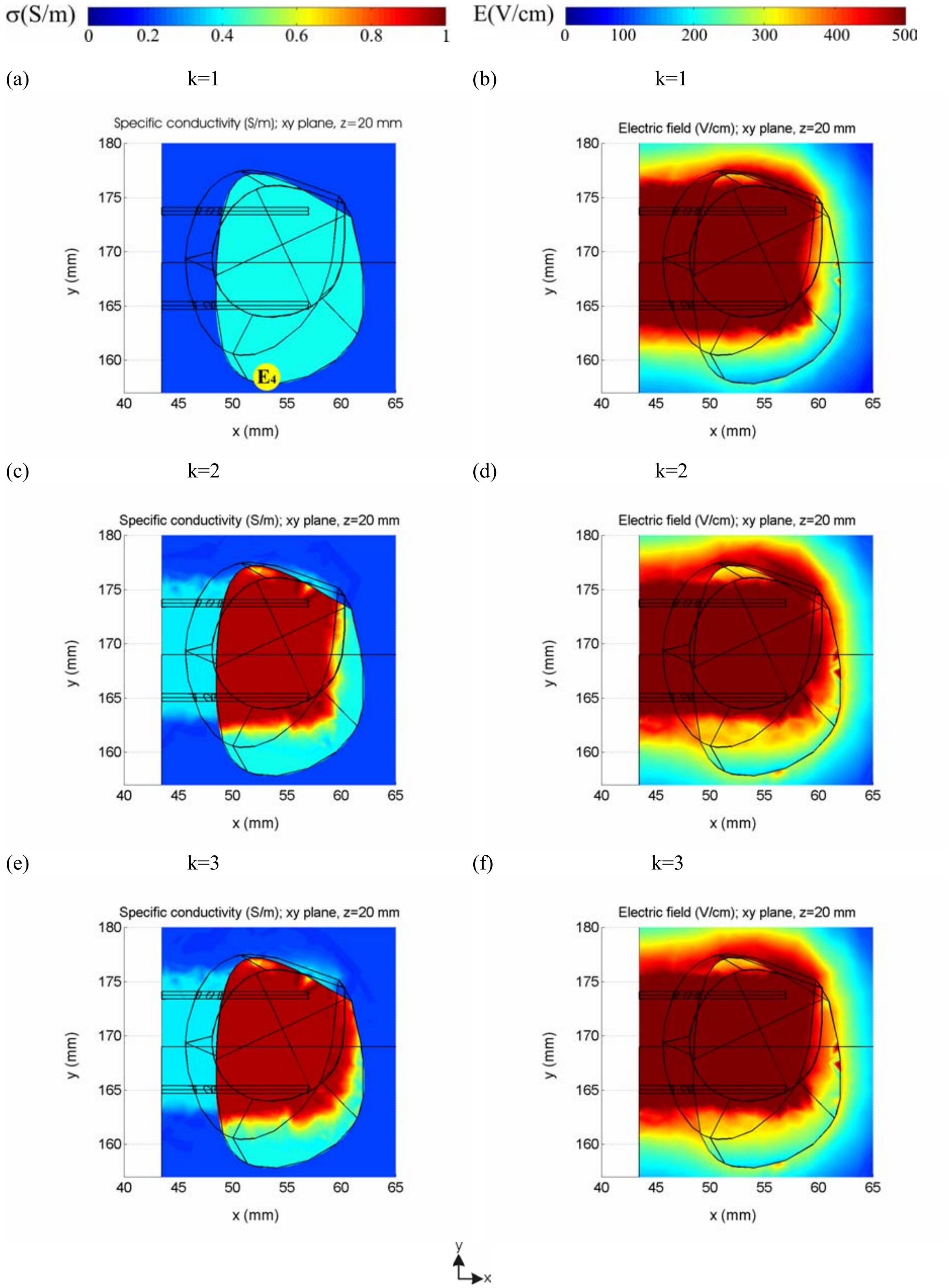

Figure 6.26: Three consecutive steps computed by the model at u=1000.0 V in xy plane (z=20 mm): (a) and (b) specific conductivity and E respectively in the first step; (c) and (d) specific conductivity and E respectively in the second step (e) and (f) specific conductivity and E respectively in the third step. The distance between two needle pairs with different polarity was d_1=3.2 mm.

6.3.3.7.2 PULSE AMPLITUDE OPTIMISATION OF TWO NEEDLE PAIRS 9.6 MM APART

Voltage was applied to two electrode pairs at distances of 9.6 mm. The initial value set for u was u_0=200 V. The value of the objective function at the end of optimisation was $f(u,d_2)$= 0.1921. The constraint on current was active, i.e. $i(u,d_2)$ was 15.99 A. The resulting optimal voltage was u=915.3 V at d_2=9.6 mm.

The electric field reached the following values at evaluation points: E_1=340.1 V/cm, E_2=267.3 V/cm, E_3=256.0 V/cm, E_4=107.7V/cm, E_5=130.1 V/cm. Compared to the previous model (d_1=3.2) the present model exceeded reversible threshold at three evaluation points (E_1, E_2, E_3), however at two points (E_4, E_5), it was far below the threshold. One of the points was also far above threshold. Thus the minimum of the objective function was higher than in the previous model, which implied that electrodes at distance d_1=3.2 mm and at applied voltage u=1000 V performed better than electrodes at distance 9.6 mm and applied voltage u=915.3 V, with respect to the defined objective function.

Specific conductivity and E distribution for the three consecutive steps in *yz*, *xz* and *xy* plane are shown in Figure 6.27, Figure 6.28, and Figure 6.29, respectively. Again we see that parts of the tumour were not permeabilised which would again require repositioning of the electrodes and therapy repetition.

6.3.3.7.3 PULSE AMPLITUDE OPTIMISATION OF FOUR NEEDLE PAIRS

Voltage was applied to four electrode pairs. All electrodes in a row were at the same potential. One row had a potential of 0 V, while the other was set to an initial value of u_0=200 V – the starting point for the optimisation.

The minimum of the objective function obtained by optimisation was $f(u)$=0.1869. Again the constraint on current was active, i.e. $i(u)$ was 16.00 A, preventing any further increase in pulse amplitude. Thus the resulting optimal voltage was u=701.0 V. The electric field reached the following values at evaluation points: E_1=276.9 V/cm, E_2=227.5 V/cm, E_3=216.7 V/cm, E_4=128.6 V/cm, and E_5=120.8 V/cm. The reversible threshold value was exceeded at only one point. The current constraint is obviously governing the extent of permeabilisation, because at higher voltages (which would cause higher currents) the E at the evaluation points would be closer to threshold value.

Specific conductivity and E distribution for the three consecutive steps in *yz*, *xz* and *xy* plane are shown in Figure 6.30, Figure 6.31, and Figure 6.32, respectively. Again we see that regions of the tumour were not permeabilised. Their permeabilisation would require repositioning of the electrodes and repetition of therapy.

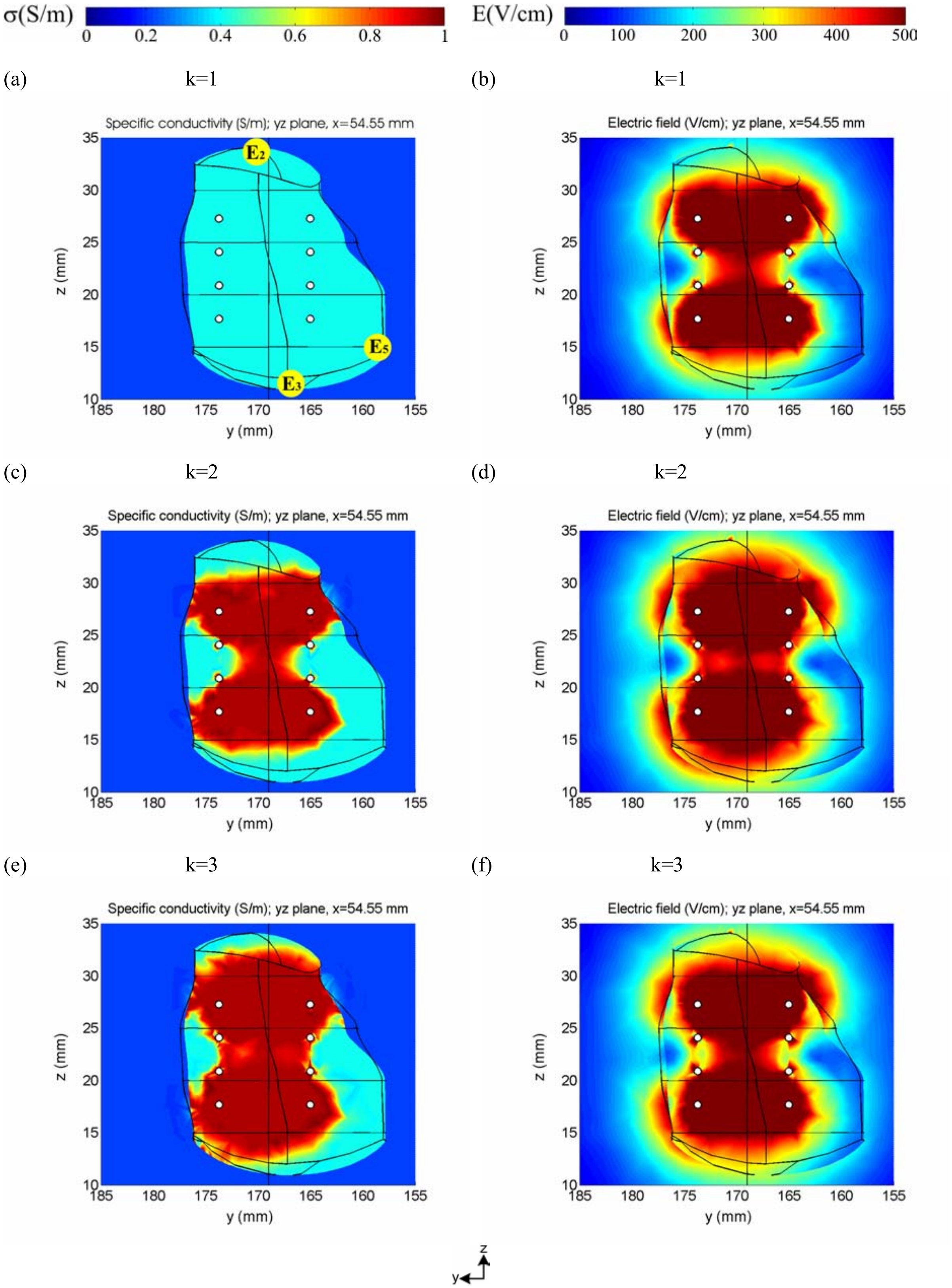

Figure 6.27: Three consecutive steps computed by the model at *u*=915.3 V in *yz* plane (*x*=54.44 mm): (a) and (b) specific conductivity and E respectively in the first step; (c) and (d) specific conductivity and E respectively in the second step; (e) and (f) specific conductivity and E respectively in the third step. The distance between two needle pairs with different polarity was d_2=9.6 mm.

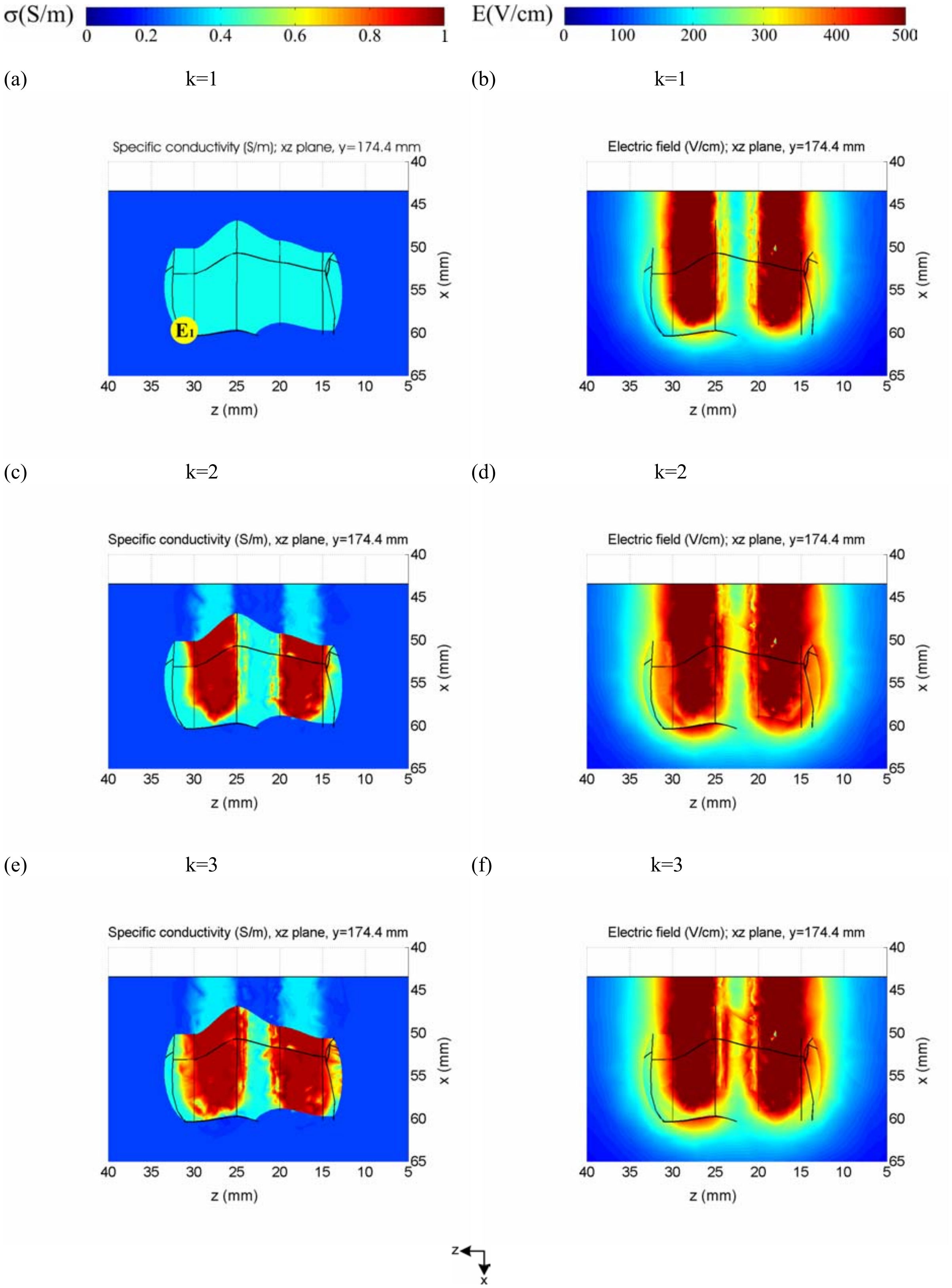
(a) k=1 (b) k=1

(c) k=2 (d) k=2

(e) k=3 (f) k=3

Figure 6.28: Three consecutive steps computed by the model at u=915.3 V in xz plane (y=174.4 mm): (a) and (b) specific conductivity and E respectively in the first step; (c) and (d) specific conductivity and E respectively in the second step; (e) and (f) specific conductivity and E respectively in the third step. The distance between two needle pairs with different polarity was d_2=9.6 mm.

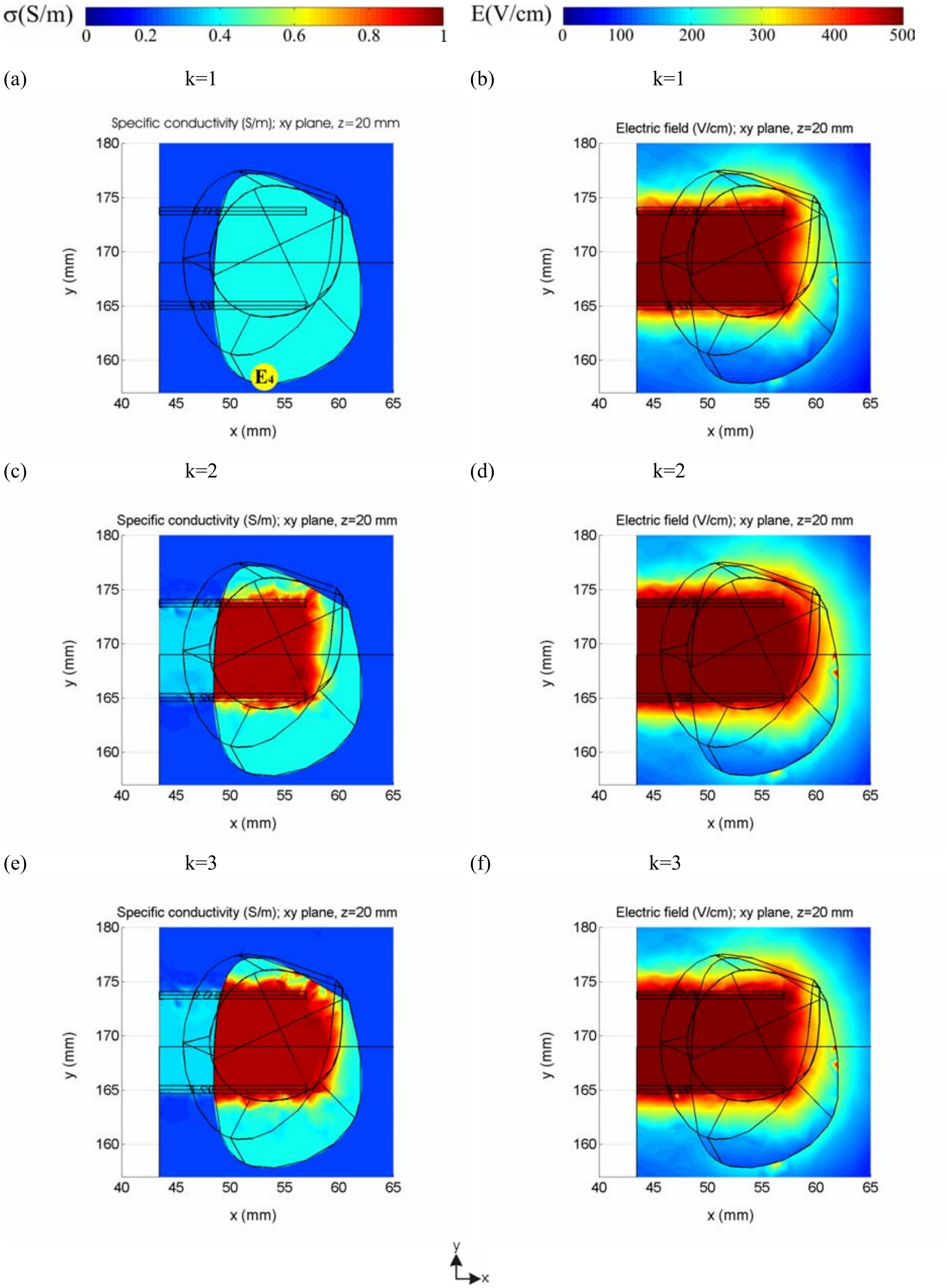
(a) k=1

(b) k=1

(c) k=2

(d) k=2

(e) k=3

(f) k=3

Figure 6.29: Three consecutive steps computed by the model at *u*=915.3 V in *xy* plane (*z*=20 mm): (a) and (b) specific conductivity and E respectively in the first step; (c) and (d) specific conductivity and E respectively in the second step; (e) and (f) specific conductivity and E respectively in the third step. The distance between two needle pairs with different polarity was d_2=9.6 mm.

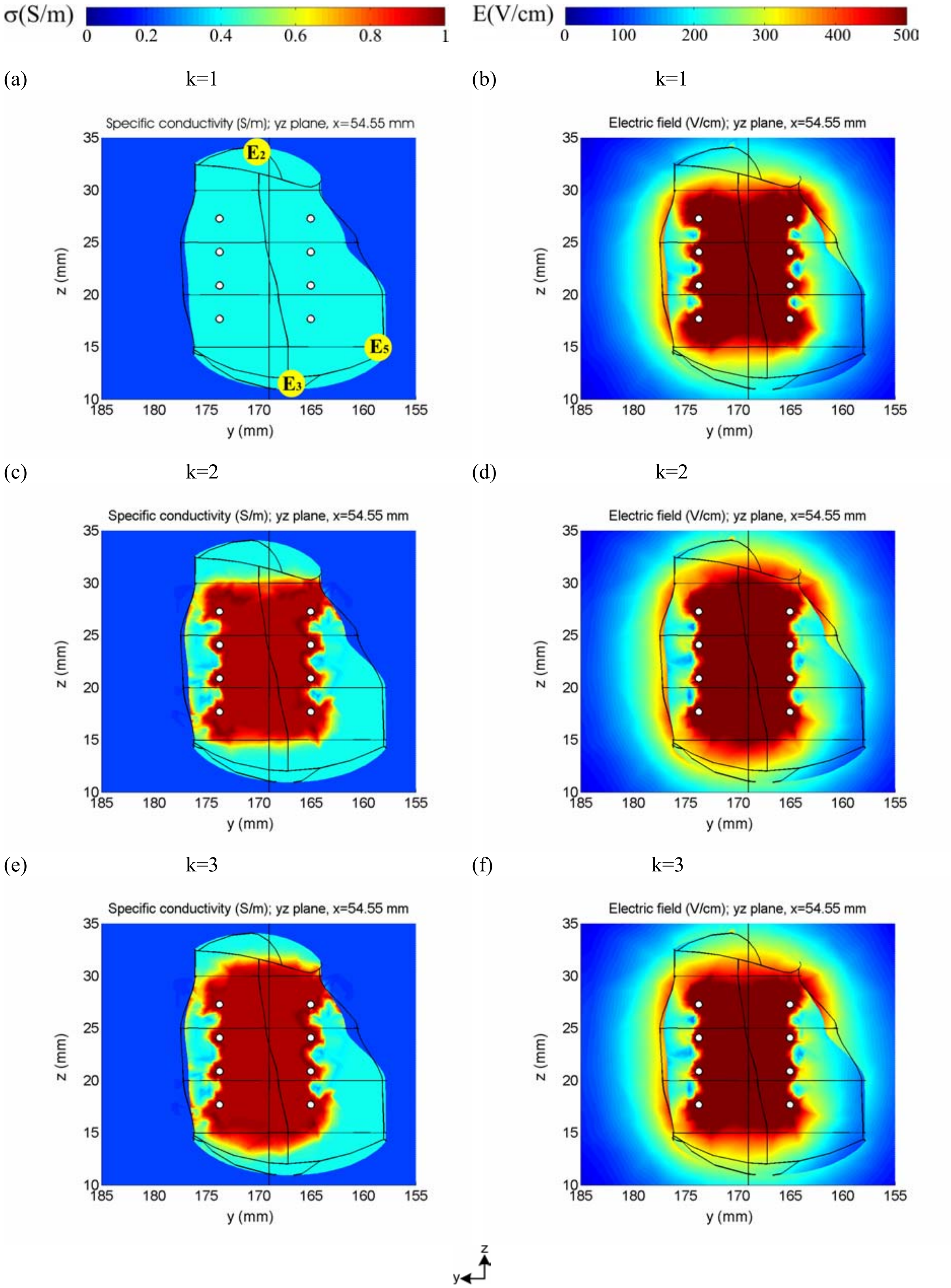

Figure 6.30: Three consecutive steps computed by the model at *u*=701.0 V in *yz* plane (*x*=54.44 mm): (a) and (b) specific conductivity and E respectively in the first step; (c) and (d) specific conductivity and E respectively in the second step; (e) and (f) specific conductivity and E respectively in the third step. Voltage was applied to four needle pairs.

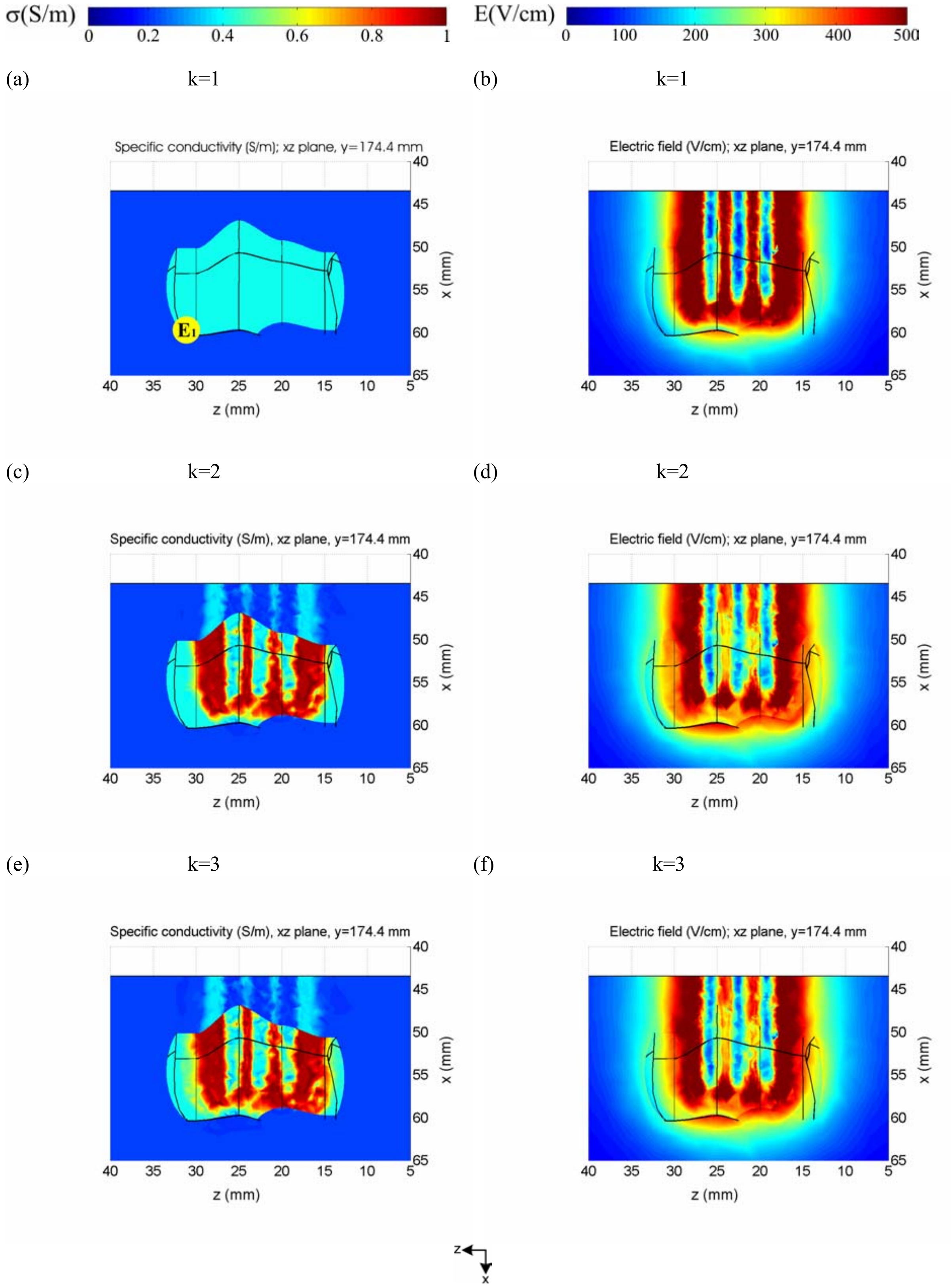

Figure 6.31: Three consecutive steps computed by the model at *u*=701.0 V in *xz* plane (*y*=174.4 mm): (a) and (b) specific conductivity and E respectively in the first step; (c) and (d) specific conductivity and E respectively in the second step; (e) and (f) specific conductivity and E respectively in the third step. Voltage was applied to four needle pairs.

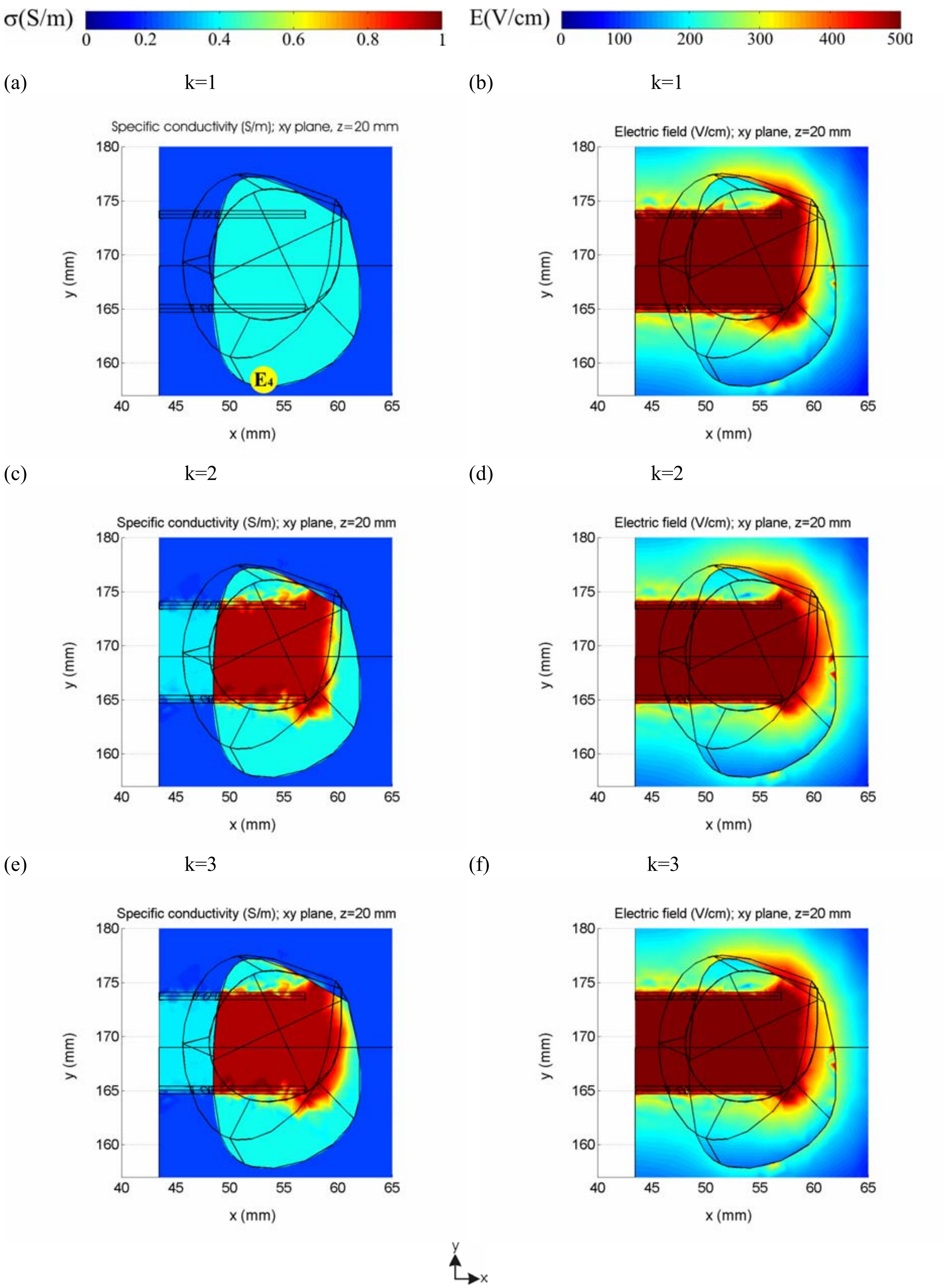

(a) k=1

(b) k=1

(c) k=2

(d) k=2

(e) k=3

(f) k=3

Figure 6.32: Three consecutive steps computed by the model at u=701.0 V in xy plane (z=20 mm): (a) and (b) specific conductivity and E respectively in the first step; (c) and (d) specific conductivity and E respectively in the second step; (e) and (f) specific conductivity and E respectively in the third step. Voltage was applied to four needle pairs.

6.3.3.7.4 PULSE AMPLITUDE OPTIMISATION OF EACH ELECTRODE PAIR FROM THE NEEDLE ARRAY

Voltage was applied to four electrode pairs. Electrodes in one row were set to potential 0 V. Electrodes in another row were each set to a different potential – subject to optimisation. Initial values were u_{01}=200 V, u_{02}=300 V, u_{03}=200 V, u_{04}=300. The same constraints on u and i were used as in the previous model.

The optimisation was repeated three times. The initial values for each subsequent optimisation were the optimised parameters obtained from the previous optimisation. Optimisation settings were refined with each optimisation.

The minimum of the objective function computed with the last optimisation was $f(u)$=0.1575. Constraint on current was again reached i.e. $i(u)$=15.99 A. The resultant optimal pulse amplitudes were u_1=802.3 V, u_2=191.9 V, u_3=671.2 V, u_4=1000.0 V. The electric field reached the following values at evaluation points: E_1=264.8 V/cm, E_2=237.1 V/cm, E_3= 275.5 V/cm, E_4=141.7 V/cm, and E_5=135.6 V/cm. At thwo points (E_1, E_3), E exceeded the reversible threshold while at the other three it was below. Despite this, the obtained pulse parameters gave superior results compared to parameters obtained in Chapters 6.3.3.7.1 to 6.3.3.7.3.

Figure 6.33, Figure 6.34, and Figure 6.35 present specific conductivity and E in *yz*, *xz* and *xy* plane, respectively in models with applied optimal pulse parameters.

6.3.3.7.5 PULSE AMPLITUDE OPTIMISATION WITHOUT CONSTRAINTS ON U AND I

As none of the previous optimisations yielded complete permeabilisation of the tumour we examined a hypothetical example, in which the pulse generator had no constraints on u and i.

Electrodes in one row were set to potential 0 V. Electrodes in another row were each set to a different potential – subject to optimisation. The initial values were u_{01}=200 V, u_{02}=300 V, u_{03}=200 V, u_{04}=300 V. There were no constraints set except a nonlinear constraint on E, which required E intensity in selected points to be above or equal to reference value E_r.

The minimum of the objective function obtained was $f(u)$=0.1762. Total current was 28.70 A with optimal potentials applied to electrodes in one row: u_1=1088.2 V, u_2=485.7 V, u_3=1200.1 V, u_4=1880.9 V. The electric field reached the following values at evaluation points: E_1=255.0 V/cm, E_2= 313.8 V/cm, E_3=474.7 V/cm, E_4=256.3 V/cm, and E_5=255.0 V/cm. According to the obtained E intensities in selected points the total volume of the tumour should be permeabilised.

Figure 6.36, Figure 6.37, and Figure 6.38 present specific conductivity and E in *yz, xz* and *xy* plane, respectively computed by models at applied optimal pulse parameters. We can see that in selected planes the complete area of the tumour was exposed to E intensities above reversible threshold in the third step computed by the time discrete model. Some regions of the tumour at its edge were exposed to E intensities just above reversible threshold, while other regions of the tumour were exposed to E intensities above irreversible threshold. Thus in the former regions, entrance of the chemotherapeutic is enabled, while in the latter regions cell death is caused due to exposure to excessive E intensities. For effective electrochemotherapy, this is a satisfactory result.

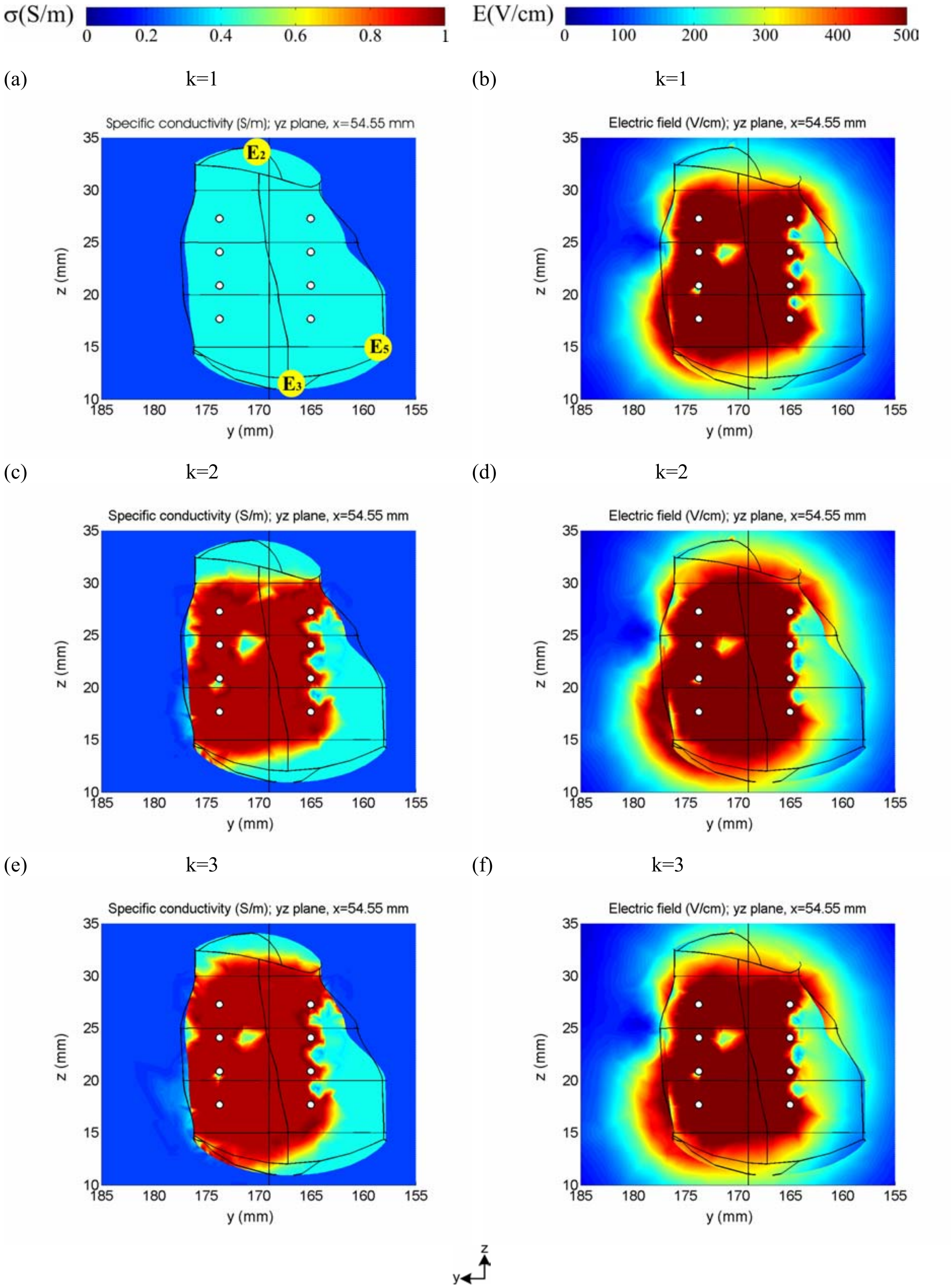

Figure 6.33: Three consecutive steps computed by the model in *yz* plane (*x*=54.55 mm). The potential assigned to needle pairs was u1=802.3 V, u2=191.9 V, u3=671.2 V, u4=1000.0 V. (a) and (b) present specific conductivity and E respectively in the first step; (c) and (d) present specific conductivity and E respectively in the second step; (e) and (f) present specific conductivity and E respectively in the third step.

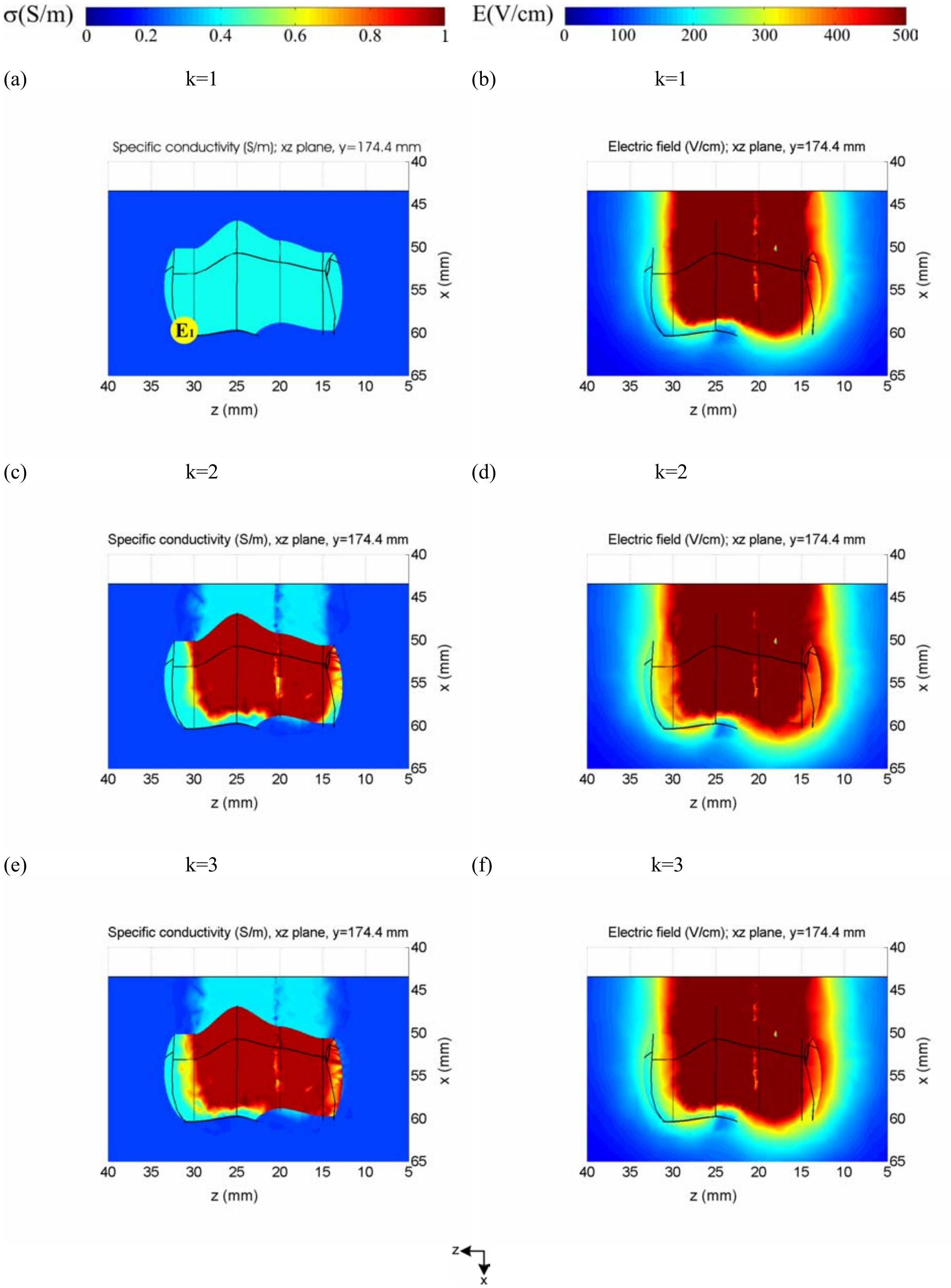

(a) k=1 (b) k=1

(c) k=2 (d) k=2

(e) k=3 (f) k=3

Figure 6.34: Three consecutive steps computed by the model in *xz* plane (*y*=174.44 mm). The potential assigned to needle pairs was *u1*=802.3 V, *u2*=191.9 V, *u3*=671.2 V, *u4*=1000.0 V. (a) and (b) present specific conductivity and E respectively in the first step; (c) and (d) present specific conductivity and E respectively in the second step; (e) and (f) present specific conductivity and E respectively in the third step.

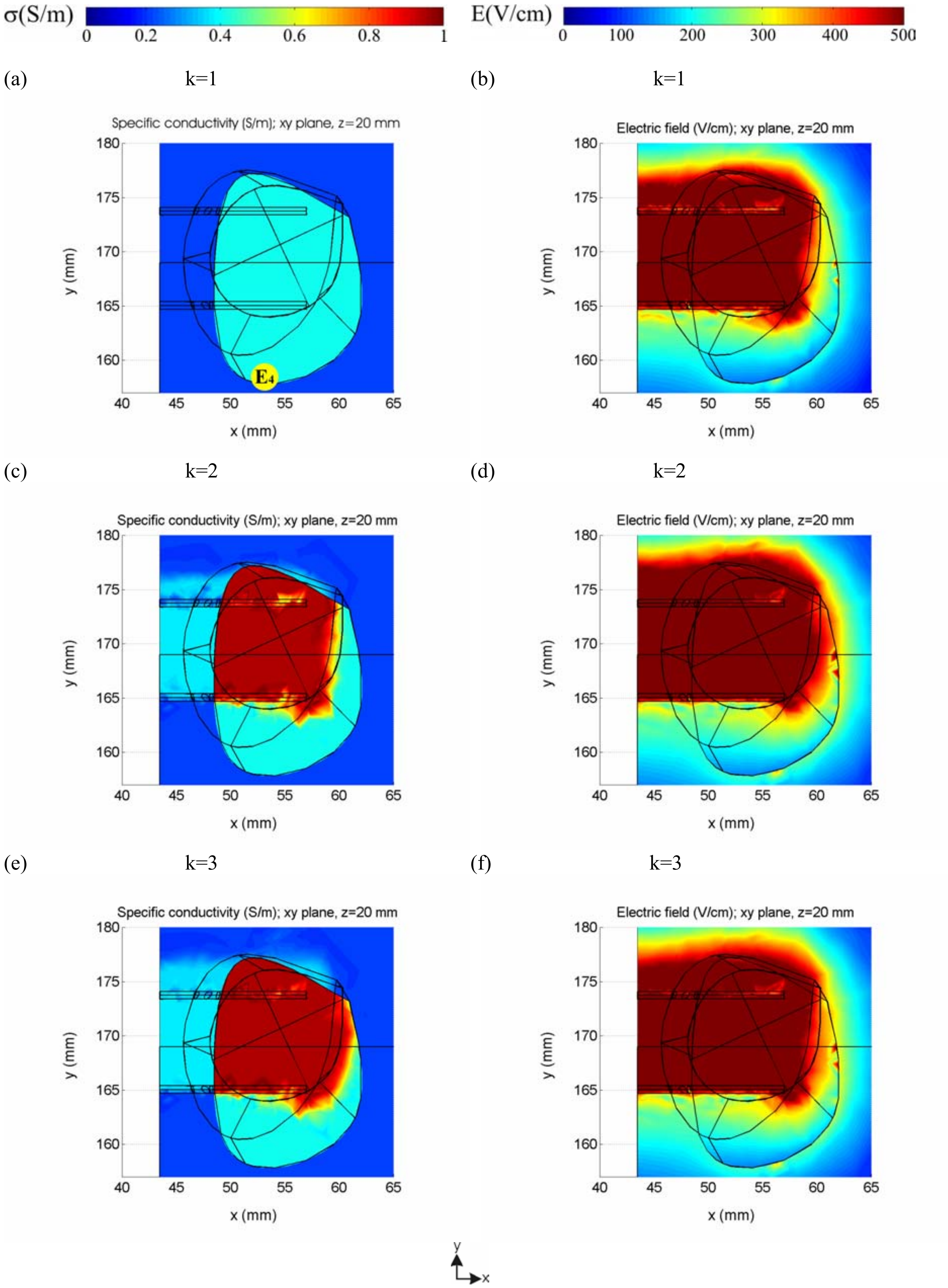

Figure 6.35: Three consecutive steps computed by the model in *xy* plane (*z*=20 mm). The potential assigned to needle pairs was *u1*=802.3 V, *u2*=191.9 V, *u3*=671.2 V, *u4*=1000.0 V. (a) and (b) present specific conductivity and E respectively in the first step; (c) and (d) present specific conductivity and E respectively in the second step; (e) and (f) present specific conductivity and E respectively in the third step.

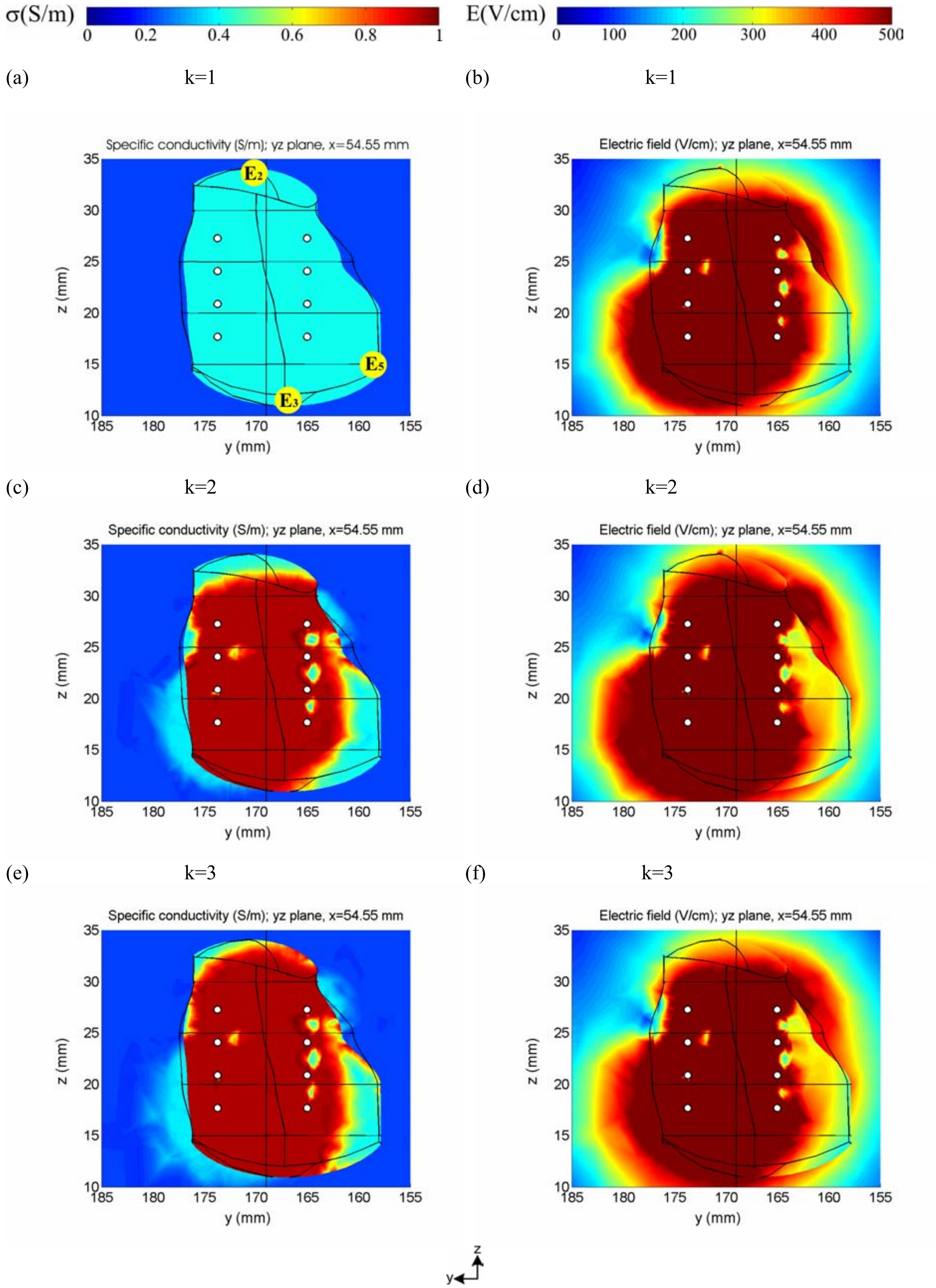

Figure 6.36: Three consecutive steps computed by the model in *yz* plane (*x*=54.55 mm). The potential assigned to needle pairs was u_1=1088.2 V, u_2=485.7 V, u_3=1200.1 V, u_4=1880.9 V. (a) and (b) present specific conductivity and E respectively in the first step; (c) and (d) present specific conductivity and E respectively in the second step; (e) and (f) present specific conductivity and E respectively in the third step.

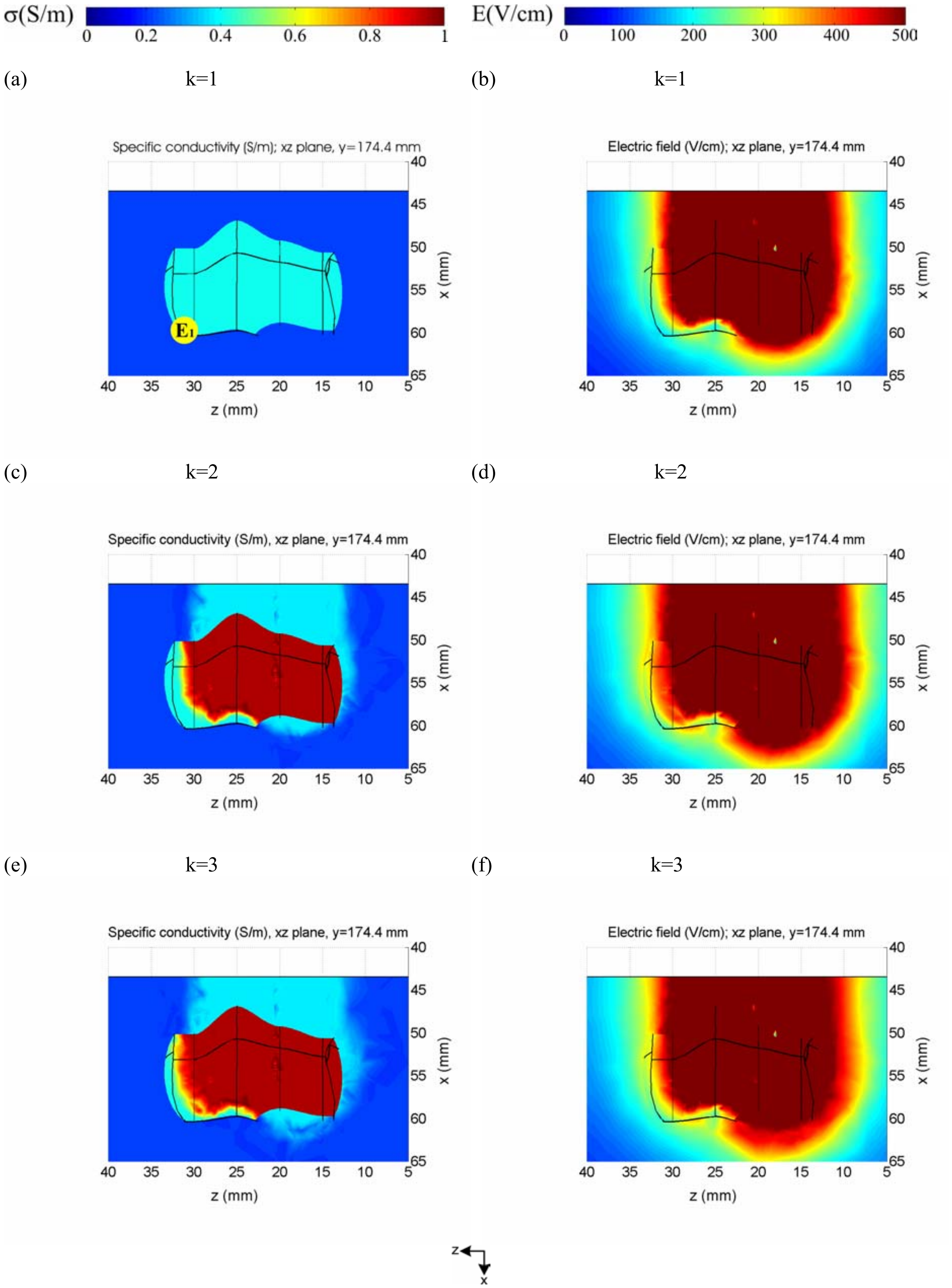
(a) k=1
(b) k=1
(c) k=2
(d) k=2
(e) k=3
(f) k=3

Figure 6.37: Three consecutive steps computed by the model in *xz* plane (y=174.44 mm). The potential assigned to needle pairs was u_1=1088.2 V, u_2=485.7 V, u_3=1200.1 V, u_4=1880.9 V. (a) and (b) present specific conductivity and E respectively in the first step; (c) and (d) present specific conductivity and E respectively in the second step; (e) and (f) present specific conductivity and E respectively in the third step.

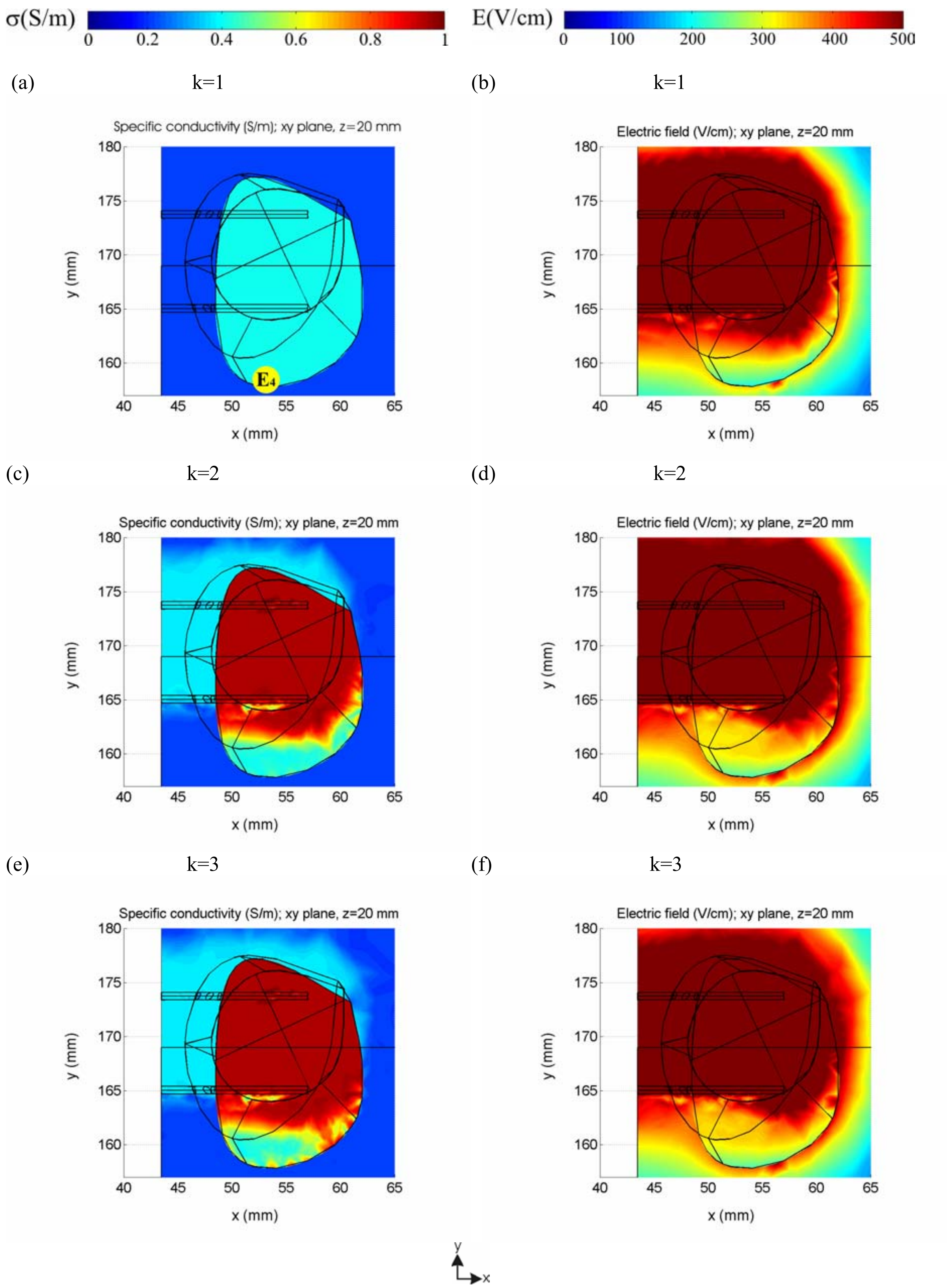

(a) k=1
(b) k=1
(c) k=2
(d) k=2
(e) k=3
(f) k=3

Figure 6.38: Three consecutive steps computed by the model in *xy* plane (*z*=20 mm). The potential assigned to needle pairs was u_1=1088.2 V, u_2=485.7 V, u_3=1200.1 V, u_4=1880.9 V. (a) and (b) present specific conductivity and E respectively in the first step; (c) and (d) present specific conductivity and E respectively in the second step; (e) and (f) present specific conductivity and E respectively in the third step.

6.3.3.8 OPTIMAL EP PARAMETERS APPLICATION ON BRAIN GEOMETRY

The optimal pulse parameters and values of E_i at the evaluation points obtained on the geometry consisting of a block with a tumour and needle array inserted are summarized in Table 6.4, where model 1 refers to the model with two electrode pairs at a distance of 3.2 mm (Chapter 6.3.3.7.1), model 2 refers to a distance of 9.6 mm between electrode pairs (Chapter 6.3.3.7.2), model 3 refers to the model with 4 needle pairs with rows at the same potential (Chapter 6.3.3.7.3) and 4 to the model with different potentials among the needle pairs (Chapter 6.3.3.7.4). Model 5 presents the example without constraints on *u* and *i* (Chapter 6.3.3.7.5). Model 6 however presents the model of the brain with a tumour where the optimal EP parameters were applied as obtained on the block geometry. Those were the same parameters as used in model 4. Comparison of the results obtained from model 4 and model 6 shows that substitution of real brain geometry with a block did not significantly deteriorate the E distribution in the tumour.

Table 6.4: Summary of EP parameters, optimisation results and E_i in evaluation points obtained in the model with a block (model 1 to 5) and the model of a brain (model 6).

Model	*f(u,d)*	*u* (V)	*i* (A)	*d*	E_1 (V/cm)	E_2 (V/cm)	E_3 (V/cm)	E_4 (V/cm)	E_5 (V/cm)
1	0.1907	1000.0	15.07	3.2	200.3	173.6	169.3	196.6	138.6
2	0.1921	915.3	15.99	9.6	340.1	267.3	256.0	107.7	130.1
3	0.1869	701.0	16.00	/	276.9	227.5	216.7	128.6	120.8
4	0.1575	*u1*=802.3 *u2*=191.9 *u3*=671.2 *u4*=1000.0	15.99	/	264.8	237.1	275.5	141.7	135.6
5	0.1762	*u1*=1088.2 *u2*=485.7 *u3*=1200.1 *u4*=1880.9	28.70		255.0	313.8	474.7	256.3	255.0
6	0.1586	*u1*=802.3 *u2*=191.9 *u3*=671.2 *u4*=1000.0	15.96	/	311.6	227.8	269.4	148.4	136.9

Figure 6.39 and Figure 6.40 present E distribution and specific conductivity respectively in the last step of the model describing permeabilisation in a brain with a tumour. We can observe that increased E values were concentrated within the tumour which is particularly advantageous because in this manner healthy brain tissue is not exposed to higher E intensities that can cause irreversible brain cell damage.

Further we established that with the particular needle array holder we can not permeabilise the entire volume of the tumour with a single needle array insertion considering the constraints on voltage and current supplied by the Cliniporator. However by employing optimisation we can determine pulse amplitude parameters that can permeabilise the tumour to a great extent. This can consequently decrease the number of needle array insertions and reduce associated tissue damage.

Unfortunately the drawback of the presented model based optimisation is the limited ability to change needle position if the model has a complex geometry. Model based optimisation namely depends on automatic mesh generation. However in a complex geometry, automatic mesh generation can fail or at least require manual tuning of mesh parameters. Therefore the problem of electrode position can be solved only by generating mesh in predefined positions and then optimising the EP parameters across those positions. On the other hand, for simple geometries as presented in Chapter 6.3.2 the electrode distance can be optimised without difficulty.

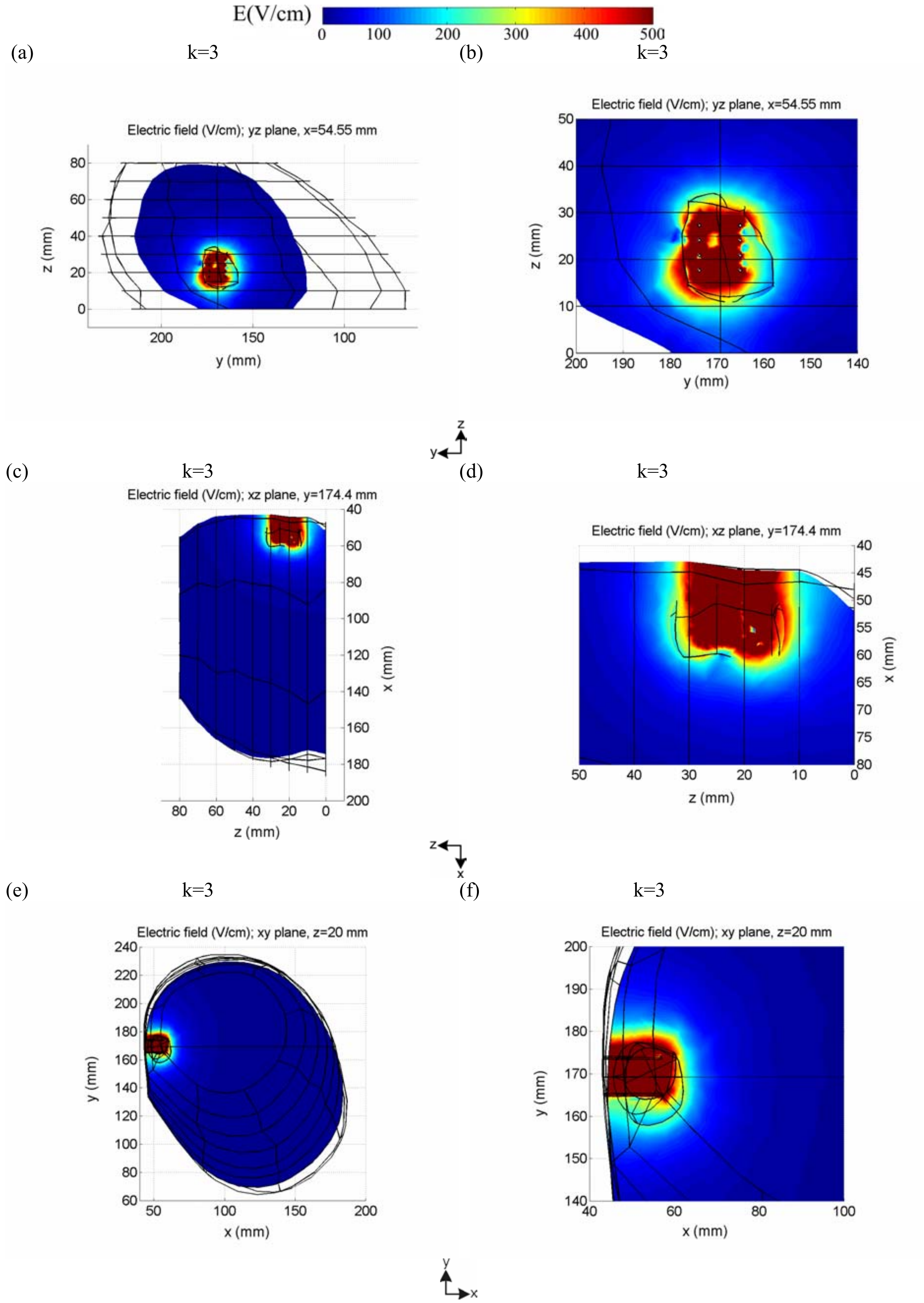

Figure 6.39: E distribution in the brain with a tumour at the end of permeabilisation at applied pulse parameters u_1=802.3 V, u_2=191.9 V, u_3=671.2 V, u_4=1000.0 V. (a) and (b) whole geometry and close up of tumour, respectively in *yz* plane (*x*=54.55 mm); (c) and (d) whole geometry and close up of tumour, respectively in *zx* plane (*y*=174.4 mm); (e) and (f) whole geometry and close up of tumour, respectively in *xy* plane (*z*=20 mm).

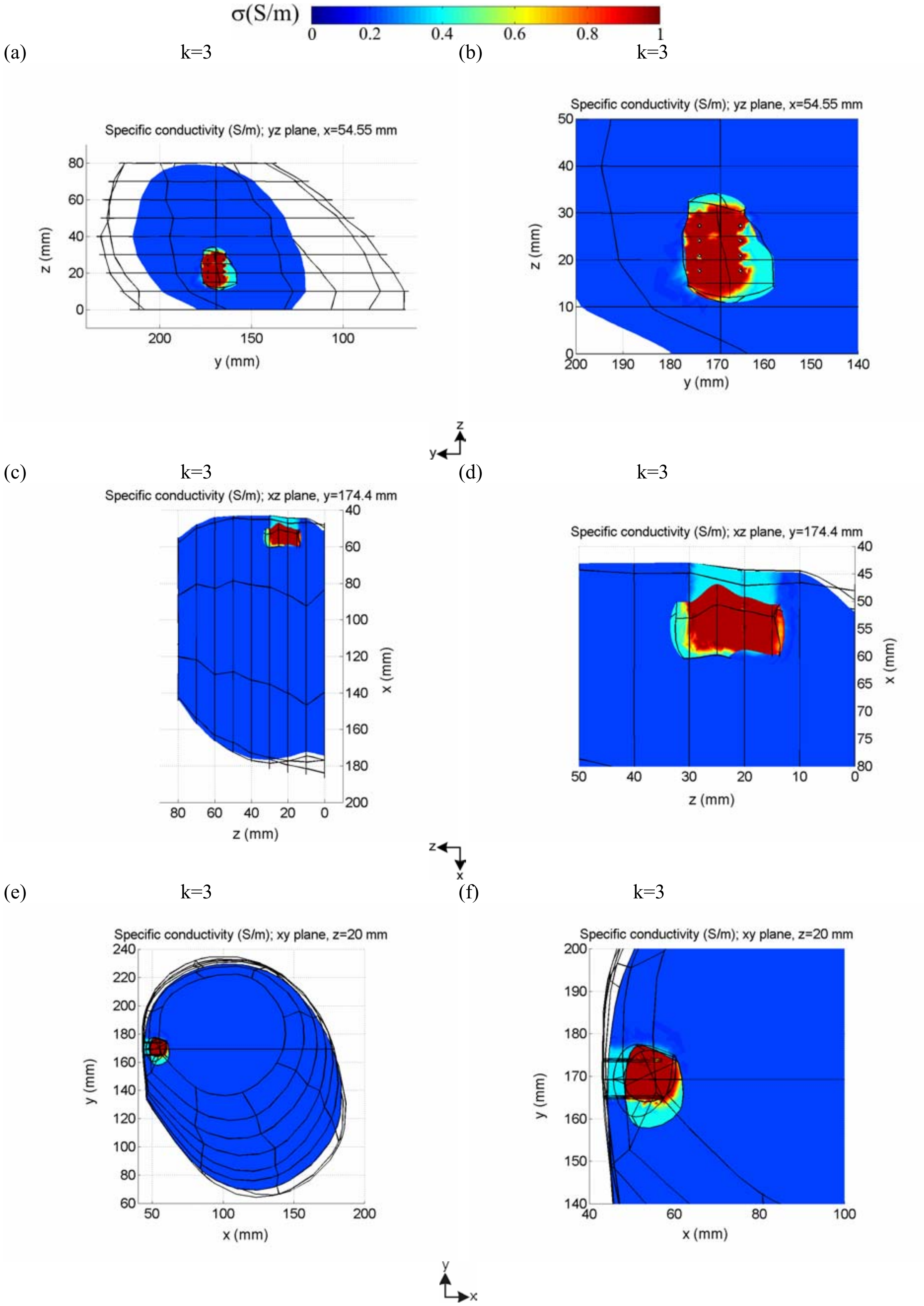

Figure 6.40: Specific conductivity of the brain with a tumour at the end of permeabilisation at applied pulse parameters u_1=802.3 V, u_2=191.9 V, u_3=671.2 V, u_4=1000.0 V. (a) and (b) whole geometry and close up of tumour, respectively in *yz* plane (*x*=54.55 mm); (c) and (d) whole geometry and close up of tumour, respectively in *zx* plane (*y*=174.4 mm); (e) and (f) whole geometry and close up of tumour, respectively in *xy* plane (*z*=20 mm).

6.4 DISCUSSION

The goal of the model based optimisation was to determine optimal EP parameters to be applied for effective electrochemotherapy by minimizing the difference between the reference value E_r and E intensities computed at selected points of the tumour. The value of E_r was selected just above the reversible threshold. Optimisation also considered the technical limitations of the generator and the requirement to have E intensity at selected points of the tumour above reversible threshold, which is needed for effective electrochemotherapy.

The feasibility of model based optimisation of EP parameters was examined first on a simple geometry representing tissue with the tumour placed between two plate electrodes. The parameter subject to optimisation was pulse amplitude. The application of the optimised pulse amplitude yielded E intensity almost equal to the reference value E_r in the selected point of the tumour. As E between plate electrodes is relatively homogeneous compared to other electrode designs, the entire tumour was also exposed to E intensities just above the reversible threshold. From the optimisation point of view this is an excellent result, however for effective electrochemotherapy it depends on determination of E_r. It is evident that the latter should be set above reversible threshold. However as the determination of threshold values depends on the accuracy of measurements and experimental conditions, we recommend a choice of E_r in the middle range between the reversible and irreversible thresholds.

In the next example the pulse amplitude and distance between the electrodes were optimised simultaneously for the geometry representing the tissue with the tumour and two plate electrodes placed on top. In this example E distribution was inhomogeneous, thus the application of optimal parameters resulted in irreversible permeabilisation of the regions of the tumour closer to the electrodes, while distant regions of the tumour were exposed to E intensities just above the reversible threshold. This sufficed for complete tumour permeabilisation, provided E_r was above true reversible threshold. The choice of a higher reference value E_r, as suggested in the previous example, would require a higher pulse amplitude, which could consequently yield a larger volume of irreversibly permeabilised healthy tissue situated just below the electrodes where the highest E intensities are present. Therefore when inhomogeneous E distribution is present the reference value for optimisation should be determined just above the true reversible threshold.

Further, we examined the feasibility of model based optimisation on a model with complex geometry. The model, generated from CT images, represented a human brain with a tumour. For the purpose of electrochemotherapy an array of needle electrodes was inserted in the model. The parameter subject to optimisation was pulse amplitude. The distance between electrode pairs was not optimised due to problems encountered with mesh generation. The first optimisation of EP parameters had no feasible solution. Namely, due to technical limitations of the pulse generator, the E distribution in the tumour could not exceed E_r. Thus in further optimisations we omitted the requirement that E intensity at selected points should exceed E_r as it can not be achieved with this particular pulse generator. Application of optimal pulse parameters obtained in such a way did not expose the entire volume of the tumour to E intensities above reversible threshold, as during optimisation the constraints on voltage or current were reached. Considering the fact that some parts of the tumour were permeabilised while others were not, the treatment should be repeated considering a new position for the electrodes which would permeabilise the areas of the tumour which remained non-permeabilised by the first needle insertion. Despite the fact that with the particular needle array holder and pulse generator we can not permeabilise the entire volume of the tumour with a single needle array insertion, we can determine the pulse amplitude to be delivered to each electrode pair separately in order to permeabilise the tumour to a great extent. This can consequently decrease the number of needle array insertions and reduce associated tissue damage.

Also, if the needle electrode holder enables switching between electrode pairs, the current constraint would probably not prevent permeabilisation of the total volume of tissue by optimised pulse amplitudes.

The purpose of the presented feasibility study was to examine the advantages and disadvantages of model based optimisation, which are listed in continuation, as well as to identify possible limitations of the approach.

The most important contribution of model based optimisation of EP parameters is the determination of optimal parameters in a non-invasive way before the treatment. The optimal parameters are also best suited to the treatment of the particular tissue with respect to its geometry and electrical properties.

Further, the optimisation enables the determination of optimal pulse amplitude to each electrode pair separately, as well as it could be used for determination of optimal potentials to be applied to 3D electrodes.

Another advantage of the approach is the information about the efficacy of permeabilisation i.e. information about whether the entire volume of the tumour was permeabilised. The latter is derived from the E distribution computed by the model. This information is extremely valuable when for example a tumour of irregular shape is treated with needle electrodes, which produce an inhomogeneous E. In such a case the use of a model providing the spatial distribution of E is of great importance.

The spatial distribution of E also provides information about the possible damage to healthy tissue when exposed to a particular electrical treatment. Based on this a decision can be made whether to permeabilise a larger area of tissue by applying higher pulse amplitudes or to reposition the electrodes and carry out the treatment under lower pulse amplitudes. The requirement that E intensity should not be exceeded in healthy tissue can also be taken into account within the optimisation procedure as a nonlinear constraint.

For model based optimisation a permeabilisation model is required. Thus the availability of an accurate model could be the major limitation to this approach. The accuracy of the presented time discrete permeabilisation model depends predominantly on the quality of the 3D geometry and determination of $\sigma(E)$ dependency. The former can be generated from CT or MRI images if available. The latter should be defined by means of experiments for each type of tissue separately.

Another important limitation is optimisation of the distance between electrodes when tissue geometry is complex. Each change in model geometry, for example a change in the distance between electrodes, requires new mesh generation. When optimising the distance between electrodes several mesh generations are thus required. However in complex geometries the automatic mesh generation can fail if initial mesh parameters are not manually tuned. To overcome this problem in complex geometries, electrode position and mesh generation should be prepared in advance. Then the discrete values of distances between the electrodes can be optimised together with pulse amplitude by employing a tree search algorithm, for example. In the case of simple geometries we did not encounter any problems when optimising the distance between electrodes.

In general, the definition of the optimisation problem in electrochemotherapy should take into consideration the technical limitations of the generator (maximum voltage, current), constraints on electrode dimensions, and the requirement that E intensity should be higher than the reversible threshold in the entire tumour. However in some cases a feasible solution to such a problem does not exist. In such cases the definition of constraints should be redesigned by taking into account only the technical limitations of the generator and electrode dimensions, while the rest of the requirements for desired E intensity could be met by repositioning the electrodes and repetition of the treatment.

Balancing the above considerations we can conclude that model based optimisation can be successfully used as a means of determining EP parameters for effective electrochemotherapy, provided an accurate model of permeabilisation is available. However in some cases the effectiveness may be limited due to the dimensions of subject tissue, limitations of the pulse generator, and electrode dimensions.

The applicability of this approach should be further verified with experimental data. The volume of permeabilised tissue after permeabilisation with optimal pulse amplitude could, for example, be validated by electric impedance tomography which should provide information about conductivity in tissue after permeabilisation.

Finally it has to be emphasised that the use of model based optimisation could be advantageous for electrogenetransfer, where optimal pulse amplitude should be determined very precisely in order to have E intensities distributed between reversible and irreversible thresholds.

7 CONCLUSION

In clinical applications of electropermeabilisation, exposure of the desired volume of tissue to E intensities which correspond to a particular therapeutic approach is crucial for therapeutic effectiveness. For example, in electrochemotherapy the entire volume of the tumour must be exposed to E intensities above reversible threshold. In this way entrance of chemotherapeutic drugs into each tumour cell is enabled. Similarly, in electrogenetransfer the whole targeted volume of tissue must be exposed to E intensities above reversible threshold to permeabilise the cell membrane but E intensities must be lower than irreversible E threshold. As soon as a cell membrane is permeabilised, E distribution in tissue can be decreased, however it should remain high enough to maintain electrophoretic transport of DNA across the permeabilised cell membrane. Electric field distribution is thus the governing factor determining the effectiveness of a particular therapeutic approach. As E distribution in tissue can be controlled by the applied pulse amplitude and distance between the electrodes, the determination of the two is referred to as the optimization problem in electropermeabilisation. Up to now, optimization of the pulse amplitude and electrode position was based on the results of experimental tests. An alternative method for determining EP parameters could be model based optimization. In such a case the model should describe E distribution in tissue due to permeabilisation.

Consequently, in this work, a time discrete model of tissue permeabilisation was developed which describes E distribution in tissue at discrete time steps during pulse application. According to the given $\sigma(E)$ dependency and E distribution, the tissue specific conductivity is altered, and subsequently used for computation of E distribution in the following time discrete step. Electric field distribution of a given geometry with given tissue electrical properties can be computed either analytically or numerically depending on the complexity of the geometry and electrode design.

An analytical approach was used to model E distribution in tissue placed between the two concentric cylindrical electrodes presented in Chapter 3. The geometry provided similar E distribution to that present around two needle electrodes of the type used for treatment of deeply seated tissue in clinics. As an analytical solution is not time consuming, the model was incorporated into a simulation environment aimed at testing the impact of different functional dependencies $\sigma(E)$ and pulse amplitudes as well as electrode distances on the course of permeabilisation. The impact of $\sigma(E)$ dependency was found to be important, thus an approach for its determination was proposed which combines experiments and the model of E distribution. Additionally, the shape of input signal was also found to influence the extent of permeabilisation. Namely, the application of a ramp signal with the same mean amplitude as that of the rectangular signal resulted in a larger radius of permeabilisation.

Also, based on the analytical model, feasibility of real time permeabilisation control by means of a closed loop control algorithm was investigated. Despite the fact that real time control was feasible, some problems related to *in vivo* control were anticipated: such as the problem of tuning controller parameters and the problem of on-line measurement of the extent of tissue permeabilisation. The only possible approach towards a solution to both problems would be model based control, which utilises a model that is capable of real time simulation of the extent of permeabilisation, such as the time discrete model presented in Chapter 3.

Further, comparison of the results obtained by analytical and numerical models for the same geometry of two concentric cylindrical electrodes showed that both methods can be used equivalently, however in the case of the numerical method, the time spent solving the model was significantly longer. Thus the latter method can not be used for real time permeabilisation control.

In Chapter 4 a method of modelling needle electrodes in the finite element model, which accelerated the solution process was proposed and evaluated using measurements on a phantom tissue. Based on the results of a criteria function, 8 faceted needle electrodes were proposed as a substitute for cylindrical ones. The results showed that such a simplification could be used without serious impact on model results. The model's relative difference in total current, which was evaluated during model validation on measurements, was 9% for gel thickness of 4 mm. This difference was not due to the approximation of needles with faceted shape nor could it be explained by geometrical inaccuracies (gel thickness, tip modelling, and inter electrode distance) between the model and the real system. The bias was due to non-ohmic low voltage behaviour. Incorporation of this effect in the model decreased the relative difference between modelled and measured current to 3% for gel thickness of 4 mm.

Current measurement was also examined as a means of finite element model validation. Provided the model geometry and material properties are known and properly modelled, a finite element model producing current results which correspond to measured results could be used for at least rough estimation of E distribution in tissue.

In Chapter 5 time a time discrete model of tissue permeabilisation in rabbit liver tissue with inserted needle electrodes was validated on experimental data. Electric field distribution in the model was described numerically – with a finite element method. Parameter estimation of S-shaped $\sigma(E)$ dependency was performed by means of experimental current results. Estimated electric field thresholds were: 460 V/cm for reversible and 700 V/cm for irreversible threshold. The obtained thresholds appear to be higher than those published in [Miklavčič *et al.*, 2000]. The reason for the difference was that previous values were determined on E distribution of non-permeabilised tissue thus the increase in conductivity due to membrane permeabilisation was not taken into account. As the new thresholds are higher, the induced TMP consequently calculated is also higher than previously published. The obtained value of induced TMP is still well within the range of values reported in literature.

The time discrete model was validated on experimental data by comparing total currents with the areas of reversibly and irreversibly permeabilised tissue. Model validation showed good agreement between the model results and experiments. Validation of the time discrete model on experimental data also lead to several hypotheses aimed at explaining the processes that occur during permeabilisation.

Based on the modelling results we assumed the presence of at least two different transport mechanisms during permeabilisation, i.e. electrophoretic transport of ions, which is reflected in a fast change of tissue conductivity and the slow transport of small molecules such as bleomycin by diffusion, which takes place predominantly subsequent to pulse application. Both transports are presumably initiated at the same threshold value, due to the fact that they depend on cell membrane permeabilisation, however their dynamics are different. Electrophoretic ion transport is facilitated by a large number of transient permeation structures that reseal after pulse application. Transport of molecules by diffusion is enabled however through long lived stable pores which are formed on the basis of transient permeation structures. As the transient permeation structures are formed very quickly - immediately after the pulse application and due to the fact that ion transport is very fast, the consequent change in tissue conductivity causes further rapid changes in E distribution and propagation of permeabilisation. At the end of permeabilisation propagation, the decreased distribution of E intensities in permeabilised tissue is found than at the beginning of the pulse application. The system behaves as if it had a specific negative feedback, preserving cells from irreversible damage [Abidor *et al.*, 1993]. We presume that after propagation of permeabilisation is terminated it is only steady E distribution which influences the origination of long lived stable pores, enabling transport of small molecules across the cell membrane.

Model based simulation also revealed that fast dynamic changes of E intensity during tissue permeabilisation influence the change in tissue conductivity. However, even if these are higher than irreversible threshold they do not necessarily cause cell necrosis. Only when steady E intensities are present for a certain period of pulse length and if they are higher than irreversible threshold, they can cause cell necrosis.

In measured current, a moderate increase was observed after the rise time, which was not predicted by the time discrete model. It was assumed that tissue heating might have increased the tissue conductivity and consequently the measured current. This implied that $\sigma(E)$ dependency should also incorporate the influence of temperature T.

The validated time discrete permeabilisation model can be used for simulation of the permeabilisation process. This is very important in clinics where electrode set-up and electrode parameters (amplitude only) should be known before treatment is performed in order to achieve effective permeabilisation of a specific tissue volume.

Thus in Chapter 6 the feasibility of model based optimisation of EP parameters for application in electrochemotherapy was investigated. The model geometry was generated from CT images of a human brain with a tumour. An array of needle electrodes was used for electrical treatment. Model based optimisation revealed that such an approach could be used for determination of optimal EP parameters. It was also revealed that the efficacy of optimisation depends on the limitations of the pulse generator. Namely, in the particular geometry, complete tumour permeabilisation was not achieved by a single needle insertion when using the Cliniporator pulse generator.

In summary, based on the above results and considerations, the validated model of tissue permeabilisation can be used for the simulation of tissue permeabilisation. It can provide information about the extent of permeabilisation at different pulse amplitudes and different electrode designs. Simulation of the permeabilisation process by a time discrete model can also show which parts of tissue are going to be exposed to pre-required E intensities at particular pulse amplitudes and electrode designs as well as indicate possible damage to healthy tissue.

The model can also provide information about the total current for different needle electrode geometries, pulse amplitudes and given tissue properties (geometry, conductivity). Based on computed current and considering E distribution, the maximal current can be determined and preset in the pulse generator in order to protect tissue against damage. Maximal current and required voltage for effective tissue electropermeabilisation for a given electrode geometry are also important in designing generator power supply and capacity.

It has to be emphasized however that effective use of a time discrete model of tissue permeabilisation requires accurate determination of $\sigma(E)$ dependency, which can be obtained only by means of experiments.

A time discrete model of tissue permeabilisation can also contribute to the effectiveness of electrochemotherapy and electrogenetransfer as it can be used for optimisation of EP parameters that are suitable to the particular treatment. In electrogenetransfer such information is of great importance as E intensities in the tissue under treatment should be in a narrow range between the reversible and irreversible threshold. The important contribution of model based optimisation is that it provides determination of optimal parameters in a non-invasive way before the treatment.

REFERENCES

Abidor I. G., Arakelyan V. B., Chernomordik L. V., Chizmadzev Y. A., Pastushenko V. F., Tarasevich M. R., "Electric Breakdown of Biayer Lipid Membranes. I. The main experimental Facts and Their Quantitative Discussion", *Bioelectrochemistry and Bioenergetics*, vol. 6, pp. 37-52, 1979.

Abidor I. G., Barbul A. I., Zhelav D. V., Doinov P., Bandrina I. N., Osipva E. M., Sukharev S. I., "Electrical properties of cell pellets and cell elctrofusion in a cntrifuge", *Biochimica et Biophysica Acta*, 1152, pp. 207-218, 1993.

Aihara H., Miyazaki J., “Gene transfer into muscle by electroporation in vivo,” *Nature Biotechnology*, vol. 16, pp. 867-870, 1998.

Barber D. C., Brown B. H., “Applied potential tomography”, *J. Phys. E.: Sci. Intsrum.*, vol. 17, pp. 723-733, 1984.

Belehradek J., Orlowski S., Poddevin B., Paoletti C., Mir L. M., "Electrochemotherapy of spontaneous mammary tumors in mice", *European Journal of Cancer*, vol. 27, no. 1, pp. 73-76, 1991.

Belehradek J., Orlowski S., Ramirez L. H., Pron B. Poddevin C., Mir L. M., "Electropermeabilisation of cells in tissue assessed by the qualitative and quantitative electroloading of bleomicyn ", *Biochim. Biophya. Acta*, 1990, pp. 155-163, 1994.

Braess, D., “Finite Elements Theory: fast solvers, and applications in solid mechanics”, Cambridge University Press, 1997.

Brandisnky K., Daskalov I, "Electric field and current distributions in electrochemotherapy",. *Biochemistry and Bioenergetics*, vol. 48, pp. 201-208, 1999.

Breeuwer M., Zylka W., Wadley J., “Detection and correction of geometric distortion in 3D CT/MR images”, *Paper CARS’99*, Paris, France, 1999.

Chandrupatla T. R., Belegundu A. D., “Introduction to Finite Elements in Engineering”, Prentice Hall, New Jersey, 1997.

Chang D. C., Reese T. S., "Changes in membrane structure induced by electroporation as revealed by rapid freezing electron microscopy", *Biophysical Journal*, vol. 58, pp. 1-12, 1990.

Chernomordik L. V., Sukarev S. I., Abidor, I. G., Chizmadzev Y. A., "The study of the BLM reversible electrical breakdown mechanisms in the presence of UO_2^{2+}", *Bioelectrochem. Bioenerg.*, vol. 9, pp. 149-155, 1982.

Chernomordik L. V., Sukarev S. I., Popov S. V., Pastushenko V. F., Sokirko A. V., Abidor I. G., Chizmadzev Y. A., "The electrical breakdown of cell and lipid membranes: the similarity of phenomenologies", *Biochimica et Biophysica Acta*, vol. 902, pp. 360-373, 1987.

Chizmadzhev Y. A., Cohen,F. S., Shcherbakov,A., Zimmerberg J., "Membranes mechanics Can Account for Fusion Pore Dilation in Stages", *Biophysical journal*. vol. 69, pp. 2489-2500, 1995.

Coburn B., "Electrical stimulation of the spinal cord: two dimensional finite element anlysis with particular reference to epidural electrodes", *Med. Biol. Eng. Comp*., vol. 18, pp 573, 1980.

Crowley J. M., "Electricalbreakdown of bimolecular lipid membranes as an electrochemical instability", *Biophysical Journal*, vol. 13, pp. 711-724, 1973.

Dakin R. J., "A tree-search algorithm for mixed integer programming problems", *Computer journal*, vol. 8, pp. 250-255, 1965.

Davalos R., Huang Y., Rubinsky B., "Electroporation: Bio-electrochemical mass transfer at the nano scale," *Microscale Theromophys. Eng.*, 4, pp. 147-159, 2000.

Davalos R., Rubinsky B., Otten D. M., "A feasibility study for Electrical Impedance Tomography as a Means to Monitor Tissue Electroporation for Molecular Medicine", *IEEE Tr. Biomed. Eng.*, 49, pp. 400-403, 2002.

Dev S.B., Dhar D., Krassowska W., "Electric Field of a Six-Needle Array Electrode Used in Drug and Gene Delivery in Vivo: Analytical Versus Numerical Solution", *IEEE Tr. Biomed. Engng*., accepted.

Duck F. A., Physical Properties of Tissue: A Comprehensive Reference Book, Academic Press, 1990.

Duliu O. G., "Computer axial tomography in geosciences: an overview", *Earth-Science Reviews*, vol. 48, pp. 265-281, 1999.

Durney C. H., "Electromagnetic dosimetry for models of humans and animals: A review of theoretical and numerical techniques"*, Proc. of IEEE*, vol. 68, pp.33-40, 1980.

EMAS Version 4 User's Manual, Brauer, J. R., and Brown, B. S. eds., Ansoft Corporation, USA, 1997.

Faes T. J., Van der Meij H. A., De Munck J. C., Heethaar R. M., "The electrical resistivity of human tissues (100 Hz-10 MHz): a meta-analysis of review studies", *Physiol. Meas*., vol. 20, pp. R1-R10, 1999.

FEMLAB User Guide and Introduction v. 2.2, Comsol AB., Sweden, 2001.

Ferber D.: "Gene Therapy: Safer and Virus-Free?", *Science*, vol. 294, pp. 1638-1642, 2001.

Fletcher R., Leyffer S., "Solving mixed integer nonlinear programs by outer approximation", *Mathematical Programming*, vol. 66, pp. 327-349, 1994.

Friedlander M. P., "A globally convergent linearly constrained method for nonlinear optimization", Ph.D. thesis, Stanford University, USA, 2002.

Gabriel B., Teissie J., "Direct observation in the milisecond time range of fluorescent molecule asymetrical interaction with the electropermeabilized cell membrane", *Biophysical Journal*, vol. 73, no. 5, pp. 2630-2637, 1997.

Gabriel B., Teissie, J., "Time courses of mammalian cell electropermeabilization observed by milisecond imaging of membrane property changes during the pulse", *Biophysical Journal*, vol. 76, no. 4, pp. 2158-2165, 1999.

Geddes L. A., Baker L. E., “The specific resistance of biological material – a compendium of data for the biomedical engineer and physiologist”, *Med. & Biol. Engng*., vol. 5, pp. 271-293, 1967.

Gehl J., Mir L. M., "Determination of optimal parameters for in vivo gene transfer by electroporation, using a rapid in vivo test for cell permeabilisation", *Biochemical and Biophysical Research Communications*, vol. 261, pp. 377-380, 1999.

Gehl J., Sorensen T. H., Nielsen K., Raskmark P., Nielsen S. L., Skovsgaard T., Mir L. M., "In vivo electroporation of skeletal muscle: threshold, efficacy and relation to electric field distribution", *Biochimica et Biophysica Acta*, vol. 1428, pp. 233-240, 1999.

Gehl J., "Electroporation: theory and methods, perspectives for drug delivery, gene therapy and research", *Acta Physiol Scand*, vol. 177, pp. 437-447, 2003.

Gilbert R. A., Jaroszeski M. J., Heller R., "Novel Electrode Design for Electrochemotherapy", *Biochimica et Biophysica Acta*, no. 1334, pp. 9-14, 1997.

Goodwin T., Tan A.., Clinically Applied Neuro Science - Computer assisted learning program, http://pbl1.medfac.unimelb.edu.au/CANs/mainmap.htm, 2003.

Gowrishankar T. R., Weaver J. C., “An approach to electrical modeling of single and multiple cells,” *Proc. Natl. Acad. Sci.*, vol. 100, pp. 3203-3208, 2003.

Grosz L., Roll C., Schonauer W., A black box solver for the solution of the general nonlinear functional eaquations by Mixed FEM, In: Finite Element Methods, Fifty years of the Courant Element, Krizek M., Neittaanmaki P., Stenberg R., eds., M. Dekker, pp. 225-234, 1994.

Hagemann G. A., Cummins R., “Computed Tomography and Nuclear Magnetic Resonance with Mathematical Applications”, Yale-New Haven Teacher Institute, 1983.

Heller R., Jaroszeski M. J., Reintgen D. S., Puleo C. A., DeConti R. C., Gilbert R., Glass L. F., "Treatment of cutaneous and subcutaneus tumors with electrochemotherapy using intralesional bleomycin", *Cancer*, vol. 83, pp. 148-157, 1998.

Heller R., Gilbert R., Jaroszeski M. J., "Clinical applications of electrochemotherapy", *Advanced Drug Delivery Reviews*, vol. 35, pp. 119-129, 1999.

Hennenberg K., Plonsey R., “Boundary element analysis of the directional sensitivity of the concentric emg electrode”, *IEEE Trans. on Biomed.. Engng*., vol. 40, pp 621-631, 1993.

Heringa A., Stegeman D. F., Uijen G. J. H., Weerd J. P. C., “Solution Methods of Electrical Field Problems in Physiology”, *IEEE Trans. Biomed. Engng.,* vol. 29, pp. 34-42, 1982.

Hibino M., Shigemori M., Hiroyasu I., Nagayama K., Kinosita, K., "Membrane conductance of an electroporated cell anlyzed by submicrosecond imaging of transmembrane potential", *Biophysical Journal*, vol. 59, pp. 209-220, 1991.

Hibino M., Itoh H., Kinosita K., "Time courses of cell electroporation as revealed by submicrosecond imaging transmembrane potential", *Biophysical Journal*, vol. 64, pp. 1789-1800, 1993.

Hofmann G.A.: Instrumentation and Electrodes for in Vivo Electroporation. In: *Methods in Molecular Medicine*. Vol. 37, Ch. 2, pp. 37-61, M. Jaroszeski, R. Heller, and R. Gilbert eds., Humana Press, Inc., Totowa, NJ, 2000.

Image processing Toolbox for Use with Matlab, *MathWorks Incorporation*, USA, 2002.

Isermann R., Lachmann K. H., Matko D., “Adaptive Control Systems”, Prentice-Hall, Inc. Engelwood Cliffs, NJ, 1992.

Jaroszeski M. J., Gilbert R., Nicolau C., Heller R., "In vivo gene delivery by electroporation", *Advanced Drug Delivery Reviews*, vol. 35, pp. 131-137, 1999.

Johnson C. R., “Numerical Methods for Bioelectric Field Problems”, *Biomedical Engineering Handbook*, Bronzion, J.D., editor, CRC Press, 1994.

Johnson C. R., “Computational and Numerical Methods for Bioelectric Field Problems”, *Critical reviews in Biomedical Engineering*, 1997.

Kak A. C., Slaney M., “Principles of Computerized Tomographic Imaging”, IEEE Press, eds. Cotellessa, Aggarwal, Wade, 1988.

Kim D. W., Bakker L.E., Pearce J.A., Kim,W.K., “Origins of impedance change in impedance cardiography by three –dimensional finite element model”, *IEE Trans. Biomed. Engng.*, vol. 35 pp.993, 1998.

Kinosita K., Tsong, T. Y., "Volage - induced pore formation and hemolysis of human erytrocytes", *Biochimica et Biophysica Acta*, vol. 471, pp. 227-242, 1977.

Kinosita K., Tsong T. Y., "Formation and resealing of pores of controlled size in human erythrocyte membrane", *Nature*, vol. 268, pp. 438-440,1977a.

Kinosita K., Tsong T. Y., "Voltage Induced conductance in human erythrocyte membranes", *Biochimica et Biophysica Acta*, vol. 554, pp. 479-497, 1979.

Klepfer R. N., Johnson C. R., Macelod R. S., “The effects of inhomogeneties and anisotropies on electrocardiographic fields: a 3-D finite element study”, *IEEE Trans. Biomed. Engng.*, vol. 44, pp. 706-719, 1997.

Kotnik T., Miklavčič D., “Analytical Description of Transmembrane Voltage Induced by Electric Field on Spheroidal Cells,” *Biophysical Journal*. Vol. 79, pp. 670-679, 2000.

Kotnik T., "Influence de la dynamique du champ electrique sur l’efficacite d l’electropermeabilisation de la membrane cellulaire", Ph.D. thesis, Faculte de medicinie Paris-Sud, Universite Paris XI, 2000.

Kubota Y., Mir L. M., Nakada I., Sasagawa H., Suzuki H., Aoyama N., "Successful treatment of metastatic skin lesions from bladder cancer by electrochmotherapy*”, J. Urol.*, 160, pp. 1426, 1998.

Loste F., Eynard N., Teissie J. “Direct Monitoring of the field strength during electropulsation,” *Bioelectrochem. Bioenerg*., vol. 47, pp. 119-127, 1998.

Maček-Lebar A., Serša G., Čemažar M., Miklavčič D., "Elektroporacija", *Medicinski Razgledi*, vol. 37, pp. 339-354, 1998.

Maček-Lebar A.: Vpliv električnih parametrov na elektroporacijo plazmaleme v in vitro pogojih*: Doktorska disertacija*. Fakulteta za elektrotehniko, Univerza v Ljubljani, 1999.

Maček-Lebar A., Serša G., Kranjc S., Grošelj A., Miklavčič D.., “Optimization of pulse parameters *in vitro* for *in vivo* electrochemotherapy”, *Anitcancer research*, vol. 22, pp.1731-1736, 2002.

Marrink S. J., Lindahl E., Edholm O., Mark A. E., “Simulation of the Spontaneous Aggregation of Phospolipids into Bilayers,” *J. Am. Chem. Soc*., 123, pp. 8638-8639, 2001.

Miklavčič D., Beravs K., Šemrov D., Čemazar M., DemŠar F., Serša G., "The importance of electric field distribution for effective in vivo electroporation of tissues", *Biophysical Journal*, vol. 74, pp. 2152-2158, 1998.

Miklavčič D., Šemrov D., Mekid H., Mir L. M., “A validated model of in vivo electric field distribution in tissue for electrochemotherapy and for DNA electrotransfer for gene therapy,” *Biochim. Biophys. Acta*, 1523, pp. 73-83, 2000.

Mir L. M., Banoun H., Paoletti C., "Introduction of definite amounts of nonpermeant molecules into living cells after electropermeabilization: Direct access to the cytosol", *Experimental Cell Reseach*, vol. 175, pp. 15-25, 1988.

Mir L. M., Orlowski S., Belehradek J., Paoletti C., "Elecrochemotherapy potentiation of antitumor effect of bleomycin by local electric pulses", *European Journal of Cancer*, vol. 27, no. 1, pp. 68-72, 1991.

Mir L. M., Orlowski S., Belehradek J. Jr., Teissié J., Rols M. P., Serša G., Miklavčič D., Gilbert R., Heller R., "Biomedical applications of electric pulses with special emphasis on antitumor electrochemotherapy", *Bioelectrochemistry and Bioenergetics*, vol. 38, pp. 203-207, 1995.

Mir L. M., Devauchelle P., Quintin-Colonna F., Delisle F., Doliger S., Fradelizi D., Belehradek J., Orlowski S., "First clinical trial of cat soft - tissue sarcomas treatment by electrochemotherapy", *British Journal o Cancer*, 1997.

Mir L. M., Glass L. F., Serša G., Teissie J., Domenge C., Miklavčič D., Jaroszeski M. J., Orlowski S., Reintgen D. S., Rudolf Z., Belehradek J., Bachaud J. M., DeConi R., Štabuc, B., Čemazar M., Coninx P., Heller R., "Effective treatment of cutaneos and subcutaneous malignant tumors by electrochemotherapy", *British Journal of Cancer*, vol. 77, no. 12, pp. 2336-2342, 1998.

Mir L. M., Orlowski S., "Mechanisms of electrochemotherapy", *Advanced Drug Delivery Reviews*, vol. 35, pp. 107-118, 1999.

Mir L. M., Bureau M. F., Gehl J., Rangara ,Rouy D., Caillaud J.M., Delaere P., Branellec D., Schwartz B., Scherman D., “High-efficieny gene transfer into skeletal muscle mediated by electric pulses,” *Proc. Natl. Acad. Sci.*, vol. 96, pp. 4262-4267, 1999.

Mir L. M., "Therapeutical perspectives of in vivo cell electropermeabilization", *Bioelectrochemistry*, vol. 53, pp. 1-10, 2000.

Mirotznik M. S., Prather D., "How to choose EM software", *IEEE Spectrum*, pp. 53-58, 1997.

Murray-Smith D.J., "Advances in Simulation Model Validation: Theory, Software and Applications", *EUROSIM'95*, pp. 75-84, 1995.

Neamtu S., Morariu V. V., Turcu I., Popescu A. H., Copasecu L. I., "Pore resealing inactivation in electroporated erythrocyte membrane irradiated with electrons", *Bioelectrochemistry and Bioenergetics*, vol. 48, pp. 441-445, 1999.

Nenonen J.T, "Solving the Inverse Problem in Magnetocardiography," *IEEE Engng. Med. Biol.*, vol. 13, pp. 487-496, 1994.

Neumann E., Schaafer-Ridder M., Wang Y., Hofschneider P. H., "Gene transfer into mouse lyoma cells by electroporation in high electric fields", *The EMBO Journal*, vol. 1, no. 7, pp. 841-845, 1982.

Neumann E., "Membrane electroporation and direct gene transfer", *Bioelectrochemistry and Bioenergetics*, vol. 28, pp. 247-267, 1992.

Neumann E., Kakorin S., "Electrooptics of membrane electroporation and vescle shape deformation", *Current Opinion in Coloid and Interface Science*, vol. 1, pp. 790-799, 1996.

Neumann E., S. Kakorin, Toensing K., "Fundamentals of electroporative delivery of drugs and genes," *Biochim. Biophys. Acta,* 48, pp. 3-16, 1999.

Nishi T., Yoshizato K., Yamashiro S., Takeshima H., Sato K., Hamada K., Kitamura I., Yoshimura T., Saya H., Kuratsu J., Ushio Y., "High - efficiency in vivo gene transfer using intraarterial plasmid DNA injection following in vivo electroporation", *Cancer Research*, vol. 56, pp. 1050-1055, 1996.

Okino M., Mohri, H., "Effects of high - voltage electrcal impulse and an anticancer drug on in vivo growing tumors", *Japanise Journal of Cancer Research*, vol. 78, pp. 1319-1321, 1987.

Optimization Toolbox for Use with Matlab, Coleman T., Branch M. A., Grace A., eds., *MathWorks Incorporation*, USA, 1999.

Panje W. R., Harrell E., Hier M. P., Goldman A., Garman G. R., Bloch I., "Electroporation therapy of head and neck cancer", *Ann.Otol.Rhinol.Laryngol.*, vol. 107, pp. 779-785, 1998.

Pavlin M.: Vpliv gostote in ureditve celic v suspenziji na vsiljeno transmembransko napetost in efektivno prevodnost. *M.Sc. Thesis*. Faculty of electrical engineering. University of Ljubljana. 2001.

Pavlin M., Pavšelj N., Miklavčič D., "Dependence of Induced Transmembrane Potential on Cell Density, Arrangement, and Cell Position Iniside a Cell System", *IEEE Transaction on Biomedical Engineering*, vol. 49, no. 6, pp. 605-612, 2002.

Pavlin M., Miklavčič, D., "Conductivity of a Suspension of Permeabilised Cells – a Theoretical Analysis," *Biophys. J.*., vol. 85, 2003.

Pavšelj N., "Porazdelitev električne poljske jakosti pred in po elektroporaciji celice", M.Sc. Thesis, Faculty of electrical Engineering, University of Ljubljana, Slovenia, 2002.

Peters M. J., De Munck J. C., “The influence of model parameters on the inverse solution based on megs and eegs”, *Acta Otolaryngol*, 491,pp.61-69, 1991.

Pliquett U., Gift E. A., Weaver J. C., “Determination of the electric field and anomalous heating caused by exponential pulses with aluminum electrodes in electroporation experiments,” *Bioelectrochem. Bioenerg.*, vol. 39, pp. 39-53, 1996.

Plonsey R., “Quantitative formulations of electrophysiological sources of potential field in volume conductors,” *IEEE Tr. Biomed. Engng.*, 31, pp. 868-872, 1984.

Plonsey R., Heppner, D. B., “Considerations of quasistationarity in electrophysiological systems”, *Bull. Math. Biphys*., vol. 29, pp. 657-664, 1967.

Plonsey R. ,”Bioelectric Phenomena,” New York: Mcgraw Hill, 1969.

Polstyanko S. , Lee, J.-F., “Fast Schwartz-Type Finite Element Electrostatic Solver,” *IEEE Tr. Magn*., vol. 37, pp. 3469-3473, 2001.

Prausnitz M. R., Corbett J. D., Gimm J. A., Golan D. E., Langer R., Weaver J. C., "Millisecond measurment of transport during and after an electroporation pulse", *Biophysical Journal*, vol. 68, pp. 1864-1870, 1995.

Prelog E., Metoda končnih elementov, Založila Univerza v Ljubljani, Fakulteta za arhitekturo, gradbeništvo in geodezijo, Ljubljana, Slovenia, 1975.

Puc M., Flisar K., Reberšek,S., Miklavcic D., "Electroporator for in vitro cell permeabilization", *Radiology and Oncology*, vol. 35, no. 3, pp. 203-207, 2001.

Puc M., Kotnik T., Mir L. M., Miklavčič D., “Quantitative model of small molecules uptake after *in vitro* cell electropermeabilisation,” *Bioelectrochemistry*, vol. 60, pp.1-10, 2003.

Pucihar G, Kotnik T, Kandušer M, Miklavčič D., "The influence of medium conductivity on electropermeabilization and survival of cells in vitro", *Bioelectrochemistry,* 54, pp. 107-115, 2001.

Ramirez L. H., Orlowski, S., An D., Bindoula G., Dzodic R., Ardouin P., Bognel C., Belehradek J., Munck J.-N., "Electrochemotherapy on liver tumours in rabbits", *British Journal of Cancer*, vol. 77, no. 12, pp. 2104-2111, 1998.

Reddinger W., CT Instrumentation & Physics, OutSource, Inc, USA, 1997.

Reddinger W., CT Image Quality, OutSource, Inc, USA, 1998.

Rols M. P., Teissie J., "Ionic - strength modulation of electrically induced permeabilization and associates fusion of mammalian cells", *European Journal of Biochemistry*, vol. 179, pp. 109-115, 1989.

Rols M. P., Teissie J., "Electropermeabilization of mammalian cells. quantitative analysis of the phenomenon", Biophysical Journal, vol. 58, pp. 1089-1098, 1990.

Rols M. P., Teissie J., "The time course of electropermeabilization," in *Electricity and magnetism in biology and medicine*, M. Blank, ed., pp. 151-154, 1993.

Rols M. P., Teissie J., "Electropermeabilization of mammalian cells to macromolecules: Control by pulse duration", *Biophysical Journal*, vol. 75, pp. 1415-1423, 1998.

Rols M. P., Delteil C., Golzio M., Dumond P., Cros S., Teissie J., "In vivo electrically mediated protein and gene transfer in murine melanoma", *Nature Biotechnology*, vol. 16, pp. 168-171, 1998.

Rush S., Abildskov J. A., McFee R., "Resistivity of body tissue at low frequency", *Circulation Reasearch*, vol. XII, pp. 40-50, 1963.

Satkauskas S., Breau M., Puc M., Mahfoudi A., Scherman D., Miklavčič D., Mir L. M., "Mechanisms of in vitro DNA electrotransfer: Respective contributions of cell electropermeabilization and DNA electrophoresis", *Molecular Therapy*, vol. 5, no. 2, pp. 1-8, 2002.

Schwan P., Key C.F., "The Conductivity of Living Tissues," *Annals of the New York Academy of Sciences*, 65, pp. 1007-1013, 1957.

Schwan H. P., "Electric Characteristics of tissue", *Biophysik*, vol. 1, pp. 198-208, 1963.

Sepulveda N., Wikswo P. J., "Finite element analysis of the cardiac defibrillation current distribution", *IEEE Tr. Biomed. Engng.*, vol. 37, pp. 354-365, 1990.

Serša G., Čemažar M., Šemrov D., Miklavčič D., "Changing electrode orientation improves the efficancy of elecrochemotherapy of solid tumors in mice", *Bioelectrochemistry and Bioenergetics*, vol. 39, pp. 61-66, 1996.

Serša I., Beravs K., Dodd N.J.F., Miklavčič D., Demšar F., "Electric Current Density Imaging of Mice Tumors," *Magn. Res. Med.*, 37, pp. 1-7, 1997.

Serša G., Štabuc B., Čemažar M., Jančar B., Miklavčič D., Rudolf Z., "Electrochemotherapy with cisplatin: Potentiation of local cisplatin antitumor effectiveness by application of electric pulses in cancer patients", *European Journal of Cancer*, vol. 34, no. 8, pp. 1213-1218, 1998.

Serša G., Čemažar M., Rudolf Z., "Electrochemotherapy: advantagaes and drawbacks in treatment of cancer patients", *Cancer Therapy*, vol. 1, pp. 133-142, 2003.

Shahidi A. V., Savard P., Nadeau R., "Forward and inverse problems of electrocardiography: Modeling and recovery of epicardial potentials in humans," *IEEE Tr. Biomed. Engng.*, vol. 41, pp. 249-256, 1994.

Simon J. R., "Transformation of intact yeast cells by electroporation," in Recombinant DNA, H R. Wu, ed., Academic Press, pp. 478-483, 1993.

Smith S. R., Foster K. R., Wolf G. L., "Dielectric properties of VX-2 carcionma versus normal liver tissue", *IEEE Trans. Biomed. Engng.*, vol. 33, pp. 522-524, 1986.

Sinigoj A. R., Osnove elektromagnetike, Založba FE in FRI, Ljubljana, Slovenia, 1999.

Somiari S., Glasspool-Malone J., Drabick J. J., Gilbert R. A., Heller R., Jaroszeski M. J., Malone R., "Theory and in vivo application of electroporative gene delivery", *Molecular Therapy*, vol. 2, no. 3, pp. 178-187, 2000.

Sugar I. P., Neumann E., "Stochastic model for electric field - induced membrane pores. electroporation", *Biophysical Chemistry*, vol. 19, pp. 211-225, 1984.

Sugar I.P., “Exact solutions of stochastic model of electroporation,” in Charge and Field Effects in Biosystems, M.J. Allen, S.F. Cleary, A.E. Sowers, D.D. Shillady eds., Birkhawser, Boston, Berlin, Basel, 1991.

Surowiec A. J., Stuchly S., Barr J. R., Swarp A., “Dielectric Properties of breast Carcionma and the Surrounding Tissuee” *IEEE Trans. Biomed. Engng.*, vol. 35, pp. 257-263, 1988.

Susil R., Šemrov D., Miklavčič D., "Electric field induced transmembrane potential depends on cell density and organization", *Electro and Magnetobiology*, vol. 17, no. 3, pp. 391-399, 1998.

Šel D., Mazeres S., Teissie J., Miklavčič D., “Finite Element Modelling of Needle Electrodes in Tissue from the Perspective of Frequent Model Computation,” *IEEE Trans. Biomed. Engng., 50, pp. 1-12,* 2003.

Šemrov D., Miklavčič D., "Calculation of the electrical parameters in electrochemotherapy of solid tumors in mice", *Computers in Biology and Medicine*, vol. 28, pp. 439-448, 1998.

Teissie J., Rols M. P., "An experimental evaluation of the critical potential difference including cell membrane electropermeabilization", *Biophysical Journal*, vol. 65, pp. 409-413, 1993.

Teissie J., Rols M. P., "Correlation between electric field pulse induced long - lived permeabilization and fusogenicity in cell membranes", *Biophysical Journal*, vol. 74, pp. 1889-1898, 1998.

Teissie J., Eynard N., Gabriel B., Rols M. P., "Electropermeabilisation of cell membranes", *Advanced Drug Delivery Reviews*, vol. 35, pp. 3-19, 1999.

Tsong T. Y., "Electroporation of cell membranes", *Biophysical Journal*, vol. 60, pp. 297-306, 1991.

Zhang L., Nolan E., Kreitschitz S., Rabussay D.P., "Enhanced delivcery of naked DNA to the skin by non-invasive in vivo electroporation", *Biochim. Biophys. Acta,* 1572, pp. 1-9, 2002.

Zylka W., Wischmann H. A., “On geometric distortions in CT Images,” *Proc. 18th Int. Conf. IEEE Eng. Med. & Biol. Society EMBS*, Amsterdam, 1996.

Weaver J. C., Chizmadzhev Y. A., “Theory of electroporation: A review”, *Bioelectrochemistry and Bioenergetics*. vol. 41, pp. 135-160, 1996.

Weaver J. C., Vaughan T.E., Chizmadzhev Y. A.: “Theory of electrical creation of aqueous pathways across skin transport barriers,” *Advanced Drug Delivery Reviews*, vol. 35, pp. 21-39, 1999.

William T. J., Zhang Y., Li C., Jirtle R. L., “The measured properties of normal and malignant human tissues from 50 to 900 MHz”, *Med. Phys,* vol. 21, pp. 4-7, 1994.

Wolf H., Rols M. P., Boldt E., Neumann E., Teissie J., "Control by pulse parametes of electric field - mediated gene transfer in mammalian cells", *Biophysical Journal*, vol. 66, pp. 524-531, 1994.

Wong T.-K., Neumann E., "Electric field mediated gene transfer", *Biochemical and Biophysical Research Comunications*, vol. 107, no. 2, pp. 584-587, 1982.

APPENDIX

The programme code of the simulation environment should be run with Matlab software (MathWork, Inc). The simulation environment is started by typing *permeabilisation* in Matlab workspace. Simulation environment consists of following programmes:

- permeabilisation.m,
- window1.m,
- window2.m,
- window3.m,
- window4.m,
- stepwise.m,
- linear.m,
- exponential.m,
- sigmoid.m.

Their programme code is given in continuation.

PERMEABILISATION.M

```
clear all;

window1;
window2;
window3;
window4;

barva=1*[0.3 0.5 0.7];
barva1=barva+0.1*[1,1,1];
barva2=[0.1 0.3 0.5];

sirina=395;
visina=260;
pozM=[sirina/2+20 visina-60 155 18];
pozP=[20 visina-60 155 18];
poz_ozP=[pozP(1)+pozP(3)/2 pozP(2)-100 20 18];

figure(1);


%
% Inner radius R0
%
poz_Rmin=pozP-[-0 5 106 0];
poz_Rmin_tx=[poz_Rmin(1) poz_Rmin(2)+20 50 18];
Rmin_hndl=uicontrol('Style','edit',...
        'Position',poz_Rmin,...
        'Back',barva1,...
        'String','1');

%
% Outer radius R1
%
poz_Rmax=pozP-[-60 5 106 0];
poz_Rmax_tx=[poz_Rmax(1) poz_Rmax(2)+20 50 18];
Rmax_hndl=uicontrol('Style','edit',...
        'Position',poz_Rmax,...
        'Back',barva1,...
        'String','4');

%
% irreversible threshold E1
%
poz_Emax=pozP-[-300 5 106 0];
poz_Emax_tx=[poz_Emax(1) poz_Emax(2)+20 50 18];
Emax_hndl=uicontrol('Style','edit',...
        'Position',poz_Emax,...
        'Back',barva1,...
        'String','63.7');

%
% length l
%
poz_l=pozP-[-0 50 106 0];
poz_l_tx=[poz_l(1) poz_l(2)+20 50 18];
l_hndl=uicontrol('Style','edit',...
        'Position',poz_l,...
        'Back',barva1,...
        'String','4');

%
%parameter B needed for exponential and s-shaped S(E) dependency
%
poz_B=pozP-[-60 50 106 0];
poz_B_tx=[poz_B(1) poz_B(2)+20 50 18];
B_hndl=uicontrol('Style','edit',...
        'Position',poz_B,...
        'Back',barva1,...
        'String','1000');
```

```
%
% non-permeabilised tissue conductivity S0
%
poz_S0=pozP-[-120 5 106 0];
poz_S0_tx=[poz_S0(1) poz_S0(2)+20 50 18];
S0_hndl=uicontrol('Style','edit',...
              'Position',poz_S0,...
              'Back',barva1,...
              'String','1');

%
% max conductivity of-permeabilised tissue S1
%
poz_S1=pozP-[-180 5 106 0];
poz_S1_tx=[poz_S1(1) poz_S1(2)+20 50 18];
S1_hndl=uicontrol('Style','edit',...
              'Position',poz_S1,...
              'Back',barva1,...
              'String','2.5');

%
% pulse amplitude
%
poz_u=pozP-[-120 50 106 0];
poz_u_tx=[poz_u(1) poz_u(2)+20 50 18];
u_hndl=uicontrol('Style','edit',...
              'Position',poz_u,...
              'Back',barva1,...
              'String','100');

%
%reversible threshold E0
%
poz_Eprag=pozP-[-240 5 106 0];
poz_Eprag_tx=[poz_Eprag(1) poz_Eprag(2)+20 50 18];
Eprag_hndl=uicontrol('Style','edit',...
              'Position',poz_Eprag,...
              'Back',barva1,...
              'String','36.2');
```

WINDOW1.M

```
barva=1*[0.3 0.5 0.7];
barva1=barva+0.1*[1,1,1];
barva2=[0.1 0.3 0.5];

sirina=395;
visina=260;
pozM=[sirina/2+20 visina-60 155 18];
pozP=[20 visina-60 155 18];
poz_ozP=[pozP(1)+pozP(3)/2 pozP(2)-100 20 18];

set(figure(1),'Position',[50 100 sirina visina],...
        'Color',barva,...
        'Name','Parameters',...
        'NumberTitle','off',...
        'MenuBar','none',...
        'Resize','off');

%
%Delete graphs
%
uicontrol('Style','push',...
        'Position',[sirina-145 10 125 25],...
        'String','Delete graphs',...
        'CallBack','figure(2); clf; figure(3); clf; figure(4); clf ');

%
%Close windows
%
uicontrol('Style','push',...
        'Position',[sirina-375 10 125 25],...
        'String','Close windows',...
        'CallBack','close(1); close (2); close (3); close (4)');

%
%inner radius R0
%
poz_Rmin=pozP-[-0 5 106 0];
poz_Rmin_tx=[poz_Rmin(1) poz_Rmin(2)+20 50 18];
uicontrol('Style','push',...
        'Position',poz_Rmin_tx,...
        'String','R0',...
        'CallBack',");

%
% outer radius R1
%
poz_Rmax=pozP-[-60 5 106 0];
poz_Rmax_tx=[poz_Rmax(1) poz_Rmax(2)+20 50 18];
uicontrol('Style','push',...
        'Position',poz_Rmax_tx,...
        'String','R1',...
        'CallBack',");

%
%irreveresible threshold E1
%
poz_Emax=pozP-[-300 5 106 0];
poz_Emax_tx=[poz_Emax(1) poz_Emax(2)+20 50 18];
uicontrol('Style','push',...
        'Position',poz_Emax_tx,...
        'String','E1',...
        'CallBack',");
```

```
%
%length l
%
poz_l=pozP-[-0 50 106 0];
poz_l_tx=[poz_l(1) poz_l(2)+20 50 18];
uicontrol('Style','push',...
          'Position',poz_l_tx,...
          'String','l',...
          'CallBack',");

%
% parameter B needed for exponential and s-shaped S(E) dependency
%
poz_B=pozP-[-60 50 106 0];
poz_B_tx=[poz_B(1) poz_B(2)+20 50 18];
uicontrol('Style','push',...
          'Position',poz_B_tx,...
          'String','B',...
          'CallBack',");

%
%field to display max pulse amplitude – not to exceed E1 anytime and anywhere between the electrodes
%
poz_umax=pozP-[-180 50 106 0];
poz_umax_tx=[poz_umax(1) poz_umax(2)+20 50 18];
uicontrol('Style','push',...
          'Position',poz_umax_tx,...
          'String','umax',...
          'CallBack',");

%
% pulse amplitude
%
poz_u=pozP-[-120 50 106 0];
poz_u_tx=[poz_u(1) poz_u(2)+20 50 18];
uicontrol('Style','push',...
          'Position',poz_u_tx,...
          'String','u',...
          'CallBack',");

%
%i before
%
poz_i0=pozP-[-240 50 106 0];
poz_i0_tx=[poz_i0(1) poz_i0(2)+20 50 18];
uicontrol('Style','push',...
          'Position',poz_i0_tx,...
          'String','i before',...
          'CallBack',");

%
%i after
%
poz_i1=pozP-[-300 50 106 0];
poz_i1_tx=[poz_i1(1) poz_i1(2)+20 50 18];
uicontrol('Style','push',...
          'Position',poz_i1_tx,...
          'String','i after',...
          'CallBack',");

%
% non-permeabilised conductivity S0
%
poz_S0=pozP-[-120 5 0 0];
poz_S0_tx=[poz_S0(1) poz_S0(2)+20 50 18];
uicontrol('Style','push',...
          'Position',poz_S0_tx,...
          'String','Sigma0',...
          'CallBack',");
```

```
%
% max conductivity of permeabilised tissue S1
%
poz_S1=pozP-[-180 5 0 0];
poz_S1_tx=[poz_S1(1) poz_S1(2)+20 50 18];
uicontrol('Style','push',...
              'Position',poz_S1_tx,...
              'String','Sigma1',...
              'CallBack','');

%
%reversible threshold E0
%
poz_Eprag=pozP-[-240 5 0 0];
poz_Eprag_tx=[poz_Eprag(1) poz_Eprag(2)+20 50 18];
uicontrol('Style','push',...
              'Position',poz_Eprag_tx,...
              'String','E0',...
              'CallBack','');

%
% Begin simulation with stepwise dependency S(E)
%
uicontrol('Style','push',...
   'Position',[sirina-375 100 170 25],...
              'String','STEP permeabilisation',...
              'CallBack','stepwise');

%
% Begin simulation with linear dependency S(E)
%
uicontrol('Style','push',...
              'Position',[sirina-190 100 170 25],...
              'String','LIN permeabilisation',...
              'CallBack','linear');

%
% Begin simulation with exponential dependency S(E)
%
uicontrol('Style','push',...
              'Position',[sirina-375 55 170 25],...
              'String','EXP permeabilisation',...
              'CallBack','exponential');

%
% Begin simulation with S-shaped dependency S(E)
%
uicontrol('Style','push',...
              'Position',[sirina-190 55 170 25],...
              'String','SIGMA permeabilisation',...
              'CallBack','sigmoid');
```

WINDOW 2.M

```
barva=1*[0.3 0.5 0.7];
barva1=barva+0.1*[1,1,1];
sirina=395;
visina=260;
pozM=[sirina/2+20 visina-60 155 18];
pozP=[20 visina-60 155 18];
poz_ozP=[pozP(1)+pozP(3)/2 pozP(2)-100 20 18];

%
%window displays change in conductivity between the electrodes at time dsicrete steps
%
set(figure(2),'Position',[50 385 sirina visina],...
        'Color',barva,...
        'Name','Change in conductivity: S=f(r)',...
        'NumberTitle','off',...
        'MenuBar','none',...
        'Resize','off');
```

WINDOW3.M

```
barva=1*[0.3 0.5 0.7];
barva1=barva+0.1*[1,1,1];
sirina=395;
visina=260;
pozM=[sirina/2+20 visina-60 155 18];
pozP=[20 visina-60 155 18];
poz_ozP=[pozP(1)+pozP(3)/2 pozP(2)-100 20 18];

%
%window displays radius of peremebilised tissue at time discrete steps
%
set(figure(3),'Position',[450 100 sirina visina],...
        'Color',barva,...
        'Name','R during permebilisation: R=f(sequence)',...
        'NumberTitle','off',...
        'MenuBar','none',...
        'Resize','off');
```

WINDOW4.M

```
barva=1*[0.3 0.5 0.7];
barva1=barva+0.1*[1,1,1];
sirina=395;
visina=260;
pozM=[sirina/2+20 visina-60 155 18];
pozP=[20 visina-60 155 18];
poz_ozP=[pozP(1)+pozP(3)/2 pozP(2)-100 20 18];


%
%window displays E between the electrodes at time discrete steps
%
set(figure(4),'Position',[450 385 sirina visina],...
        'Color',barva,...
        'Name','E0 and E during permebilisation: E=f(r)',...
        'NumberTitle','off',...
        'MenuBar','none',...
        'Resize','off');
```

STEPWISE.M

```
Eprag=str2num(get(Eprag_hndl,'string'));
R0=str2num(get(Rmin_hndl,'string'));
R1=str2num(get(Rmax_hndl,'string'));
S0=str2num(get(S0_hndl,'string'));
S1=str2num(get(S1_hndl,'string'));
Emax=str2num(get(Emax_hndl,'string'));
l=str2num(get(l_hndl,'string'));
f=1; %to plot S(E)

barva=1*[0.3 0.5 0.7];
barva1=barva+0.1*[1,1,1];
barva2=[0.1 0.3 0.5];
I1=[];

sirina=395;
visina=260;
pozM=[sirina/2+20 visina-60 155 18];
pozP=[20 visina-60 155 18];
poz_ozP=[pozP(1)+pozP(3)/2 pozP(2)-100 20 18];

A=S1/S0; %conductivity ration
Rpor=[];
E30=[];
E31=[];
E00=[];
KON=[];
KON1=[];
KON2=[];
E3=[];
tok=[];
tok1=[];
tok2=[];
SS0=[];
SS=[];
SS1cel=[];
I1=[];
RR1=[];

korak=15; %no. of time discrete steps
plus=0.01;
deli=50;
delta=(Emax-Eprag)/deli;
konst=(S1-S0)/(Emax-Eprag);
n=konst*Eprag-S0;

umax=Emax*(log(R1/R0)*R0); %max. pulse amplitude

%
% display max. pulse amplitude
%
poz_umax=pozP-[-180 50 106 0];
poz_umax_tx=[poz_umax(1) poz_umax(2)+20 50 18];
umax_hndl=uicontrol('Style','edit',...
    'Position',poz_umax,...
    'Back',barva1,...
    'String',umax);

%
% read pulse amplitude
%
u=str2num(get(u_hndl,'string'));

%%%%%%%%%%%%%%%%%%%%%%%%%%%%%%%%%%%%%%%%%%%%
% E in non-permebilised tissue
for r=R0:plus:R1
    e00=u/(log(R1/R0)*r);
    E00=[E00 e00];
    KON=[KON Eprag];   %E0
    KON1=[KON1 Emax];   %E1
    KON2=[KON2 u/(log(R1/R0)*R1)];
end
%%%%%%%%%%%%%%%%%%%%%%%%%%%%%%%%%%%%%%%%%%
```

```
%%%%%%%%%%%%%%%%%%%%%%%%%%%%%%%%%%%%%%%%%
%current before
i0=2*pi*l*S0*u/log(R1/R0);

% display
poz_i0=pozP-[-240 50 106 0];
poz_i0_tx=[poz_i0(1) poz_i0(2)+20 50 18];
i0_hndl=uicontrol('Style','edit',...
                'Position',poz_i0,...
                'Back',barva2,...
                'String',i0);
%%%%%%%%%%%%%%%%%%%%%%%%%%%%%%%%%%%%%%%%%%%

rpor=u/(log(R1/R0)*Eprag);
rpor=round(rpor*100)/100;

if rpor>R1
   rpor=R1;
end
%%%%%%%%%%%%%%%%%%%%%%%%%%%%%%%%%%%%%%%%%%%

%%%%%%%%%%%%%%%%%%%%%%%%%%%%%%%%%%%%%%%%%%%
% E, if raidus of permeabilisation  between inner and outer radius
if rpor<R1
   E31=E00;
   E0skup=E00;
   Rpor=[R0 rpor];
   SS1old(1:length(E00))=S0;

   %%%%%%%%%%%%%%%%%%%%%%%%%%%%%%%%%%%%%%
   %no. of steps
   %%%%%%%%%%%%%%%%%%%%%%%%%%%%%%%%%%%%%%

   for veliki=1:(korak-1)
      E0=[];
      E1=[];

      %if r during permebilisation exceeds R1
      if rpor>=R1
         E1=E00;
         sigma(1:length(E00))=S1;
         i1=2*pi*l*S1*u/log(R1/R0);
         E31=[E31; E1];
         SS1cel=[SS1cel; sigma];
         I1=[I1 i1];
         Rpor=[Rpor R1];
      end

      %%%%%%%%%%%%%%%%%%%%%%%%%%%%%%%%%%%%%%
      %if r during permebilisation below R
      %%%%%%%%%%%%%%%%%%%%%%%%%%%%%%%%%%%%%%

      if rpor<R1
         EE=E0skup;
         SS1=[];

         %%%%%%%%%%%%%%%%%%%%%%%%%%%%%%%%
         % S(E)
         %%%%%%%%%%%%%%%%%%%%%%%%%%%%%%%%%


         for m=1:length(EE)
            if EE(m)>=Eprag
               ss1=S1;
            else
               ss1=S0;
            end
            SS1(m)=ss1;
         end

         %%%%%%%%%%%%%%%%%%%%%%%%%%%%%%%%%
         % end S(E)
         %%%%%%%%%%%%%%%%%%%%%%%%%%%%%%%%%
```

```
% compare S at k with S at k-1
for nn=1:length(SS1)
   if SS1old(nn)>=SS1(nn)
      SS1(nn)=SS1old(nn);
   end
end

SS1old=SS1;
SS1cel=[SS1cel; SS1];


%%%%%%%%%%%%%%%%%%%%%%%%%%%%%%%%%%
% new E and r
%%%%%%%%%%%%%%%%%%%%%%%%%%%%%%%%%%
RR1=[R0];
RR2=[];
SS2=[];
AA=[];
rr1=R0;

for jj=1:length(SS1)-1
   S00=SS1(jj+1);
   S01=SS1(jj);
   A=S01/S00;

   if S01~=S00
      RR1=[RR1 rr1];
      SS2=[SS2 S01];
      AA=[AA A];
   end
   rr1=rr1+plus;
end

SS2=[SS2 S00];
RR2=[RR1(2:length(RR1)) R1];

SP=SS2(1)./SS2;
E0skup=[];

imen=0;
for ena = 1:length(RR1)
   imen=imen+SP(ena)*log(RR2(ena)/RR1(ena));
end

for dva=1:length(RR1)
   E0=[];
   RR1(1)=RR1(1)-plus;
   a=round((RR1(dva)+plus)*100)/100;
   b=round((RR2(dva))*100)/100;

   for r=a:plus:b
      e0=SP(dva)*(u/imen)*(1/r);
      E0=[E0 e0];

      %new r
      razl=Emax;
      if dva==length(RR1)
         if (e0-Eprag)<= razl
            if (e0-Eprag)>0
               razl=e0-Eprag;
               rpor=r;
            end
         end
      end
   end
   E0skup=[E0skup E0];
end

Rpor=[Rpor rpor];
E30=E0skup;
E31=[E31; E30];
```

```
            %%%%%%%%%%%%%%%%%%%%%%%%%%%%%%%%
            % end new E and r
            %%%%%%%%%%%%%%%%%%%%%%%%%%%%%%%%

        end %
        %%%%%%%%%%%%%%%%%%%%%%%%%%%%%%%%%%%%%%%%%
        %end  if r during permebilisation below R
        %%%%%%%%%%%%%%%%%%%%%%%%%%%%%%%%%%%%%%%%%

    end
    %%%%%%%%%%%%%%%%%%%%%%%%%%%%%%%%%%%%%%%%%%%%%
    %end of no. of steps
    %%%%%%%%%%%%%%%%%%%%%%%%%%%%%%%%%%%%%%%%%%%%%

    %%%%%%%%%%%%%%%%%%%%%%%%%%%%%%%%%%%%%%%%%%%%%
    %i after permeabilisation
    A=S1/S0;
    i1=(S1*l*2*pi*u)/((log(rpor/R0)+A*log(R1/rpor)));
    poz_i1=pozP-[-300 50 106 0];
    poz_i1_tx=[poz_i1(1) poz_i1(2)+20 50 18];
    i1_hndl=uicontrol('Style','edit',...
        'Position',poz_i1,...
        'Back',barva2,...
        'String',i1);
    %%%%%%%%%%%%%%%%%%%%%%%%%%%%%%%%%%%%%%%

    %begin store current
    for stt=1:length(Rpor)
        A=S1/S0;
        rpori=Rpor(1,stt);
        i1=(S1*l*2*pi*u)/((log(rpori/R0)+A*log(R1/rpori)));
        I1=[I1 i1];
    end
    %end store current

    %plot radius of permeabilisation
    figure(3);
    ip=0:korak;
    plot(ip,Rpor);
    hold on;
    grid

    %plot E
    for ie=1:korak;
        figure(4)
        grid
        r3rise=R0:plus:R1;
        plot(r3rise,E31(ie,:),r3rise,E31(1,:),'r',r3rise,KON);
        hold on;
        grid;
    end

    %plot conductivity
    for ie=1:korak-1;
        figure(2)
        if ie == korak-1
            plot(r3rise,SS1cel(ie,:),'r','linewidth',2);
        else
            plot(r3rise,SS1cel(ie,:));
        end
        axis([1 4 0.0002 0.00065]);
        hold on;
        grid;
    end
end
```

LINEAR.M

```
Eprag=str2num(get(Eprag_hndl,'string'));
R0=str2num(get(Rmin_hndl,'string'));
R1=str2num(get(Rmax_hndl,'string'));
S0=str2num(get(S0_hndl,'string'));
S1=str2num(get(S1_hndl,'string'));
Emax=str2num(get(Emax_hndl,'string'));
l=str2num(get(l_hndl,'string'));
B=str2num(get(B_hndl,'string'));
f=4; %to plot S(E)

barva=1*[0.3 0.5 0.7];
barva1=barva+0.1*[1,1,1];
barva2=[0.1 0.3 0.5];
I1=[];

sirina=395;
visina=260;
pozM=[sirina/2+20 visina-60 155 18];
pozP=[20 visina-60 155 18];
poz_ozP=[pozP(1)+pozP(3)/2 pozP(2)-100 20 18];

A=S1/S0; %conductivity ration
Rpor=[];
E30=[];
E31=[];
E00=[];
KON=[];
KON1=[];
KON2=[];
E3=[];
tok=[];
tok1=[];
tok2=[];
SS0=[];
SS=[];
SS1cel=[];
I1=[];
RR1=[];

korak=15; %no. of time discrete steps
plus=0.01;
deli=50;
delta=(Emax-Eprag)/deli;
konst=(S1-S0)/(Emax-Eprag);
n=konst*Eprag-S0;


umax=Emax*(log(R1/R0)*R0); %max. pulse amplitude

%
% display max. pulse amplitude
%
poz_umax=pozP-[-180 50 106 0];
poz_umax_tx=[poz_umax(1) poz_umax(2)+20 50 18];
umax_hndl=uicontrol('Style','edit',...
    'Position',poz_umax,...
    'Back',barva1,...
    'String',umax);

%
% read pulse amplitude
%
u=str2num(get(u_hndl,'string'));

%%%%%%%%%%%%%%%%%%%%%%%%%%%%%%%%%%%%%%%%%%%%%
% E in non-permebilised tissue
for r=R0:plus:R1
    e00=u/(log(R1/R0)*r);
    E00=[E00 e00];
    KON=[KON Eprag];   %E0
    KON1=[KON1 Emax];   %E1
```

```
   KON2=[KON2 u/(log(R1/R0)*R1)];
end
%%%%%%%%%%%%%%%%%%%%%%%%%%%%%%%%%%%%%%%%%%

rpor=u/(log(R1/R0)*Eprag);
rpor=round(rpor*100)/100;

if rpor>R1
   rpor=R1;
end

%%%%%%%%%%%%%%%%%%%%%%%%%%%%%%%%%%%%%%%%%
%current before
i0=2*pi*l*S0*u/log(R1/R0);

% display
poz_i0=pozP-[-240 50 106 0];
poz_i0_tx=[poz_i0(1) poz_i0(2)+20 50 18];
i0_hndl=uicontrol('Style','edit',...
   'Position',poz_i0,...
   'Back',barva2,...
   'String',i0);
%%%%%%%%%%%%%%%%%%%%%%%%%%%%%%%%%%%%%%%%%%%

%%%%%%%%%%%%%%%%%%%%%%%%%%%%%%%%%%%%%%%%%%%%%%%%%%%%%
% if E at R1 above E1
%%%%%%%%%%%%%%%%%%%%%%%%%%%%%%%%%%%%%%%%%%%%%%%%%%%%%
if E00(length(E00))>=Emax
   E3=E00;
   Rpor(1:(korak+1))=R1;

   %plot E
   figure(4);
   r3rise=R0:plus:R1;
   plot(r3rise,E3,r3rise,KON);
   xlabel('radius');
   ylabel('E');
   axis([1 10 0 45]);
   grid;
   hold on;

   %plot r
   figure(3);
   ip=0:korak;
   plot(ip,Rpor);
   xlabel('k');
   ylabel('radius');
   grid;
   hold on;
end
%%%%%%%%%%%%%%%%%%%%%%%%%%%%%%%%%%%%%%%%%%%%%%%%%%%%%
%end  if E at R1 above E1
%%%%%%%%%%%%%%%%%%%%%%%%%%%%%%%%%%%%%%%%%%%%%%%%%%%%%%

%%%%%%%%%%%%%%%%%%%%%%%%%%%%%%%%%%%%%%%%%%%%%%%%%%%%%
% if r<R0
%%%%%%%%%%%%%%%%%%%%%%%%%%%%%%%%%%%%%%%%%%%%%%%%%%%%%
if rpor<=R0
   E3=E00;
   Rpor(1:(korak+1))=rpor;

   %plot E
   figure(4);
   r3rise=R0:plus:R1;
   plot(r3rise,E3,r3rise,KON);
   xlabel('radius');
   ylabel('E');
   axis([1 10 0 45]);
   grid;
   hold on;

   %plot radius
   figure(3);
   ip=0:korak;
```

```
   plot(ip,Rpor);
   xlabel('k');
   ylabel('radius');
   grid;
   hold on;
end
%%%%%%%%%%%%%%%%%%%%%%%%%%%%%%%%%%%%%%%%%%%%%%%%%%%%%%%%%%%%
%end  if r<R0
%%%%%%%%%%%%%%%%%%%%%%%%%%%%%%%%%%%%%%%%%%%%%%%%%%%%%%%%%%%%

%%%%%%%%%%%%%%%%%%%%%%%%%%%%%%%%%%%%%%%%%%%%%%%%
% E, if raidus of permeabilisation  between inner and outer radius
%%%%%%%%%%%%%%%%%%%%%%%%%%%%%%%%%%%%%%%%%%%
if E00(length(E00))<=Emax
   E31=E00;
   E0skup=E00;
   Rpor=[R0 rpor];
   SS1old(1:length(E00))=S0;

   %%%%%%%%%%%%%%%%%%%%%%%%%%%%%%%%%%%%%%%%%%%
   %no. of steps
   %%%%%%%%%%%%%%%%%%%%%%%%%%%%%%%%%%%%%%%%%%%

   for veliki=1:(korak-1)
      E0=[];
      E1=[];

      %if r during permebilisation exceeds R1
      if E0skup(length(E00))>=Emax
         E1=E00;
         sigma(1:length(E00))=S1;
         i1=2*pi*l*S1*u/log(R1/R0);
         E31=[E31; E1];
         SS1cel=[SS1cel; sigma];
         I1=[I1 i1];
         Rpor=[Rpor R1];
      end

      %%%%%%%%%%%%%%%%%%%%%%%%%%%%%%%%%%%%%%%%%%%
      %if r during permebilisation below R
      %%%%%%%%%%%%%%%%%%%%%%%%%%%%%%%%%%%%%%%%%%%

      if E0skup(length(E00))<=Emax
         EE=E0skup;
         SS1=[];

         %%%%%%%%%%%%%%%%%%%%%%%%%%%%%%%%%%%%
         % S(E)
         %%%%%%%%%%%%%%%%%%%%%%%%%%%%%%%%%%%%%

         for m=1:length(EE)
            if EE(m)>Emax
               ss1=S1;
            elseif EE(m)<=Eprag
               ss1=S0;
            else
               for kk=1:deli
                  if EE(m)<=Eprag+kk*delta
                     if EE(m)>Eprag+(kk-1)*delta
                        ss1=konst*(Eprag+(kk-0.5)*delta)-n;
                     end
                  end
               end
            end
            SS1(m)=ss1;
         end

         %%%%%%%%%%%%%%%%%%%%%%%%%%%%%%%%%%%%%
         % end S(E)
         %%%%%%%%%%%%%%%%%%%%%%%%%%%%%%%%%%%%%


         % compare S at k with S at k-1
         for nn=1:length(SS1)
```

```
   if SS1old(nn)>=SS1(nn)
      SS1(nn)=SS1old(nn);
   end
end

SS1old=SS1;
SS1cel=[SS1cel; SS1];


%%%%%%%%%%%%%%%%%%%%%%%%%%%%%%%%%
% new E and r
%%%%%%%%%%%%%%%%%%%%%%%%%%%%%%%%%
RR1=[R0];
RR2=[];
SS2=[];
AA=[];
rr1=R0;

for jj=1:length(SS1)-1
   S00=SS1(jj+1);
   S01=SS1(jj);
   A=S01/S00;

   if S01~=S00
      RR1=[RR1 rr1];
      SS2=[SS2 S01];
      AA=[AA A];
   end
   rr1=rr1+plus;
end

SS2=[SS2 S00];
RR2=[RR1(2:length(RR1)) R1];

SP=SS2(1)./SS2;
E0skup=[];

imen=0;
for ena = 1:length(RR1)
   imen=imen+SP(ena)*log(RR2(ena)/RR1(ena));
end

for dva=1:length(RR1)
   E0=[];
   RR1(1)=RR1(1)-plus;
   a=round((RR1(dva)+plus)*100)/100;
   b=round((RR2(dva))*100)/100;

   for r=a:plus:b
      e0=SP(dva)*(u/imen)*(1/r);
      E0=[E0 e0];

      %new r
      razl=Emax;
      if dva==length(RR1)
         if (e0-Eprag)<= razl
            if (e0-Eprag)>0
               razl=e0-Eprag;
               rpor=r;
            end
         end
      end
   end
   E0skup=[E0skup E0];
end

Rpor=[Rpor rpor];
E30=E0skup;
E31=[E31; E30];


%%%%%%%%%%%%%%%%%%%%%%%%%%%%%%%%
% end new E and r
%%%%%%%%%%%%%%%%%%%%%%%%%%%%%%%%
```

```
        end %
        %%%%%%%%%%%%%%%%%%%%%%%%%%%%%%%%%%%%%%%%%
        %end  if r during permebilisation below R
        %%%%%%%%%%%%%%%%%%%%%%%%%%%%%%%%%%%%%%%%%

    end
    %%%%%%%%%%%%%%%%%%%%%%%%%%%%%%%%%%%%%%%%%%%%%
    %end of no. of steps
    %%%%%%%%%%%%%%%%%%%%%%%%%%%%%%%%%%%%%%%%%%%%%

    %plot radius of permeabilisation
    figure(3);
    ip=0:korak;
    plot(ip,Rpor);
    hold on;
    grid

    %plot E
    for ie=1:korak;
        figure(4)
        grid
        r3rise=R0:plus:R1;
        plot(r3rise,E31(ie,:),r3rise,E31(1,:),'r',r3rise,KON);
        hold on;
        grid;
    end

    %plot conductivity
    for ie=1:korak-1;
        figure(2)
        if ie == korak-1
            plot(r3rise,SS1cel(ie,:),'r','linewidth',2);
        else
            plot(r3rise,SS1cel(ie,:));
        end
        axis([1 4 0.0002 0.00065]);
        hold on;
        grid;
    end
end
```

EXPONENTIAL.M

```
Eprag=str2num(get(Eprag_hndl,'string'));
R0=str2num(get(Rmin_hndl,'string'));
R1=str2num(get(Rmax_hndl,'string'));
S0=str2num(get(S0_hndl,'string'));
S1=str2num(get(S1_hndl,'string'));
Emax=str2num(get(Emax_hndl,'string'));
l=str2num(get(l_hndl,'string'));
B=str2num(get(B_hndl,'string'));
f=4; %to plot S(E)

barva=1*[0.3 0.5 0.7];
barva1=barva+0.1*[1,1,1];
barva2=[0.1 0.3 0.5];
I1=[];

sirina=395;
visina=260;
pozM=[sirina/2+20 visina-60 155 18];
pozP=[20 visina-60 155 18];
poz_ozP=[pozP(1)+pozP(3)/2 pozP(2)-100 20 18];

A=S1/S0; %conductivity ration
Rpor=[];
E30=[];
E31=[];
E00=[];
KON=[];
KON1=[];
KON2=[];
E3=[];
tok=[];
tok1=[];
tok2=[];
SS0=[];
SS=[];
SS1cel=[];
I1=[];
RR1=[];

korak=15; %no. of time discrete steps
plus=0.01;
deli=50;
delta=(Emax-Eprag)/deli;
konst=(S1-S0)/(Emax-Eprag);
k2=(S0-S1)/(exp((Eprag-Emax)/B)-1);


umax=Emax*(log(R1/R0)*R0); %max. pulse amplitude

%
% display max. pulse amplitude
%
poz_umax=pozP-[-180 50 106 0];
poz_umax_tx=[poz_umax(1) poz_umax(2)+20 50 18];
umax_hndl=uicontrol('Style','edit',...
   'Position',poz_umax,...
   'Back',barva1,...
   'String',umax);

%
% read pulse amplitude
%
u=str2num(get(u_hndl,'string'));

%%%%%%%%%%%%%%%%%%%%%%%%%%%%%%%%%%%%%%%%%%%%%%%%%%%%
% E in non-permebilised tissue
for r=R0:plus:R1
   e00=u/(log(R1/R0)*r);
   E00=[E00 e00];
   KON=[KON Eprag];   %E0
   KON1=[KON1 Emax];   %E1
```

```
   KON2=[KON2 u/(log(R1/R0)*R1)];
end
%%%%%%%%%%%%%%%%%%%%%%%%%%%%%%%%%%%%%%%%%%


rpor=u/(log(R1/R0)*Eprag);
rpor=round(rpor*100)/100;

if rpor>R1
   rpor=R1;
end

%%%%%%%%%%%%%%%%%%%%%%%%%%%%%%%%%%%%%%%%%
%current before
i0=2*pi*l*S0*u/log(R1/R0);

% display
poz_i0=pozP-[-240 50 106 0];
poz_i0_tx=[poz_i0(1) poz_i0(2)+20 50 18];
i0_hndl=uicontrol('Style','edit',...
   'Position',poz_i0,...
   'Back',barva2,...
   'String',i0);
%%%%%%%%%%%%%%%%%%%%%%%%%%%%%%%%%%%%%%%%%%%

%%%%%%%%%%%%%%%%%%%%%%%%%%%%%%%%%%%%%%%%%%%%%%%%%%%%%
% if E at R1 above E1
%%%%%%%%%%%%%%%%%%%%%%%%%%%%%%%%%%%%%%%%%%%%%%%%%%%%%
if E00(length(E00))>=Emax
   E3=E00;
   Rpor(1:(korak+1))=R1;

   %plot E
   figure(4);
   r3rise=R0:plus:R1;
   plot(r3rise,E3,r3rise,KON);
   xlabel('radius');
   ylabel('E');
   axis([1 10 0 45]);
   grid;
   hold on;

   %plot r
   figure(3);
   ip=0:korak;
   plot(ip,Rpor);
   xlabel('k');
   ylabel('radius');
   grid;
   hold on;
end
%%%%%%%%%%%%%%%%%%%%%%%%%%%%%%%%%%%%%%%%%%%%%%%%%%%%%
%end  if E at R1 above E1
%%%%%%%%%%%%%%%%%%%%%%%%%%%%%%%%%%%%%%%%%%%%%%%%%%%%%%

%%%%%%%%%%%%%%%%%%%%%%%%%%%%%%%%%%%%%%%%%%%%%%%%%%%%%
% if r<R0
%%%%%%%%%%%%%%%%%%%%%%%%%%%%%%%%%%%%%%%%%%%%%%%%%%%%%
if rpor<=R0
   E3=E00;
   Rpor(1:(korak+1))=rpor;

   %plot E
   figure(4);
   r3rise=R0:plus:R1;
   plot(r3rise,E3,r3rise,KON);
   xlabel('radius');
   ylabel('E');
   axis([1 10 0 45]);
   grid;
   hold on;

   %plot radius
   figure(3);
```

```
   ip=0:korak;
   plot(ip,Rpor);
   xlabel('k');
   ylabel('radius');
   grid;
   hold on;
end
%%%%%%%%%%%%%%%%%%%%%%%%%%%%%%%%%%%%%%%%%%%%%%%%%%%%%%%%%%%%
%end  if r<R0
%%%%%%%%%%%%%%%%%%%%%%%%%%%%%%%%%%%%%%%%%%%%%%%%%%%%%%%%%%%%

%%%%%%%%%%%%%%%%%%%%%%%%%%%%%%%%%%%%%%%%%%%%%%%%%
% E, if raidus of permeabilisation  between inner and outer radius
%%%%%%%%%%%%%%%%%%%%%%%%%%%%%%%%%%%%%%%%%%%
if E00(length(E00))<=Emax
   E31=E00;
   E0skup=E00;
   Rpor=[R0 rpor];
   SS1old(1:length(E00))=S0;

   %%%%%%%%%%%%%%%%%%%%%%%%%%%%%%%%%%%%%%%%%%%
   %no. of steps
   %%%%%%%%%%%%%%%%%%%%%%%%%%%%%%%%%%%%%%%%%%%

   for veliki=1:(korak-1)
      E0=[];
      E1=[];

      %if r during permebilisation exceeds R1
      if E0skup(length(E00))>=Emax
         E1=E00;
         sigma(1:length(E00))=S1;
         i1=2*pi*l*S1*u/log(R1/R0);
         E31=[E31; E1];
         SS1cel=[SS1cel; sigma];
         I1=[I1 i1];
         Rpor=[Rpor R1];
      end

      %%%%%%%%%%%%%%%%%%%%%%%%%%%%%%%%%%%%%%%%%%%
      %if r during permebilisation below R
      %%%%%%%%%%%%%%%%%%%%%%%%%%%%%%%%%%%%%%%%%%%

      if E0skup(length(E00))<=Emax
         EE=E0skup;
         SS1=[];

         %%%%%%%%%%%%%%%%%%%%%%%%%%%%%%%%%%%%
         % S(E)
         %%%%%%%%%%%%%%%%%%%%%%%%%%%%%%%%%%%%%

         for m=1:length(EE)
            if EE(m)>Emax
               ss1=S1;
            elseif EE(m)<=Eprag
               ss1=S0;
            else
               for kk=1:deli
                  if EE(m)<=Eprag+kk*delta
                     if EE(m)>Eprag+(kk-1)*delta
                        ss1=k2*(exp(((Eprag+(kk-0.5)*delta)-Emax)/B)-1)+S1;
                     end
                  end
               end
            end
            SS1(m)=ss1;
         end

         %%%%%%%%%%%%%%%%%%%%%%%%%%%%%%%%%%%%%
         % end S(E)
         %%%%%%%%%%%%%%%%%%%%%%%%%%%%%%%%%%%%%


         % compare S at k with S at k-1
```

```
for nn=1:length(SS1)
   if SS1old(nn)>=SS1(nn)
      SS1(nn)=SS1old(nn);
   end
end

SS1old=SS1;
SS1cel=[SS1cel; SS1];


%%%%%%%%%%%%%%%%%%%%%%%%%%%%%%%%%%
% new E and r
%%%%%%%%%%%%%%%%%%%%%%%%%%%%%%%%%%
RR1=[R0];
RR2=[];
SS2=[];
AA=[];
rr1=R0;

for jj=1:length(SS1)-1
   S00=SS1(jj+1);
   S01=SS1(jj);
   A=S01/S00;

   if S01~=S00
      RR1=[RR1 rr1];
      SS2=[SS2 S01];
      AA=[AA A];
   end
   rr1=rr1+plus;
end

SS2=[SS2 S00];
RR2=[RR1(2:length(RR1)) R1];

SP=SS2(1)./SS2;
E0skup=[];

imen=0;
for ena = 1:length(RR1)
   imen=imen+SP(ena)*log(RR2(ena)/RR1(ena));
end

for dva=1:length(RR1)
   E0=[];
   RR1(1)=RR1(1)-plus;
   a=round((RR1(dva)+plus)*100)/100;
   b=round((RR2(dva))*100)/100;

   for r=a:plus:b
      e0=SP(dva)*(u/imen)*(1/r);
      E0=[E0 e0];

      %new r
      razl=Emax;
      if dva==length(RR1)
         if (e0-Eprag)<= razl
            if (e0-Eprag)>0
               razl=e0-Eprag;
               rpor=r;
            end
         end
      end
   end
   E0skup=[E0skup E0];
end

Rpor=[Rpor rpor];
E30=E0skup;
E31=[E31; E30];


%%%%%%%%%%%%%%%%%%%%%%%%%%%%%%%%%
% end new E and r
```

```
      %%%%%%%%%%%%%%%%%%%%%%%%%%%%%%%%%%%

    end %
    %%%%%%%%%%%%%%%%%%%%%%%%%%%%%%%%%%%%%%%%%%%%%
    %end  if r during permebilisation below R
    %%%%%%%%%%%%%%%%%%%%%%%%%%%%%%%%%%%%%%%%%%%%%

  end
  %%%%%%%%%%%%%%%%%%%%%%%%%%%%%%%%%%%%%%%%%%%%%%%%%
  %end of no. of steps
  %%%%%%%%%%%%%%%%%%%%%%%%%%%%%%%%%%%%%%%%%%%%%%%%%

  %plot radius of permeabilisation
  figure(3);
  ip=0:korak;
  plot(ip,Rpor);
  hold on;
  grid

  %plot E
  for ie=1:korak;
    figure(4)
    grid
    r3rise=R0:plus:R1;
    plot(r3rise,E31(ie,:),r3rise,E31(1,:),'r',r3rise,KON);
    hold on;
    grid;
  end

  %plot conductivity
  for ie=1:korak-1;
    figure(2)
    if ie == korak-1
      plot(r3rise,SS1cel(ie,:),'r','linewidth',2);
    else
      plot(r3rise,SS1cel(ie,:));
    end
    axis([1 4 0.0002 0.00065]);
    hold on;
    grid;
  end
end
```

SIGMOID.M

```
Eprag=str2num(get(Eprag_hndl,'string'));
R0=str2num(get(Rmin_hndl,'string'));
R1=str2num(get(Rmax_hndl,'string'));
S0=str2num(get(S0_hndl,'string'));
S1=str2num(get(S1_hndl,'string'));
Emax=str2num(get(Emax_hndl,'string'));
l=str2num(get(l_hndl,'string'));
B=str2num(get(B_hndl,'string'));
f=5; %to plot S(E)

barva=1*[0.3 0.5 0.7];
barva1=barva+0.1*[1,1,1];
barva2=[0.1 0.3 0.5];
I1=[];

sirina=395;
visina=260;
pozM=[sirina/2+20 visina-60 155 18];
pozP=[20 visina-60 155 18];
poz_ozP=[pozP(1)+pozP(3)/2 pozP(2)-100 20 18];

A=S1/S0; %conductivity ration
Rpor=[];
E30=[];
E31=[];
E00=[];
KON=[];
KON1=[];
KON2=[];
E3=[];
tok=[];
tok1=[];
tok2=[];
SS0=[];
SS=[];
SS1cel=[];
I1=[];
RR1=[];

korak=15; %no. of time discrete steps
plus=0.01;
deli=50;
delta=(Emax-Eprag)/deli;
konst=(S1-S0)/(Emax-Eprag);
aa=(Eprag+Emax)/2;


umax=Emax*(log(R1/R0)*R0); %max. pulse amplitude

%
% display max. pulse amplitude
%
poz_umax=pozP-[-180 50 106 0];
poz_umax_tx=[poz_umax(1) poz_umax(2)+20 50 18];
umax_hndl=uicontrol('Style','edit',...
   'Position',poz_umax,...
   'Back',barva1,...
   'String',umax);

%
% read pulse amplitude
%
u=str2num(get(u_hndl,'string'));

%%%%%%%%%%%%%%%%%%%%%%%%%%%%%%%%%%%%%%%%%%%%%%%%
% E in non-permebilised tissue
for r=R0:plus:R1
   e00=u/(log(R1/R0)*r);
   E00=[E00 e00];
   KON=[KON Eprag];   %E0
   KON1=[KON1 Emax];   %E1
   KON2=[KON2 u/(log(R1/R0)*R1)];
```

```
end
%%%%%%%%%%%%%%%%%%%%%%%%%%%%%%%%%%%%%%%%%%


rpor=u/(log(R1/R0)*Eprag);
rpor=round(rpor*100)/100;

if rpor>R1
   rpor=R1;
end

%%%%%%%%%%%%%%%%%%%%%%%%%%%%%%%%%%%%%%%%%
%current before
i0=2*pi*l*S0*u/log(R1/R0);

% display
poz_i0=pozP-[-240 50 106 0];
poz_i0_tx=[poz_i0(1) poz_i0(2)+20 50 18];
i0_hndl=uicontrol('Style','edit',...
   'Position',poz_i0,...
   'Back',barva2,...
   'String',i0);
%%%%%%%%%%%%%%%%%%%%%%%%%%%%%%%%%%%%%%%%%%%

%%%%%%%%%%%%%%%%%%%%%%%%%%%%%%%%%%%%%%%%%%%%%%%%%%%%%
% if E at R1 above E1
%%%%%%%%%%%%%%%%%%%%%%%%%%%%%%%%%%%%%%%%%%%%%%%%%%%%%
if E00(length(E00))>=Emax
   E3=E00;
   Rpor(1:(korak+1))=R1;

   %plot E
   figure(4);
   r3rise=R0:plus:R1;
   plot(r3rise,E3,r3rise,KON);
   xlabel('radius');
   ylabel('E');
   axis([1 10 0 45]);
   grid;
   hold on;

   %plot r
   figure(3);
   ip=0:korak;
   plot(ip,Rpor);
   xlabel('k');
   ylabel('radius');
   grid;
   hold on;
end
%%%%%%%%%%%%%%%%%%%%%%%%%%%%%%%%%%%%%%%%%%%%%%%%%%%%%
%end  if E at R1 above E1
%%%%%%%%%%%%%%%%%%%%%%%%%%%%%%%%%%%%%%%%%%%%%%%%%%%%%%

%%%%%%%%%%%%%%%%%%%%%%%%%%%%%%%%%%%%%%%%%%%%%%%%%%%%%
% if r<R0
%%%%%%%%%%%%%%%%%%%%%%%%%%%%%%%%%%%%%%%%%%%%%%%%%%%%%
if rpor<=R0
   E3=E00;
   Rpor(1:(korak+1))=rpor;

   %plot E
   figure(4);
   r3rise=R0:plus:R1;
   plot(r3rise,E3,r3rise,KON);
   xlabel('radius');
   ylabel('E');
   axis([1 10 0 45]);
   grid;
   hold on;

   %plot radius
   figure(3);
   ip=0:korak;
```

```
   plot(ip,Rpor);
   xlabel('k');
   ylabel('radius');
   grid;
   hold on;
end
%%%%%%%%%%%%%%%%%%%%%%%%%%%%%%%%%%%%%%%%%%%%%%%%%%%%%%%%%%
%end  if r<R0
%%%%%%%%%%%%%%%%%%%%%%%%%%%%%%%%%%%%%%%%%%%%%%%%%%%%%%%%%%

%%%%%%%%%%%%%%%%%%%%%%%%%%%%%%%%%%%%%%%%%%%%%%%
% E, if raidus of permeabilisation  between inner and outer radius
%%%%%%%%%%%%%%%%%%%%%%%%%%%%%%%%%%%%%%%%%
if E00(length(E00))<=Emax
   E31=E00;
   E0skup=E00;
   Rpor=[R0 rpor];
   SS1old(1:length(E00))=S0;

   %%%%%%%%%%%%%%%%%%%%%%%%%%%%%%%%%%%%%%%%%
   %no. of steps
   %%%%%%%%%%%%%%%%%%%%%%%%%%%%%%%%%%%%%%%%%

   for veliki=1:(korak-1)
      E0=[];
      E1=[];

      %if r during permebilisation exceeds R1
      if E0skup(length(E00))>=Emax
         E1=E00;
         sigma(1:length(E00))=S1;
         i1=2*pi*l*S1*u/log(R1/R0);
         E31=[E31; E1];
         SS1cel=[SS1cel; sigma];
         I1=[I1 i1];
         Rpor=[Rpor R1];
      end

      %%%%%%%%%%%%%%%%%%%%%%%%%%%%%%%%%%%%%%%%%
      %if r during permebilisation below R
      %%%%%%%%%%%%%%%%%%%%%%%%%%%%%%%%%%%%%%%%%

      if E0skup(length(E00))<=Emax
         EE=E0skup;
         SS1=[];

         %%%%%%%%%%%%%%%%%%%%%%%%%%%%%%%%%%%
         % S(E)
         %%%%%%%%%%%%%%%%%%%%%%%%%%%%%%%%%%%%

         for m=1:length(EE)
            if EE(m)>Emax
               ss1=S1;
            elseif EE(m)<=Eprag
               ss1=S0;
            else
               for kk=1:deli
                  if EE(m)<=Eprag+kk*delta
                     if EE(m)>Eprag+(kk-1)*delta
                        ss1=((S1-S0)/(1+exp(-((Eprag+(kk-0.5)*delta)-aa)/B)))+S0;
                     end
                  end
               end
            end
            SS1(m)=ss1;
         end

         %%%%%%%%%%%%%%%%%%%%%%%%%%%%%%%%%%%%
         % end S(E)
         %%%%%%%%%%%%%%%%%%%%%%%%%%%%%%%%%%%%


         % compare S at k with S at k-1
         for nn=1:length(SS1)
```

```
    if SS1old(nn)>=SS1(nn)
        SS1(nn)=SS1old(nn);
    end
end

SS1old=SS1;
SS1cel=[SS1cel; SS1];


%%%%%%%%%%%%%%%%%%%%%%%%%%%%%%%%%
% new E and r
%%%%%%%%%%%%%%%%%%%%%%%%%%%%%%%%%
RR1=[R0];
RR2=[];
SS2=[];
AA=[];
rr1=R0;

for jj=1:length(SS1)-1
    S00=SS1(jj+1);
    S01=SS1(jj);
    A=S01/S00;

    if S01~=S00
        RR1=[RR1 rr1];
        SS2=[SS2 S01];
        AA=[AA A];
    end
    rr1=rr1+plus;
end

SS2=[SS2 S00];
RR2=[RR1(2:length(RR1)) R1];

SP=SS2(1)./SS2;
E0skup=[];

imen=0;
for ena = 1:length(RR1)
    imen=imen+SP(ena)*log(RR2(ena)/RR1(ena));
end

for dva=1:length(RR1)
    E0=[];
    RR1(1)=RR1(1)-plus;
    a=round((RR1(dva)+plus)*100)/100;
    b=round((RR2(dva))*100)/100;

    for r=a:plus:b
        e0=SP(dva)*(u/imen)*(1/r);
        E0=[E0 e0];

        %new r
        razl=Emax;
        if dva==length(RR1)
            if (e0-Eprag)<= razl
                if (e0-Eprag)>0
                    razl=e0-Eprag;
                    rpor=r;
                end
            end
        end
    end
    E0skup=[E0skup E0];
end

Rpor=[Rpor rpor];
E30=E0skup;
E31=[E31; E30];


%%%%%%%%%%%%%%%%%%%%%%%%%%%%%%%%
% end new E and r
%%%%%%%%%%%%%%%%%%%%%%%%%%%%%%%%
```

```
      end %
      %%%%%%%%%%%%%%%%%%%%%%%%%%%%%%%%%%%%%%%%%%%%%%%%%%
      %end  if r during permebilisation below R
      %%%%%%%%%%%%%%%%%%%%%%%%%%%%%%%%%%%%%%%%%%%%%%%%%%

   end
   %%%%%%%%%%%%%%%%%%%%%%%%%%%%%%%%%%%%%%%%%%%%%%%%%%%%%%%
   %end of no. of steps
   %%%%%%%%%%%%%%%%%%%%%%%%%%%%%%%%%%%%%%%%%%%%%%%%%%%%%%%

   %plot radius of permeabilisation
   figure(3);
   ip=0:korak;
   plot(ip,Rpor);
   hold on;
   grid

   %plot E
   for ie=1:korak;
      figure(4)
      grid
      r3rise=R0:plus:R1;
      plot(r3rise,E31(ie,:),r3rise,E31(1,:),'r',r3rise,KON);
      hold on;
      grid;
   end

   %plot conductivity
   for ie=1:korak-1;
      figure(2)
      if ie == korak-1
         plot(r3rise,SS1cel(ie,:),'r','linewidth',2);
      else
         plot(r3rise,SS1cel(ie,:));
      end
      axis([1 4 0.0002 0.00065]);
      hold on;
      grid;
   end
end
```

ORIGINAL CONTRIBUTIONS TO THE RESEARCH AREA

Based on the presented results in this work the author demands the recognition of her original scientific contributions to the research area which are summarized in continuation.

DEVELOPMENT OF THE TIME DISCRETE MODEL OF TISSUE ELECTROPERMEABILISATION

A time discrete model of tissue permeabilisation was developed. The model describes the dynamics of electropermeabilisation at time discrete intervals. It describes changes in tissue specific conductivity during permeabilisation, which had not yet been provided by any other model of tissue permeabilisation.

The most important model outputs are electric field distribution, specific conductivity and total current computed at time discrete intervals during permeabilisation.

Model verification was performed by a parametric study. The analysis showed that the model behaves in accordance with experimental observations.

Model validation was performed on experimental *in vivo* measurements of current and areas of reversibly and irreversibly permeabilised tissue. The model validation showed very good agreement between the model and measurements.

Electric field distribution in time discrete steps within the model can be described either analytically or numerically, depending on the complexity of the geometry.

MODEL BASED ANALYSIS OF THE COURSE OF PERMEABILISATION AFFECTED BY DIFFERENT FUNCTIONAL DEPENDENCIES $\sigma(E)$

The time discrete model was extended to describe the arbitrary dependency between specific conductivity and electric field intensity $\sigma(E)$. For time discrete models with a numerical description of electric field distribution, special purpose functions were designed to be used with Femlab software. For the time discrete model with an analytical description of electric field distribution between two concentric electrodes, the analytical solution was extended to describe arbitrary dependency $\sigma(E)$.

Model based analysis of the impact of different dependencies $\sigma(E)$ on the course of permeabilisation were carried out by performing a parametric study considering the model with an analytical description of E distribution. The analysis has shown the importance of having accurate information about $\sigma(E)$ dependency for each type of tissue.

ESTIMATION OF ELECTRIC FIELD THRESHOLD VALUES BASED ON MEASURED CURRENT AND CR^{51}-EDTA UPTAKE

A method for determination of the functional dependency σ(E) was proposed. The method is based on current measurements and permeabilisation model. Measurements of Cr^{51}-EDTA uptake can also be used to increase the accuracy of σ(E) determination.

DEVELOPMENT OF THE SIMULATION ENVIRONMENT FOR MONITORING ELECTROPERMEABILISATION BASED ON THE ANALYTICAL MODEL OF THE ELECTRIC FIELD DISTRIBUTION BETWEEN TWO CONCENTRIC ELECTRODES

A simulation environment was developed based on a time discrete model of tissue permeabilisation between two concentric cylindrical electrodes. The simulation environment provides the means for monitoring the radius of permeabilisation, electric field intensity and specific conductivity at time discrete steps during permeabilisation at user supplied parameters. As the electric field distribution between two concentric cylindrical electrodes is similar to the distribution around needle electrodes this simulation environment could be used for approximate but fast determination of the extent of permeabilisation before treatment in clinics.

DETERMINATION OF THE OPTIMAL NEEDLE ELECTRODE GEOMETRY FOR MODELLING WITH A FINITE ELEMENT METHOD

An optimal needle electrode geometry for modelling with a finite element method from the perspective of frequent model computation was proposed.

OPTIMISATION OF ELECTROPERMEABILISATION PULSE PARAMETERS BASED ON A TIME DISCRETE MODEL OF ELECTROPERMEABILISATION

Optimisation of electropermeabilisation parameters was undertaken by a nonlinear constrained optimisation method, which considered limitations of power supply and other requirements related to application in electrochemotherapy. The parameters subject to optimisation were pulse amplitude and the distance between electrodes. The results showed that model based optimisation is an adequate approach for determination of optimal electropermeabilisation parameters.

The optimisation procedure, which is based on a validated time discrete model of tissue permeabilisation, could thus be used in clinics for determination of optimal pulse parameters in a non-invasive way before treatment.

DECLARATION

The author herewith declares that the content of the thesis is a result of her own research work supervised by mentor prof. dr. Damijan Miklavčič. The assistance of other colleagues is stated in the Acknowledgements. Published research results of other authors are listed amongst References.

Davorka Šel

IZJAVA

Izjavljam, da sem avtor te disertacije, ki je nastala kot plod raziskovalnega dela pod mentorstvom prof. dr. Damijana Miklavčiča. Izkazano pomoč drugih sodelavcev sem v celoti navedla v zahvali (ang. *Acknowledgements*). Že objavljeni dosežki drugih avtorjev so navedeni v literaturi (ang. *References*).

Davorka Šel